TUBULAR REACTOR FOR LIQUID-PHASE PROPYLENE POLYMERIZATION

Ravindra Radhakisan Tupe

Promotion Committee:

Prof. dr. ir. L. van Wijngaarden	Chairman, University of Twente, The Netherlands
Prof. Dr. –Ing. habil G. Weickert	Promoter, University of Twente, The Netherlands
Prof. Dr. L. Böhm	University of Aachen, Germany
Dr. A. B. Mathur	Indian Petrochemicals Corporation Limited, India
Prof. dr. ir. W. P. M. van Swaaij	University of Twente, The Netherlands
Prof. dr. ir. G. F. Versteeg	University of Twente, The Netherlands
Prof. dr. P. D. Idema	University of Amsterdam, The Netherlands
Prof. Dr. rer. nat. K-H. Reichert	Technical University Berlin, Germany
Prof. Dr. J. Mejzlík	Polymer Research Institute, Brno, Czech Republic

The research described in this thesis was performed at the University of Twente, The Netherlands. The work has been financially supported by the Dutch Polymer Institute (Project Number: #115), The Netherlands.

Publisher:

Wöhrmann Print Service
Groupe CPI
P. O. Box 92, 7200 AB
Zutphen, The Netherlands

Thesis cover design: Ide Engelsma, Kiran Thumma and Ravindra Tupe

ISBN 90-365-2379-6

TUBULAR REACTOR FOR LIQUID-PHASE PROPYLENE POLYMERIZATION

DISSERTATION

to obtain
the doctor's degree at the University of Twente,
on the authority of the rector magnificus,
prof. dr. W.H.M. Zijm,
on account of the decision of the graduation committee,
to be publicly defended
on Thursday June 08th 2006 at 13.15 hrs

by

Ravindra Radhakisan Tupe
born on September 11th 1976
in Mumbai, Maharashtra, India

This dissertation is approved by the promoter,
Prof. Dr. –Ing. habil G. Weickert

...to my family, friends and teachers

Summary

Olefin polymerization processes at elevated reaction temperature and pressure, using heterogeneous catalysts, are of great commercial interest, and certainly account for a very active field of research and development. Among the present conventional processes is the liquid-phase propylene polymerization, which is one of the most important industrial processes in polypropylene (PP) manufacture. This process became vital after the remarkable developments in high performance catalysts both in terms of improved activity and stereospecificity. However, in order to use such novel catalysts to develop innovative technologies or new products, the fundamental information of the catalyst performance, kinetically and morphologically, is required. Therefore, the present thesis is aimed at highlighting the important aspects of a novel tubular reactor process for the catalytic polymerization of liquid-phase propylene. The characteristics of the tubular reactor for catalytic liquid-phase propylene polymerization is understood based on the key element of "time-scale" analysis involved at different stages of polymerization. This covers the time starting from the insertion of the first monomer molecule at the active sites to the residence time of industrial scale reactors. The "time-scale" analysis in interpreting the reactor behavior is very important for a better understanding of the nature of the polymeric material produced at different stages of polymerization processes. The strategies applied in the present study and the most important outcomes are summarized in the following four categories:

i) Kinetic studies using isoperibolic calorimeter

Experimental investigations:

Prior to the analysis of the tubular reactor process, a proper selection of catalyst type is imperative. The main emphasis of the kinetic study falls on analyzing the overall kinetic response of the catalyst during polymerization. The kinetics of liquid-phase propylene polymerization were investigated in a fully filled 5.05 l batch reactor (Calorimeter) under isoperibolic conditions. The polymerization experiments were performed, for 45 to 60 min, using a highly active supported catalyst of type $MgCl_2/TiCl_4$ with Phthalate as an internal donor, Silane as an external donor and Triethylaluminum (TEA) as a cocatalyst. Different process parameters, such as temperature, cocatalyst concentration and precontacting time ($t_{Precont}$) for catalyst, cocatalyst and external donor, were varied in the range of 60 to 80 ^{o}C, 0.05 to 0.20 kg.m^{-3} and 5 to 60 min, respectively. The operating

pressure was maintained within the range of 40 to 55 bar. In addition, the influence of hydrogen on the polymerization kinetics has been studied by varying the mole ratio of hydrogen to liquid propylene (X) from 0.00025 to 0.1, much more than in most of other studies [⊕].

The initial polymerization rates were estimated using two approaches, one by extrapolating the reaction rate to time zero (R_{po}) and another by using an adiabatic temperature rise approach (R_{po_ATR}). For a given catalyst type, the difference between the two estimated rates was almost constant within a range of 4 % independent of polymerization conditions. The polymerization rate (R_p) increased by 2 fold with every 10 ^oC rise in temperature, and interesting to note that even at 80 ^oC this increment in rate was measured [◊]. It seems that experiments done with a completely filled reactor exhibit the effect of "reactor filling" on the dynamics of active catalyst particles during the reaction. From an Arrhenius plot of R_{po} and catalyst decay (k_d), an apparent activation energy for propagation reaction (E_p = 65.1 kJ.mol^{-1}) was estimated to be much higher than an apparent activation energy for deactivation reaction (E_d = 24.7 kJ.mol^{-1}). As a result of this difference, the polymer yield basically increases with increasing temperature. The reason can be seen in overheating and catalyst deactivation in case of partially filled reactors where the gas and liquid phase are more or less in equilibrium. In case of cocatalyst influence, the R_p and polymer yield enhanced by 10 % for an increase in the TEA concentration from 0.05 to 0.10 kg.m^{-3}. Furthermore, a strong dependency of the activation-decay behavior of catalyst on the $t_{Precont}$ was studied, and noticed that the k_d value was enhanced by 50 % when $t_{Precont}$ was changed from 30 to 60 min.

The most striking effect on the catalyst activity was seen in the presence of hydrogen. The catalyst activity was enhanced by 89 % when the X value was increased from 0.0 to 0.01, and the degree of enhancement was found to be temperature independent at least within the given window of operating conditions. The most widely accepted hypothesis for such an activation effect of hydrogen is due to the regeneration of active species via chain transfer at "dormant" (2,1 - inserted) sites. However, at high hydrogen concentration, the catalyst activity was decreasing with increasing X value from 0.01 to 0.1 at reaction temperature of 70 ^oC. The retardation effect on the catalyst activity was

[⊕] In case of polymerization tests performed at high hydrogen amount ($0.015 < X > 0.1$), the experiments were carried out using a capillary type tubular reactor operating under isoperibolic conditions.

[◊] Note that this is not always the case for experiments performed in a partially filled reactor in the presence of a monomer gas-phase operated under equilibrium conditions.

understood based on two reported facts: i) the decrease in active centers caused by the time lag of the recovery of polymerization center from metal-hydride (Ti-H) bond formed by the chain transfer by hydrogen and ii) a thermal instability in the active centers.

At similar hydrogen concentration, the weight-average molecular weight (M_w^{avg}) of the produced PP sample was estimated to be increased by an average value of 23 % for the rise in temperature from 60 to 70 ^oC. Typically, the average molecular weights of the produced polymer were decreasing with increasing the hydrogen concentration. In addition, the polydispersity index (PDI) or the molecular weight distribution (MWD) for different PP samples represented a narrow distribution with increasing reaction temperature. On the other hand, the increasing level of hydrogen during polymerization reaction resulted in an increase PDI value for all PP samples studied.

Kinetic model development:

A detailed and "improved" kinetic model has been derived by combining the two distinct kinetic mechanisms based on the "Natta approach" and the "dormant site approach". The "improved" kinetic model is a step-further in comparison with the "standard" kinetic model (containing the dormant site approach), which includes the chain transfer effect of dissociatively adsorbed as well as molecular hydrogen on the activity and molecular properties. The kinetic model developed for R_{po} and average probability of chain termination (q), which stands for the inverse average molecular weight, was capable of exhibiting the dependency on the polymerization temperature and concentrations of monomer, catalyst and hydrogen quantitatively. In particular, a deep analysis of the kinetic model has been performed to understand the characteristic influence of hydrogen on the R_{po} and q.

It was noticed that the model could predict the acceleration-retardation behavior of catalyst activity over a wide range of hydrogen concentrations ($0.0 < X < 0.1$), and was found to be in good statistical agreement with the experimental values. A careful but qualitative inspection of the values of predicted kinetic constants did explain the increasing phenomenon of catalyst activity at low values of X ($0.0 < X > 0.01$). Ultimately, it has been observed that the influence of hydrogen on the waking-up of dormant sites was indeed the rate determining step, especially when the X values were considered below 0.01. In other words, at low range of hydrogen concentration ($0.0 < X > 0.01$), the reactivation of dormant sites can be interpreted as reason for increasing the catalyst activity by "freeing" the blocked polymerization sites. On the other hand, at

higher hydrogen concentration ($0.01 < X > 0.1$), the distinct effect of adsorbed as well as molecular hydrogen seems to play a role in deciding the nature of produced active sites due to the hydrogen chain transfer. Therefore, during reaction, the delay in recovery of some of the active sites, which are attached to the hydrogen, could act as a rate determining step. It appeared that the relation between the formation of total number of active Ti-H bond due to the transfer and reactivation reaction with adsorbed as well as molecular hydrogen, and its reinitiation for further propagation with monomer was a key element in determining the effect of hydrogen on the decreasing catalyst activity [▽].

Furthermore, the dependency of q on X values between 0.0 and 0.01 was very steep and increased with increasing X value; however, for X values between 0.01 and 0.1, its effect on q was slightly (linearly) dampened out, and thus, leads to classify a hydrogen response on q with two distinct regions. Typically, at X values between 0.0 and 0.01 hydrogen act as a strong chain transfer agent enhancing the chain transfer phenomenon of active polymer chains. Next, at X values between 0.01 and 0.1, the dampened response of q can be classified from the decreasing response of catalyst activity, suggesting the slow recoveries of active sites, which are attached to the hydrogen. Therefore, as polymerization reaction proceeds, the polymer chain initiated from these active centers may probably exhibit a subsequent delay in the chain termination of these chains.

Additionally, it was observed that over a wide range of polymerization rate the catalyst deactivation depends on its activity change (may be due to temperature, pressure, hydrogen concentration, etc). In order to analyze the decay behavior, the spontaneous deactivation of an active catalyst was mainly considered with 1^{st} order decay rate with respect to the overall catalyst concentration. The deactivation of catalyst has been interpreted being just an “activity-dependent probability”.

The influence of hydrogen on the average molecular weights of the polymer samples was also discussed with the help of deconvolution analysis of MWD curves obtained using a gel permeation chromatography (GPC). The MWD curves were deconvoluted using a four site model. The results obtained describe the influence of temperature and hydrogen quantitatively.

[▽] Therefore, the reactions for first monomer addition (initiation) were considered separately, which was important especially in the case of initiation of active sites containing Ti-H bond.

ii) Aspects of novel (capillary type) tubular reactor

Kinetics and morphology analysis:

A novel (capillary type) tubular reactor (with an inside diameter of 0.004 m and reactor length of 5.65 m) set-up has been developed for conducting the catalytic polymerization reaction. The reactor behavior was systematically analyzed by carrying out polymerization experiments under isoperibolic condition, with pulse injections of the preactivated catalyst into a continuous liquid propylene flow at short residence times (τ = 40 - 43 s). The experiments were performed within the temperature range of 40 to 80 ^{o}C and reactor pressure ranging from 40 to 65 bar. A constant (2.70 kg.hr^{-1}) mass flow rate for liquid propylene was used while performing the polymerization experiments, yielding an average axial velocity (v_z) of 0.14 m.s^{-1} and Reynolds number (Re) of ≈ 3700. The experiments were conducted using the same catalyst type that has been used for the kinetic investigations performed with an isoperibolic calorimeter. Good reproducibility was found from a number of experiments performed at high hydrogen concentrations, i. e., at X values of 0.0219, 0.0510 and 0.0981, respectively.

The temperature profiles generated during the polymerization run describe the kinetic response of the catalyst at an early stage of polymerization. Interestingly, it was noticed that the catalyst exhibit the similar thermal characteristics in batch as well as in tubular reactor under the similar reaction conditions. However, the initial catalyst activity determined from tubular reactor experiments showed 14 - 30 % higher values compared to the batch reactor data. The high activity can be judged on the basis of two factors, one with respect to the dynamic behavior of tubular reactor in terms of mixing and heat transfer and another with regard to the influence of "early stage" processes on the subsequent polymerization reaction [∅].

The MWD curves for produced PP samples were found to be broadened by a factor of 1.3 with increasing X value from 0.0219 to 0.0981. The detailed analysis of the MWD curves was also carried out by applying a deconvolution method with a four site model. The broadening in MWD reflect the particular kinetic response intrinsic to each type of active sites, and exhibit a constant change in their performance with increasing values of X. At high hydrogen concentration (0.0219 < X > 0.0981), the mass fraction of polymer

[∅] As per the literature reviewed, the reason for such finding may believed to be mainly due to the differing time (polymerization yield) pertaining to the particular methods.

originating from different families of active sites found to be enhanced especially for the low molecular weight part. For instance, mass fractions of site type 1 and 2 were increased by 70 % and 28 %, respectively, when X value increased from 0.0219 to 0.0981, which clearly represents the sensitivity of different sites towards the presence of hydrogen.

In order to understand the effect of reactor behavior on the morphology of produced polymer, off line characterization techniques such as scanning elector microscopy (SEM), energy dispersive X-ray spectrometry (EDX), particle size distribution (PSD) and differential scanning calorimetry (DSC) were used. From the SEM analysis, it was observed that polymer particle tend to replicate the shape and texture of the catalyst, thus indicating a well controlled morphology of the polymer particle, which is not unexpected in case of a prepolymerized PP catalyst. Even the interpretation of PSD data suggested that the morphology of the polymer particles was intact and no problem of fines formation or particle agglomeration. The response of the tubular reactor on polymer morphology examined from the SEM and PSD analysis did exhibit the potential in extending the application of tubular reactor to a macro scale level of polymer production at least in the form of "prepolymerization reactor tool". Additionally, it was interesting to see that the dynamics of the tubular reactor did not show any significant influence on the crystallization ability of the polymer chains in comparison with the DSC data of PP sample prepared from batch reactor experiments.

Reactor model development and validation:

The nature of the temperature profiles obtained from tubular reactor experiments were evaluated by comparing with the output of the mathematical model. The analysis of thermal response of the tubular reactor together with the reactor model was very essential, and was carried out based on following important factors: a) reaction kinetics (heat production), b) heat transfer to the cooling media, and c) mixing dynamics of the reactor fluid. The model predictability for reaction rates, polymer yield and average molecular weights was assessed with respect to the experimental data, and observed to be in well accordance with the real reactor performance. More significantly, the "early stage" kinetic experiments together with the reactor model enabled us to characterize the catalyst performance over a shortened time of reaction. More importantly, the temperature profiles in tubular reactor were observed as a fingerprint for a given reactor-catalyst-heat transfer system and could be used as a "high-output" tool for characterization of both catalyst and monomer quality.

iii) Characteristics of scale-up tubular reactor

In order to explore the possibilities of extending the concept of tubular reactor to a macro scale level of real polymer production, the characteristics of scale-up tubular reactor has been investigated based on the developed reactor model. The simulation was carried out for the tubular reactor with an inside diameter of 0.1 m and reactor length of 5000 m, resulting into the reactor volume of 39 m^3. The reactor behavior was predicted in terms of the reactor thermal response (in the range of 60 to 80 ^oC), varying concentration of chemical constituents like active catalyst and hydrogen, and the polymer properties mainly the molecular weights and their distributions.

In most of the cases studied, the loading of the active catalyst was optimized to have the maximum reactor temperature difference (ΔT) in the range of 10 - 14 ^oC with the overall conversion value up to 30 %. With these settings, the predicted (optimum) annual production capacity of the tubular reactor was found to be 214 $kton.yr^{-1}$. The nature of the profile predicted for cumulative polymer yield, average molecular weights and polydispersity index as a function of hydrogen amount were found to be intrinsic to the type of the catalyst used throughout this research work. The unique characteristic of tubular reactor in allowing the multiple injection of hydrogen along the reactor length facilitated to predict the "Bimodal" nature of MWDs of the PP samples. The polydispersity indices of the predicted "Bimodal" molecular weight distributions are ranging from 34.1 to 70.2.

iv) Non-ideal behavior of tubular reactor

The atypical non-ideal behavior of the tubular reactor was highlighted by performing the selective experimental analysis on the dynamics of non-isothermal laminar flow of a reacting fluid in a scale-up tubular reactor. The tubular reactor geometry was scaled-up with respect to the ratios of inside tube diameter, tube length and reactor volume with respect to the "capillary type" reactor, and their values were 5.3, 0.2 and 5.6, respectively. The methodology discussed with the help of these experiments could assist in carrying out the statistical analysis of catalytic polymerization in a tubular reactor operating under laminar flow regime. It has been observed that the investigations presented to understand the non-ideal response of the reactor were very important in understanding the relation between reaction kinetics and the scaling dimensions of tubular reactor.

Finally, I want to express my hope that the different investigations presented in this thesis will help our industrial professionals to design the research framework for the future investigation of this reactor concept.

Contents

Chapter 1

General introduction

1.1 Tubular reactor: An overview

The discoveries of Ziegler's organometallic polymerization catalysts and Natta's stereoselective polymerization during the 1950's have initiated a chain of innovations promoting the rapid growth of polyolefin industry. Over the last five decades, a remarkable progress of catalytic olefin polymerization has greatly simplified the polyolefin production by eliminating deactivation, solvents, and polymer purification steps; see Figure 1.1. Presently, propylene is polymerized with a highly active and stereoselective magnesium chloride-supported catalysts in solvent-free gas phase and liquid pool processes to produce polypropylene (PP) economically (with an ever widening product slate). At the same time, the most advanced processes meet the stringent ecological requirements. It appears that the catalyst design, polymer reaction engineering, and polymer process technologies are being pushed forward to produce the novel polyolefin materials meeting the demands of highly diversified industries.

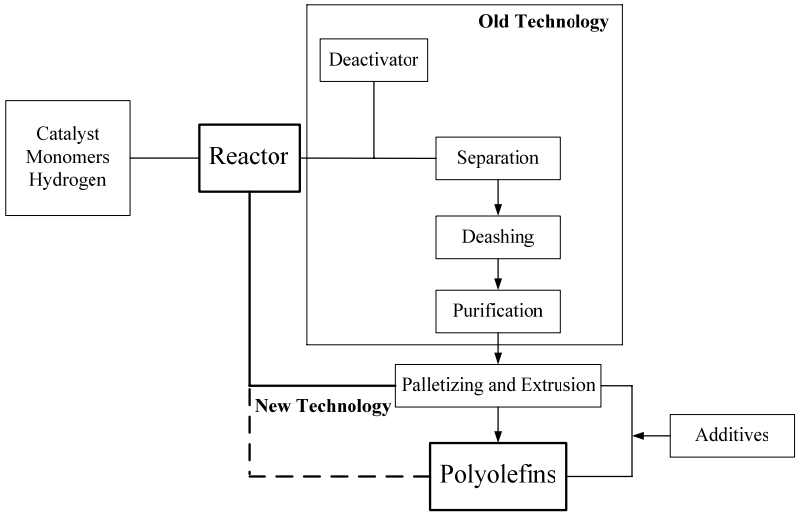

Figure 1.1: Simplified process chart of polyolefin production (see also Mülhaupt (2003) [21]).

The demand for new materials creates high motivations and new challenges for engineers to develop the novel process technologies for polyolefin production. As an example, the research work presented in this thesis is directed towards the analysis of liquid-phase processes for catalytic propylene polymerization using a tubular reactor concept.

The "time-scale" analysis of the different processes is important for a better understanding of the nature of the polymeric material produced at different stages of polymerization processes. A general overview of time-scale observed for the polyolefin processes is given below,

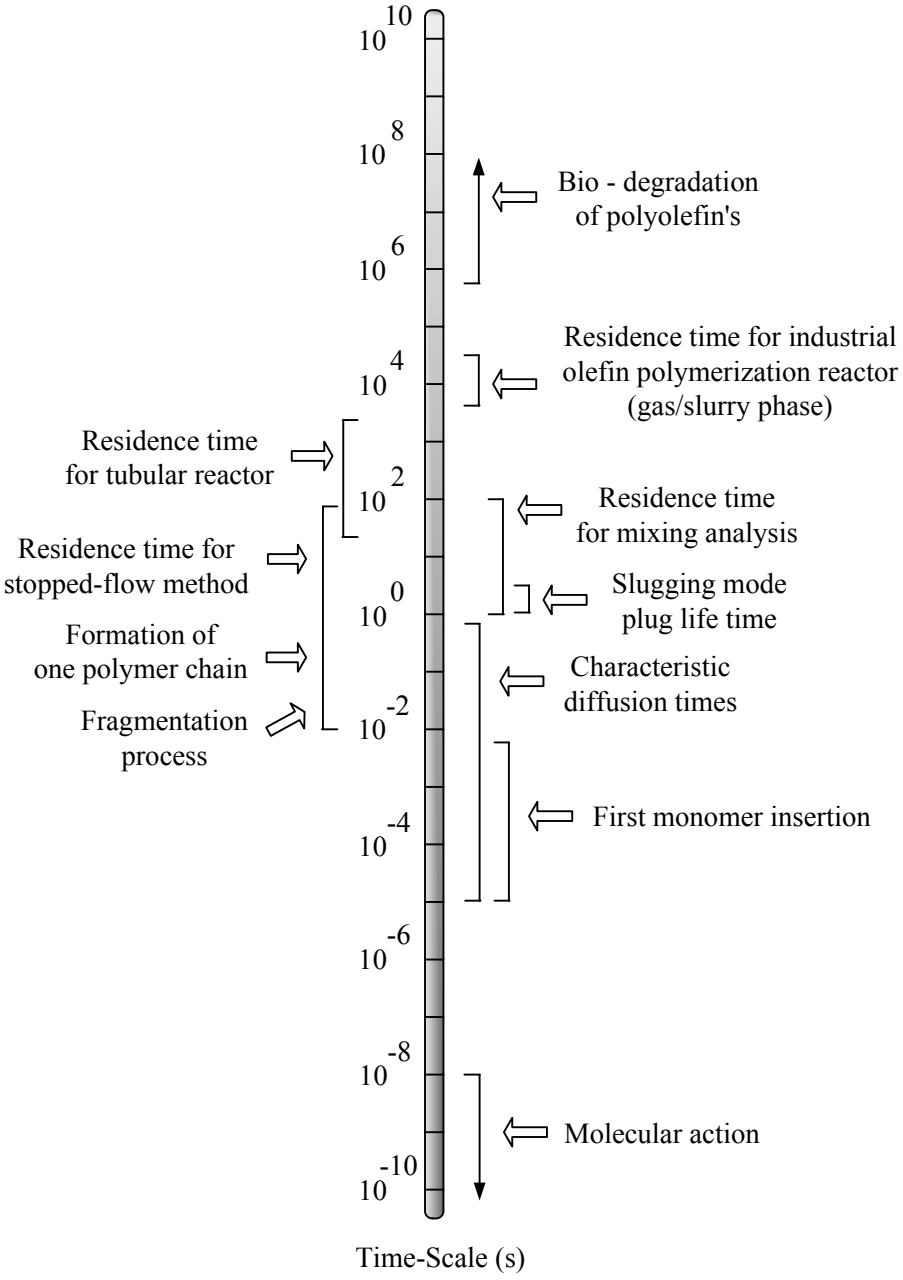

Tubular reactors have been used for the high pressure free radical polymerization of ethylene. Their principle was discovered in the 1930's and further developed by Union Carbide and by BASF [1, 3, 25]. Several experimental studies were reported in the literature, regarding the free radical polymerization of vinyl monomers such as styrene, methyl methacrylate, and vinyl acetate [6, 7, 10, 22, 24, 26].

The versatility of tubular reactors in polymerization processes is mainly due to its design simplicity and good heat transfer capabilities. Tubular reactor operations have become increasingly attractive for controlling both the residence time distribution of the active polymer molecules and the reaction temperatures [9, 19, 27]. In spite of having all these positive features, the usage of tubular reactors exhibits some limitations, due to two main obstacles, namely the "reactor fouling and plugging". Fortunately, there are several solutions discussed in the literature to overcome these obstacles [22].

The concept of tubular reactor is novel for the continuous catalytic polymerization of olefins. Stopped-flow techniques have been widely employed in the field of polymer science to investigate the cationic, anionic, free radical and group-transfer polymerizations [20]. Only, bench-scale setups referred to as "Stopped-flow" or "Quenched-flow" techniques have been used by several research groups for studying the catalytic olefin polymerization [4, 5, 12]. This technique was first developed by T. Keii and M. Terano in 1987, to evaluate the specific kinetic parameters of the polymerization of propylene with $MgCl_2$-supported Ziegler-Natta (ZN) catalyst [12].

The main advantage of stopped-flow polymerization method is seen in a possibility of carrying out the kinetic and morphological studies of catalytic olefin polymerization at its very early stages, which directly reflects the nature of active sites just after their formation.

This method provide a profound understanding of many controversial problems, such as the non-uniformity of the active sites [12], obtaining reliable kinetic parameters [4, 12], formation of active sites at different stages [20], the role of cocatalyst [16], the effects of hydrogen [15] and electron donor [17, 18], etc. Mori et al. (1997) [20] reported the characteristics of stopped-flow technique compared with the conventional one; they are shown in Table 1.1.

Table 1.1: Characteristics of a conventional process and the stopped-flow technique reported by Mori et al. (1997) [20] (i)

Characteristic	Conventional polymerization	Stopped-flow polymerization
Polymerization time	7200 s – 36000 s	~ 0.25 s
Catalyst activity	Varies with time	Constant (iii)
Chain transfer reaction	Inevitable	Negligible
Polymerization time versus lifetime (ii)	Polymerization time > > lifetime	Polymerization time < lifetime (iv)

(i) The comparison based on the typical results for propylene polymerization with an $MgCl_2$ – supported ZN catalyst; (ii) Lifetime of growing chain; (iii) However, for time-scale ~ 0.25s, the change in catalyst activity is depending on the process conditions; (iv) Similarly, the polymerization time can also be kept in the range of lifetime of the growing polymer chain by selecting the optimized experimental conditions.

Hence, the kinetic information can be derived for the different time-scales, which referred to the average time required for one polymer chain formation, the time required for the phase transition of growing particle, and the relevant time for the polymer production in various commercial processes (being in the order of 7200 to 36000 s).

From the stopped-flow experiments, the kinetic constants like k_p, k_{tr}, and $[C^*]$ can be determined, together with the following interrelations [12]:

$$Y = k_p[M][C^*]t \tag{1.1}$$

$$P_n^{avg} = \frac{M_n^{avg}}{M_o} = \frac{k_p\,[M]\,t}{1 + k_{tr}\,t} \tag{1.2}$$

According to Keii (2004) [13], the equation (1.2) for P_n^{avg} was derived based on the so-called "ideal" kinetic model for a polymerization reaction at a constant rate of monomer consumption, in which the propagation (growing) and transfer reactions of the growing polymer chains occur, and the rates of these reactions per growing polymer chain were assumed to be constant, independent of the chain length of growing polymer chain. The author reported that the P_n^{avg} estimated from equation (1.2) is the number-average degree of polymerization at $t >> 1/k_{tr}$. On the other hand, Busico et al. (1999) [4] proposed the modified form of the interrelations between Y and $1/P_n^{avg}$:

$$Y = k_p[M]C_{st}^* \left\{ t + \frac{1}{\langle f_i \rangle}\left[\exp\left(-\langle f_i \rangle t\right) - 1\right] \right\} \tag{1.3}$$

$$P_n^{avg} = \frac{\langle f_t \rangle \langle f_i \rangle + \langle f_i \rangle \left[1 - \exp\left(-\langle f_i \rangle t\right)\right]}{k_p[M]\langle f_i \rangle + k_p[M]\langle f_i \rangle t + k_p[M]\left[\exp\left(-\langle f_i \rangle t\right) - 1\right]} \quad (1.4)$$

In the case of propylene polymerization, Busico et al. (1999) [4] observed an acceleration period (in spite of a long pre-contact between the catalyst and co-catalyst). Therefore, the term $<f_i>$ was included in equation (1.4), as they believed that the process of acceleration was responsible for the induction period. Selected literature data for k_p, $<f_t>$, C^*, and $<f_i>$, are given in Table 1.2, parts (a) and (b).

Table 1.2: Kinetic results for catalytic olefin polymerization under stopped-flow conditions

(i) Experiments performed in a heptane solution saturated with propylene, and with $TiCl_4/MgCl_2/C_6H_5COOC_2H_5/Al(C_2H_5)_3$; (ii) Approximate values obtained by means of equation (1.2); (iii) Experiments performed in a toluene solution saturated with ethylene and/or propylene, and with rac-Me_2Si(2-methyl-4-phenyl-1-indenyl)$_2ZrCl_2$ and Methylaluminoxane cocatalyst; (iv) Best - fit values obtained by means of equation (1.3) and (1.4).

(a) From Keii et al. (1987) [12] (i):

Monomer	**T** (°C)	**k_p** (ii) ($m^3.kmol^{-1}.s^{-1}$)	**$[C^*]/[Ti]$** (% kmol)
Propylene	0	375	5.1
	10	496	6.0
	20	1060	6.0
	30	1630	5.0
	40	2280	7.8

(b) From Busico et al. (1999) [4] (iii):

Monomer	**T** (°C)	**k_p** (iv) ($m^3.kmol^{-1}.s^{-1}$)	**$<f_t>$** (iv) (s^{-1})	**$[C^*]$** (iv) (kmol.(kmol Zr)$^{-1}$)	**$<f_i>$** (iv) (s^{-1})
Ethylene	20	2.6E+05	7	0.046	-
	40	1.1E+06	17	0.100	-
	60	2.8E+06	35	0.230	-
Propylene	40	4.7E+03	2.3	0.580	8.2

Table 1.3: Data for t_{chain} (based on the experiments performed under stopped-flow conditions) ([12] (i), [4] (ii)).

T (°C)	t (s)	[M] (kmol.m^{-3})	k_p (m^3.kmol^{-1}.s^{-1})	P_n^{avg}	t_{chain} (s)
Propylene; $TiCl_4/MgCl_2/C_6H_5COOC_2H_5/Al(C_2H_5)_3$ (i); (iii)					
0	0.21	1.48	3.75E+02	116	0.210
10	0.12	1.00	4.96E+02	59	0.120
20	0.10	0.72	1.06E+03	76	0.100
30	0.14	0.50	1.63E+03	114	0.140
40	0.13	0.37	2.28E+03	109	0.130
Propylene; rac-Me_2Si(2-methyl-4-phenyl-1-indenyl)$_2ZrCl_2$; Methylaluminoxane (ii); (iv)					
	0.19			160	0.100
	0.25			170	0.106
	0.33			240	0.150
40	0.46	0.34	4.70E+03	330	0.207
	0.64			370	0.232
	0.84			410	0.257
	1.06			530	0.332
Ethylene; rac-Me_2Si(2-methyl-4-phenyl-1-indenyl)$_2ZrCl_2$; Methylaluminoxane (ii); (iv)					
	0.07			990	0.047
	0.11			1280	0.061
20	0.15	0.081	2.60E+05	1660	0.079
	0.18			1800	0.085
	0.26			1800	0.085
	0.06			1900	0.029
	0.11			2660	0.041
40	0.18	0.059	1.10E+06	2750	0.042
	0.22			3300	0.051
	0.46			3280	0.051
	0.05			2300	0.018
	0.07			2600	0.021
60	0.08	0.045	2.80E+06	2510	0.020
	0.11			2930	0.023
	0.15			2860	0.023

(iii) Experiments performed in a heptane solution saturated with propylene; (iv) Experiments performed in a toluene solution saturated with ethylene and/or propylene.

In general, the stopped-flow method seems to give lower values of [C^*] and higher values of k_p as compared to the pilot-scale polymerization methods used for kinetic studies. The difference in the kinetic parameters obtained was believed to be mainly due to the differing time (polymerization yield) pertaining to the particular methods.

Keii et al. (1987) [12] found that the effect of transfer reactions was negligible for the polymerization times below 0.2 - 0.3 s. The average time for polymer chain formation (t_{chain}) can be calculated as a ratio between degree of polymerization and the rate of propagation related to one active site:

$$t_{chain} = \frac{P_n^{avg}}{k_p [M]} \tag{1.5}$$

The calculated t_{chain} data from the stopped-flow experiments pertaining to ethylene and propylene polymerization are summarized in Table 1.3. The t_{chain} values vary between 0.01 to 0.33 s, depending on the type of monomer and catalyst, reaction temperature and pressure. The t_{chain} can certainly be modified by changing [M] and k_p. The latter parameter is temperature controlled and it will in fact depend on the catalyst used.

The next important effect on the polymerization kinetics is the “phase transition” of growing particle during the early stages of polymerization. The time-scale for such an event is believed to be in the order of 0.01 s to a few minutes depending upon the monomer concentration and initial propagation frequency. Initially, the catalyst forms an apparently continuous phase, within which the polymer is distributed. After the phase transition, polymer forms a continuous phase in which the catalyst fragments are distributed.

An effect of phase transition on the early stage polymerization kinetics of propylene polymerization was described for the first time by Pater et al. (2001) [23]. The experiments performed at low polymerization rates yielded the pre-polymerization levels from 0.3 to 50 g-PP.g-cat^{-1}. Up to 2 g-PP.g-cat^{-1}, the polymerization rate was found to decrease. Pater et al. (2001) [23] explained the phenomenon in terms of a phase transition being controlled by various factors in the polymerization process. The first factor for decreasing the polymerization rates was polymer-induced “dilution” effect. The second factor mentioned was a monomer concentration decrease near the active centers upon increasing polymerization yield.

Performances of a ZN catalyst in an olefin polymerization within a time period typical for commercial processes are strongly dependent on the conditions of initial stage of polymerization. The stopped-flow technique describes the performance of active sites at the very beginning of polymerization. However, the pilot plant data reflect the processes operative in the later stages of polymerization, such as catalyst deactivation, various types of chain transfer reactions, and fragmentation of catalyst particles. All these processes influence the propagation reaction. Mori et al. (1997) [20] noted that the kinetic parameters obtained in pilot plants were resulted from superimposing the individual factors generated during the polymerization. On the contrary, Busico et al. (1999) [4] observed that for the metallocene catalyzed propylene polymerization the productivity measured under stopped-flow method was close to the values reported for "conventional" polymerization conditions.

The kinetic history of polymerization reactions occurring during the polymer formation leave their fingerprints in the polymer properties, such as molecular weight and its distribution, and subsequently in the polymer morphology [14]. The control of molecular weight and its distribution is often used to improve certain mechanical and physical properties of a polymer product (reflecting the market demands).

The complex kinetics of polymerization reactions with heterogeneous catalyst (like $MgCl_2$-supported ZN catalyst) could lead to the broadening of molecular weight distribution (MWD) of polymer being prepared. Several theories have been reported in the literature about the broadening effect of the MWD [8, 11, 12, 15]. Keii et al. (1984) [11] and Liu et al. (2001) [15] discussed the potential reasons for the MWD broadening, such as variations for the rate constants of propagation and transfer reactions with the growing polymer chain lengths, the existence of monomer diffusion limitations due to polymer layers, and a non-uniformity of active centers. The currently prevailing view is that the multiplicity of active sites is the main reason for observed effects.

Galvan et al. (1986) [8] studied for the first time the combined effect of multiplicity of active sites and monomer diffusion limitations as a result of growing polymer layers. They developed a model based on a two-site theory for heterogeneous ZN polymerizations, and used it to predict the degree of polymerization and polymer polydispersity, using a concept of multiplicity of sites and monomer mass transfer. In their studies, two cases have been compared, namely with and without the monomer

diffusion limitations. In both cases, they found that broadening in MWD is a consequence of the presence of different types of sites.

However, the stopped-flow polymerization technique has set a new insight into the theory of broad MWD [12]. MWD of PP obtained at an initial polymerization stage showed similar values (MWD = 3.2 – 4.3) up to 0.2 s and remained constant up to a residence time of 10 s (MWD = 3.6). As stated earlier, the transfer reactions in such experiments are negligible and at very low residence time, the polymer layer can be ignored. These two facts cannot explain the broadening of MWD. Thus, the only feasible reason for the broad MWD was non-uniformity of active centers, as proposed by Keii et al. (1984) [11] on another basis.

A proper characterization of morphology development of nascent structures during the catalytic olefin polymerization might throw some light on its influence on the polymer properties. In spite of its recognized importance, this phenomenon is still not described properly because of the difficulties associated with the experimental studies at fragmentation stage. Recently, Di Martino et al. (2004) [5] introduced the "quenched-flow" reactor for the first time as an effective method for this purpose. The authors reported number of experiments performed in a "high-pressure quenched-flow" reactor for the observation of polyethylene (PE) morphology under the industrial conditions (80 ^{o}C, 8 bar) and at very short residence times (ranging from 0.2 to 0.7 s). They combined a reactor and off-line SEM observations for the experimental data acquisition about particle fragmentation. Initial striking results in their analysis showed that not all parts of the catalyst polymerize at the same time, and they have also noticed that certain types of structures developed at very early stages of polymerization. They have mentioned that this technique would provide a unique guidance for the formulation and validation of the mathematical models applied for a prediction of the particle morphology.

It is encouraging to know that different tools have been developed to understand the various aspects of catalytic olefin polymerization. In fact, if the changes in reaction kinetics and morphology appears together in the early stage of polymerization, then the effects discussed above in this chapter, should be present in all polymerization reactions with $MgCl_2$-supported ZN catalyst. However, the results may not be always possible to scale-up to the industrial conditions. This may be a limitation for a comparative analysis of different reaction stages involved during polymerization process. Still, it cannot be denied that the methods, such as "stopped-flow" have created a well knowledgeable

foundation for the catalytic olefin polymerization with respect to the reaction kinetics and morphology.

This provides a motivation to design a "multi-purpose pilot-plant", which can be used in the wide range of different time-scales for catalytic olefin polymerization, and is also useful for studying other elemental processes. From know-how of the stopped-flow method, an idea was developed to design a pilot-scale tubular reactor especially for liquid-phase catalytic polymerization of propylene. This novel technique can be useful as a strategic control tool for the better understanding of the scale-up tubular reactor concept for the polymer production on the industrial level. It is envisaged that the tubular reactor will allow studying the performance of the catalyst system at high temperatures (up to 200 ^{o}C) and pressures (up to 150 bar), with respect to the polymer yield and product properties, such as molecular weight and its distribution and polymer morphology, etc.

1.2 Objectives

The basic concept of the research work presented in this thesis, is to study the catalytic olefin polymerization using an optimized non-isothermal tubular reactor system. The main objective of the present work is to extract the kinetic information (under near-industrial conditions) by analyzing the temperature profiles generated over the effective length of the tubular reactor, together with their dynamic behavior. The thermal response of the reactor is a result of an exothermic polymerization initiated after the injection of an active catalyst in the continuous flow of monomer. The rise in the reactor temperature is a measure of catalyst activity and, accordingly, of the polymerization rate. Several polymerization runs for the reactor analysis will be performed with a short residence time in the reactor, thus reducing the reaction time from hours to minutes. The emerging temperature profiles will depend on several factors, such as, reaction kinetics (heat production), mixing dynamics of reaction fluid and heat transfer to the cooling media. The influence of these three variables on the thermal response of reactor will be quantified by means of an appropriate calibration method for a reactor system (together with a thermocouple dynamics). One of the methods for calibration is to use a kinetically well characterized catalyst type for polymerization. Finally, the polymerization rate data from the tubular reactor is possible to measure via a detail analysis of reactor calibration, together with mixing and heat transfer model.

Another important goal is to use the information obtained from the pilot-scale tubular reactor plant for the development of a scale-up model for tubular reactor technology applicable for the real industrial-scale polymer production. The reactor potential in the catalytic polymerization of propylene is seem to be important in the development of new catalysts types performing at high temperature as well as in the development of novel polymer products. Furthermore, the obtained experimental data from the pilot-scale (capillary type) tubular reactor and the predicted behavior of scale-up tubular reactor can be used to describe the non-ideal behavior of the reactor.

1.3 Thesis outline

The experimental part, including description of all chemical and their purification (if any), is described in **Chapter 2**. The experimental set-ups, such as batch reactor and tubular reactor, used in this study are explained in detail. The batch reactor set-up enables to assess the kinetics of liquid-pool propylene polymerization. Similarly, a continuous mode tubular reactor pilot plant was designed and implemented for the kinetic analysis of catalytic liquid-phase propylene polymerization. The complete experimental recipe for the experiments performed in both types of reactors is outlined. The data acquisition system used in the tubular reactor pilot plant is also summarized along with the expected performance of the control unit. The procedures for the assessment of polymers prepared via DSC, GPC, IV, PSD, SEM, and EDX measuring techniques are also illustrated.

The $MgCl_2$-supported ZN catalyst system used in this study is kinetically characterized to use it as one of the calibration method for the reactor. The state-of-the-art for this catalyst type based on the reaction kinetics and polymer properties is presented in **Chapter 3**. The kinetic studies were performed under near-industrial conditions in an over pressurized fully filled batch reactor (calorimeter) with liquid-phase propylene (also see Al-haj Ali, 2006 [2]). Relevant experiments were carried out to study the effects of various process parameters, such as temperature, pre-contacting time for catalyst and co-catalyst, amount of co-catalyst and hydrogen, etc. The experimental findings are discussed based on the calculated polymer yield, initial reaction rate, deactivation behavior of the catalyst and the average molecular weights. This chapter provides a unique opportunity in understanding the overall performance of the catalyst for liquid-phase propylene polymerization.

The interpretation of the several important facts observed from the experimental data measured during the kinetic investigations (reported in Chapter 3) is a key element in improving the process stability and efficiency. **Chapter 4** reports the detailed discussions on the experimental data from the batch reactor in terms of the reaction rate and polymer properties, based on the "improved" kinetic mechanism. Especially, this chapter presents the development of a detailed kinetic model describing an overall hydrogen influence observed in catalyzed propylene polymerization. The catalyst activity and average probability of chain termination are modeled as a function of hydrogen by combining the two distinct kinetic mechanisms derived from Natta model and dormant site model. Furthermore, the different and often contradictory observations regarding the role of hydrogen in propylene polymerization (reported by several researchers) are reviewed and discussed with respect to the present kinetic investigations.

In **Chapter 5**, the performance of a novel (capillary type) tubular reactor is compared with the batch reactor for the catalytic liquid-phase propylene polymerization on the basis of kinetics (initial activity) and polymer properties. The reactor behavior is systematically analyzed by carrying out the pulse experiments with an isoperibolic reaction mode. The polymerization experiments were carried out with the injection of preactivated catalyst slurry into a continuous flow of liquid propylene, with a short residence time inside the reactor and at near-industrial polymerization conditions. In order to understand the effect of reactor behavior on the morphology of produced PP samples, off line characterization techniques such as SEM, EDX, PSD and DSC were used, and relevant parameters are discussed such as temperature, hydrogen concentration and quenching agent.

A detailed analysis of mathematical model for the non-isothermal tubular reactor for catalytic liquid-phase propylene polymerization is described in **Chapter 6**. The reactor model analysis is done based on the selected experimental data obtained from the polymerization tests. The predicted profiles of reactor temperature and the experimental one are explained based on the reactor fluid mixing and heat transfer model. The model predictability for reaction rates, polymer yield and average molecular weights is also evaluated with the experimental data. In this chapter, the model capability in elaborating the reactor behavior with respect to varying process variables and parameters during polymerization reaction is explored. For instance, the reactor model is simulated for different reactor lengths. In addition, it is demonstrated that based on the model predictions, the optimal process conditions can be developed for catalytic polymerization reactions using this tubular reactor concept.

The prospects and important issues for the future process design of scale-up tubular reactor for catalytic liquid-phase propylene polymerization is investigated based on the selected simulation runs performed using the developed mathematical model, in **Chapter 7**. The purpose of the present analysis is to demonstrate the theoretical strategy in studying the response of the tubular reactor at industrial scale. The reactor behavior is predicted in terms of the reactor thermal response, varying concentration of chemical constituents like active catalyst and hydrogen and the polymer properties mainly the molecular weights and their distributions. Strictly speaking, the predictions reported in this chapter are based on the kinetic peculiarities of the catalyst type used in the present work. Several points related to the optimized process recipes for such reactors are mentioned. The performance of the catalyst in the reactor is analyzed and described. Further, the kinetic data and polymer properties obtained are discussed in detail.

In **Appendix I**, the experimental analysis is demonstrated for predictions of various non-ideal behavior of scaled-up tubular reactor during the catalytic polymerization reactions. The polymerization experiments were carried out with the injection of active catalyst slurry into a continuous inlet flow of liquid propylene and the flow disturbances in the tubular reactor were created by the continuous cycle of pressurization and expansion. The catalyst response with respect to the temperature and pressure profiles over the reactor length is analyzed at near-industrial polymerization conditions. For this analysis, the tubular reactor dimension was scaled-up using the following ratios of inside tube diameter, tube length and reactor volume in comparison to that of "capillary type" reactor used earlier, and there values are 5.3, 0.2 and 5.6, respectively. The design of pilot plant set-up and the data acquisition is found to be very successful in performing the catalytic polymerization experiments. The characteristic performance of the reactor is discussed based on the detected region of nonlinear transport and thermal response of the reactor during reaction.

Nomenclature

$[C^*]$	: Catalyst efficiency (kmol.kmol[Metal]$^{-1}$)
C_{st}^*	: Stationary concentration of polymerization centers (kmol.kmol[Metal]$^{-1}$)
$<f_i>$	: Average frequency of an "initiation" process (s^{-1})
$<f_t>$	: Average turnover frequencies of chain transfer process (s^{-1})
k_p	: Rate constant for propagation reaction ($m^3.kmol^{-1}.s^{-1}$)

k_{tr} : Rate constant for transfer reaction (s^{-1})
[M] : Monomer concentration ($kmol.m^{-3}$)
M_o : Molecular weight of monomer ($kg.kmol^{-1}$)
M_n^{avg} : Number-average molecular weight ($kg.kmol^{-1}$)
P_n^{avg} : Number-average degree of polymerization
t : Polymerization time (s)
t_{chain} : Average time for formation of one polymer chain (s)
T : Reaction temperature (^oC)
Y : Polymer yield ($kmol[M].kmol[Metal]^{-1}$)

Sub- and superscripts

chain : Representing polymer chain
i : Initiation
n : Number-based
o : Initial or zero
p : Propagation
st : Stationary
tr : Transfer
* : Active

Abbreviations

DSC : Differential scanning calorimetry
EDX : Energy dispersive X-ray spectrometry
GPC : Gel permeation chromatography
IV : Intrinsic viscometry
$MgCl_2$: Magnesium dichloride
MWD : Molecular weight distribution
PE : Polyethylene
PP : Polypropylene
PSD : Particle size distribution
SEM : Scanning elector microscopy
ZN : Ziegler-Natta

Literature

[1] Agrawal, S. and Han, C. D. (**1975**), AIChE Journal, 21 (3), 449 - 465.

[2] Al-haj Ali, M. (**2006**), Doctorate Thesis, University of Twente, Enschede, The Netherlands.

[3] Brandolin, A., Capiati, N. J., Farber, J. N. and Valles, E. M. (**1988**), Ind. Eng. Chem. Res., 27, 784 - 790.

[4] Busico, V., Cipullo, R. and Esposito, V. (**1999**), Macromol. Rapid. Commun., 20 (3), 116 - 121.

[5] Di Martino, A., McKenna, T. F., Broyer, J. P., Weickert, G., Schweich, D. and De Bellefon, C. (**2004**), DECHEMA Monographs, Wiley-VCH Verlag, 138, 173 - 179.

[6] Dowding, P. J., Goodwin, J. W. and Vincent, B. (**2000**), Colloid. Polym. Sci., 278, 346 - 351.

[7] Fan, S., Gretton-Watson, S. P., Steinke, J. H. G. and Alpay, E. (**2003**), Chemical Engineering Science, 58, 2479 - 2490.

[8] Galvan, R. and Tirrell, M. (**1986**), Chemical Engineering Science, 41 (9), 2385 - 2393.

[9] Hammer, J. W. and Ray, W. H. (**1986a**), Chemical Engineering Science, 41 (12), 3083 - 3093.

[10] Hammer, J. W. and Ray, W. H. (**1986b**), Chemical Engineering Science, 41 (12), 3095 - 3100.

[11] Keii, T., Doi, Y., Suzuki, E., Tamura, M., Murata, M. and Soga, K. (**1984**), Makromol. Chem., 185, 1537 - 1557.

[12] Keii, T., Terano, M., Kimura, K. and Ishii K. (**1987**), Makromol. Chem. Rapid. Commun, 8, 583 - 587.

[13] Keii, T. (**2004**), Heterogeneous Kinetics, Kodansha Ltd. and Springer-Verlag Berlin Heidelburg.

[14] Kiparissides, C. (**1996**), Chemical Engineering Science, 51 (10), 1637 - 1659.

[15] Liu, B., Matsuoka, H. and Terano, M. (**2001**), Macromol. Symp., 165, 3 - 10.

[16] Liu, B., Nitta, T., Nakatani, H. and Terano, M. (**2002**), Macromol. Chem. Phys., 203, 2412 - 2421.

[17] Liu, B., Nitta, T., Nakatani, H. and Terano, M. (**2003**), Macromol. Chem. Phys., 204, 395 - 402.

[18] Matsuoka, H., Liu, B., Nakatani, H. and Terano, M. (**2001**), Macromol. Rapid. Commun., 22, 326 - 328.

[19] Melo, P. A., Biscaia Jr., E. C. and Pinto, J. C. (**2001**), Chemical Engineering Science, 56, 6793 - 6800.

[20] Mori, H. and Terano, M. (**1997**), TRIP, 5 (10), 314 - 321.

[21] Mülhaupt, R. (**2003**), Macromol. Chem. Phys., 204, 289 - 327.

[22] Ouzineb, K., Graillat, C. and McKenna, T. (**2003**), Journal of Applied Polymer Science, 91, 2195 - 2207.

[23] Pater, J. T. M., Weickert, G., Loos, J. and van Swaaij, W. P. M. (**2001**), Chemical Engineering Science, 56, 41075 - 4120.

[24] Paquet Jr., D. A. and Ray, W. H. (**1994**), AIChE Journal, 40 (1), 73 - 87.

[25] Yoon, B. J. and Rhee, H. (**1985**), Chem. Eng. Commun., 34, 253 - 265.

[26] Yoon, W. J. and Choi, K. Y. (**1996**), Polymer Engineering and Science, 36 (1), 65 - 77.

[27] Zacca, J. J. and Ray, W. H. (**1993**), Chemical Engineering Science, 48 (22), 3743 - 3765.

Chapter 2

Description of experimental techniques

Abstract: The experimental part including the description of all chemical and their purification is presented in this chapter. The experimental set-ups such as batch reactor (isoperibolic calorimeter) and tubular reactor pilot plant are described in detail. The batch reactor set-up enables to evaluate the kinetics of the catalytic liquid-phase propylene polymerization. Similarly, a continuous mode tubular reactor pilot plant was designed and implemented for the kinetic analysis of catalytic liquid-phase propylene polymerization over a short period of reaction time. The complete experimental recipes for the experiments performed in batch as well as in tubular reactors are outlined. The data acquisition system used in the tubular reactor pilot plant is also outlined along with the expected performance of the control unit. The procedures for the polymer characterization using the DSC, GPC, IV, PSD, SEM, and EDX measuring techniques are explained.

2.1 Materials

The liquid propylene used in this work was a commercially available "polymerization grade monomer" with a purity above 99.5 % and sourced from Praxair. It was purified by passing through three columns, shown in Figure 2.1 (a). These purification columns consist of oxidized R3-12 catalyst (BASF), reduced R3-12 catalyst (BASF) and molecular sieves, respectively. The purification step removes CO, CO_2, H_2O, O_2 and propane from the liquid propylene. n-Hexane (purity > 99 %, pro synthesis, Merck), nitrogen (purity > 99.998 %, Praxair) and hydrogen (purity > 99.999 %, Hoekloos) were purified in individual systems containing a reduced 3R-11 catalyst (BASF) and molecular sieves (13X, 3Å and 4Å, Sigma-Aldrich); see Figure 2.1 (b).

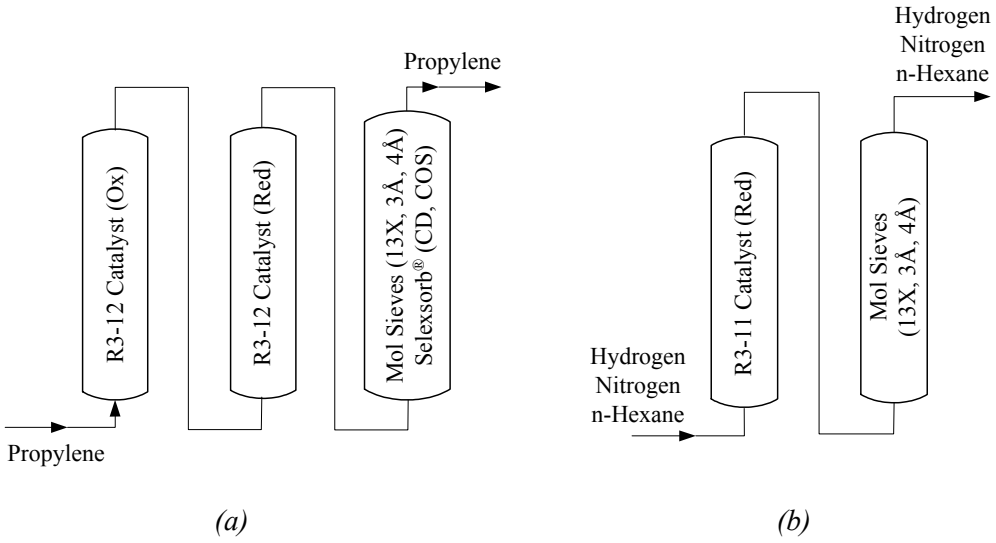

Figure 2.1: Schematic of purification columns for (a) propylene and (b) n-hexane, nitrogen and hydrogen.

Carbon dioxide (purity > 99.7 %, O_2 < 500 ppm, H_2O < 150 ppm, Hoekloos) and helium (purity > 99.9997 %, CO + CO_2 < 50 ppb, H_2O < 20 ppb, O_2 < 10 ppb, hydrocarbons < 100 ppb, Air Products) were used directly from the cylinder. The quenching agents used in this study were ethanol (purity > 99.7 %, Lamers & Pleuger) and/or hydrochloric acid (1N standard solution, ACROS Organics). The ethanol and hydrochloric acid was also used for polymer washing.

The catalyst studied in this work was $MgCl_2$-supported Ziegler-Natta (ZN) catalyst of the type [$MgCl_2$/$TiCl_4$/Internal donor (Phthalate) – $AlEt_3$/External donor (alkoxy silane)]. Tri

ethylaluminum (TEA) was used as a cocatalyst and a scavenger. The catalyst system was stored and handled in a glove box under nitrogen atmosphere containing less than 0.1 ppm H_2O and O_2.

2.2 Reactor systems

2.2.1 Liquid-pool batch reactor

2.2.1.1 Pilot plant

Figure 2.2 illustrates the 5.05 l stirred-tank batch polymerization reactor operated as a calorimeter. The cooling and heating system of the reactor consist of two water baths, a cold water tap and an oil bath for heating the cover plate. The cover plate was heated slightly above the reactor temperature to prevent the condensation of propylene on the cover plate during the reaction.

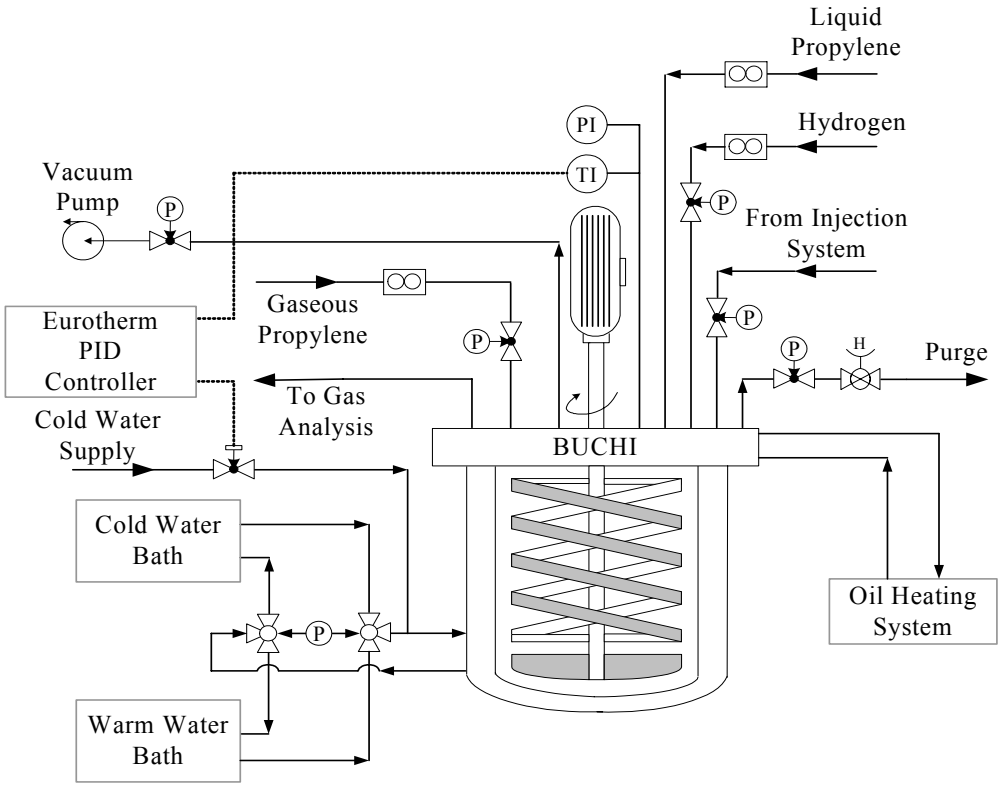

Figure 2.2: Batch reactor set-up for liquid-phase propylene polymerization.

The chemical components for reactions can be added to the reactor using the mass flow controller (MFC). The (suspended) catalyst, cocatalyst and external donor mixture was prepared in the glove box and transferred from a glass vial into the reactor by means of a pneumatic injection system. After injecting the catalyst mixture, the transfer line was rinsed with n-hexane to ensure that all the material was introduced into the reactor.

An isoperibolic mode was mainly applied for all the polymerization runs. This means the temperature control system keep the jacket temperature constant and the rise in reactor temperature was caused by highly exothermic polymerization reaction. All the experimental data were collected every three seconds using Data Acquisition and Control Unit (DACU), and analyzed further for kinetic investigation.

2.2.1.2 Polymerization procedure

Prior to every experiment, the reactor was heated to 90 ^{o}C and flushed with the 6 cycles of evacuation and pressurization, wherein 5 bar of nitrogen was used for pressure series. At the end of flushing procedure, the reactor was left at vacuum. Gaseous propylene was added up to 5 bar and evacuated again. The reactor was flushed with propylene for two times, without evacuating it.

Further, the liquid propylene was added to the reactor and heated up to the reaction temperature. When the temperature reached to its set point, hydrogen was added to the reactor. The reactor temperature and pressure were monitored as a function of time. As soon as both became stable for an interval of three minutes, the reaction was started by injecting the preactivated catalyst into the reactor.

The experiments were executed under isoperibolic conditions. Thus, just after the catalyst injection, the temperature control system becomes active in order to keep the jacket temperature at its set point, whereas the reaction temperature slightly increases reaching quasi steady state after about 1.5 min in case of using a fully pre-activated catalyst. The heat of polymerization is measured under quasi steady state conditions.

The polymerization reaction was finally terminated by rapidly purging the unreacted propylene followed by a few cycles of nitrogen flushing. After each experiment, the

resulting polymer was dried under vacuum at 50°C for four hours. The detailed experimental conditions are provided in Chapter 3 and 4.

2.2.2 Tubular reactor

2.2.2.1 Pilot plant

Experimental set-up for "capillary type" non-isothermal tubular reactor is shown in Figure 2.3. The reactor was made up of stainless steel with 4 mm of inside diameter and 7.8 m of length, and folded up in the vertical sections of 43 cm. It can withstand pressure up to 200 bar and temperature up to 200 ^{o}C. Presently, the set-up can be operated up to 60 bar (120 bar with hydrogen) and 97 ^{o}C.

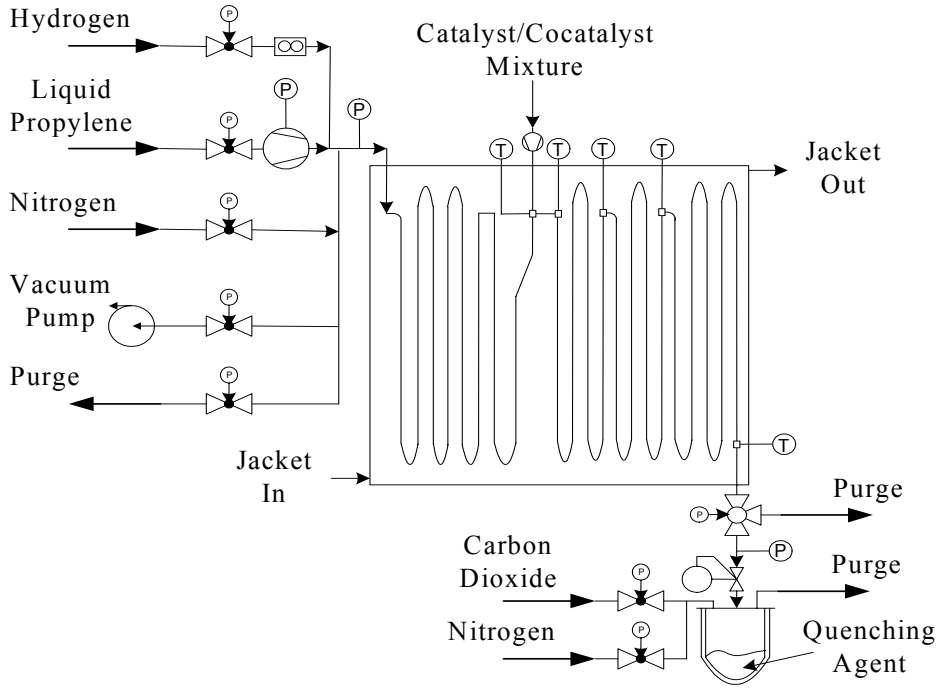

Figure 2.3: Schematic of tubular reactor set-up for liquid-phase propylene polymerization.

Two pressure sensors in the reactor were located at 40 cm before and after the jacket. A five K-type (0.5 mm) thermocouples were placed over the reactor length starting at the catalyst injection point (so-called mixing cell) and ending just before the exit of the reactor. The pressure in the reactor was maintained with a back-pressure valve (BP66, GO). The complete reactor was submerged in a 47 l cylindrical stainless steel jacket,

which was heated and controlled by a water bath (T4500, Tamson). The water bath can be replaced by an oil heating system in order to carry out the experiment for temperatures above 97 ^{o}C. A circular motion of water in the jacket was obtained using a water pump with a capacity of 20 l.min^{-1}, which provided the tubular reactor a cross-current heat exchange.

The liquid propylene was stored in two 3.3 l jacketed vessels with an inner diameter of 6 cm. These vessels can be filled up to 80 % at saturation pressure of liquid propylene. A normal storage temperature for these vessels is 50 ^{o}C. The liquid level was measured with a pressure difference sensor (ST3000, Honeywell) connected 30 cm below the vessels. The line connecting a pressure difference sensor was heated with an electrical heater up to 100 ^{o}C.

The heated propylene at its saturation pressure then pumped with a high pressure liquid compression pump (HPLC, LCP 4000.1, Techlab) at a constant volumetric flow rate of 90 ml.min^{-1}. This pump can be operated up to 99 ml.min^{-1} and 150 bar discharge pressure. The pump head contains two sapphire pistons, which were linked in parallel and work in opposite cycle to decrease the pressure fluctuations. At the inlet of HPLC pump, liquid propylene naturally cooled down from 50 ^{o}C to 35 ^{o}C, preventing the gas formation in the pump head. Hydrogen can be added to the propylene feed stream using a thermal MFC (5850TR, Brooks). The feed stream to the reactor was preheated to the reaction temperature in the first eight vertical sections of the tubular reactor; see Figure 2.3.

The catalyst injection point was placed at the exit of preheating section. Therefore, the actual reactor length available for the reaction was 5.65 m. The catalyst injection unit consists of two Williams pumps (WP) (CP125V125) with oscillating controllers (MK XII) and illustrated in Figure 2.4. The two WP's were used to inject the catalyst slurry and n-hexane, respectively. These pumps were modified to pump the slurry. The pumps were mounted upside down as shown in Figure 2.5, in order to have a direct inlet from the vessel above the pump. The inlet at the top (1) and the outlet at the side (2) contain a spring loaded check valve to direct the flow. The pneumatic piston (3) can pump up to 0.1 ml.stroke^{-1}, and with 42 - 62 strokes.min^{-1}. The discharge pressure was constant at 139 bar. The bleeder (4) was used to purge the gas from the pump. The stroke length adjuster (5) alters the volume of the injection chamber. The catalyst slurry and n-hexane were stored in a 50 ml removable vessels placed above the WP. Nitrogen, n-hexane and

purge connections were used to clean the injection system. To keep the solid catalyst particle in suspension, helium was bubbled through the mixture.

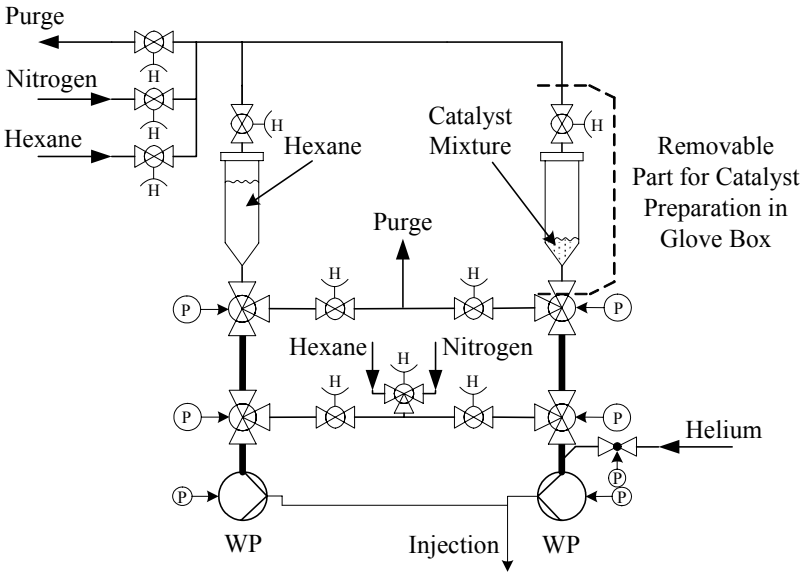

Figure 2.4: Injection unit design.

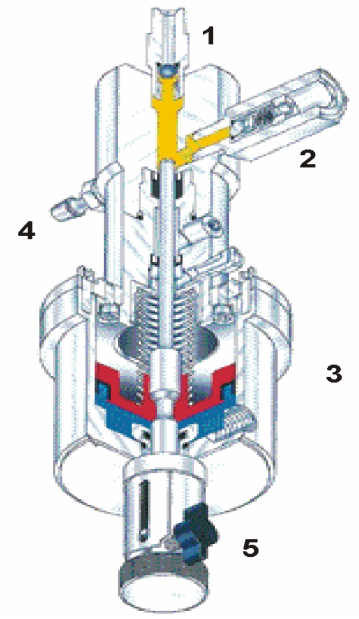

Figure 2.5: Cross-section of upside down mounted WP.

The two WP's were connected to each other with a capillary tube having an inside diameter of 1 mm (see Figure 2.4); this provided the cleaning of catalyst injection line during the experiment, especially for pulse experiments. WP can pump the solutions up to 0.1 ml.stroke^{-1} with a stroke rate up to 62 strokes.min^{-1} [$]. This makes it possible to run the pumps in a fast injection of catalyst or in a pulsed mode (where a few large strokes create one large injection as a pulse). As shown in Figure 2.4, the catalyst slurry was injected through one WP whereas the second WP was used to clean the (1 mm) injection tube with solvent. Injection of the catalyst slurry occurred in counter current mode in a mixing cell as shown in Figure 2.6.

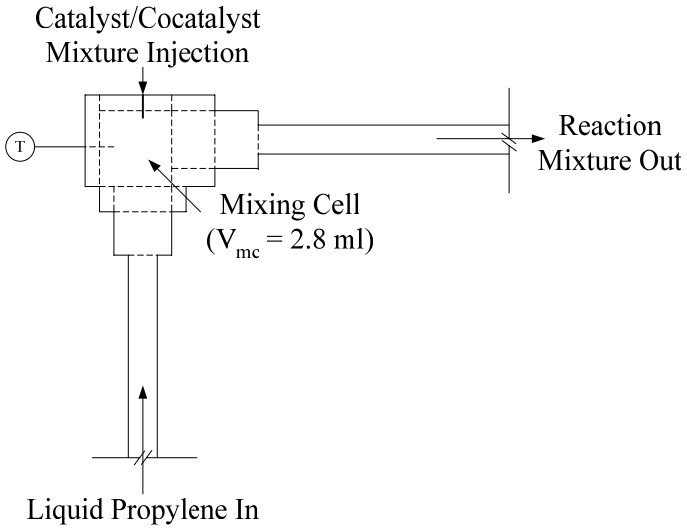

Figure 2.6: Schematic of mixing cell.

The reactor outlet was connected to the jacketed glass expansion vessel, wherein the reaction mixture was expanded to the atmospheric pressure. The expansion vessel jacket has the same temperature as that of reactor jacket to prevent the expanding propylene from recondensating. The expansion vessel was partly filled with a quenching agent and CO_2 in order to quench the polymerization reaction. Gaseous propylene was purged from the expansion vessel through a 22 cm inside diameter purge line.

The complete set-up was operated from outside of the concrete bunker. All the experimental data were collected using DACU, and analyzed further for kinetic investigation.

[$] The maximum stroke rate may vary between individual pumps.

2.2.2.2 Safety measures

Special safety precautions are required while working with a liquid-phase polymerization reactor due to an exothermic nature of the reaction and the usage of explosive chemicals at high pressures.

A complete reactor set-up was placed inside a concrete bunker and mainly controlled from outside the bunker. In case of an explosion, the concrete bunker has a shutter in the ceiling to direct the blast. A gas detection system (Dräger) for carbon monoxide, hydrogen and propylene was connected to a general alarm and an emergency stop of the setup. Several exhausts were placed in the bunker to remove the dangerous gases.

To prevent the system from reaching the pressure above its design limit a pressure relief valve was mounted on the reactor, which can purge the reactor above 160 bar. Similarly, two pressure relief valves were placed on the monomer storage vessels and set at 60 bar. The emergency switch can be activated when a dangerous situation occurs. The emergency stop was used to purge the reactor by setting all the valves in their original positions. All data acquisition remains active in order to find the origin of the dangerous situation. The HPLC pump has a manual input for the upper pressure set-point at which the pump gives an alarm and shuts itself off.

To decrease the response time and reduce the load on the PC software, safety procedures were implemented in a Programmable Logic Controller (PLC, Mitsubishi), which was connected to the relay switches. This system has three goals,

1. The first was to stop the experiment. The experiment was stopped by switching off the WP, closing the catalyst storage, monomer supply and hydrogen supply.
2. Secondly, the pressure was kept below a preset value, which was near the experimental pressure, by purging the reactor.
3. The last goal was to prevent the expansion vessel from exceeding 0.5 bar overpressure. This was implemented by a three way valve between the reactor and the back pressure valve, which redirects the flow directly to the purge.

2.2.2.3 Data acquisition and control

A schematic of data flow and control signals is shown in Figure 2.7. Data acquisition from the set-up and transfer of control signals to the set-up was carried out using a

DACU (3825A, Hewlett-Packard). The DACU contained a 20 channel FET multiplexer (44710A), 20 channel relay multiplexer (44705A), 16 channel switch cards (44725A) and a four channel voltage digital to analog converter (DAC) card (44727A).

The multiplexer cards received the data from sensors throughout the setup. The switch cards were connected to a relay switch box, which operates the pneumatic actuators and the valves. The valves can also be operated manually. The DAC card operates the set-point of the MFC and the pressure regulator for the back pressure valve. The DACU can be operated by manual input or with a PC controlled software package called HP Visual Engineering Environment (HP-VEE) version 5.0. Data to and from the DACU was transferred over an IEEE-488 interface bus.

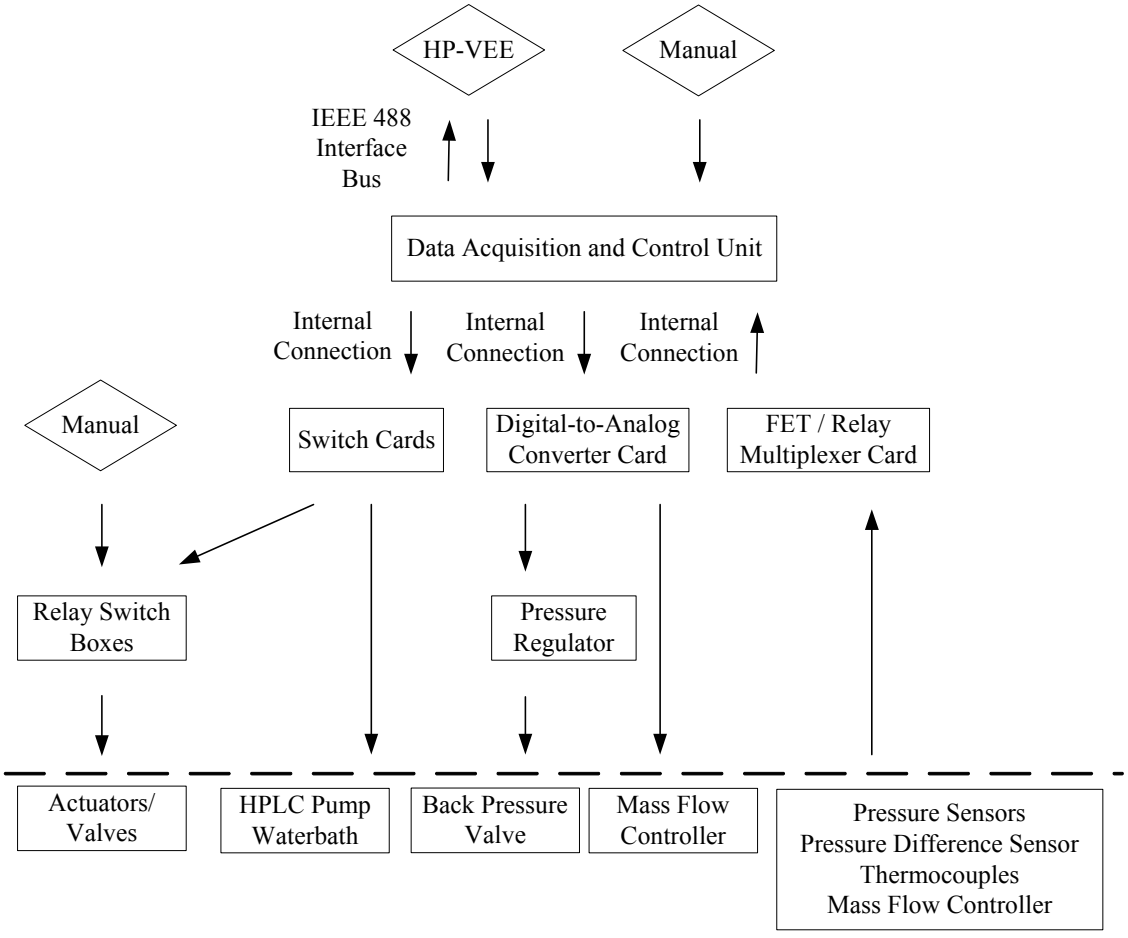

Figure 2.7: Schematic of data flow and control signals.

To acquire a reactor pressure and temperature data at an optimum rate, a selection on data intervals was made (see Table 2.1). Sensors, which record the actual reaction data (such as inlet and outlet pressure, five reactor thermocouples), were set at a minimal recording intervals. Other sensors (13 in total) which record the data regarding supply system, heating system and expansion section were set at an interval of 5 seconds (s). Individual sensors of the setup can be recorded by a sub program to obtain the high speed data from a specific system. To record pulses, a specific group of reactor thermocouples can be recorded with minimal loss of resolution. However, to reduce the amount of data stored, recording intervals can be increased when required.

Table 2.1: Overview of measurement intervals

Number of Pressure Sensors	Number of Thermocouples	Measurement Intervals (s)
0	1	0.22
0	2	0.27
0	4	0.37
1	0	0.09
2	5	0.56
1 (High Speed)	0	0.0002 – 0.02*

* Burst Time = 1195 (Interval).

For high speed pressure measurements, a four channel track-and-hold card (44730A) combined with a high speed voltmeter card (44702B) can be added to a second DACU to obtain data up 100 kHz. Data can only be obtained in a burst method, where an increase in measurement frequency reduces the burst time.

The setup was controlled via the HP-VEE programmed control panel and it consists of,

- Leakage testing ("Leakage test"): The reactor was pressurized and the pressure drop was monitored.
- Flushing ("Flush PFR"): Impurities were removed with the cycles of vacuum and pressurized nitrogen.
- Water bath program with timer ("Water Bath")

- Back-pressure program ("BPV401"): To pressurize the reactor with liquid propylene or nitrogen. A controlling method can be selected such as proportional or linear.
- Pulse injections ("WP Stroke"): A pulse can be executed with the desired number of catalyst injections followed by the desired number of solvent injections.
- Monomer storage vessels ("Fill MSV"): The monomer storage vessels can be automatically flushed, filled to the desired level and purged.
- Hydrogen addition ("MFC_H2"): Hydrogen flow can be set and started after which the stability is checked.

2.2.2.4 Calibration

The HPLC pump was calibrated by pumping n-hexane at a different set of flow rates. The collected n-hexane was weighed and compared with the set flow rate of the pump. The back pressure set point was varied and its response was checked using a nitrogen flow to the reactor. The calibration for the back pressure valve controller is shown in Figure 2.8. A linear relationship is observed between the set pressure and set voltage to the back pressure valve.

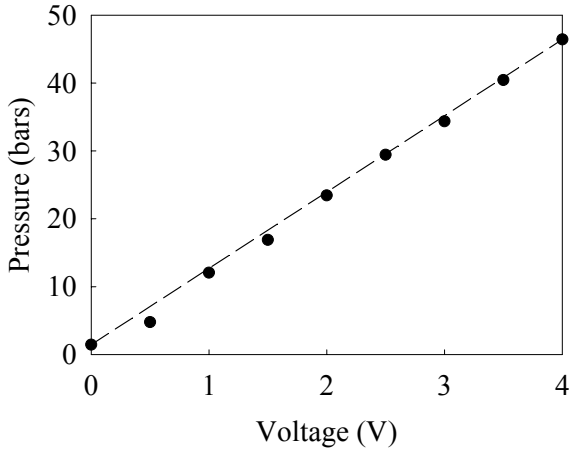

Figure 2.8: Back pressure valve calibration curve.

For the WP, the stroke rate was set using an analog control button. For continuous injection, the stroke rate was calibrated and given in Figure 2.9. The large deviation from factory settings has no influence on the performance of the pump and it may have appeared due to the modification made for in-house purpose. Low settings of stroke rates

must be checked prior to the experiments, due to a large sensitivity in the analog control button.

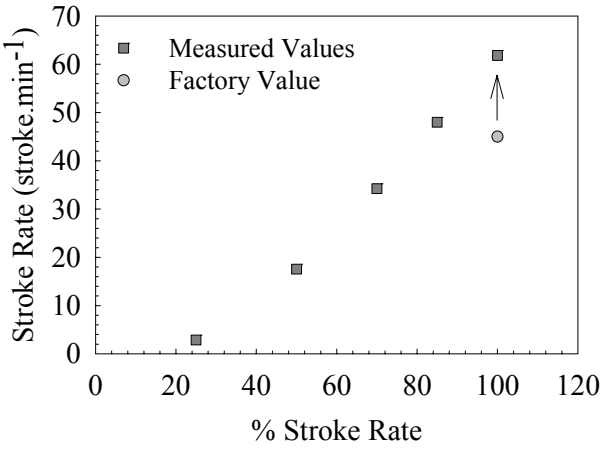

Figure 2.9: Stroke rate calibration for WP.

With the high speed recording method (Table 2.1), a WP was connected to a 150 ml cylinder filled with n-hexane and a pressure sensor. Further, n-Hexane was injected through the WP into the cylinder and pressure changes above 5 bar were recorded. The stroke rate was kept constant (62 strokes.min^{-1}) and the stroke volume was varied. The injection time was recorded at time intervals of 2 ms. The results presented in Figure 2.10 show a linear increase of the stroke time with increasing stroke volume.

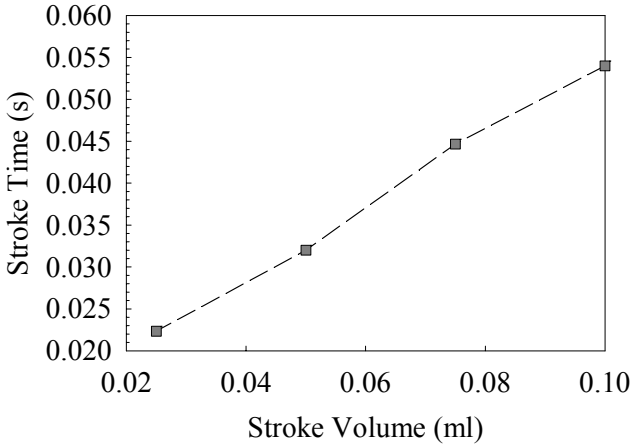

Figure 2.10: Measured injection time as a function of stroke volume at maximum stroke rate (62 strokes.min^{-1}).

The maximum stroke time recorded was 0.054 s. All the thermocouples used in this study were calibrated and shows similar (dynamic) thermal response upon step change in the reactor temperature. The average response time of the thermocouples to the step change was in the order of ≈ 30 ms per unit ^{o}C change in the temperature. Figure 2.11 show an average thermocouple dynamics.

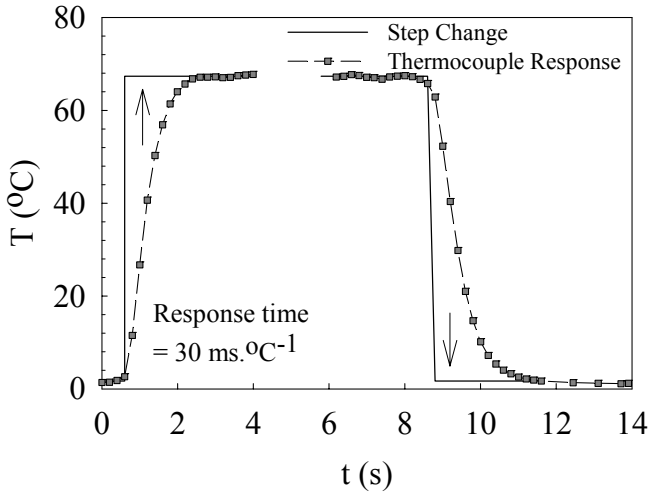

Figure 2.11: Thermocouple dynamics

2.2.2.5 Polymerization procedure

Start-up of the system begins with the heating up of jacket to the reaction temperature. During the heating period of jacket, the liquid propylene and n-hexane storage vessels were filled. The monomer storage vessels were usually filled up to ≈ 80 % at 35 ^{o}C in order to keep the feed line pressure at 16 bar. After the dissolved nitrogen was purged, these vessels were heated to 50 ^{o}C. A leakage test was carried out with the nitrogen at reaction pressure. Further, the reactor was cleaned by thorough flushing. The flushing procedure consists of 20 cycles of pressurization with nitrogen (up to 20 bar) and evacuation using vacuum pump, in an alternate manner, respectively. The injection is also flushed with nitrogen and n-hexane.

The WP and injection tubes were filled with n-hexane to avoid leakage from the reactor to the injection system. The WP stroke rate and stroke volume were set at maximum. Both the pumps were checked by injecting n-hexane into a flow of nitrogen in the reactor. The catalyst, cocatalyst and external donor mixture was prepared in a glove box under the

nitrogen atmosphere containing less than 0.1 ppm of H_2O and O_2. n-hexane was used as a solvent for catalyst preparation. All components were mixed in a glass vial not more than 30 min before injection, and transferred to a 50 ml removable vessel, which is then refitted. Connections to the refitted vessel are flushed and a helium flow of 25 - 45 $ml_n.s^{-1}$ was started.

The expansion vessel was filled with 300 ml of quenching agent (ethanol or aqueous hydrochloric acid (HCl)) and a CO_2 flow was started. The back-pressure valve was set at reaction pressure. Then the flow of propylene and hydrogen was started with the required set-point to the reactor. When the reactor pressure and temperature were stable, the preactivated catalyst injections were started. The data from an electronic counter on the WP was transferred to the HP-VEE to control a series of injections. An injection sequence started with a set number of catalyst injections followed by two hexane injections.

After the experiment, the hydrogen flow was stopped and reactor was depressurized over 60 s. The HPLC pump was stopped and the reactor was cleaned with a nitrogen flow for 5 min. The catalyst vessel and WP were purged and cleaned with n-hexane and nitrogen. The quenching agent with polymer was removed and washed. When ethanol was used as a quenching agent, 20 ml of 1 N HCl solution was added. The solution was mixed for an hour and filtrated over a glass filter with a Schlenk set-up. The powder is dried for four hours at 50°C in a vacuum oven.

2.3 Analytical techniques

2.3.1 Differential scanning calorimetry (DSC)

The DSC 821^e from Mettler–Toledo GmbH was used to study the thermal history over the temperature range of 30 ^oC to 230 ^oC. The polymer samples weighing of approximately 5.5 mg were placed in a 40 μL aluminum crucible and kept under a nitrogen atmosphere with flow rate of 60 $ml.min^{-1}$ for about 50 min. The thermal history was obtained over the two cycles of heating and one cycle of cooling. The heating and cooling rate of about 20 $K.min^{-1}$ was employed. For data acquisition and evaluation, the software package Star^{e}V5.12 was used.

2.3.2 Gel permeation chromatography (GPC)

The polypropylene (PP) samples were characterized by their molecular weight and molecular weight distribution (MWD) using GPC technique. GPC measurements presented in this work were carried out employing a Waters Alliance GPCV 2000 apparatus with TSK columns at 155 °C using 1,2,4-trichlorobenzene as a solvent. These measurements were performed at Basell R&D Center, Ferrara, Italy.

GPC is a method to separate the molecules by size. The separation is usually carried out in columns that are packed with a gel or some other porous material and completely filled with solvent. The same solvent was used to dissolve the sample before introducing it into the column and also for elution. Small molecules can diffuse into the pores of the gel, large ones are excluded, and others of intermediate size can penetrate through some of the larger pores. The molecules are constantly diffusing back and forth between the pores and interstices. Solvent pumped through the columns flows only in the interstices, sweeping along all sample molecules present at that location. The molecules in the pores stay behind until they diffuse back out. The large molecules are always or mostly excluded from the pores and eluted first, the small ones, which are mostly inside the pores come out last. This method results in chromatograms that relate the amount of solute with the retention time. The chromatogram is further converted into MWD using well-known calibration methods.

2.3.3 Intrinsic viscometry (IV)

An Ubbelohde viscometer of type DSV-D15 KP (edition 2000) from Lauda was used to measure the viscosity-average molecular weight (M_v^{avg}). A viscometer consists of glass tube having an inside diameter of 5 mm. The test solution was prepared by dissolving the polymer in the decahydronaphthalene solvent (purity > 98 %, ACROS Organics) with a concentration of 1 mgPolymer.mlSolvent^{-1}. The suitable quantity of polymer dissolved solution is transferred into the glass tube. The glass tube was replaced into the thermostat to maintain the test temperature. For data acquisition and measurement, the software package PVS 2.49e was used.

The Hagenbach correction factors were taken from the Ubbelohde operating instruction manual. The value of intrinsic viscosity ([η]) for a linear polymer in a specific solvent is related to the polymer M_v^{avg} through the empirical Mark-Houwink equation,

$$[\eta] = K\left(M_v^{avg}\right)^a \tag{2.1}$$

where, the values of Mark-Houwink constants "K" and "a" amend with polymer type, solvent and temperature [].

2.3.4 Particle size distribution (PSD)

PSD was measured using Microtrac particle size analyzer (SRA 150), which uses laser diffraction analysis technique. Measurements were done in a wet mode using ethanol. Approximately 10-20 mg (1 spatula) of polymer sample is required for each measurement. The Analyzer automatically makes three measurements and gives average value for each sample.

2.3.5 Scanning electron microscopy (SEM) and energy dispersive X-ray spectrometry (EDX)

The surface and cross sectional morphologies of the samples were investigated using a Philips environmental SEM XL-30 ESEM FEG (Philips, Eindhoven, The Netherlands) equipped with EDX for local and area distribution analysis of elements.

Imaging of the samples was performed in high vacuum mode using the acceleration voltages of 1-1.2 kV and a secondary electron detector. No additional coating of the sample surface was done because charging is not an issue for the chosen imaging conditions.

For the investigation of cross section, the polymer particles were embedded in SPURR low viscosity epoxy resin (SPI Supplies) and cut with a razor blade at room temperature. The samples for cross-section analysis were then placed on the sample mount and

[] In this work, for PP samples, the values of Mark-Houwink constants are (industrial settings obtained from Basell R&D Center, Ferrara, Italy), K = 0.000238 $cm^3.g^{-1}$ and a = 0.725.

transferred into SEM chamber as quick as possible so as to minimize the contact of samples with moisture and oxygen in the atmosphere.

Qualitative EDX analyses were carried out in wet-mode at accelerating voltages of 5 kV, 10 kV and 20 kV respectively.

Chapter 3

Kinetics of liquid-phase propylene polymerization: I. Experimental study

Abstract: In this work, kinetic studies were carried out for liquid-phase propylene polymerization using $MgCl_2$-supported Ziegler-Natta catalyst type in a batch reactor. The state-of-the-art for the catalyst based on the reaction kinetics and polymer properties is reported here. The kinetic studies were performed under near-industrial conditions in an over pressurized fully filled batch reactor (calorimeter) with liquid propylene and operating with an isoperibolic reaction condition. Relevant experiments were carried out to study the effects of various process parameters, such as temperature, cocatalyst, precontacting time for catalyst, cocatalyst and external donor, and hydrogen. A reaction rate was found to be enhanced with the increase in reaction temperature. Similar trend was observed for deactivation reaction rate constant. No drastic change has been observed on the initial polymerization rate as well as on the polymer yield by increasing the cocatalyst concentration up to 0.10 $kg.m^{-3}$. A possible mechanism of over reduction of metal centers by cocatalyst exhibits a lower initial activity for precontacting time for catalyst and cocatalyst and external donor above 30 min. The experimental findings concerning hydrogen response on the catalyst activity and polymer properties is also reported in this chapter.

Keywords: kinetics (polym.), polypropylene, Ziegler-Natta polymerization

3.1 Introduction

The behavior of $MgCl_2$-supported Ziegler-Natta (ZN) catalysts has been widely studied due to their commercial importance. A great deal of efforts has been made on the enhancement of catalyst performance, such as activity and stereospecificity. The progress in catalyst design for polyethylene (PE) and polypropylene (PP) production has brought revolutionary industrial developments together with an immense deal of scientific publications and patents. It is worth mentioning that scientific literature has successfully built the conceptual knowledge bridge between the catalyst design, polymer reaction engineering and polymer process technologies. One of the outcomes of knowledge bridging is the understanding of novel processes, for example a non-isothermal tubular reactor for catalytic polymerization of liquid-phase propylene.

It is known that polymerization processes often entail more than one polymerization reactor in series, for example a bulk (liquid monomer) or gas-phase (fluidized bed, vertically stirred bed or horizontally stirred bed) reactor followed by a (second) gas-phase reactor. Pater (2001) [15] reviewed that more than 50 % of the worldwide PP production capacity utilizes processes in which the first reactor operates with liquid propylene. In open literature only few numbers of publications have dealt with the kinetics of ZN catalyzed polymerization of liquid propylene (for example [15, 17, 18, 19]). The reactor used in these reported studies was always partially filled with liquid propylene that means polymerization was carried out in the presence of gas-phase, and could led to have some drawbacks depending on details of the experimental procedures.

In this respect, the main emphasis of the present kinetic study falls on performing the polymerization experiments in a fully filled batch reactor with liquid propylene using $MgCl_2$-supported ZN catalyst type, under a near-industrial conditions. The main objective of this work is to understand the overall catalyst performance by analyzing its kinetic response during polymerization with different process conditions. Therefore, the relevant experiments were carried out to study the effects of various process parameters, such as temperature, cocatalyst concentration, precontacting time for catalyst, cocatalyst and external donor, and hydrogen concentration. The process parameters like temperature, cocatalyst concentration and precontacting time were varied in the range of 60 to 80 ^oC, 0.05 to 0.20 $kg.m^{-3}$ and 5 to 60 min, respectively. Under the completely filled reactor all the hydrogen is dissolved in the liquid propylene and no gas-liquid mass transfer is

present. The influence of hydrogen on the polymerization kinetics has been studied by varying the mole ratio of hydrogen to liquid propylene (X) from 0.00025 to 0.1.

The catalyst used here was a highly active supported catalyst of type $MgCl_2/TiCl_4$ with Phthalate as an internal donor, Silane as an external donor and Triethylaluminum (TEA) as a cocatalyst. The details about chemicals, experimental techniques and their recipes used for this study are given in Chapter 2. The experimental results obtained here have been used to investigate the influence of before mentioned parameters on the initial reaction rate, yield, decay rate and molecular properties of the produced PP, respectively.

3.2 Polymerization rate

3.2.1 Using lumped propagation and deactivation constants

In general, the kinetic of ZN catalyst can be explained by applying a first-order model with the assumptions [19] that (a) the rate of polymerization (R_p' or R_p) is directly proportional to monomer and active site concentrations, (b) the active site concentration decreases in accordance with the first-order decay, and there are no monomer concentration and temperature gradients in the growing polymer particles. Thus, the R_p' obtained from the laboratory scale reactor can be written as,

$$R_p' = -R_M = k_p' C_{m,a} C^* \qquad (\text{kmol.m}^{-3}.\text{hr}^{-1}) \quad (3.1)$$

The $C_{m,a}$ shown in equation (3.1) is the monomer concentration near the active metal sites, and possibly estimated from the bulk monomer concentration ($C_{m,b}$) using an appropriate model for monomer-polymer systems (see equation 3.2).

$$C_{m,a} = \kappa C_{m,b} \qquad (3.2)$$

Similarly, the C^* used in equation (3.1) can also be represented in terms of moles of active sites injected per unit reaction volume, such as,

$$C^* = \frac{m_c^*}{V_r M_{cat}} \qquad (3.3)$$

The accurate amount of active metal (Ti) sites per mass of preactivated catalyst is difficult to estimate. It is often assumed that all Ti atoms present on the catalyst mass take

part in the complexation with cocatalyst and electron donors; and a fraction (χ) of these complexed metal atoms are active for the polymerization. Let's say,

$$m_c^* = m_{c\max}^* f(H_2) \tag{3.4}$$

and,

$$m_{c\max}^* = \chi m_c \tag{3.5}$$

Therefore, the mass active sites can be expresses in the following form,

$$m_c^* = \chi m_c f(H_2) \tag{3.6}$$

Substituting the new definition of $C_{m,a}$ and C^* from equation (3.2) and (3.3) into equation (3.1) leads to the standard form of reaction rate,

$$R_p = \frac{R_p' M_{mon} V_r}{m_c} = k_p M f(H_2) \quad (\text{kg.gCat}^{-1}.\text{hr}^{-1}) \tag{3.7}$$

where, the propagation reaction rate constant (k_p) is in the form of,

$$k_p = \frac{k_p' \kappa \chi}{M_{cat}} \tag{3.8}$$

The initial rate of polymerization can be written as,

$$R_{po} = \frac{R_{po}' M_{mon} V_r}{m_{co}} = k_p M f(H_2) \quad (\text{kg.gCat}^{-1}.\text{hr}^{-1}) \tag{3.9}$$

When the rate constants of various deactivation processes are lumped into one single parameter "k_d" , the decrease in the concentration of active sites can be described as,

$$\frac{dC^*}{dt} = -k_d C^* \tag{3.10}$$

Integrating equation (3.10) under isothermal conditions leads to,

$$C^* = C_o^* e^{-k_d t} \tag{3.11}$$

It is important to note that the reasons for real or apparent deactivation of active centers are numerous. Therefore, the fitting of experimental rate profiles with equations based on equation (3.10) might estimate low C^* even when low reaction rates are caused by other processes [15].

Further, assuming an isothermal condition, equations (3.3), (3.6), (3.9) and (3.11) can be combined and rearranged to obtain the relationship for Rp depending on time.

$$R_p = R_{po} e^{-k_d t} \quad (\text{kg.gCat}^{-1}.\text{hr}^{-1}) \quad (3.12)$$

Samson et al. (1998) [17] successfully shown that the experimental reaction rates and polymer yield could be determined from the reactor temperature profiles using the calorimetry method (according to equation (3.13) and (3.14), respectively). The multiplier shown in equation (3.15) is estimated based on the obtained polymer yield at the end of reaction, and thus used as a constant over the period of complete reaction time.

$$R_p = Multiplier\ (T_r - T_j) \quad (\text{kg.gCat}^{-1}.\text{hr}^{-1}) \quad (3.13)$$

and,

$$Yield = \int_o^{t_f} R_p\, dt \quad (3.14)$$

where,

$$Multiplier = \frac{U\,A}{m_c\, dH_r} = \text{Constant} \quad (3.15)$$

Using equation (3.12) a complete reaction rate - time curve (under an isothermal condition) should be able to describe by two parameters: (a) the initial reaction rate (R_{po}) (after complete activated catalyst, without any deactivation) and (b) the deactivation constant (k_d). These two parameters are extracted by fitting experimental rate profiles with equation (3.12). The temperature dependency of k_p and k_d can be described as,

$$k_p = k_{po} e^{\frac{-E_p}{R_g T}} \quad (3.16)$$

$$k_d = k_{do} e^{\frac{-E_d}{R_g T}} \quad (3.17)$$

3.2.2 From adiabatic temperature rise

In this method, the initial polymerization rate (R_{po_ATR}) can be estimated from the initial (adiabatic) temperature rise under isoperibolic conditions assuming that the heat produced is only heating-up the liquid propylene. Therefore, the initial isoperibolic temperature rise during the first seconds after the injection of preactivated catalyst in a completely filled reactor can be interpreted as "quasi-adiabatic" if the data acquisition is fast enough.

Figure 3.1 shows a typical temperature profile for a fully preactivated catalyst with the temperature change shown after catalyst injection being directly proportional to the polymerization rate. The differential ("slope") method combined with the assumption of adiabatic conditions can be used to determine the R_{po_ATR} (from line C; see Figure 3.1). Therefore,

$$R_{po\_ATR} = \frac{M_o\, C_P}{m_{co}\, dH_r}\left(\frac{dT}{dt}\right)_i \qquad (\text{kg.gCat}^{-1}.\text{hr}^{-1}) \quad (3.18)$$

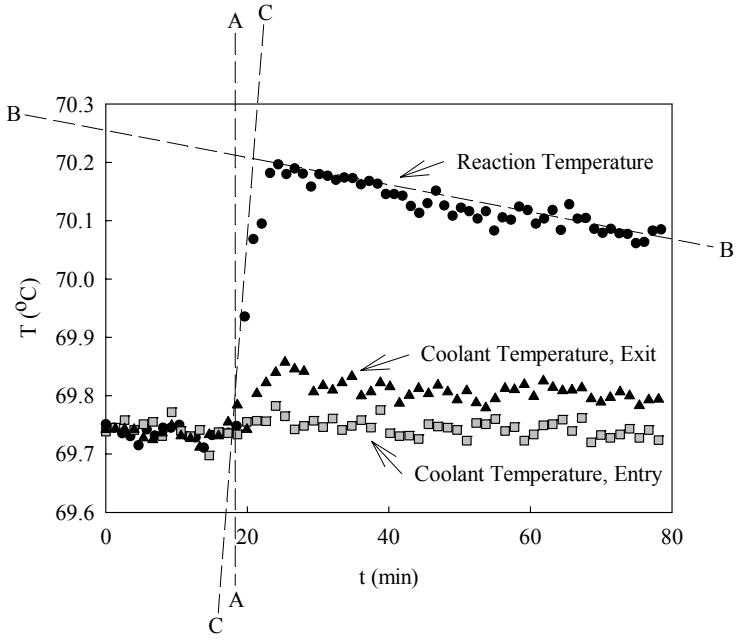

Figure 3.1: Liquid propylene polymerization at 70°C: Isoperibolic temperature profile and parameter estimation; A-catalyst injection, B-extrapolation to time zero, C-isoperibolic temperature gradient (for experimental conditions see Run33).

This allows estimating two types of initial polymerization rates: R_{po}, by extrapolating, line B (equation 3.12); and R_{po_ATR}, line C (equation 3.18); see Figure 3.1.

3.3 Results and discussion

In this section, the influence of different process parameters on the reaction kinetic as well as on the molecular properties of the produced PP is illustrated. As mentioned above, all the experiments were carried out in a completely filled isoperibolic calorimeter with liquid propylene so that no gas-liquid mass transfer is operative in the reactor.

Table 3.1 (a) illustrate the experimental recipes for polymerization tests carried out to study the effect of temperature, cocatalyst concentration and precontacting time on the reaction kinetics. The overall summary of results, presenting the R_{po}, R_{po_ATR}, yield and k_d for these experiments is given in Table 3.1 (b). Based on these experiments, the initial activity and decay behavior of catalyst is studied. These two parameters are estimated using equation (3.12).

Table 3.1: Polymerization tests carried out to study the effect of temperature, cocatalyst concentration and precontacting time on the reaction kinetics

(a) Experimental conditions [$]

Experiment Code	T_{avg} (^oC)	P_{avg} (bar)	m_o^M (kg)	m_o^{Cat} (mg)	m_o^{Cocat} (mg)	$t_{Precont}$ (min)
Run31	60.6	46.0	2.26	3.78	1040	30
Run32	70.1	40.8	2.11	3.85	250	30
Run33	70.1	40.6	2.11	3.85	500	30
Run34	70.0	41.0	2.11	3.85	1000	30
Run35	70.1	40.4	2.11	3.85	1000	5
Run36	70.1	36.0	2.08	3.85	1000	60
Run37	80.5	46.9	1.96	3.78	1040	30

[$] For all experiments a 50 mg of external donor was used and these experiments were carried out in the absence of hydrogen.

Table 3.1: Continue…

(b) Data for R_{po}, R_{po_ATR}, yield and k_d

Experiment Code	$R_{p\,o}$ (kg.gCat^{-1}.hr^{-1})	$R_{p\,o\_ATR}$ (kg.gCat^{-1}.hr^{-1})	Yield (kg.gCat^{-1})		k_d (hr^{-1})
			Exp.	Model	
Run31	8.5	8.1	9.5	9.5	0.260
Run32	13.8	15.6	11.3	11.5	0.373
Run33	15.3	16.2	12.7	13.2	0.303
Run34	14.7	16.8	12.7	13.0	0.231
Run35	15.1	17.8	12.9	13.1	0.288
Run36	10.9	13.0	8.1	8.3	0.578
Run37	27.5	28.9	21.6	22.1	0.430

As already stated above, the fine-tuned isoperibolic operation of the used 5.05 l reactor for polymerization reaction allows measuring quasi steady state polymerization rates from temperature changes down to 0.2 K just 1.5 minutes after catalyst injection. In such operations the jacket temperatures was kept constant, which resulted in the reactor temperature rise after addition of the preactivated catalyst (see Figure 3.1). With the present batch reactor tool, it is advisory to keep the maximum temperature difference between the reactor and jacket temperature below 1.5 ^{o}C in order to maintain the stable jacket temperature. However, the limitations may vary from one reactor system to another. The catalyst used in this study is already precontacted with the cocatalyst and external donor prior adding to the reactor. It has been found that an activation phenomenon of catalyst is instantaneous, and thus was not considered while calculating the reaction kinetic data. As noted earlier, it is possible to estimate R_{po_ATR}, using equation (3.18), and can be compared with R_{po} determined from equation (3.12) after fitting experimental rate profiles. The comparison of these two reaction rates is shown in Figure 3.2 (a) and Figure 3.2 (b). For a given catalyst type, there is hardly any difference between the rates within ca. 4 % of scatter. This represents the degree of catalyst activity, suggesting that the metal sites present on the surface of the catalyst are completely active.

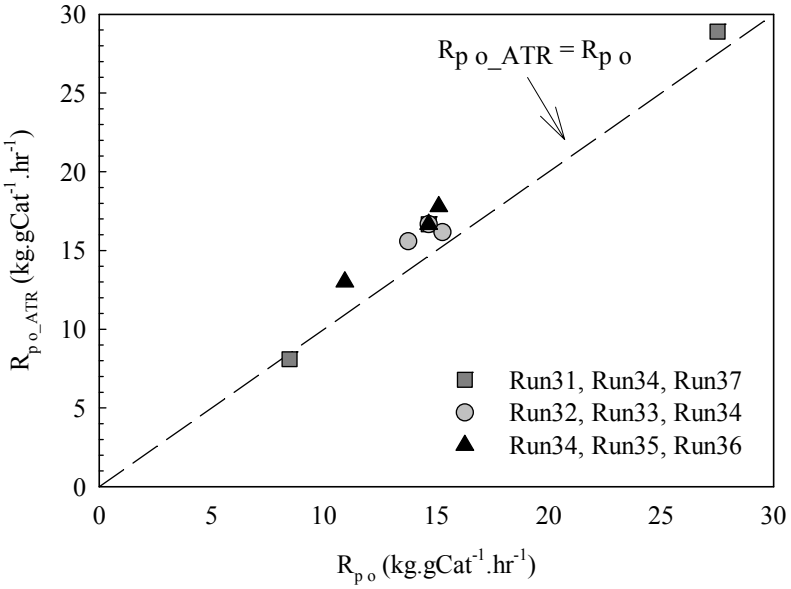

(a) Experimental conditions and kinetic data are given in Table 3.1 (a) and Table 3.1 (b).

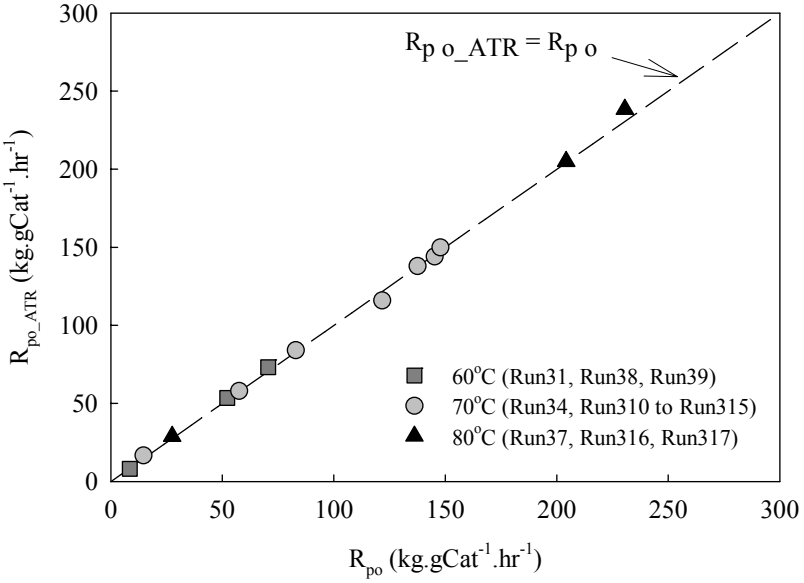

(b) Experimental conditions and kinetic data are given in Table 3.2 (a) and Table 3.3 (a)

Figure 3.2: Plot of $R_{p\,o}$ (calculated by extrapolating the polymerization rate to time zero, equation (3.12) and shown in dotted lines) versus $R_{p\,o\_ATR}$ (calculated using adiabatic rise temperature approach, equation (3.18) and shown in points).

3.3.1 Influence of temperature

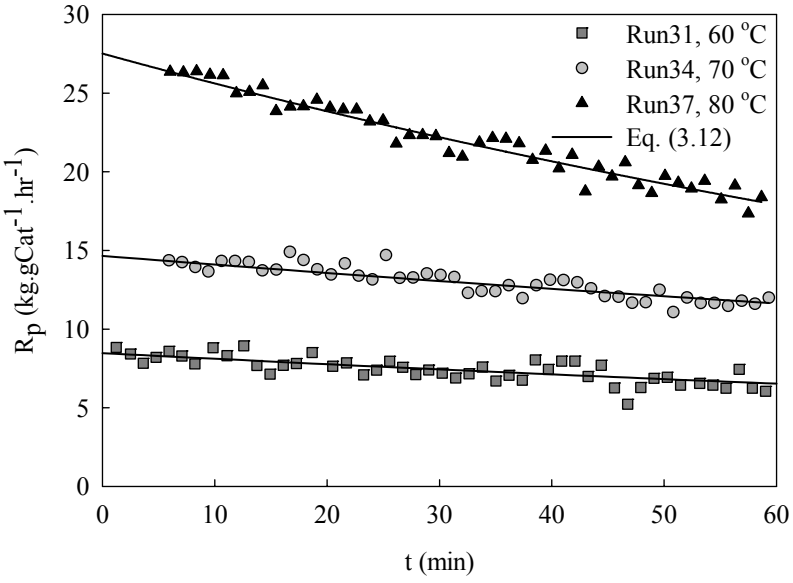

Figure 3.3: Experimental and calculated reaction rate profiles for polymerization experiment performed at different reaction temperatures.

Figure 3.3 shows the kinetic curves and its dependency on the reaction temperature. The kinetic curves in the range from 60 to 80 ^{o}C are fitted by equation (3.12) with a good agreement. The estimated parameters are shown in Table 3.1 (b). It appears that the R_p is strongly influenced by temperature, both at the initial activity as well as at the decay rate. The R_{po} was approximately doubled with every 10 ^{o}C increase in the temperature, and interesting to note that even at 80 ^{o}C this increment in rate was observed (see Figure 3.4 (a)). Similar trends were noticed for the yield and k_d (see Table 3.1 (b) and Figure 3.4 (c)).

It is often quoted that catalyst activity decreases at relatively high temperatures (> 70 ^{o}C), and the most general explanation mentioned for such phenomenon is the one which proposes a deactivation of the active centers [15, 17, 19, 24]. However, the decreasing effect in the R_{po} above 70 ^{o}C was not observed in the present study. Note that this is not always the case for experiments performed in a partially filled reactor in the presence of a monomer gas-phase operated under equilibrium conditions [15, 19]. It seems that experiments done with a completely filled reactor exhibit the effect of "reactor filling" on the dynamics of active catalyst particles during the reaction, and may vary from one catalyst type to another.

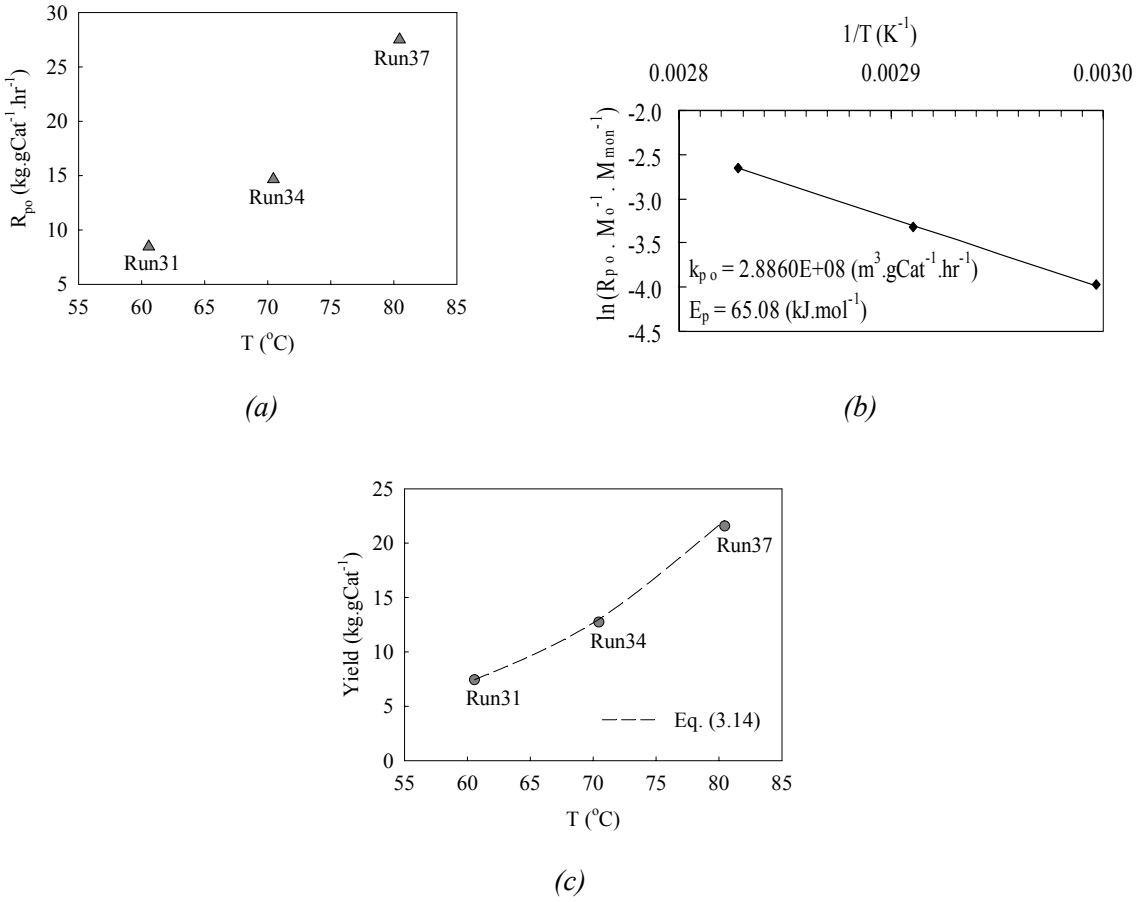

Figure 3.4: Effect of reaction temperature on (a) R_{po} measured at different temperature series experiments, (b) Arrhenius plot for R_{po} and (c) polymer yield obtained after 60 min of reaction time.

Figure 3.4 (b) shows an Arrhenius plot for R_{po}, enabling the estimation of apparent activation energy (E_p) together with the Arrhenius constant (k_{po}) for propagation reaction. The estimated value of these two parameters is indicated in Figure 3.4 (b).

In a similar way, an apparent activation energy (E_d) and Arrhenius constant (k_{do}) for deactivation reaction is determined based on the decay data given in Table 3.1 (b) and the estimated values are 24.6809 kJ.mol^{-1} and 1834.1 hr^{-1}, respectively. The E_p seems to be much higher than E_d. As a result of this difference, the polymer yield basically increases with increasing temperature (shown in Figure 3.4 (c)).

3.3.2 Influence of cocatalyst

It is known that TEA strongly affects the polymerization kinetics, and, in the case of propylene, also the polymer stereoregularity [11]. One of the explanations reported is the removal of internal donor from the surface of the catalyst, resulting in the enhanced coordination of external donor, which led to the formation of highly isotactic and highly active sites [19]. The kinetic behavior, however, is difficult to generalize for a wide range of olefin and catalyst types. A typical kinetic curves (with a preactivated catalyst) obtained for reactions carried out with different TEA concentration, are shown in Figure 3.5.

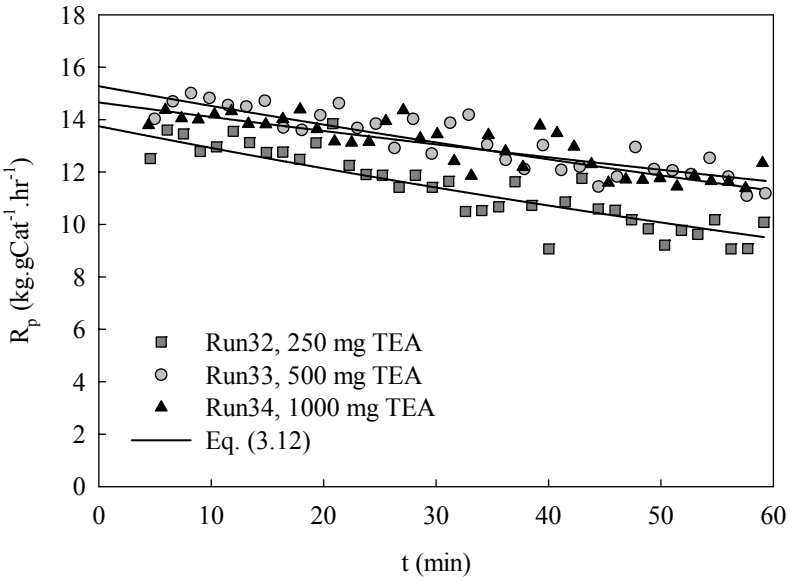

Figure 3.5: Experimental and calculated reaction rate profiles for the polymerization experiment performed at different cocatalyst concentration.

It was noticed that during the decay period the reaction rate for Run33 and Run34 was differing by 12 - 16 % compared to Run32 as the polymerization reaction proceeds (see Figure 3.5). This may be due to a lowering of the effective concentration of TEA by some reaction of TEA with catalyst (alkylation of titanium and complexation with electron donors), especially in the low TEA concentration region [3, 11, 19]. The estimated values of R_{po} and k_d for the experiments carried out with different TEA concentration are given in Table 3.1 (b).

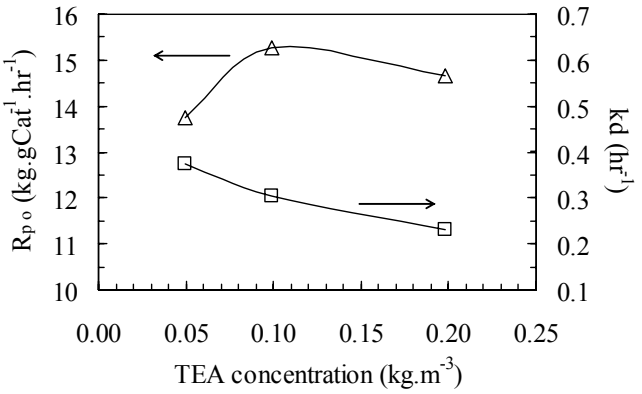

(a) Run32, Run33, Run34

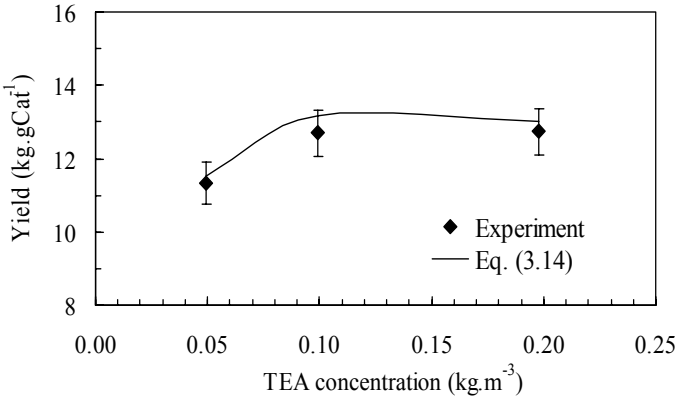

(b) Run32, Run33, Run34

Figure 3.6: Effect of cocatalyst concentration on (a) R_{po}, k_d and (b) polymer yield obtained after 60 min of reaction time, respectively.

From Figure 3.6, it is seen that R_{po} and polymer yield exhibit increment by 10 - 11 % as the TEA concentration increased by 50 % from Run32 to Run33. The values of R_{po} and polymer yield were stable within an experimental error for the TEA concentration above 0.10 kg.m^{-3}. Several studies dealing with the similar effect of TEA on the polymerization kinetics with $MgCl_2$-supported ZN catalyst type has been reported [3, 22]. They have mentioned the increase in R_{po} upon an increase of TEA concentration may be attributed to the progressive activation of the potential catalytic sites by its interaction (alkylation) with metal-alkyl. The kinetic results observed at TEA concentration above 0.10 kg.m^{-3} can be explained, by the need to have a minimum of TEA in the reaction medium in order to avoid contamination by poison (scavenging effect of cocatalyst) or to stabilize the

polymerization centers. It can also be seen from the decrease in the values of k_d from 0.373 to 0.231 hr^{-1} with the TEA concentration increased from 0.05 to 0.20 $kg.m^{-3}$.

3.3.3 Influence of precontacting time

Figure 3.7 shows an effect of precontacting time ($t_{Precont}$) for catalyst, cocatalyst and external donor on the R_p. In these experiments, the catalyst, cocatalyst and external donor mixture was precontacted for 5, 30 and 60 min respectively, before adding to the reactor.

As the $t_{Precont}$ was increased from 30 to 60 min, the R_p during the decay period (> 10 min) for Run36 found to be ≈ 40 % lower compared to Run34 and Run35. Similar effect has been observed for the R_{po} and polymer yield of Run36, which were approximately 28 % and ≈ 37 % lower in comparison with Run34 and Run35, respectively. The influence of $t_{Precont}$ above 30 min on the reaction kinetics can also be seen from the 50 % increment in the k_d value for Run36 with respect to Run34 and Run35.

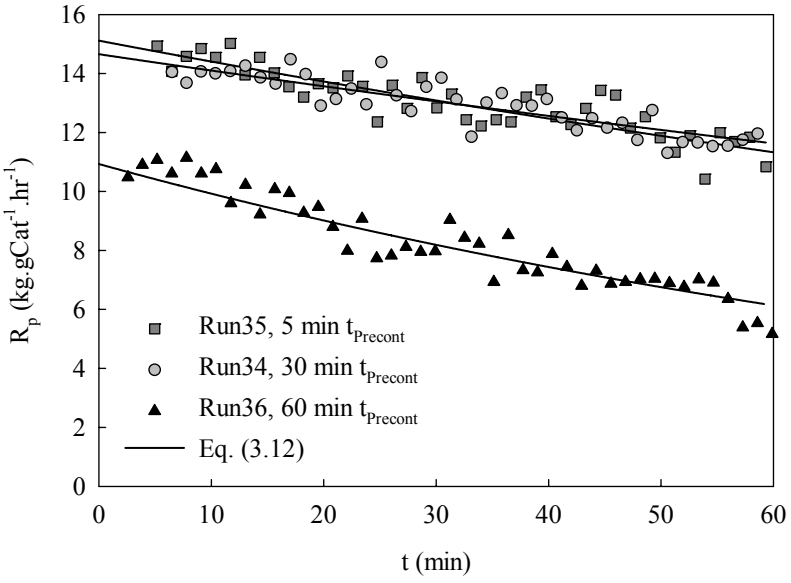

Figure 3.7: Experimental and calculated reaction rate profiles for the polymerization experiment performed at different precontacting time for catalyst, cocatalyst and external donor.

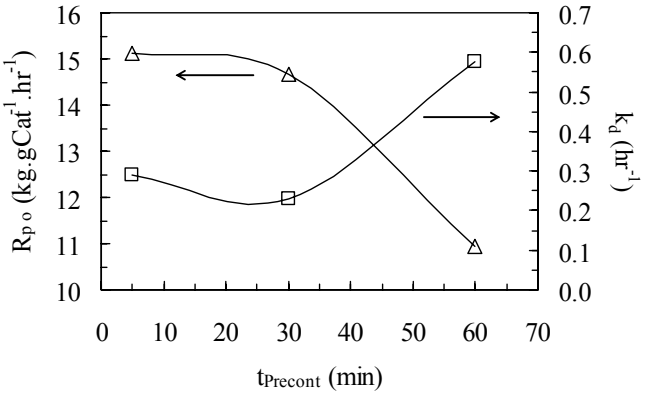

(a) Run34, Run35, Run36

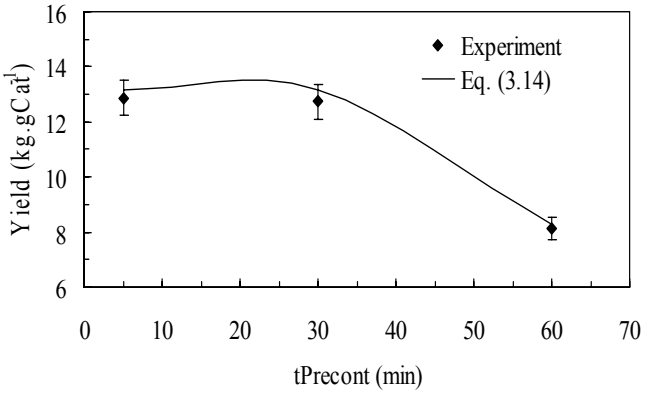

(b) Run34, Run35, Run36

Figure 3.8 Effect of precontacting time for catalyst, cocatalyst and external donor on (a) R_{po}, k_d and (b) polymer yield obtained after 60 min of reaction time, respectively

Several authors [3, 7, 8, 14, 16, 19] have studied the effect of $t_{Precont}$ on polymerization kinetics with $MgCl_2$-supported ZN catalyst type. A common fact is noticed that the activity decay is caused due to the decrease in the number of active sites. One hypothesis has been reported by Fregonese et al. (2001) [8] that the decrease in number of active sites occurred via over reduction of metal centers, for example, Ti^{3+} reduced to Ti^{2+} by TEA, because TEA is a strong reducing agent. It is also noted that Ti^{2+} is less active than Ti^{3+} in ethylene polymerization and completely inactive in the polymerization of propylene [3, 9]. Judging from the variation in the k_d value above $t_{Precont}$ of 30 min, the hypothesis of transformation of metal centers seems to be reasonable.

3.3.4 Influence of hydrogen

In this work, the raw experimental data consisting of reactor temperature and pressure profiles for all the hydrogen experiments were obtained from Al-haj Ali (2006) [2]. These data were further processed according to the calorimetry method [17], in order to obtain the reaction rate profiles from the temperature profiles, and the prepared polymer was characterized by its molecular properties. In this section, the influence of hydrogen concentration on the reaction kinetics as well as on the molecular properties is illustrated. As mentioned earlier, hydrogen (with different amounts) was injected into the completely filled reactor with liquid propylene, and thus a factor, X was used as a variable for the interpretation of the obtained kinetic results. Few experiments with high values of X were performed using a tubular reactor technique (with short residence time of around 40 - 43 s). Due to such a short residence of tubular reactor, the initial activity obtained from the tubular reactor as well as from batch reactor is discussed together in order to understand the hydrogen influence over a wide range.

Table 3.2: Polymerization tests carried out to study the effect of hydrogen on the reaction kinetics as well as on the molecular properties

(a) Experiment conditions in batch rector[†]

Experiment Code	T_{avg} (^oC)	P_{avg} (bar)	m_o^M (kg)	m_o^{Cat} (mg)	X ($molH_2o.molPPYo^{-1}$)
Run38	59.9	44.3	2.25	3.78	0.00133
Run39	61.0	46.2	2.25	1.54	0.00981
Run310	71.5	47.7	2.12	3.78	0.00025
Run311	71.9	44.8	2.10	3.78	0.00050
Run312	72.3	40.4	2.07	3.78	0.00143
Run313	72.6	42.8	2.08	3.78	0.00248
Run314	71.1	49.1	2.13	1.54	0.00516
Run315	71.3	46.9	2.12	1.54	0.00971
Run316	81.2	46.8	1.94	1.54	0.00190
Run317	80.6	47.1	1.96	1.54	0.01238

[†] For all experiment runs a 1040 mg of cocatalyst (TEA), 50 mg of external donor (Silane) and 30 min of precontacting time was used.

Table 3.2: Continue…

(b) Experiment conditions in tubular reactor[‡]

Experiment Code	T_{avg} (°C)	P_{avg} (bar)	m_{fr}^{M} (kg.hr^{-1})	$m_o^{Cat\ \#}$ (mg)	X (molH_2o.molPPYo^{-1})
Run318	70.0	65.0	2.73	0.76	0.0219
Run319	70.0	55.0	2.71	3.31	0.0510
Run320	70.0	55.0	2.71	3.20	0.0981

[‡] The total amount of catalyst used over the period of reaction.

Table 3.3: Data for R_{po}, yield, k_d and molecular weights

(a) Obtained from batch reactor

Experiment Code	Rp_o (kg.gCat^{-1}.hr^{-1})	Rp_{o_ATR} (kg.gCat^{-1}.hr^{-1})	Yield (kg.gCat^{-1})		k_d (hr^{-1})	M_w^{avg} (kg.kmol^{-1})	PDI
			Exp.	Model			
Run38	52.2	53.5	35.2	36.7	0.762	266000	6.5
Run39	70.6	73.2	35.1	36.5	1.250	*104000*	-
Run310	57.5	60.9	43.2	44.5	0.532	1120000	6.4
Run311	83.0	84.0	56.7	58.8	0.717	834000	6.6
Run312	121.7	115.9	45.5	49.1	1.187	361000	6.8
Run313	137.5	138.4	65.6	70.1	1.194	*291000*	-
Run314	145.2	144.0	62.1	67.1	1.410	244000	7.3
Run315	147.8	149.9	58.7	64.9	1.578	*133000*	-
Run316	204.2	205.0	59.8	64.2	2.007	*334000*	-
Run317	230.6	238.3	60.0	66.2	2.637	130000	5.7

Table 3.3: Continue…

(b) Obtained from tubular reactor[ℓ]

Experiment Code	Activity ($kg.gCat^{-1}.hr^{-1}$)	Yield ($g.gCat^{-1}$)	M_w^{avg} ($kg.kmol^{-1}$)	PDI
Run318	129.3	1437.9	73000	7.3
Run319	86.0	948.8	64000	8.6
Run320	61.5	679.2	43000	9.5

[ℓ] Data obtained for average residence time of approximately 40 s in a tubular reactor.

Table 3.2 show the experimental recipes used to carry out a number of polymerization tests. Table 3.3 gives an overall summary of results, presenting the R_{po}, R_{po_ATR}, yield, k_d, activity, weight-average molecular weight (M_w^{avg}) and polydispersity index (PDI). Figure 3.9 illustrates the kinetic rate profiles obtained from the batch reactor experiments and its dependency on the hydrogen concentrations analyzed at reaction temperatures of 60, 70 and 80 ^oC, respectively. These rate profiles were fitted with equation (3.12) to estimate the R_{po} and k_d. It appears that these two parameters are strongly influenced due to the presence of hydrogen. The catalyst activity was significantly increased by approximately 89 % for an increment in the X value from 0.0 to 0.01; see Table 3.2 (a) and Table 3.3 (a), and the degree of rise was found to be temperature independent at least within the given window of operating conditions. Another important fact observed is the impact of hydrogen on the R_{po} leveled off between the X values of 0.00248 and 0.01 at reaction temperature of 70 ^oC (Figure 3.10). Compared to the case for the absence of hydrogen, the estimated yield for 30 min of reaction time in a batch reactor was increased by factor 4 - 6 times at the X value of 0.01. The acceleration factor for polymer yield found to be nearly constant under the operation conditions, similar to the effect noted for R_{po}. However, from the tubular reactor experiments with high hydrogen concentration (> X value of 0.01), it was noticed that the catalyst activity seem to be decreased by 14 % as the X value increased from 0.01 to 0.02, and the activity still further decreases to 86 and 61.5 ($kg.gCat^{-1}.hr^{-1}$) at the X values of 0.05 and 0.1, respectively. Therefore, it can be concluded that R_{po} showed an acceleration period up to X value of 0.01 and above this value of X, a retardation period is observed for the same; see Figure 3.11. van Putten (2004) [23] has used the same catalyst type (as used in this study) for the gas-phase polymerization of propylene, and observed a similar effect of hydrogen on the R_{po}.

(a) At 60 °C

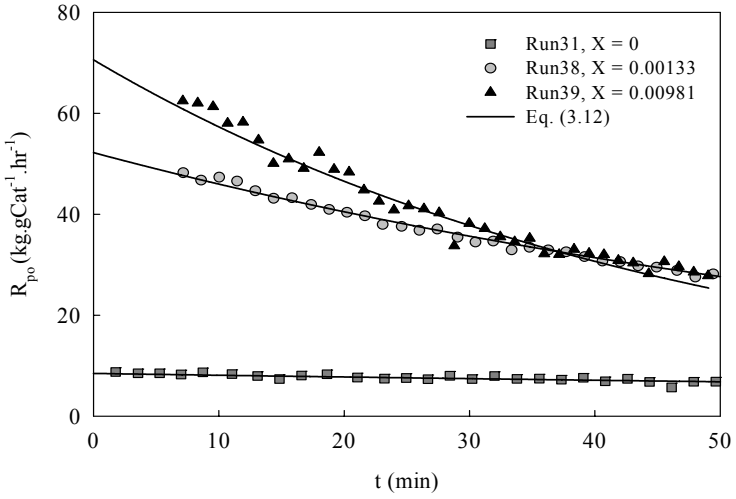

(b) At 70 °C

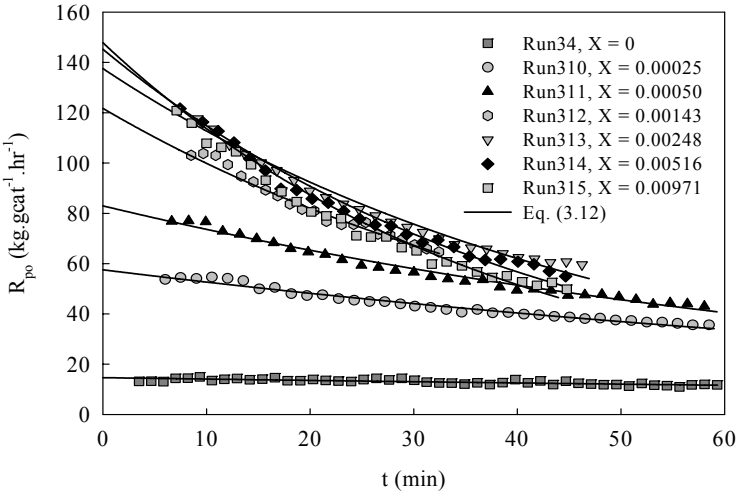

(c) At 80 °C

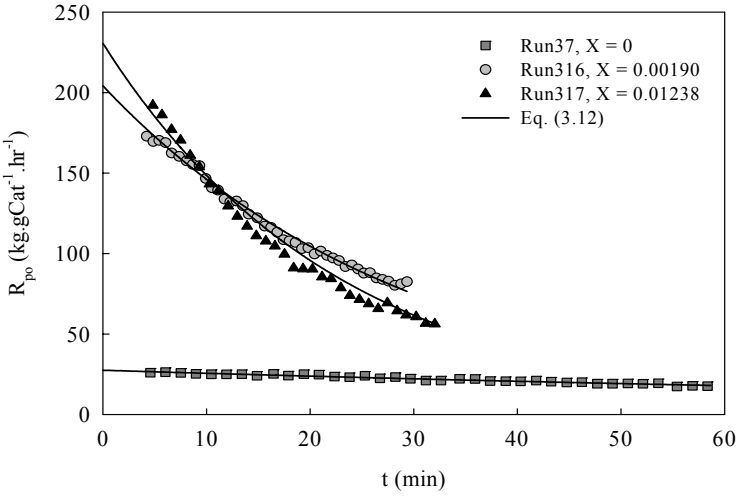

Figure 3.9: Hydrogen response on the rate of polymerization.

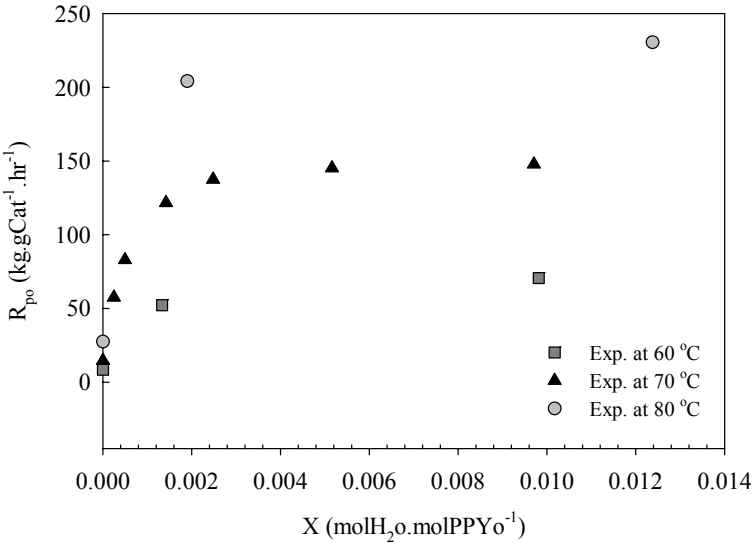

Figure 3.10: Influence of hydrogen on the R_{po}, data obtained from the batch reactor.

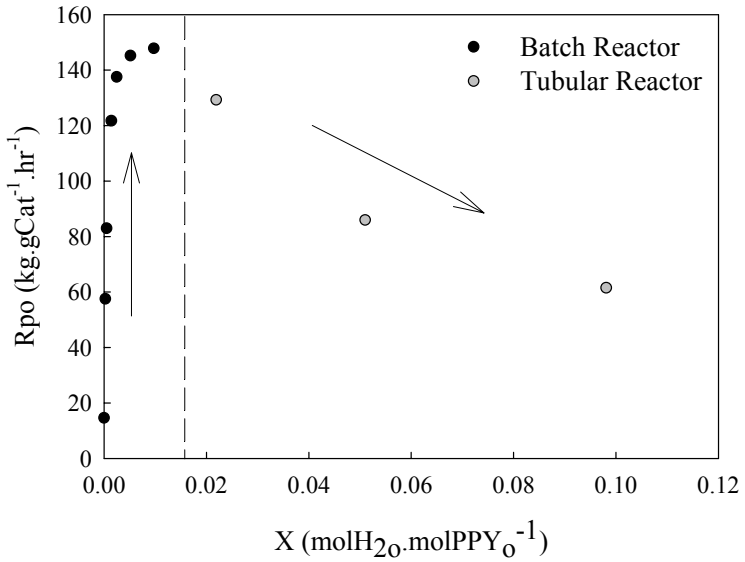

Figure 3.11: R_{po} obtained over a wide range of mole ratio of hydrogen to liquid propylene at 70 °C.

The rate enhancement effect of hydrogen (< X value of 0.02) for $MgCl_2$-supported ZN catalyst in propylene polymerization has been studied by several researchers who proposed the different hypothesis to interpret the mechanism [4, 6, 11, 12, 15, 18, 20]. The most widely accepted hypothesis for such activation effect of hydrogen is due to the regeneration of active species via chain transfer at "dormant" (2,1 - inserted) sites. The effect concerning the decreasing catalyst activity at high hydrogen concentrations (> X values of 0.02) especially for propylene polymerization has been observed by very few authors. Keii et al. (1970) [10] explained this retardation in the activity was due to an adsorption of hydrogen on the surface of $TiCl_3$ and also observed a thermal instability in the active centers. In another study performed by Soga et al. (1982) [21], the authors reported that the decreasing trend in polymerization rate with increasing partial pressure of hydrogen may be attributed to the decrease in active centers caused by the time lag of the recovery of polymerization center from metal-hydride (Ti-H) bond formed by the chain transfer via hydrogen.

The deactivation constant was increased with hydrogen concentration; see Table 3.3 (a), and trend was quite similar to the R_{po}. It exhibits that over a wide range of polymerization rate the catalyst deactivation depends on its activity. Al-haj Ali et al. (2006) [1] concluded that this influence can be interpreted as being just an activity-dependent probability. Samson et al. (1998) [17] also reported that with increasing hydrogen concentration, the concentration of the relatively unstable "Ti-H" active centers also increases and so does the deactivation rate.

The effects of hydrogen on the molecular properties of PP prepared in this study are summarized in Table 3.3. The part of M_w^{avg} values reported in Table 3.3 (shown in italic), were estimated using the viscosity average molecular weights (M_v^{avg}) measured by intrinsic viscometry (see Figure 3.12). The correlation applied for such estimation was obtained by calibrating M_w^{avg} measured by GPC. The average molecular weight was found to be decreased with the increasing hydrogen concentration over a wide range; see Table 3.3. Soares et al. (1996) [20] found that at same hydrogen concentration the average molecular weights of PP has decreased with increasing polymerization temperature. However, in the present case, the dependency of molecular weights on temperature is found to be different. In contrary to the effect stated by Soares et al. (1996) [20], the M_w^{avg} of the produced polymer was found to increase by an average value of ~ 24 % for the temperature increment from 60 to 70 ^oC. This increase was noted for both X value of 0.0014 and 0.01 (see Table 3.3).

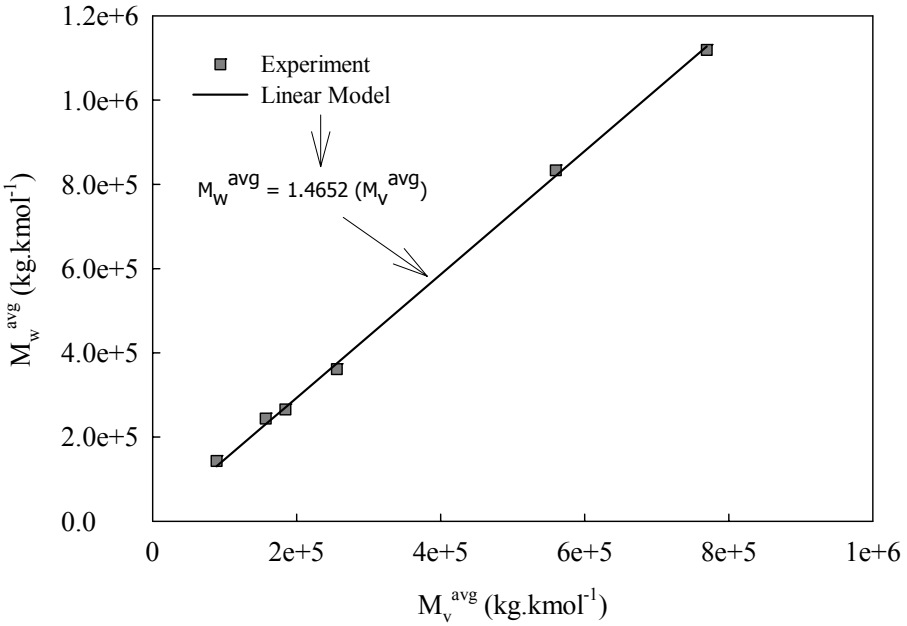

Figure 3.12: The relationship between M_w^{avg} and M_v^{avg}.

However, the usual effect of temperature on molecular weights can be seen for the M_w^{avg} values obtained at 70 and 80 ^oC (given in Table 3.3), but not found to be so drastic. In another important study, Chadwick et al. (1995) [5] stated that the effect of hydrogen on polymer molecular weight is dependent on the nature of alkoxysilane used as an external donor in polymerization. The author studied an effect of hydrogen and different external donors on regio- and stereospecificity in propylene polymerization with $MgCl_2$-supported ZN catalyst type. For example, at a given hydrogen concentration, methoxysilanes typically give higher molecular weight polymer than ethoxysilanes [5]. The PDI of PP samples at different hydrogen concentration, reaction temperatures and reactor conditions is provided in Table 3.3. According to Al-haj Ali et al. (2006) [1], the increasing level of hydrogen resulted in an increase PDI for PP prepared from batch experiments, and may have been caused due the activation of catalyst sites, which are dormant in the absence of hydrogen. In addition, at given level of hydrogen, a composition of dormant sites might differ from the composition of active sites. The PDI value for Run317 represented a narrow distribution compared to the other experiments performed at 70 ^oC (Run310, Run311, Run312 and Run314). This indicates that PDI narrows with increasing reaction temperature, and such phenomenon has also been observed by Kissin et al (2004) [13].

Note: The results discussed in section 3.3.4 concerning the influence of hydrogen on the catalyst activity and polymer properties are valid for the X values ranging between 0.0 and 0.1.

All the effects of hydrogen on the catalyst activity as well as on the molecular properties of PP are discussed in detail in Chapter 4, on the basis of improved kinetic model.

3.4 Conclusions

The influence of temperature, cocatalyst concentration, precontacting time and hydrogen concentration on the polymerization kinetics was studied using $MgCl_2$-supported ZN catalyst type with the combination of an alkoxy silane as an external donor and TEA as a cocatalyst in a completely filled batch reactor with liquid-phase propylene. With the comparison of R_{po} and R_{po_ATR}, it was possible to represent the degree of catalyst activity. The kinetics can be described with simple first-order decay up to a reaction temperature of 80 ^{o}C. It was interesting to note that the R_{po} increased with increasing reaction temperature even at 80 ^{o}C. Similar effect has been observed for decay constant.

The increase in TEA concentration showed enhancement in the reaction rate, suggesting that a minimum TEA concentration should be present in the system in order to have its activating as well as scavenging effect during the polymerization reaction. In addition, it was important to note that the combine effect of TEA and external donor on the stereoregularity of polymer cannot be neglected and has to de studied. A pronounced effect of precontacting time for catalyst, cocatalyst and external donor on the $R_{po,}$ polymer yield and k_d was noticed. A hypothesis of metal center transformation seems to play an important role in the increased decay in the reaction rate at higher regime of $t_{Precont}$ values (> 30 min).

At low hydrogen concentration below the X value of 0.01, the R_{po} found to be increasing indicating the “waking-up” of phenomena of dormant sites due to hydrogen. However, at high hydrogen concentration ($0.01 < X <= 0.1$), the R_{po} observed to be decreasing explaining the fact that different nature of hydrogen takes part into the chain transfer reactions. Very few researches have reported this fact assuming that Ti-H active center formed after chain transfer with (adsorbed) hydrogen may show a slow propagation rate. The k_d has shown an increasing trend with increasing hydrogen amount.

The molecular weight of produced polymer was found to decrease with increasing hydrogen concentration. However, molecular weight for PP sample prepared at 70 ^{o}C (Run314) showed higher value compared to the sample prepared at 60 ^{o}C (Run38) and

may lead to the conclusion that the propagation reaction seems to have higher activation energy than the termination reactions. This effect could be considered as an unusual with respect to the published literatures, and should be indicated as a very special for the catalyst type used in the present work. The PDI values for PP produced from batch polymerization experiments increased slightly with the hydrogen concentration, but decreased with temperature.

Nomenclature

A : Heat transfer area (m^2)
$C_{m,a}$: Monomer concentration near active sites ($kmol.m^{-3}$)
$C_{m,b}$: Bulk monomer concentration ($kmol.m^{-3}$)
C_p : Specific heat ($kJ.kg^{-1}.K^{-1}$)
C_o^* : Initial active site concentration ($kmol.m^{-3}$)
C^* : Active site concentration ($kmol.m^{-3}$)
dHr : Heat of reaction ($kJ.kg^{-1}$)
E_d : Activation energy for deactivation reaction ($kJ.mol^{-1}$)
E_p : Activation energy for propagation reaction ($kJ.mol^{-1}$)
$f(H_2)$: Hydrogen response function
H_2 : Hydrogen concentration ($kg.m^{-3}$)
H_{2o} : Initial moles of hydrogen present during reaction (mole)
k_{do} : Arrhenius constant for deactivation reaction (hr^{-1})
k_d : Rate constant for deactivation constant (hr^{-1})
$k_p^{'}$: Rate constant for propagation constant ($m^3.kmol^{-1}.hr^{-1}$)
k_{po} : Arrhenius constant for propagation reaction ($m^3.gCat^{-1}.hr^{-1}$)
k_p : Rate constant for propagation reaction ($m^3.gCat^{-1}.hr^{-1}$)
m_c^* : Mass of active sites (g)
$m_{c\,max}^*$: Maximum mass of active sites (g)
$m_{co,}\ m_o^{Cat}$: Initial mass of preactivated catalyst (mg)
m_c : Mass of preactivated catalyst (gCat)
m_o^{Cocat} : Initial mass of cocatalyst (mg)
m_o^M : Initial mass of propylene (kg)
m_{fr}^M : Mass flow rate of liquid propylene ($kg.hr^{-1}$)
M_o : Initial concentration of monomer ($kmol.m^{-3}$)
M_{cat} : Molecular weight of catalyst ($kg.kmol^{-1}$)

M_{mon} : Molecular weight of monomer ($kg.kmol^{-1}$)
M : Concentration of monomer ($kmol.m^{-3}$) or Chain length on weight basis
P_{avg} : Average reactor pressure (bar)
PPY_o : Initial moles of liquid propylene present during reaction (mole)
R_g : Universal gas constant ($kJ.mol^{-1}.K^{-1}$)
R_M : Reaction rate for monomer consumption ($kmol.m^{-3}.hr^{-1}$)
R_{po}' : Initial rate of polymerization ($kmol.m^{-3}.hr^{-1}$)
R_p' : Rate of polymerization ($kmol.m^{-3}.hr^{-1}$)
R_{po} : Initial rate of polymerization ($kg.gCat^{-1}.hr^{-1}$)
R_{po_ATR} : Initial rate of polymerization from ATR ($kg.gCat^{-1}.hr^{-1}$)
R_p : Rate of polymerization ($kg.gCat^{-1}.hr^{-1}$)
t_f : Final reaction time (min or hr)
$t_{Precont}$: Precontacting time (min)
t : Polymerization time (min)
T_{avg} : Average reactor temperature (^oC)
T_j : Jacket temperature (^oC)
T_r : Reactor temperature (^oC)
T : Temperature (^oC)
U : Overall heat transfer coefficient ($kJ.m^{-2}.K^{-1}.hr^{-1}$)
V_r : Reactor volume or reaction volume (m^3)
X : Mole ratio of hydrogen to liquid propylene

Greek letters

κ : Sorption coefficient for monomer-polymer system
χ : Fraction

Sub- and superscripts

avg : Average
c, cat, Cat : Catalyst
Cocat : Cocatalyst
d : Deactivation
f : Final

fr	: Flow rate
g	: Gas
j	: Jacket
m, mon, M	: Monomer
o	: Zero or initial
p	: Propagation or polymer
r	: Reactor
*	: Active

Abbreviations

ATR	: Adiabatic temperature rise
GPC	: Gel permeation chromatography
$MgCl_2$	: Magnesium dichloride
PDI	: Polydispersity index
PE	: Polyethylene
PP	: Polypropylene
TEA	: Triethylaluminum
$TiCl_3$	: Titanium trichloride
$TiCl_4$	: Titanium tetrachloride
ZN	: Ziegler-Natta

Literature

[1] Al-haj Ali, M., Betlem, B., Roffel, B. and Weickert G. (**2006**), AIChE Journal, 52, 5, 1866 - 1876.

[2] Al-haj Ali, M. (**2006**), Doctorate Thesis, University of Twente, Enschede, The Netherlands.

[3] Barbè, P. C., Cecchin, G. and Noristi, L. (**1987**), Advances in Polymer Science, 81.

[4] Chadwick, J. C., Miedema, A. and Sudmeijer, O. (**1994**), Macromol. Chem. Phys., 195, 167 - 172.

[5] Chadwick, J. C., van Kessel, G. M. M. and Sudmeijer, O. (**1995**), Macromol. Chem. Phys., 196, 1431 - 1437.

[6] Chadwick, J. C., Morini, G., Albizzati, E., Baldontin G., Mingozzi, I. and Christofori, A. (**1996**), Macromol. Chem. Phys., 197, 2501 - 2510.
[7] Chien, J. C. W., Weber, S. And Hu, Y. (**1989**), Journal of Polymer Science: Part A: Polymer Chemistry, 27, 1499 - 1514.
[8] Fregonese, D., Mortara, S. and Bresadola, S. (**2001**), Journal of Molecular Catalysis A: Chemical, 172, 89 - 95.
[9] Kashiwa, N. and Yoshitake, J. (**1984**), Macromol. Chem., 185, 1133 - 1138.
[10] Keii, T., Okura, I., Soga, K. and Kojima, A. (**1970**), Journal of Polymer Science: Part A-1, 8, 2717 - 2719.
[11] Keii, T. (**1982**), Macromol. Chem., 183, 2285 - 2304.
[12] Kissin, Y. V., Rishina, L. A. (**2002**), Journal of Polymer Science: Part A, Polymer Chemistry, 40, 1353 - 1365.
[13] Kissin, Y. V., Ohmishi, R. and Konakazawa, T. (**2004**), Macromol. Chem. Phys., 205, 284 - 301.
[14] Liu, B., Nitta, T., Nakatani, H. and Terano, M. (**2003**), Macromol. Chem. Phys., 204, 395 - 402.
[15] Pater, J. T. M. (**2001**), Doctorate Thesis, University of Twente, Enschede, The Netherlands.
[16] Pino, P. and Rotzinger, B. (**1984**), Macromol. Chem. Suppl., 7, 41 - 54.
[17] Samson, J. J. C., Weickert, G., Heerze, A. E. and Westerterp, K. R. (**1998**), AIChE Journal, 44, 6, 1424 - 1437.
[18] Samson, J. J. C., Bosman, P. J., Weickert, G. and Westerterp, K. R. (**1999**), Journal of Polymer Science: Part A, Polymer Chemistry, 37, 219 - 232.
[19] Shimizu, F. (**2001**), Doctorate Thesis, University of Twente, Enschede, The Netherlands.
[20] Soares, J. B. P. and Hamielec, A. E. (**1996**), Polymer, 37 (20), 4607 - 4614.
[21] Soga, K. and Siono, T. (**1982**), Polymer Bulletin, 8, 261 - 268.
[22] Spitz, R., Bobichon, C. and Guyot, A. (**1989**), Makromol. Chem., 190, 707 - 717.
[23] van Putten, I. (**2004**), Doctorate Thesis, University of Twente, Enschede, The Netherlands.
[24] Vaquero, J. L. H., Lingl, G. M. and Gaitan, J. M. P. (**2004**), Macromol. Symp., 213, 367 - 383.

Chapter 4

Kinetics of liquid-phase propylene polymerization: II. Modeling

Abstract: The development of a detailed kinetic model describing an overall hydrogen influence observed in catalyzed propylene polymerization is presented. The kinetic model has been developed based on the obtained experimental data from the polymerization tests performed with a wide range of hydrogen concentrations. Kinetic mechanisms were selected to describe the effect of hydrogen on catalyst activity and molecular weight distribution of the polymer. In this chapter, different and often contradictory observations regarding the role of hydrogen in propylene polymerization (reported by several researchers) are reviewed and discussed with respect to the present kinetic investigations. The catalyst activity and average probability of chain termination were modeled as a function of hydrogen by combining the two distinct kinetic mechanisms derived from Natta model and dormant site model. The strong acceleration effect of hydrogen on catalyst activity was observed below 0.01 mole ratio of hydrogen to propylene, however, above this mole ratio of hydrogen to propylene, hydrogen seem to depress the catalyst activity. The catalyst decay behavior was related to the reaction rate, and found that the deactivation of catalyst increases with its increasing activity. The average molecular weight of the produced polymer was found to be decreasing with increasing concentration of hydrogen during polymerization reaction in the whole range studied. A complex kinetic parameter the so-called chain termination probability has been used for deconvolution analysis of molecular weight distribution of produced polymer. The GPC curves were deconvoluted using a four site model, and the results obtained concerning the influence of temperature and hydrogen on the catalytic propylene polymerization reflects the specific kinetic effects inherent to the nature of catalyst site.

Keywords: kinetics (polym.), modeling, propylene polymerization, Ziegler-Natta catalyst

4.1 Introduction

One of the important aspects for $MgCl_2$-supported Ziegler-Natta (ZN) catalysts for olefin polymerization is its performance in the presence of hydrogen during reaction. For instance, the conventional effect of hydrogen in the propylene polymerization with $MgCl_2$-supported ZN catalyst is on the catalyst activity and polymer molecular weight. Most of the studies done on the catalytic propylene polymerization have shown that an introduction of hydrogen during the polymerization reaction results in a considerable enhancement of catalyst activity, in addition to decreasing the molecular weight of the polymer produced. Moreover, these studies are focused on the qualitative description of the hydrogen effect and on searching for the most probable mechanism for these observations. Furthermore, from the end-use user point of view, the consequences of hydrogen response on the thermal, rheological and morphological properties of polypropylene (PP) prepared from gas- and liquid-phase propylene polymerization processes were recently reported by Stern et al. (2005) [42].

In this chapter, different and often contradictory observations regarding the role of hydrogen in propylene polymerization are reviewed and discussed with respect to the kinetic investigations carried out in this study. The present work focuses on the development of a detail kinetic model describing an overall hydrogen influence observed especially in the catalyzed propylene polymerization. The kinetic model analyses are carried out based on the obtained experimental data from the polymerization tests performed in the presence of wide range of hydrogen concentrations (discussed in Chapter 3). Important kinetic mechanisms were selected for deriving the effects of hydrogen on the catalyst activity as well as on the molecular properties of the polymer produced. As per the author knowledge, the present study discussed here is the state-of-the-art concerning the hydrogen effect on the catalytic liquid-phase propylene polymerization.

4.2 Literature analysis: Role of hydrogen

The dependency of catalyst productivity on the concentration of hydrogen, the most used molecular weight modifier in industrial practice, varies with the nature of catalyst and monomer. Several kinetic studies were performed to understand the hydrogen influence on the different catalyst type, such as $TiCl_3$, $MgCl_2$-supported ZN and Metallocences.

Selected literatures are reported in this section dealing with the effect of hydrogen on the polymerization rate and polymer properties during the catalytic polymerization of olefins. In 1959, Natta et al. [28] performed the olefin polymerization experiments using hydrogen as a transfer agent to regulate the average molecular weight, and also observed a considerable decrease in polymerization rate in the presence of hydrogen for both ethylene and propylene, using $TiCl_3$ and $AlEt_3$ or $AlEt_2Cl$ catalysts. Hoffman et al. (1963) [16] investigated the "Natta" mechanism in which hydrogenation of a catalyst-growing chain bond occurs; yielding a catalyst hydride site (Ti-H) and a dead chain with a hydrogen atom incorporated at the end. They have performed a number of polymerization runs with propylene using $TiCl_3$-$AlEt_2X$ catalyst under conventional conditions in the presence of hydrogen gas to which tritium has been added as a tracer. Their study concluded that an appearance of a secondary mechanism (chain transfer to hydrogen) produced a lower molecular weight fraction of both the isotactic and atactic portions of the polymers.

Keii (1970 and 1972) and coworkers [19, 20] performed several polymerization experiments with propylene using AA-grade $TiCl_3$ at different hydrogen concentration. In particular, the study has been performed on propylene polymerization using AA-$TiCl_3$/$Al(C_2H_5)_2Cl$/toluene/hydrogen shown an abnormal effect of hydrogen on the reaction rates [20]. The stationary polymerization rate was decreasing above 7.5 cmHg pressure of hydrogen in the reactor. The authors suggested that such effect on the rate comes from the mixture of AA-$TiCl_3$/$Al(C_2H_5)_2Cl$/toluene/hydrogen. Their results were discussed on the basis of Natta's findings. Later, Keii et al. (1984) [20] especially studied the effect of hydrogen on the molecular properties of PP samples prepared with the catalyst type such as $MgCl_2/TiCl_4/C_6H_5COOC_2H_5/Al(C_2H_5)_3$, and they observed a significant decreased in the number-average molecular weight (M_n^{avg}) by addition of hydrogen to the reaction system.

Soga et al. (1982) [39] performed slurry polymerization of propylene in n-heptane at 40 ^oC for 30 min with the catalyst type of $MgCl_2/TiCl_4$/TEA/EB under pressure of propylene (35 cmHg) and hydrogen (10 - 35 cmHg). They have noticed that the rate of polymerization gradually decreases with an increase in the partial pressure of hydrogen. The authors believed that this result may be attributed to the decrease in active centers caused by the time lag of the recovery of polymerization center from the metal-hydride (C_o^H or Ti-H) bond formed by the chain transfer via hydrogen.

In another interesting study performed by Guastalla et al. (1983) [14] (especially for low temperature (17 ^{o}C) slurry propylene polymerization) suggested that the catalyst activity did not rise with increasing hydrogen concentrations, but still significantly decreased the polymer molecular weight.

Spitz et al. (1989) [40] carried out propylene polymerization with an improved catalyst type of $MgCl_2/TiCl_4$/Phthalate – TEA/Silane, in the presence of hydrogen; and activity found to be increased by almost 3 times of the initial rate and of about twice of the productivity. This increasing effect in activity has been observed by increasing hydrogen partial pressure from 0 to 0.3 bar with a total system pressure of 4 bar at 70 ^{o}C.

In 1992, Busico et al. [9] investigated the polyinsertion of propylene over a highly isospecific $MgCl_2$-supported/$TiCl_4$ catalyst in the presence of high partial pressures of hydrogen (ranging from 0 to 50 bar) as a chain transfer agent. With the application of advanced polymer analysis techniques, the authors focused their work on finding a possible link between the rate enhancement and the use of stereospecific monomers.

Similarly, Chadwick et al. (1995 and 1996) [12, 13] analyzed the hydrogen performance on the stereochemistry level after characterizing the PP prepared from propylene polymerization with $MgCl_2$-supported ZN catalyst type. The authors found that the effect of hydrogen on the catalyst activity and on the polymer molecular weight is dependent on the type of internal and external electron donors present in the catalyst system.

Chadwick et al. (1996) [13] also observed that the stereoregularity of isotactic polymer chain increased with increasing hydrogen concentration during polymerization. This result indicated that not only a regioirregular but also a stereoirregular insertion may slow down the rate of chain propagation, leading to an increased chance of chain transfer. A similar conclusion has been drawn by Bukatov et al. (1994) [10]. While, in earlier investigation, Pijpers et al. (1972) [30] believed that hydrogen rate enhancement may be due to an improved monomer access at the active sites via increased chain migration or reduced competition with terminal double bond.

Kahraman et al. (1996) [18] performed the detail kinetic studies on propylene polymerization using a prepolymerized high-active ZN catalyst. They commented that hydrogen consumption depends on the characteristics of the catalyst and the amount of reactive impurities in the raw materials. In their study, a hydrogen quantity was varied

from 600 Nml to 3000 Nml in a 2500 ml of n-heptane slurry. The authors observed a constant activity up to 1000 Nml of hydrogen amount, and above this amount of hydrogen the reaction rate started decreasing. They concluded that a decrease in rate is a result of decreasing effective monomer concentration near the catalytically active sites due to adsorbed hydrogen.

Another interesting study on propylene polymerization with catalyst type of LYNX 900 and cocatalyst as diethyl aluminium chloride was performed by Soares et al. (1996) [35]. They concluded, "effect of hydrogen on the activity of catalyst for propylene polymerization is reversible".

In an elegant work, Mori et al. (1999) [27] evaluated the effect of hydrogen in the propylene polymerization experiments carried out by stopped-flow ($t <= 0.2$ s) as well as using a conventional slurry process ($t >= 30$ min). With the stopped-flow experiments, they observed that polymer yield and molecular weight were apparently proportional to the polymerization time; indicating that the nature of active sites on the catalyst was constant and that the chain transfer and termination reactions were negligible regardless of the presence of hydrogen. However, with the conventional slurry polymerization process, the authors observed an activity enhancement with the addition of hydrogen to the reactor, and thus, concluded that only feasible reason for such phenomena is the reactivation of dormant sites by hydrogen.

An interesting work on the liquid-phase propylene polymerization using highly active catalyst of type $MgCl_2/TiCl_4$/EB - TEA/PEEB at near-industrial conditions has been reported by Samson et al. (1999) [31]. From the obtained kinetic data, the authors examined that hydrogen attributed to the two important facts, one is in reactivation of dormant metal sites and another is in stimulating the initiation process resulting in the significant decrease in an induction period. Besides this paper, a few more studies were reported on the influence of hydrogen on the kinetics of liquid-phase propylene polymerization using highly active catalyst type [29, 33].

The sensitivity of metallocene catalyst towards the hydrogen during ethylene polymerization has also been studied by Blom et al. (1999, 2001 and 2002) and Soares et al. (2000) [5, 6, 7, 36]. Blom et al. (1999) [5] found a bimodal molecular weight distribution (MWD) for polyethylene (PE) prepared using $Cp_2^*ZrCl_2/MAO/SiO_2$ catalyst type, and concluded that this effect might be due to the formation of two different active sites

among which one strongly hydrogen sensitive site, which might be activated by the presence of hydrogen. Meier (2000) [26] has evaluated an effect of hydrogen on the (gas and liquid-phase) propylene polymerization using metallocene catalyst of type rac-$Me_2Si[Ind]_2ZrCl_2$/MAO/SiO_2(PQ). In the gas-phase analysis, the author observed the similar broadening effect on the MWD as stated above, and described the MWD curves using a "two-site" Schulz-Flory distribution model. A key model parameter, i. e., an average chain termination probability (q: inverse of average molecular weight) seem to be linearly related to the hydrogen concentration (in the low concentration regime below =< 0.0016 $molH_2.molPPY^{-1}$).

A linear relation was observed between q and hydrogen conceratration in the research work carried out by Kissin et al. (2002) [23] on the slurry polymerization of propylene using $MgCl_2/TiCl_4$/Phthalate - TEA/Silane catalyst type. The molecular weight remained constant at higher hydrogen concentrations (> 0.01 C_H/C_{Pr}). The authors suggested that monomer plays a role in hydrogen transfer reactions by forming a complex with the polymer, which further reacts with hydrogen molecules. The concentration of such complex may be dependent on the hydrogen concentration at low values (< 0.01 C_H/C_{Pr}), and became hydrogen independent (saturated) at high concentrations of hydrogen (from 0.01 to 0.08 C_H/C_{Pr}).

Kissin et al. (2002) [23] also reported the chemical mechanism of catalyst activation in their study. On the basis of kinetic data, the authors mentioned that only about 10 % of the potentially active species are engaged in propylene chain-growth reactions in the absence of hydrogen. They concluded that the addition of hydrogen, which reacts with the stable Ti-$CH(CH_3)_2$ species as well as with other stable Ti-$CH(CH_3)R$ species, and restores the Ti-H (or C_o^H) bond, causes the activation of propylene polymerization reactions.

In 2004, van Putten [44] has carried out gas-phase propylene polymerization using $MgCl_2/TiCl_4$/Phthalate - TEA/Silane catalyst type with varying mole ratio of hydrogen to propylene (X) ranging from 0 to 0.12. The author found that the initial catalyst activity represented by "R_{po}" increases with increasing hydrogen concentration to a maximum of approximately 44 $kg.gCat^{-1}.hr^{-1}$ at a concentration of 1.1 mole % of hydrogen; i.e., 3 times higher than the initial activity observed in the absence of hydrogen (see Figure 4.1). However, the author observed that above the concentration of 1.8 mole % of hydrogen the initial activity was found to be decreasing. From the GPC analysis of the produced PP,

the author reported that an average molecular weight of polymer decreases rapidly with increasing hydrogen concentration followed by a slower decrease of the molecular weight at the higher hydrogen concentration, shown in Figure 4.1.

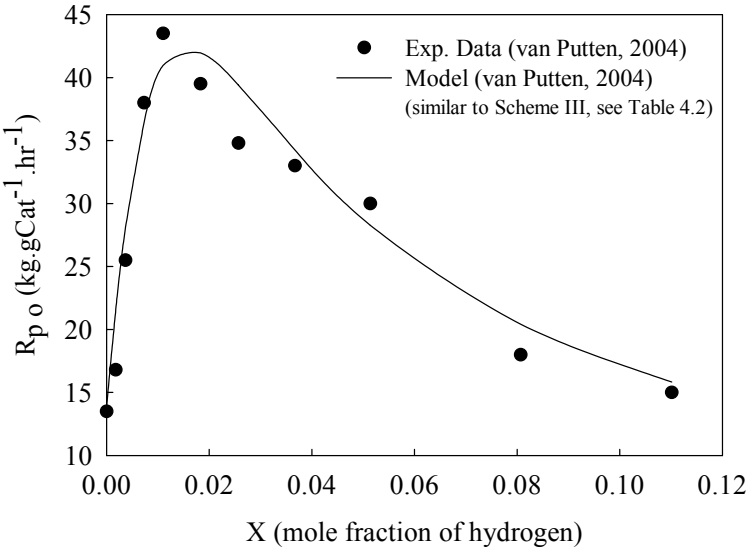

(a)

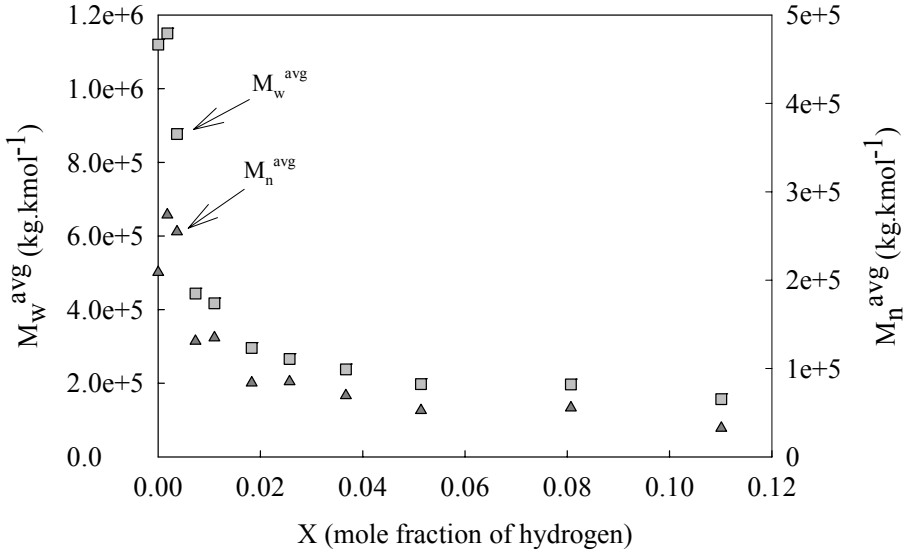

(b)

Figure 4.1: Influence of hydrogen on (a) initial activity and (b) average molecular weights of the produced PP, reported by van Putten (2004) [44].

The experimental findings discussed above regarding the hydrogen influence on polymerization of ethylene and propylene were carried out mostly in gas-phase, slurry-phase or in liquid-phase with partially filled reactor. Depending on the details of experimental procedure, the use of partially filled reactor for liquid-phase polymerization could have some drawbacks, especially when a prepolymerization step and heating between pre- and main polymerization is required. Recently, Al-haj Ali (2006) [3] has performed a comprehensive comparison between liquid-phase propylene polymerization carried out in a partially filled and in the completely filled reactor under isoperibolic conditions.

For the first time, in case of completely filled reactor with liquid-phase propylene, Al-haj Ali et al. (2006) [2] reported the hydrogen response on the polymerization kinetics and molecular properties of PP. The author has used the same catalyst type of $MgCl_2/TiCl_4$/Phthalate - TEA/Silane as used by van Putten (2004) [44], for the polymerization performed under near-industrial conditions, and varied the values of X up to 0.01. The author found that initial catalyst activity has strongly enhanced in the presence of hydrogen, as well as the deactivation rate of catalyst.

In our previous study [43], it is reported that the liquid propylene polymerization tests have been performed in a tubular reactor using a similar catalyst type as used by van Putten (2004) [44] and Al-haj Ali (2006) [2]. The experiments were carried out in the presence of high values X, in the range of 0.02 to 0.1 (see Chapter 3). The most striking effect observed in these experiments is that the catalyst activity decreases above the X values of 0.02. Now, it is possible to understand the influence of hydrogen on the propylene polymerization reaction at near-industrial operating conditions, and also with a wide range of hydrogen concentrations.

4.3 Kinetic model for catalytic propylene polymerization

The relevant chemical complexities involved in the process of catalytic propylene polymerization led to the postulation of a kinetic mechanism composed of several reaction steps [8]. Typically, in case of $MgCl_2$-supported ZN catalyst, the polymerization reactions occur at several reactive sites on the catalyst particle. In general, each class of sites will have different reaction rates associated with it; see Shaffer et al. (1997) [32]. It is difficult to estimate a complete set of kinetic constants for all active sites separately with

good statistical agreement. Therefore, the complicated kinetics of the multi-site ZN catalysts are often dealt with by lumping the kinetic constants of different types of active sites into one or into a reduced number of kinetic parameters. For the present study, the reaction mechanisms reported are considered with a lumped kinetic constant assuming "quasi-single" site approach.

Natta et al. (1959) [28] were among the first to report the effects of hydrogen on catalyzed olefin polymerizations. They performed polymerization of ethylene and propylene in the presence of hydrogen, using $TiCl_3$ and $AlEt_3$ or $AlEt_2Cl$ catalysts. The authors obtained the following formula for the rate of propylene polymerization with $TiCl_3/AlEt_3$,

$$R^H = R^o - \frac{1}{\frac{A}{\sqrt{pH_2}} + B} \tag{4.1}$$

In the case of M_n^{avg} for both PE and PP, the authors found that the experimental data were fitted well using the equation (4.2), which is similar in form to the Langmuir isotherm for dissociative adsorption.

$$\frac{1}{M_n^{avg}} = a + b\sqrt{pH_2} \tag{4.2}$$

The authors derived the equation (4.1) and (4.2) based on the fact that the chain termination and subsequent reinitiation could be represented by the following reaction mechanism, where PH represents the terminated chain [∇].

$$Cat - P + H_2 \longrightarrow Cat - H + PH \tag{4.3}$$

$$Cat - H + M \longrightarrow Cat - P \tag{4.4}$$

Based on this simple scheme, the authors attributed the observed rate decreases in the presence of hydrogen to slow reactivation of the Cat-H bond and demonstrated that the effect could be reversed by simply removing hydrogen. However, this mechanism does

[∇] A complete derivation of rate of polymerization and M_n^{avg} based on Natta's model is given in Appendix 4A.

not explain the existence of a term involving the square-root hydrogen pressure in the equation (4.1) and (4.2), respectively.

From the experimental findings, the authors derived that at steady state conditions the concentration of "Cat-H" actives sites will be a function of active sites concentration representing the "Cat-P" bond and partial pressure of hydrogen present during the reaction. For the presence of square-root dependency of hydrogen pressure in equation (4.1) and (4.2), the authors postulated the hypothesis that the hydrogen may be involved with the process of dissociative adsorption on the surface of catalyst, and further suggesting that a hydrogen atom participates in the rate determine step, for example see equation (4.4).

$$Cat - P + H_{ads} \longrightarrow Cat + PH \tag{4.5}$$

This assumes a pre-established equilibrium for the dissociative adsorption of hydrogen on the catalyst surface.

Dissociative adsorption of hydrogen on the catalyst surface:

$$H_2 \quad \underset{k_r}{\overset{k_f}{\rightleftharpoons}} \quad 2\,H_{ads} \tag{4.6}$$

Therefore,

$$H_{ads} = \sqrt{\frac{k_f}{k_r}}\sqrt{H_2} = \sqrt{K_H}\sqrt{H_2} \tag{4.7}$$

Keii (1972) [20] examined this hypothesis proposed by Natta et al. (1959) [28] by performing the hydrogen/deuterium exchange reaction on the surface of several $TiCl_3$/organo-metal catalyst types. The author observed a rapid equilibration of this exchange over the γ- $TiCl_3/Al(C_2H_5)_3$ catalyst type.

On the basis of relations shown in equation (4.2), Keii (1972 and 1984) [20, 21] and coworkers stated that the chain transfer reaction by hydrogen may be regarded as one of the elementary steps involved in the hydrogenation of olefins over metal surfaces. The authors interpreted their results using the Horiuti-Polanyi mechanism for olefin hydrogenations in which adsorbed hydrogen atoms attack the adsorbed alkyls; see Horiuti et al. (1934) [17]. Keii (1972) [20] has also reported that if the dissociative adsorption of

hydrogen does occur then it will result in a lowering of polymerization rate via two mechanisms: (i) reduction of number of active centers available for polymerization, and (ii) temporary deactivation of polymerization centers following the chain transfer.

In 1982, Soga et al. [39] proposed a different kinetic scheme for the transfer reaction of active polymer chains by hydrogen. However, they have postulated this hypothesis based on the experimental findings obtained for their catalyst type used during the polymerization; see their results stated in section 4.2.

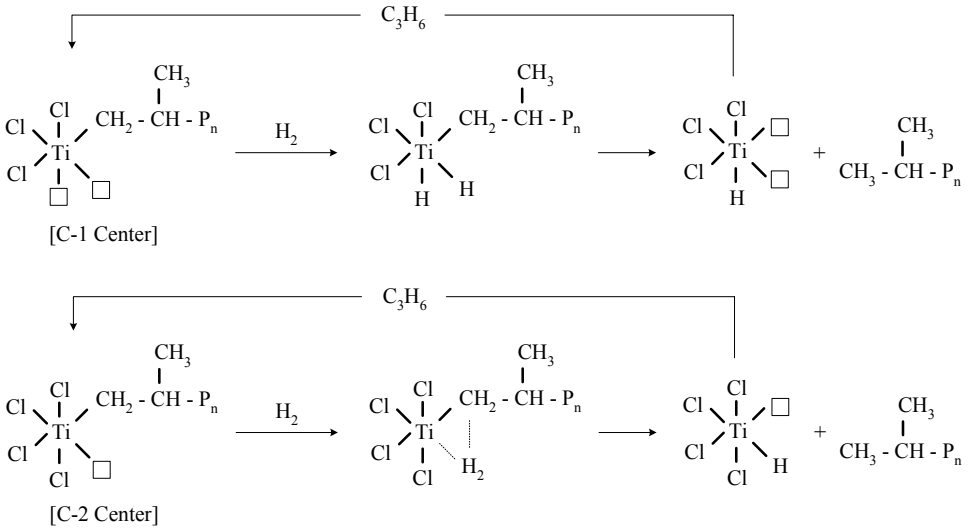

Figure 4.2: Mechanism for chain transfer by hydrogen proposed by Soga et al. (1982) [39].

The authors considered that the dissociative adsorption of hydrogen proceeds only on the C-1 center having two vacant sites. According to the authors perception the results obtained in their studies strongly suggest that a plausible mechanism for the chain transfer by hydrogen proceeds according to the model given Figure 4.2. It was also mentioned that addition of EB to the catalyst mixture leads to the blocking of one of the vacant sites of C-1 and consequently C-1 become inactive and turns into C-2.

Further, the investigation done by Busico et al. (1992) [9] on the catalytic polyinsertion of propylene in the presence of hydrogen revealed that propylene may propagate via 1,2-insertion (k_{pp} or k_{sp}) and/or 2,1- insertion (k_{ps} or k_{ss}). The propylene polyinsertion mechanism reported by the authors is presented in Figure 4.3.

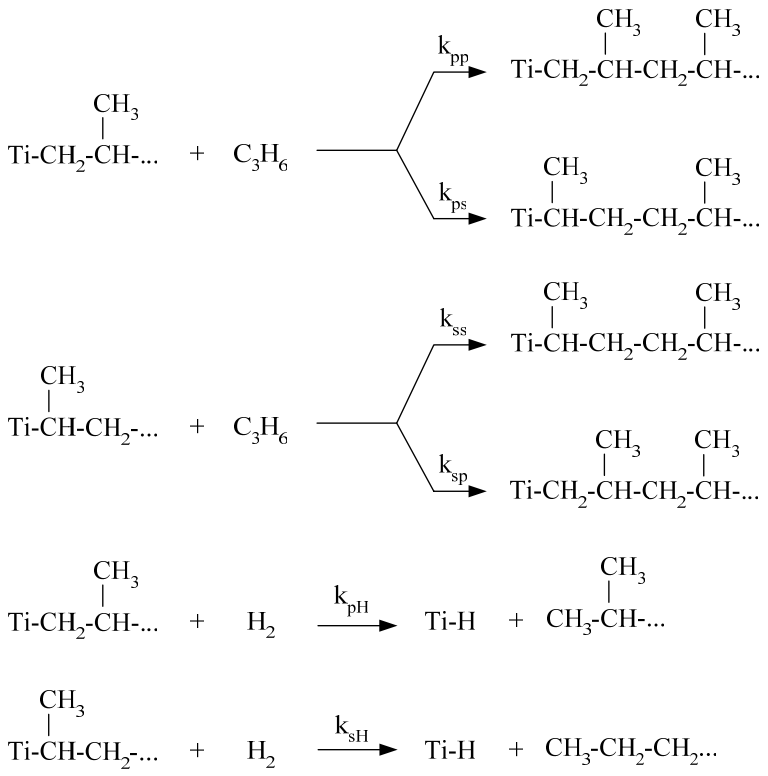

Figure 4.3: Propylene polyinsertion mechanism reported by Busico et al. (1992) [9].

The author demonstrated on basis of the analysis of gas chromatogram from such polymerization that each hydrooligomer with a given degree of polymerization can be put into one of the two categories. For instance, one containing all possible diastereoisomers from a regioregular 1,2- insertion mechanism, and the other containing all possible diastereoisomers created by a 1,2- insertion mechanism with a 2,1- inserted terminal end. Furthermore, these results were also supported by the end group analysis of Chadwick et al. (1994) [11].

Recently, Weickert et al. (2002) [47] modeled the effect of hydrogen on the reaction rate and (instantaneous) average molecular weight based on the "dormant site theory" along with a standard kinetic scheme and assuming a single site approach (see Table 4.1). The authors derived an equation for "q" leading to an expression that corresponds to Mayo equation, and also taken into account the deviation from Mayo equation for low hydrogen concentration region.

Table 4.1: Kinetic mechanism for catalytic propylene polymerization reported by Weickert et al. (2002) [47]

Chain propagation:	$C_j + M \xrightarrow{k_p} C_{j+1}$	*j = 0,1,2,…*
Chain transfer to hydrogen:	$C_j + H_2 \xrightarrow{k_h} C_0 + D_j$	*j = 1,2,3,…*
Chain transfer to monomer:	$C_j + M \xrightarrow{k_m} C_1 + D_j$	*j = 1,2,3,…*
Dormant site formation:	$C_j + M \xrightarrow{k_s} S_{j+1}$	*j = 0,1,2,…*
Dormant sites reactivation by H_2:	$S_j + H_2 \xrightarrow{k_{reh}} C_o + D_j$	*j = 1,2,3,…*
Dormant sites reactivation by monomer:	$S_j \xrightarrow[+M]{k_{rem}} C_j$	*j = 1,2,3,…*
Deactivation:	$C_j \xrightarrow{k_d} D_j$	*j = 0,1,2,…*

According to kinetic scheme presented in Table 4.1, the authors assumed that polymerization reaction starts with a rapid propagation step to generate active polymer chains (C_{j+1}) with chain length of j. Polymer molecular weight is controlled by chain transfer agent such as hydrogen to create a dead polymer chain (D_j) and a vacant active site. Chain transfer may also occur due to reaction with the monomer itself; however, such reaction leads to the formation of a live polymer chain of length unity (see Table 4.1).

In this mechanism, they have also considered the formation of dormant site (especially due to the mis-insertion of monomer). The response of hydrogen is derived based on the reactivation of dormant sites. Finally, the mechanism of deactivation may occur spontaneously (but with active sites only); see Table 4.1. For instantaneous modeling, the authors have neglected the deactivation reaction because of its larger time constant. Therefore, the increase in the R_{po} could be explained by increasing the overall concentration of active centers.

van Putten (2004) [44] has used the same kinetic mechanism as shown in Table 4.1, for describing the influence of hydrogen during the gas-phase propylene polymerization on the reaction rate and on the average molecular properties of the produced PP. On the basis of obtained experimental results, the author reported that the decreasing reaction rate at higher hydrogen concentration ($0.02 < X < 0.12$) could not be described by the kinetic model proposed by Weickert et al. (2002) [47]. The author has modeled this effect by considering the different initiation reaction for the Ti-H (Cat-H) bond assuming a slow insertion of first monomer (see equation (4.5) and (4.9)) together with the kinetic mechanism presented in Table 4.1.

Al-haj Ali et al. (2006) [2] used the same kinetic mechanism as shown in Table 4.1 and showed that kinetic model fits the experimental data with the good statistical agreement. However, the authors have performed the catalytic liquid-phase propylene polymerization tests at low hydrogen concentration (X = 0.0 to 0.01) compared to the gas-phase experiments performed by van Putten (2004) [44].

The kinetic model described by Weickert et al. (2002) [47] did not consider the square-root dependency for the reaction rate as well as for the average molecular properties of polymer. Therefore, the Natta's hypothesis given by equation (4.5) to (4.7) and further examined by Keii (1972) [20] can not be explained by using the reaction mechanism given in Table 4.1.

Several kinetic schemes reported above vary in their opinion especially in terms of hydrogen influence on the catalytic propylene polymerization, for example, from hydrogen adsorption hypothesis to the dormant site theory. Therefore, it is important to summarize the available information on the reaction mechanism, in order to understand the overall performance of the catalytic olefin polymerization process, qualitatively as well as quantitatively. In this chapter, relevant kinetic reactions are selected to represent the catalytic propylene polymerization process performed under near-industrial conditions. Basically, two different opinions in terms of kinetic modeling suggested by Natta et al. (1959) [28] and Weickert et al. (2002) [47] are studied together, to observe the hydrogen effect in more detail, on the performance of catalyst during the polymerization reactions.

In modeling the kinetics of propylene polymerization and the corresponding hydrogen influence, it is necessary to reconsider the standard kinetic scheme assuming a "quasi-single" site approach, for example see Table 4.1. It is unanimously assumed that polymerization of propylene with $MgCl_2$-supported ZN catalysts type involves a stepwise insertion of the monomer into a transition metal-carbon bond generating the active polymer chains (C_{j+1}) with chain length of j. Albizzati et al. (1996) [1] reported that coordination of the monomer to the transition metal before the insertion step is generally assumed. Such propagation reactions are shown in equation (4.8), (4.9) and (4.10). The reactions for first monomer addition (initiation) are considered separately (see equation (4.8) and (4.9)), and it is important especially in the case of initiation of active sites containing Ti-H bond (here, C_o^H).

Propagation:
first monomer unit (Initiation):

$$C_o + M \xrightarrow{k_i} C_1 \tag{4.8}$$

$$C_o^{\,H} + M \xrightarrow{k_{iH}} C_1 \tag{4.9}$$

additional units (Propagation):

$$C_j + M \xrightarrow{k_p} C_{j+1} \qquad (j = 1,2,3,...\infty) \tag{4.10}$$

The insertion of propylene in the metal-carbon bond may take place in two different ways, like 1,2- or primary insertion or 2,1- or secondary insertion (the so called "dormant site") (see Figure 4.4). Equation 4.11 shows the dormant site formation reaction with the addition of monomer unit to the active polymer chain, and results in the "slipping" polymer chain (S_{j+1}). The reactivation of dormant sites is reported usually due to hydrogen, and may be due to monomer (in an over-pressurized reactor system); see equation (4.12) and (4.13).

Dormant site formation reaction with:
monomer:

$$C_j + M \xrightarrow{k_{dm}} S_{j+1} \qquad (j = 0,1,2,3,...\infty) \tag{4.11}$$

Dormant site reactivation reaction by:
molecular hydrogen:

$$S_j + H_2 \xrightarrow{k_{rh}} C_o^{\,H} + D_j \qquad (j = 1,2,3,...\infty) \tag{4.12}$$

monomer:

$$S_j + M \xrightarrow{k_{rm}} C_{j+1} \qquad (j = 1,2,3,...\infty) \tag{4.13}$$

The relative importance of the different chain transfer reactions depends on the catalyst type used and on the process conditions. Following two types of chain transfer reactions are considered to be most important chain terminating process in propylene polymerization with heterogeneous catalysts.

Chain transfer reaction of an active polymer center with:
molecular hydrogen:

$$C_j + H_2 \xrightarrow{k_{th}} C_o^{\,H} + D_j \qquad (j = 1,2,3,...\infty) \tag{4.14}$$

monomer:

$$C_j + M \xrightarrow{k_{tm}} C_1 + D_j \qquad (j = 1,2,3,...\infty) \tag{4.15}$$

The spontaneous deactivation of an active catalyst is mainly considered with 1st order decay rate with respect to the overall catalyst concentration; see Weickert et al. (2002) [47].

Deactivation:

$$C_j \xrightarrow{k_d} D_j \qquad (j = 0,1,2,3,...\infty) \tag{4.16}$$

In the present study, an influence of adsorbed hydrogen is taken into account for two important reactions, such as: (i) dormant site reactivation reaction followed by chain transfer reaction and (ii) successive chain transfer reactions for active polymer chains. These reactions are shown in following equations,

Dormant site reactivation reaction followed by chain transfer reaction with adsorbed hydrogen:

$$S_j + H_{ads} \xrightarrow{k_{rah1}} S_j^{\,H} \qquad (j = 1,2,3,...\infty) \tag{4.17}$$

$$S_j^{\,H} + H_{ads} \xrightarrow{k_{rah2}} C_o^{\,H} + D_j \qquad (j = 1,2,3,...\infty) \tag{4.18}$$

Chain transfer reactions for active polymer chains with adsorbed hydrogen:

$$C_j + H_{ads} \xrightarrow{k_{tah1}} C_j^{\,H} \qquad (j = 1,2,3,...\infty) \tag{4.19}$$

$$C_j^{\,H} + H_{ads} \xrightarrow{k_{tah2}} C_o^{\,H} + D_j \qquad (j = 1,2,3,...\infty) \tag{4.20}$$

The “improved” kinetic model presented above consisting of equation (4.6) to (4.20), is used for modeling of hydrogen influence on initial reaction rate and molecular properties.

The "improved" kinetic model discussed in this section is a step-further in comparison with the kinetic model used by van Putten (2004) [44] and Al-haj Ali et al. (2006) [2], which includes the effect of dissociatively adsorbed as well as molecular hydrogen on the activity and molecular properties, too. The developed kinetic model is quite flexible in terms of selecting the reaction mechanism, and thus can be reduced to different forms applicable for the analysis of an experimental data together with different process parameters such as temperature, pressure, monomer concentration, etc.

4.4 Model for initial polymerization rate

The "improved" kinetic model (see section 4.3) explains the influence of various chemical constituents on the interpretation of overall polymerization rate. The assumption used here are similar to those reported (earlier) by Natta et al. (1959), Keii (1972) and Weickert et al. (2002) [20, 28, 47] (also see assumption reported in Chapter 3). The hypothesis of long chain polymerization has been used in defining the reaction rate [2, 44]. Therefore,

$$R_p = k_p M C \tag{4.21}$$

On the basis of the "improved" kinetic mechanism proposed in section 4.3, an instantaneous active site concentration (C) after the mass of preactivated catalyst injected to the completely filled reactor with liquid propylene will be,

$$C = C_{max} - S - C_o^H \tag{4.22}$$

The quasi steady state assumption [47] is applied to obtain the net reaction rate for dormant sites based on the kinetic model shown above, and can be written as,

$$rS = 0 = k_{dm} M C - k_{rm} M S - k_{rh} H_2 S - k_{rah1} \sqrt{K_H} \sqrt{H_2} S \tag{4.23}$$

The resulting dormant site concentration (S) according to equation (4.23), will be,

$$S = \left[\frac{k_o}{1 + k_1 X + k_2 \frac{\sqrt{X}}{\sqrt{M}}} \right] C \tag{4.24}$$

where,

$$k_o = \frac{k_{dm}}{k_{rm}} \qquad k_1 = \frac{k_{rh}}{k_{rm}} \qquad k_2 = \frac{k_{rah1}\sqrt{K_H}}{k_{rm}} \qquad X = \frac{H_2}{M} \tag{4.25}$$

Similarly, the quasi steady state assumption is applied to obtain the concentration of C_o^H,

$$rC_o^H = 0 = k_{th} H_2 C + k_{tah2}\sqrt{K_H}\sqrt{H_2} C^H + k_{rh} H_2 S + k_{rah2}\sqrt{K_H}\sqrt{H_2} S^H - k_{iH} M C_o^H \tag{4.26}$$

$$C_o^H = \frac{k_{th}}{k_{iH}}\frac{H_2}{M} C + \frac{k_{tah2}\sqrt{K_H}}{k_{iH}}\frac{\sqrt{H_2}}{M} C^H + \frac{k_{rh}}{k_{iH}}\frac{H_2}{M} S + \frac{k_{rah2}\sqrt{K_H}}{k_{iH}}\frac{\sqrt{H_2}}{M} S^H \tag{4.27}$$

The concentrations of C^H and S^H can be derived as,

$$rC^H = 0 = k_{tah1}\sqrt{K_H}\sqrt{H_2} C - k_{tah2}\sqrt{K_H}\sqrt{H_2} C^H \tag{4.28}$$

$$C^H = \frac{k_{tah1}}{k_{tah2}} C \tag{4.29}$$

and,

$$rS^H = 0 = k_{rah1}\sqrt{K_H}\sqrt{H_2} S - k_{rah2}\sqrt{K_H}\sqrt{H_2} S^H \tag{4.30}$$

$$S^H = \frac{k_{rah1}}{k_{rah2}} S \tag{4.31}$$

Substituting the derived form of C^H and S^H into equation (4.27),

$$C_o^H = k_3 X C + k_4 \frac{\sqrt{X}}{\sqrt{M}} C + k_5 X S + k_6 \frac{\sqrt{X}}{\sqrt{M}} S \tag{4.32}$$

where,

$$k_3 = \frac{k_{th}}{k_{iH}} \qquad k_4 = \frac{k_{tah1}\sqrt{K_H}}{k_{iH}} \qquad k_5 = \frac{k_{rh}}{k_{iH}} \qquad k_6 = \frac{k_{rah1}\sqrt{K_H}}{k_{iH}} \tag{4.33}$$

The concentration of C can be obtained from equation (4.22), (4.24) and (4.32),

$$C = \frac{C_{\max}\,(1+k_1\,X+k_2\,\frac{\sqrt{X}}{\sqrt{M}})}{1+k_o+(k_1+k_3+k_ok_5)\,X+(k_2+k_4+k_ok_6)\,\frac{\sqrt{X}}{\sqrt{M}}+k_2k_4\,\frac{X}{M}+(k_1k_4+k_2k_3)\,\frac{X^{1.5}}{\sqrt{M}}+k_1k_3\,X^2} \tag{4.34}$$

Therefore, according to equation (4.21), the initial rate of polymerization (R_{po}) in the presence of hydrogen will be,

$$R_{po}(H_2) = \frac{k_p\,M_o\,C_{\max}\,(1+k_1\,X+k_2\,\frac{\sqrt{X}}{\sqrt{M}})}{1+k_o+(k_1+k_3+k_ok_5)\,X+(k_2+k_4+k_ok_6)\,\frac{\sqrt{X}}{\sqrt{M}}+k_2k_4\,\frac{X}{M}+(k_1k_4+k_2k_3)\,\frac{X^{1.5}}{\sqrt{M}}+k_1k_3\,X^2} \tag{4.35}$$

In the absence of hydrogen, i.e. at X value of 0, R_{po} (0) from equation (4.35) then be,

$$R_{po}(0) = \frac{k_p\,M_o\,C_{\max}}{(1+k_o)} \tag{4.36}$$

Therefore, rearranging equation (4.35) and (4.36) will give an "improved" (roof) model for R_{po} in the presence of hydrogen and can be represented as,

$$R_{po}(H_2) = \frac{R_{po}(0)\left(1+k_1\,X+k_2\,\frac{\sqrt{X}}{\sqrt{M}}\right)}{\left(1+K_a\,X+K_b\,\frac{\sqrt{X}}{\sqrt{M}}+K_c\,\frac{X}{M}+K_d\,\frac{X^{1.5}}{\sqrt{M}}+K_e\,X^2\right)} \tag{4.37}$$

where,

$$K_a = \frac{(k_1+k_3+k_ok_5)}{(1+k_o)} \quad K_b = \frac{(k_2+k_4+k_ok_6)}{(1+k_o)} \quad K_c = \frac{(k_2k_4)}{(1+k_o)} \quad K_d = \frac{(k_1k_4+k_2k_3)}{(1+k_o)}$$

$$K_e = \frac{(k_1k_3)}{(1+k_o)} \tag{4.38}$$

An equation (4.37) for R_{po} represents the combination of hydrogen adsorption hypothesis together with a dormant site theory. Especially, the effect of adsorbed and molecular hydrogen is considered on the "waking-up" of the dormant sites, as well as on the chain transfer of the "operational" catalyst sites. Several schemes for R_{po} were developed by selecting the required kinetic reactions shown in section 4.3.

Table 4.2: Kinetic schemes for R_{po} [i, ii, iii]

Scheme	Conditions	Final equation
I	-	Equation (4.37)
II	Set $k_{th} = 0$ and $k_{rh} = 0$, thus $K_a = 0$, $K_d = 0$ and $K_e = 0$	$R_{po}(H_2) = \frac{R_{po}(0)\left(1 + k_2 \frac{\sqrt{X}}{\sqrt{M}}\right)}{\left(1 + K_b \frac{\sqrt{X}}{\sqrt{M}} + K_c \frac{X}{M}\right)}$
III	Set $k_{tah1} = 0$, $k_{tah2} = 0$, $k_{rah1} = 0$ and $k_{rah2} = 0$, thus $K_b = 0$, $K_c = 0$ and $K_d = 0$	$R_{po}(H_2) = \frac{R_{po}(0)\left(1 + k_1 X\right)}{\left(1 + K_a X + K_e X^2\right)}$
IV	$C = C_{max} - S$ and $k_{iH} = k_i$, therefore constants k_3, k_5, K_e are neglected. Set $k_{tah1} = 0$, $k_{tah2} = 0$, $k_{rah1} = 0$ and $k_{rah2} = 0$, thus $K_b = 0$, $K_c = 0$ and $K_d = 0$	$R_{po}(H_2) = \frac{R_{po}(0)\left(1 + k_1 X\right)}{\left(1 + K_a X\right)}$

i. Initiation reaction shown in equation (4.8) is instantaneous. ii. Long chain hypothesis is used for rate of polymerization. iii. Required component concentration is determined based on the quasi steady state assumption for the respective reaction rates.

The individual effect of adsorbed and molecular hydrogen on the reaction kinetic can be discussed using Scheme II and Scheme III, respectively. Scheme III shown in Table 4.2 is resembled to the kinetic model used by van Putten (2004) [44]. Scheme IV only takes into account the dormant site theory and also assumes that initiation velocity for C_o and C_o^H is the same in contrast to the other schemes, and thus, represents the model same as used by Weickert et al. (2002) [47]. All the schemes are reported in Table 4.2 and they were fitted with the experimental data of reaction rate determined over a wide range of hydrogen concentration.

4.5 Model for average chain termination probability

The term "q" is dependent on the type of catalyst and the process conditions, like temperature, pressure, hydrogen concentration, etc. Therefore, adopting the kinetic mechanism described by equation (4.6) to (4.20), the parameter q can be related to the polymerization kinetic rates and polymerization conditions. This parameter is usually described as the ratio of all transfer rates to the propagation rate. It is well known that different types of chain transfer reaction are observed in the coordination polymerization, such as β-hydrogen transfer to the metal and monomer, chain transfer to alkylaluminum, chain transfer with hydrogen and chain transfer with the monomer. However, it is expected that chain transfer reactions with hydrogen and monomer as well as the dormant site formation and its reactivation are more effective ones (as their direct consequences on the reaction kinetic can be seen) than other kind of termination reactions stated above. Therefore, only selected reactions are chosen in modeling the hydrogen influence on q.

With the quasi steady state assumption, according to the reaction mechanism proposed above the net reaction rate for an active site with the chain length of j can be written as,

$$rC_j = 0 = k_p M C_{j-1} - k_p M C_j - k_{tm} M C_j - k_{th} H_2 C_j - k_{tah1} \sqrt{K_H} \sqrt{H_2} C_j - k_{dm} M C_j + k_{rm} M S_{j-1} \tag{4.39}$$

Similarly, the net reaction rate for dormant site can be obtained by rewriting equation (4.23) for the chain length of j leads to,

$$rS_j = 0 = k_{dm} M C_{j-1} - k_{rm} M S_j - k_{rh} H_2 S_j - k_{rah1} \sqrt{K_H} \sqrt{H_2} S_j \tag{4.40}$$

Equation (4.40) will give the concentration of dormant sites with chain length of j,

$$S_j = \left[\frac{k_{dm} M}{k_{rm} M + k_{rh} H_2 + k_{rah1} \sqrt{K_H} \sqrt{H_2}} \right] C_{j-1} \tag{4.41}$$

Combining equation (4.39) and (4.41), and rearranging,

$$\left(k_p\,M + k_{tm}\,M + k_{th}\,H_2 + k_{tah1}\sqrt{K_H}\,\sqrt{H_2} + k_{dm}\,M\right) C_j = \left(k_p\,M + k_{rm}\,M\left[\frac{k_{dm}\,M\,\alpha}{k_{rm}\,M + k_{rh}\,H_2 + k_{rah1}\sqrt{K_H}\,\sqrt{H_2}}\right]\right) C_{j-1} \tag{4.42}$$

or, in terms of average chain propagation probability (p),

$$C_j = p\,C_{j-1} \tag{4.43}$$

The q can now be determined by,

$$q = 1 - p \tag{4.44}$$

Combining and rearranging equations (4.42), (4.43) and (4.44), and implementing the long chain hypothesis results in the "improved" (roof) model of q,

$$q = \left[\frac{k_{tm}}{k_p} + \frac{k_{th}}{k_p}\frac{H_2}{M} + \frac{k_{tah1}\sqrt{K_H}}{k_p}\frac{\sqrt{H_2}}{M} + \frac{k_{dm}}{k_p}\left(1 - \frac{\alpha}{1 + k_1\,X + k_2\dfrac{\sqrt{X}}{\sqrt{M}}}\right)\right] \tag{4.45}$$

or,

$$q = \left[A_1 + A_2\,X + A_3\frac{\sqrt{X}}{\sqrt{M}} + \left(\frac{A_4 + A_5\,X + A_6\dfrac{\sqrt{X}}{\sqrt{M}}}{1 + k_1\,X + k_2\dfrac{\sqrt{X}}{\sqrt{M}}}\right)\right] \tag{4.46}$$

where,

$$A_1 = \frac{k_{tm}}{k_p} \qquad A_2 = \frac{k_{th}}{k_p} \qquad A_3 = \frac{k_{tah1}\sqrt{K_H}}{k_p} \qquad A_4 = \frac{k_{dm}}{k_p}(1-\alpha) \qquad A_5 = \frac{k_{dm}\,k_1}{k_p} \qquad A_6 = \frac{k_{dm}\,k_2}{k_p} \tag{4.47}$$

Table 4.3: Kinetic schemes for q [i, ii, iii]

Scheme	Conditions	Final equation
I	-	Equation (4.46)
II	Set $k_{th} = 0$ and $k_{rh} = 0$, thus $A_2 = 0$ and $A_5 = 0$	$q = \left[A_1 + A_3 \frac{\sqrt{X}}{\sqrt{M}} + \left(\frac{A_4 + A_6 \frac{\sqrt{X}}{\sqrt{M}}}{1 + k_2 \frac{\sqrt{X}}{\sqrt{M}}} \right) \right]$
III / IV	Set $k_{tah1} = 0$, $k_{tah2} = 0$, $k_{rah1} = 0$ and $k_{rah2} = 0$, thus $A_3 = 0$ and $A_6 = 0$	$q = \left[A_1 + A_2 X + \left(\frac{A_4 + A_5 X}{1 + k_1 X} \right) \right]$
V	k_{rm}, k_o, k_1, k_2 are neglected. Set $k_{th} = 0$, $k_{dm} = 0$, $k_{rh} = 0$, $k_d = 0$, $k_{rah1} = 0$ and $k_{rah2} = 0$, thus $A_2 = 0$ and $A_4 = 0$ $A_5 = 0$ and $A_6 = 0$	$q = \left[A_1 + A_3 \frac{\sqrt{X}}{\sqrt{M}} \right]$
VI	k_{rm}, k_o, k_1, k_2 are neglected. Set $k_{dm} = 0$, $k_{rh} = 0$, $k_d = 0$, $k_{tah1} = 0$, $k_{tah2} = 0$, $k_{rah1} = 0$ and $k_{rah2} = 0$, thus $A_3 = 0$, $A_4 = 0$, $A_5 = 0$ and $A_6 = 0$	$q = \left[A_1 + A_2 X \right]$

i. Initiation reaction shown in equation (4.6) is instantaneous. ii. Long chain hypothesis is used for rate of polymerization. iii. Required component concentration is determined based on the quasi steady state assumption for the respective reaction rates.

The expression for q shown in equation (4.46) can be divided into parts, the first part will be the termination probability obtained from chain transfer reactions (i.e., q_{min}), and the second part describing the effect on the molecular properties comes from the dormant sites theory (i.e., dq).

$$q_{\min} = \left(A_1 + A_2 X + A_3 \frac{\sqrt{X}}{\sqrt{M}} \right) \tag{4.48}$$

$$dq = \left(\frac{A_4 + A_5 X + A_6 \frac{\sqrt{X}}{\sqrt{M}}}{1 + k_1 X + k_2 \frac{\sqrt{X}}{\sqrt{M}}} \right) \tag{4.49}$$

Similar to reaction rate, different schemes were developed by selecting the required kinetic reactions shown in section 4.3. The scheme I includes all the kinetic reactions explained above, and thus the final form for q is obtained as given in equation (4.46). The individual effect of adsorbed and molecular hydrogen on the chain termination can be discussed using Scheme II and Scheme III/IV, respectively. Scheme III/IV shown in Table 4.3 is resembled to the kinetic model used by van Putten (2004) [44] and Al-haj Ali et al. (2006) [2]. Scheme V only takes into account the Natta's hypothesis and thus, represent the similar model equation as used by Natta et al. (1959) [28]. The linear approach is shown by Scheme VI in which the chain transfer reaction with molecular hydrogen and monomer is only considered as a chain terminating reactions. All the schemes are reported in Table 4.3 and they were fitted with the experimental data of q estimated over a wide range of hydrogen concentration.

4.6 Model analysis

The model analysis is done based on the experimental data obtained from the catalytic liquid-phase propylene polymerization. In order to understand the kinetic model performance for the hydrogen influence, polymerization tests for liquid propylene were carried out with a wide range of hydrogen concentrations using $MgCl_2/TiCl_4$/Phthalate – TEA/Silane catalyst type. For the present study, X values representing the mole ratio of hydrogen to liquid propylene were varied from 0 to 0.1 [⊗].

All the experiments were performed in an over pressurized (completely filled) reactor with liquid propylene and therefore the injected amount of hydrogen was believed to be completely dissolved in the liquid propylene. Experimental conditions and results are reported in Chapter 3.

In the present work, the "improved" kinetic model given in section 4.3 was used for deriving kinetic models for reaction rate as well as average probability of chain termination. Several schemes for R_{po} are discussed in section 4.4, and are developed based on the literature studies described above.

[⊗] This is an extremely wide range compared to the data published so far; see for example Samson et al. (1999), Pater (2001) and Al-haj Ali et al. (2006) [2, 29, 31].
Note: The results discussed in the section 4.6 concerning the influence of hydrogen on the catalyst activity and polymer properties are valid for the X values ranging between 0.0 and 0.1.

4.6.1 Catalyst activity

First, let us revise the fact reported in Chapter 3 that the catalyst activity enhances with increasing concentration of hydrogen, up to the X values of 0.01, during the propylene polymerization. Until the X value of 0.002, the obtained results on catalyst activity exhibit the similar accelerating effect in the initial activity of the catalyst during the polymerization tests, which were carried out in the presence of hydrogen and at different reaction temperatures (see Chapter 3). This effect can be clearly seen from the Figure 4.4 in which the normalized R_{po} (determined at different temperatures) is plotted against the X values. Figure 4.4 also shows that between the X values of 0.002 and 0.012 the enhancement in the initial catalyst activity levels off.

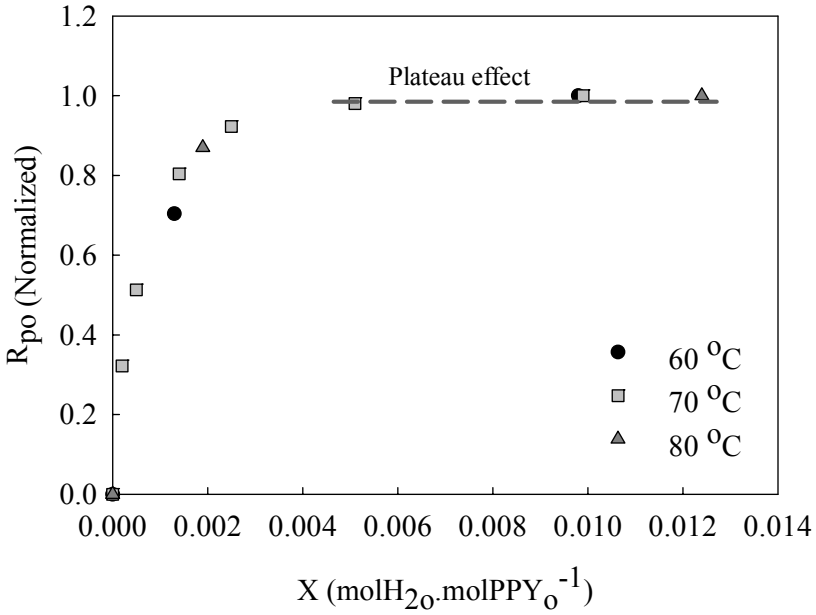

Figure 4.4: Normalized R_{po} as function of X obtained from batch reactor data.

For X values ranging between 0.015 and 0.1, the striking effect of hydrogen on the catalyst activity can be seen from the Figure 4.5. It was noticed that the catalyst activity seem to be decreased by 14 % as the X value increased from 0.01 to 0.02, and further decreases to 86 and 61.5 ($kg.gCat^{-1}.hr^{-1}$) at the X values of 0.05 and 0.1, respectively. However, at present, these effects have been only studied for reaction temperatures of 70 ^oC. So to conclude, the hydrogen influence on catalyst activity can be classified into two regions, such as, "activation effect" up to the X value of 0.01 and above this value of X a "retardation effect". Although the direction and magnitude of the hydrogen effect varies

from one catalyst/donor/monomer type to another, the bulk of experimental data using today's higher activity $TiCl_4$ catalysts show that hydrogen enhances the polymerization rate for propylene (particularly at low hydrogen concentration) [□]. Very few authors [14, 19, 28, 39, 44] observed the decreasing reaction rate with increasing hydrogen concentration.

The results obtained by van Putten (2004) [44], see Figure 4.1 and show a similar response of the catalyst activity towards hydrogen. It is important to note that the author used the same catalyst type as used in this work. However, the magnitude of the hydrogen effect on catalyst activity observed in her study is 3 fold lower in comparison with findings presented in Figure 4.5.

Table 4.4: Constants used in the kinetic models for R_{po} at 70 ^oC [*]

Constants	Scheme I	Scheme II	Scheme III	Scheme IV
k_1	47		16568	20080.6
k_2	4521	4875		
K_a	119.2		1323.5	1849.3
K_b	5.37	0.000862		
K_c	3766	64360		
K_d	260.3			
K_e	384.3		26649.5	

[*] Shown in Table 4.2 and Figure 4.5.

Figure 4.5 and Figure 4.6 indicate that model predictions for R_{po} by Scheme I, and found to be in good statistical agreement with the experimental values, at least at 70 ^{o}C. Scheme II and Scheme III representing the individual effect of adsorbed and molecular hydrogen, respectively; also seem to be in agreement with the obtained experimental values. However, at X value of 0.1, the predicted values for R_{po} by Scheme II showed a deviation

[□] Chadwick et al. (1994) [11] reported that several researchers has observed the hydrogen activation effect when using $MgCl_2/TiCl_4$/ Phthalate ester – TEA/Alkoxysilane type catalyst for performing propylene polymerization. However, a more precise description on catalyst types can be found in Busico et al. (1992), Chadwick et al. (1995) and Chadwick et al. (1996) [9, 12, 13].

of about 11 % in comparison with the experimental value. The constants estimated from the experimental data fitting are given in Table 4.4 and Table 4.5.

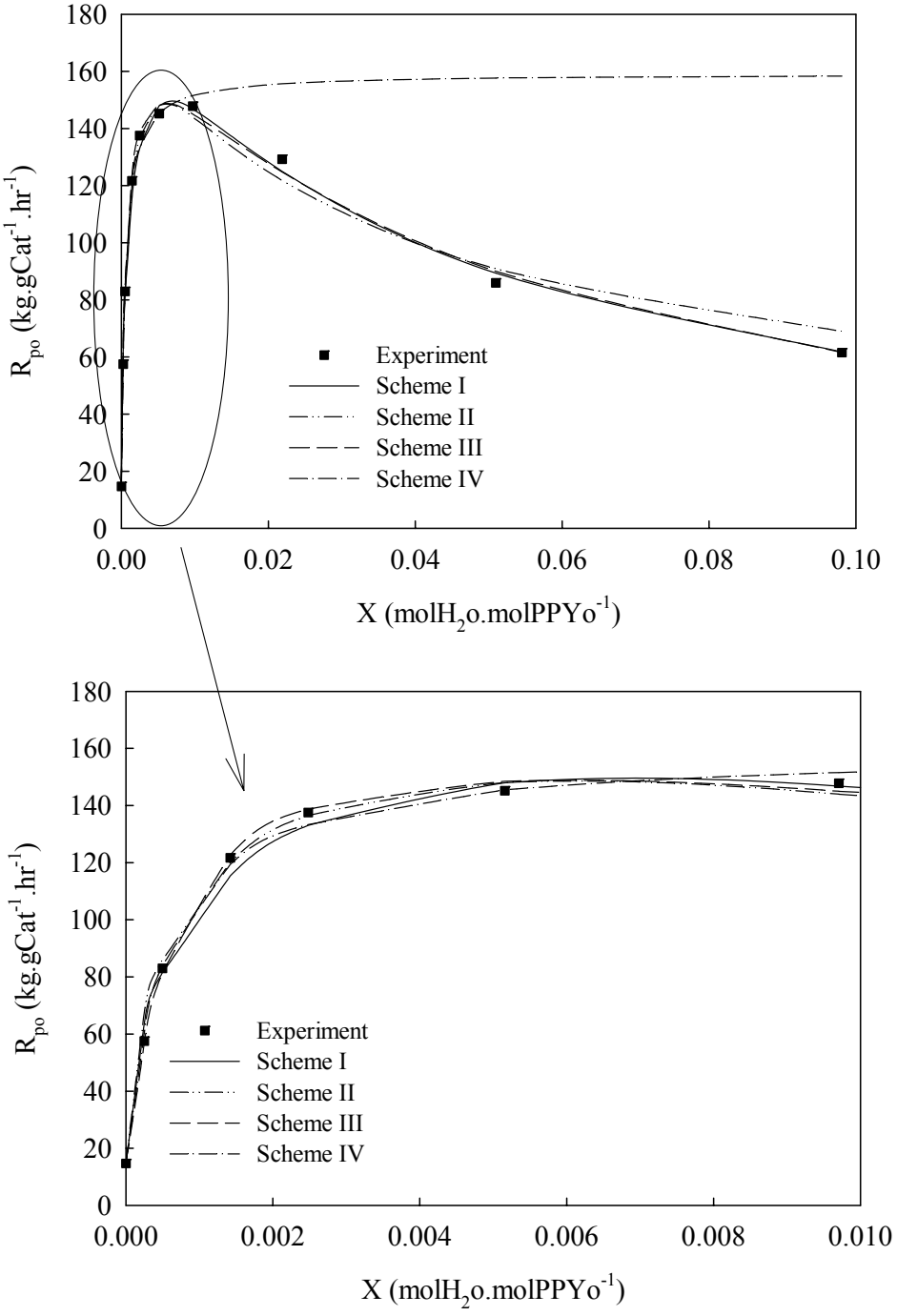

Figure 4.5: Analysis of kinetic models for R_{po} over a wide range of X values at 70 °C (schemes for R_{po} are shown in Table 4.2 and experimental values are provided in Chapter 3).

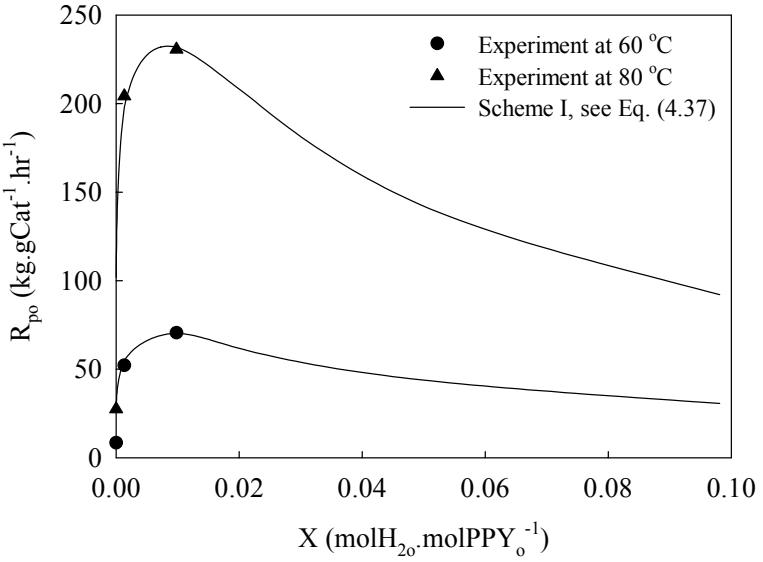

Figure 4.6: Model predictions for R_{po} over a wide range of X values at 60 and 80 ^{o}C, respectively (experimental values are provided in Chapter 3).

Table 4.5: Constants used in the kinetic roof model for R_{po} [*]

Constants	**Scheme I (at 60 ^{o}C)**	**Scheme I (at 80 ^{o}C)**
k_1	25	37
k_2	3821	3509
K_a	109	102.9
K_b	2.8	7.6
K_c	8766	2866
K_d	75.3	473.5
K_e	295	560

[*] Shown in Table 4.2 and Figure 4.6

On the other hand, the conditions adopted by Scheme IV exhibit a strong influence on the prediction of R_{po} mainly above the X values of 0.01; see Figure 4.5. The model predicts the "plateau" effect for R_{po} even at high concentrations of hydrogen. This effect is explained by several researchers, however not in the range of hydrogen concentration used in this study. For example, Al-haj Ali et al. (2006) [2] explained this plateau effect by reviewing the fact that in the presence of hydrogen a limiting maximum number of active centers are realized in the catalyst types, and further stated that the concentration of the blocked sites is very low at high hydrogen concentrations. However, this does not seem to be in agreement with the experimental findings of this work. The rate expression according to Scheme IV predicted a high R_{po} values with the deviation of 17 %, 46 % and 61 % in comparison with the data points noted at X values of 0.02, 0.05 and 0.1, respectively.

The analysis of all the schemes at low values of X (< 0.01) revealed that the "activation effect" of hydrogen on the catalyst should indeed discover from the reactivation of dormant sites in the presence of hydrogen. A careful but qualitative inspection of the values of kinetic constants k_1 and k_2 present in equation (4.37) explained this phenomenon very well (see also Table 4.4 and Table 4.5). For example, in case of the simple kinetic expression given by Scheme IV, it is observed that the estimated values of k_1 seems to be factor 10 higher than K_a, thus depicting that the influence of hydrogen on the waking-up of dormant sites is the rate determining step, especially when the X values are considered below 0.01. However, the estimation of these kinetic constants will depend on the hypothesis made during the kinetic modeling. This clearly indicates that with a wide range of hydrogen concentration during the polymerization runs, the nature of hydrogen attached to the polymerization center and its subsequent effect are the important factors in analyzing the reaction rates.

At high hydrogen concentrations, the so-called "retardation effect" on catalyst activity during propylene polymerization was observed in this work; see Figure 4.5, and very few authors have reported this phenomena. The literatures stated above exhibit operational limitations may be with respect to the experimental set-ups, or may be due to the scope of research.

The model prediction by first three schemes over a wide range of X values seems to explain the decreasing trend in R_{po}. For instance, in a Scheme III, the kinetic constant K_e showed a high value as compared to the other kinetic constants. The K_e parameter is

defined with different individual kinetic constants representing a relation between the formation of total number of active metal-hydride bond due to the transfer and reactivation reaction with molecular hydrogen, and its reinitiation for further propagation with monomer. The term k_{iH} involved in defining the K_e is happened to be important in analyzing the performance of catalyst activity especially at high hydrogen concentrations.

Qualitatively, the high value of K_e for Scheme III (Table 4.4) may be resulted due to the slow recovery of these active metal-hydride bonds, meaning the term k_{iH} should have a relatively very low value compared to other kinetic constants (see equation (4.38)). The high value was also observed for the term K_c used in Scheme II (Table 4.4) representing the similar kinetic phenomena in analyzing the catalyst activity, however, this kinetic constant deal with the influence of adsorbed hydrogen (see equation (4.38)).

From the above discussion, it can be clearly noticed that in the low range of hydrogen concentration the reactivation of dormant sites is the broadly acknowledged reason for increasing the catalyst activity by "freeing" the blocked polymerization sites. On the other hand, at higher hydrogen concentration, the distinct effect of adsorbed as well as molecular hydrogen seems to play a role in deciding the nature of produced active sites due to the hydrogen chain transfer. Therefore, during reaction, the delay in recovery of some of the active sites, which are attached to the hydrogen, could act as a rate determining step.

4.6.2 Average chain termination probability

The q values were estimated based on the instantaneous values of weight-average molecular weight (M_w^{avg}); see Appendix 4B. At low hydrogen concentration ($0.0 < X < 0.01$), the dependency of q is steep and increases rapidly with increasing X value. However, as X value increases further ($0.01 < X < 0.1$), its effect on molecular weight seem to get slightly dampens out, and thus, leads to classify a hydrogen response on q with two distinct regions. This transition of q can also be classified from the decreasing response of catalyst activity in the high hydrogen concentration region, suggesting that the slow recoveries of active sites, which are attached to the hydrogen. Therefore, as polymerization reaction proceeds, the polymer chain initiated from these active centers will probably exhibit a subsequent delay in the chain termination of these chains.

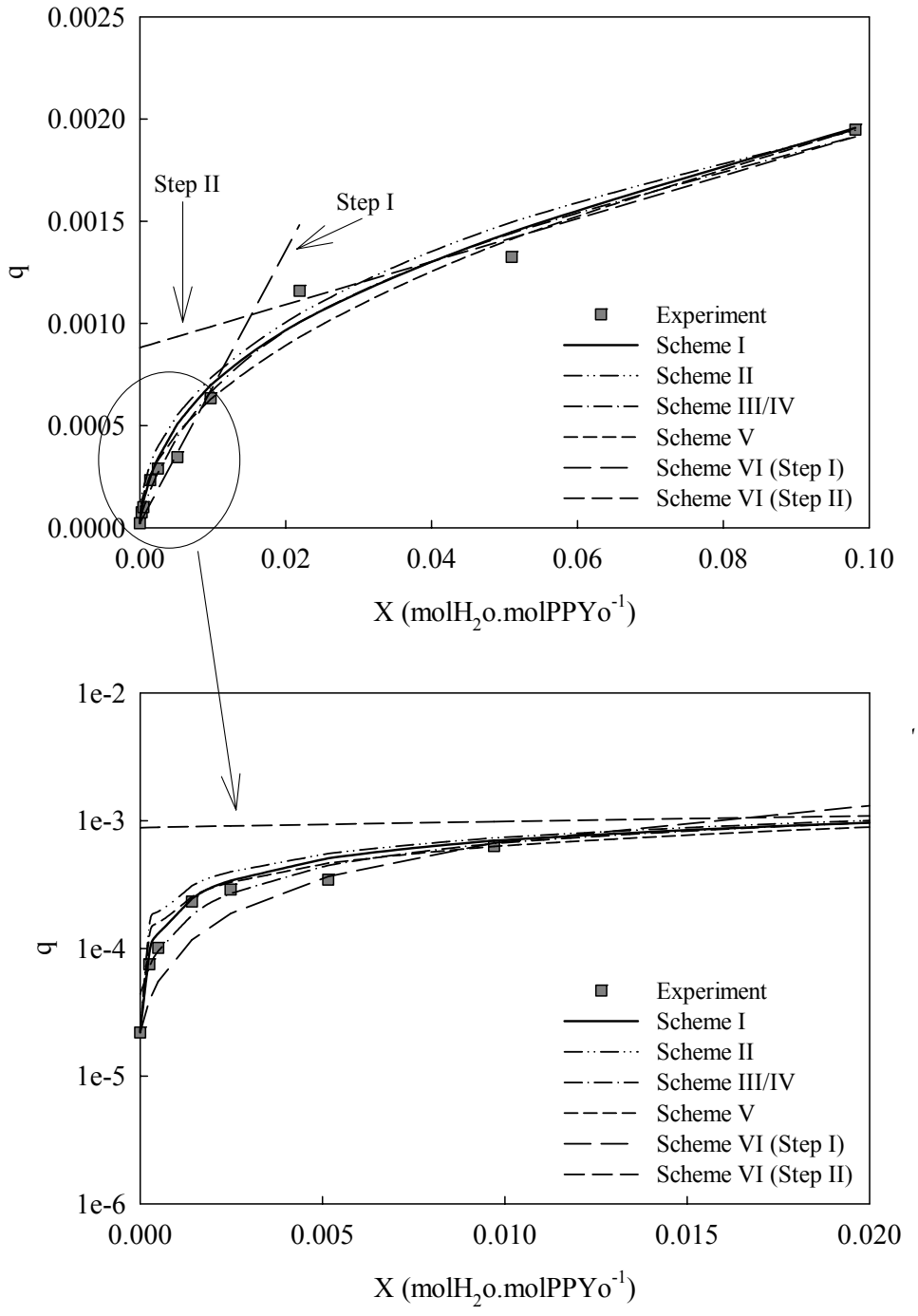

Figure 4.7: Analysis of kinetic models for q over a wide range of X values at 70 °C (schemes for q are shown in Table 4.3).

The simplest check is possible using a Scheme VI given in Table 4.3, allowing a two-step linear approach for a raw interpretation of q estimated over a wide range of X values. From the determined constants for Scheme VI given in Table 4.6, it indicates that a chain transfer ability of hydrogen is factor 6 times higher in step I (at X < 0.01) compared to step II (X>0.01). In step II, it is interesting to note that the chain transfer reaction due to monomer happens to play an important role, however, this hypothesis is constructed only based on the estimated slope values; see Table 4.6. According to step II, the value of parameter q at X value of 0.0 is much higher than predicted by other schemes, and considered to be an extrapolation mistake. This two-step linear approach deviate in their respective regimes, like step I predicted the higher values of q for the X values > 0.01 and similarly step II calculated the higher values of q for the X values < 0.01. These deviations are reported in Table 4.7. The complexities involved due to the presence of hydrogen in the polymerization of propylene using $MgCl_2$-supported ZN type catalyst cannot be explained by a linear approach shown by Scheme VI. The complexities mainly concerning the chain transfer reaction caused either by an adsorbed or by the molecular hydrogen present during the reaction; see Keii (1972) [20]. Therefore, several schemes were derived in order to interpret the result obtained for q, and they are tabulated in Table 4.3.

Table 4.6: Constants used in the kinetic models for q at 70 ^oC [*]

Constants	Scheme I	Scheme II	Scheme III/IV	Scheme V	Scheme VI (Step I)	Scheme VI (Step II)
k_1	137.522		79.89811			
k_2	249.706	25.533079				
A_1	0.000022	0.000022	0.000022	0.000022	0.000022	0.000881
A_2	0.00652146		0.007838841		0.06666	0.010519
A_3	0.0233723	0.033496047		0.12601829		
A_4	1.73609E-9	5.601885E-9	2.176136E-5			
A_5	0.171744		0.1010212			
A_6	0.0205736	0.12816481				

[*] Shown in Table 4.3 and Figure 4.7.

Table 4.7: % deviation for q calculated for all the schemes used in modeling q with reference to experimental q values at 70 ^{o}C.

X ($molH_2o.molPPYo^{-1}$)	Scheme I	Scheme II	Scheme III/IV	Scheme V	Scheme VI (Step I)	Scheme VI (Step II)
0.000000	0.24	0.26	99.38	0.23	0.23	3915.08
0.000249	18.77	92.96	7.07	58.29	48.73	1074.97
0.001421	5.00	32.70	22.05	9.07	49.90	284.62
0.002481	17.28	37.26	7.12	13.59	35.24	213.54
0.009707	9.98	15.59	4.53	0.83	5.55	55.13
0.021900	13.24	9.74	13.22	19.51	27.80	4.12
0.051000	9.16	12.79	8.74	6.57	158.15	6.96
0.098100	0.44	0.16	1.71	0.13	236.81	1.79

Schemes I to IV for q have been derived using the similar assumption applied while deriving the schemes for R_{po}. Scheme I for q has been formulated considering a complete "improved" kinetic model discussed in the section 4.3 of this chapter. The kinetic models used by van Putten (2004) [44] and Al-haj Ali et al. (2006) [2] led to the common equation for q, and can be seen from Scheme III/IV given in Table 4.3. The implication of Natta's hypothesis regarding the effect of adsorbed hydrogen on the molecular properties of polymer can be obtained in the form of Scheme II and V for q, wherein, Scheme II also considers the effect of dormant polymerization centers on the molecular weights of polymer (shown in Table 4.3).

Figure 4.7 shows that Scheme I indicate an optimum fit for q values over a wide range of X values. In addition, the other schemes such as II, III/IV and V exhibit a good agreement with the experimental findings for q. However, these schemes seem to be deviating at few values of X (especially in the lower regime); see Figure 4.7. This can be observed from the % deviation values given in Table 4.7.

From the comparison of constants obtained for Scheme II and III/IV (see Table 4.6), it has been understood that the individual influence of adsorbed as well as molecular hydrogen on the dormant site reactivation and their successive chain transfer is compensative, and presumed that an equilibrium condition is obtained between an adsorbed and the molecular hydrogen. This effect may be more pronounced in the high hydrogen concentration region ($0.01 < X < 0.1$).

4.7 Catalyst decay behavior

The deactivation behavior of the catalyst as a function of R_{po} is shown in Figure 4.8, and found that deactivation of the catalyst increases with increasing activity (independent of reaction temperature); see also Chapter 3 of this thesis. Pater (2001) [29] has noticed the similar phenomena for deactivation process with $MgCl_2$-supported ZN catalyst type, and reported that catalyst deactivation relates to its initial activity, independent on the reason for the activity change (may be due temperature, pressure, hydrogen concentration, etc). From Figure 4.8, the critical points marked by "a", "b" and "c" indicate the sudden increase in catalyst deactivation; however, the velocity of this change varies with the reaction temperature. Interestingly, this figure shows, also, that at hydrogen concentrations, $X < 0.0051$, the dependence of k_d on R_{po} can be described reasonably well using a linear relationship •. However, increasing hydrogen concentration introduces deviations from linearity; whether such a deviation becomes noticeable depends on the polymerization temperature. In addition, extrapolation of such linear model also predicts the deactivation of catalyst at 0.0 value of R_{po}, which is difficult to explain at this moment.

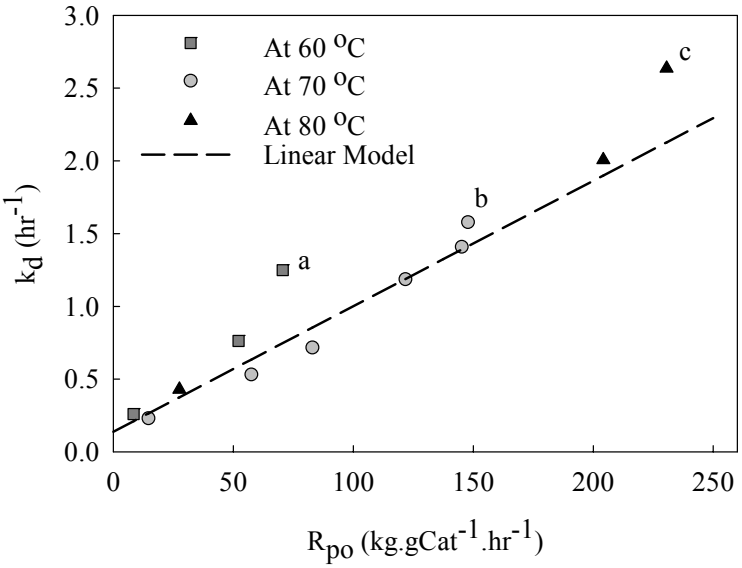

Figure 4.8: The relationship between k_d and R_{po}.
(experimental values are provided in Chapter 3; see Table 3.2 (a) and Table 3.3 (a)).

• The values of k_d and R_{po} plotted in Figure 4.8 as a function of hydrogen concentration and reaction temperature.

In another attempt, Al-haj Ali (2006) [3] has modeled the complete relationship between k_d and R_{po} by applying a "two-term" function. The first term explains the linear behavior and the second term describe the deviation from the linearity. Just to have an idea, the empirical model is presented here,

$$k_d = \left(k_{d1} R_{po} + \left(k_{do} e^{\left(\frac{-E_{act\,d}}{R_g T} \right)} \right) \left(1 + k_{d2} X \right) \right) \tag{4.50}$$

where,

k_{do} = 1.7E-4 (hr^{-1}), k_{d1} = 8.38E-3 ($gCat.kg^{-1}$), k_{d3} = 288.2 and $E_{act\,d}$ = -20E3 ($J.mol^{-1}$)

The author observed a good agreement between experimental and predicted values, however, the physical reasoning of deviation observed in catalyst deactivation at higher values of R_{po} is not mentioned, and it is still unclear. In addition, similar to linear model, the model shown in equation (4.50) predicts the deactivation of catalyst at 0.0 value of R_{po}.

Theoretically, the dependency of k_d on R_{po} can be modeled using variety of empirical and semi-empirical models. The proper selection of these will be crucial from the point of view of understanding the kinetic process and the reactor behavior in general. For instance, another effort is presented here to understand this phenomenon, the R_{po} and k_d has been normalized and analyzed with a semi-empirical equation shown in Figure 4.9 [◊]. Normalizing the curves shown in Figure 4.8 led to the "master" curve presented in Figure 4.9 up to the critical region indicated for R_{po}, which are pointed out by "a", "b" and "c". However, these curves deviate above the critical region of R_{po}. In this region, the velocity of change in k_d in terms of slope was found to be increased by factor 4 as temperature increased from 60 to 70 ^oC and decreased further by factor 3 with temperature increased

[◊] The relative R_p and relative k_d constant has been calculated using following equations:

$$R_{po\_rel} = \frac{R_{po}(i) - R_{po}(1)}{R_{po}^{Max} - R_{po}(1)} \tag{4.51}$$

$$k_{d\_rel} = \frac{k_d\left(R_{po}(i)\right) - k_d\left(R_{po}(1)\right)}{k_d\left(R_{po}^{Max}\right) - k_d\left(R_{po}(1)\right)} \tag{4.52}$$

from 70 to 80 °C. With the semi-empirical model shown in Figure 4.9, the model prediction display a good agreement with the experimental data, and also indicate that the predicted profile start at origin. However, with such semi-empirical models, the sensitivity of constants has to be validated from one catalyst and process type to another.

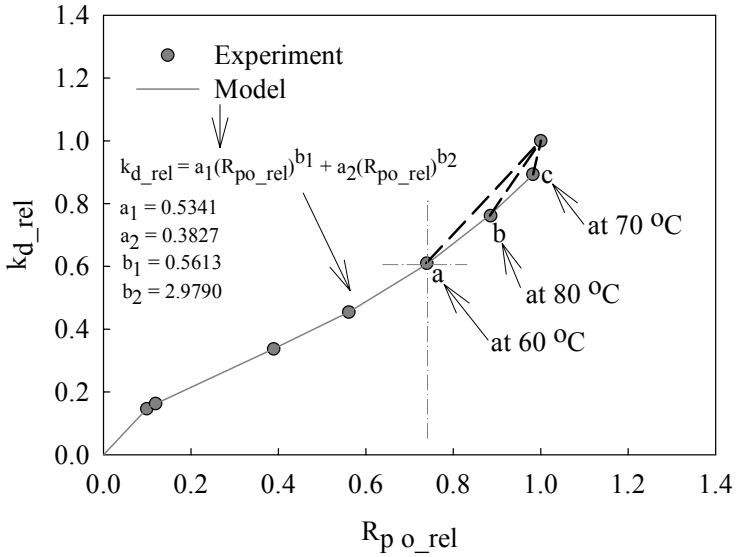

Figure 4.9: Experimental and calculated relative k_d as a function of relative R_{po}

The results shown in Figure 4.9 demonstrate that the deactivation can be interpreted as being just an "activity-dependent probability" but only up to the critical values of R_{po} at individual reaction temperatures. The high R_{po} obtained at high hydrogen concentration (see Chapter 3: Run39, Run315 and Run317) direct to the fact that there is some deactivation processes linked to hydrogen, chiefly at high hydrogen concentration. A similar relation between deactivation process and hydrogen has been observed for $MgCl_2$-supported ZN catalyst type used for propylene polymerization by Spitz et al. (1989) [41].

The mechanisms involved in the termination of the chain growth in olefin polymerization with ZN type catalysts has been studied thoroughly in the last five decades and they are mentioned in the above sections presented in this chapter. It is generally accepted that the termination mechanisms are valid for the wide range of catalyst types used in polymerization of olefins (for more precise information see Böhm (1978), Busico et al. (1992), Chadwick et al., (1995) and Albizzati et al. (1996) [1, 8, 9, 12]). However, that generalization is not obvious: for instance, the behavior of hydrogen may be different for the new generation of catalysts. If the present study is considered then it is clear that

hydrogen in the low concentration range (for X vales below 0.01) activates the polymerization in addition to acting as a powerful transfer agent. At high hydrogen concentration (for X values above 0.01), it is observed that hydrogen is also associated with some deactivation processes yielding a decrease in the catalyst activity. At X value of 0.01 (and may be above), the polymerization center such as C_o^H is believed to be exhibiting a high probability for deactivation than propagation. In other words, the deactivation process for C_o^H polymerization centers may be fast as compared to the deactivation of other active catalyst centers (for example $k_{do}^H > k_d$).

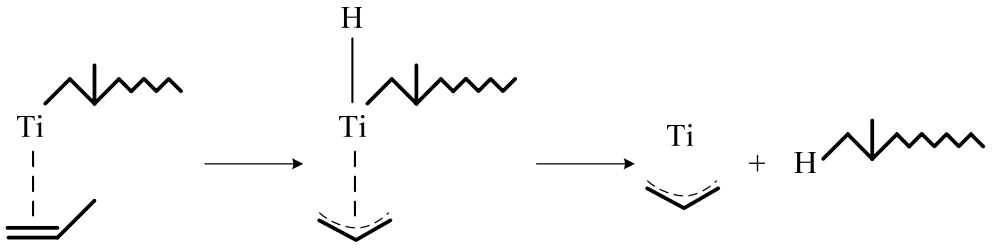

Figure 4.10: Mechanism for polymer chain deactivation proposed by Guyot et al. (1993) [15].

Guyot et al. (1993) [15] proposed another mechanism for the deactivation of active centers, i.e., a coordinated propylene monomer either inserts into the growing polymer chain or decomposes into an inactive π-allyl species and H atom, which adds to the growing polymer chain, giving a saturated isobutyl chain end (see Figure 4.10). According to the authors, the formation of π-allyl species accounts for the high deactivation observed at high temperature (with high initial activation). Al-haj Ali et al. (2006) [2] reviewed an additional reason that a catalyst site might show an increase deactivation behavior due its destabilization during the polymerization reaction.

4.8 Analysis of molecular weight distributions

The experimental data regarding average molecular weights of produced PP is discussed in Chapter 3. As reported in Chapter 3, M_w^{avg} of few PP samples were analyzed using GPC technique and for rest of the samples the values of M_w^{avg} were obtained from the viscosity-average molecular weights (M_v^{avg}). At a particular reaction temperature level, the obvious influence of hydrogen has been observed on the average molecular weights of polymer.

Another approach for the analysis of polyolefin polymerization kinetics prepared with heterogeneous polymerization catalysts is reported here. The basis for this analysis has been reviewed by Soares et al. (1996) [35] that under most polymerization conditions the effect of multiple site types on the kinetics is far more important than mass and heat transfer resistances. The cornerstone of the approach is based on the analysis of MWD data that is performed under the assumption that heterogeneous Ti-based catalysts contain several types of active centers, which differ in kinetic properties (see Appendix 4B).

Under these conditions, each site type will instantaneously produce polymer that is assumed to have a Flory's most probable MWD. Therefore, an instantaneous MWD of the accumulated polymer made with $MgCl_2$-supported ZN catalysts can be considered as an average of that produced by the individual site types, weighed by the weight fraction of polymer produced by each site type. In this respect, the MWD of a few PP samples were determined by GPC analysis following the procedure discussed in Chapter 2 of this thesis. The GPC curves of these respective PP samples were resolved into Flory components using the deconvolution method described in Appendix 4B. The predicted GPC curves were obtained by estimating the individual M_w^{avg} and mass fractions of Flory components given in equation (4B.12).

In this section, the GPC curves of selected PP samples are discussed in order to understand the influence of temperature and hydrogen as a transfer agent on the molecular weights of the polymer samples. The GPC curves of six PP samples are reported here, such as, Run38 (60 ^oC, X = 0.00133), Run310 (70 ^oC, X = 0.00025), Run311 (70 ^oC, X = 0.00050), Run312 (70 ^oC, X = 0.00143), Run314 (70 ^oC, X = 0.00516) and Run317 (80 ^oC, X = 0.01238) [◊]. These curves were deconvoluted using a "four site" model to interpret the effect of different site types on the kinetics of polymerization reaction.

The deconvolution analysis of these GPC curves are discussed using the following three groups,

1. Temperature effect is analyzed by comparing Run38 and Run312, as they are prepared with similar amount of hydrogen.
2. Hydrogen influence as a transfer agent is evaluated by comparing Run310, Run311 and Run314 together.

[◊] The experimental conditions for these runs are given in Chapter 3.

3. Run317 is interpreted individually to see the effect of high temperature and high hydrogen concentration on the MWD.

The data regarding molecular weights and mass fractions for individual Flory component are given in Table 4.8. It was noticed that the Four Flory components (1 - 4 in order of increasing molecular weight) described the MWD of these polymer in an acceptable manner. In general, the contribution from mass fraction of an individual Flory component in modeling the MWD of different PP samples was found to be not deviating significantly. It can be presumed that the contribution of each site is independent of the polymerization conditions, especially for the range of hydrogen concentration studied in this work. For the same catalyst type, Al-haj Ali (2006) [3] assumed a constant contribution of mass fraction and found a good fit between experimental and model GPC curves. The author has used following constant values of mass fractions, $m_1 = 0.08$, $m_2 = 0.4$, $m_3 = 0.37$ and $m_4 = 0.15$.

Table 4.8: Hydrogen effect on molecular weights and contents (mass fractions) of Flory components in propylene polymerization reactions [$]

Experiment Code	Center	M_w^{avg} (kg.kmol^{-1})	Fraction	Experiment Code	Center	M_w^{avg} (kg.kmol^{-1})	Fraction
Run38	1	16300	0.07	Run310	1	98700	0.10
	2	82000	0.37		2	304000	0.36
	3	231000	0.41		3	956000	0.34
	4	817000	0.15		4	3190000	0.20
Run311	1	76100	0.10	Run312	1	36100	0.09
	2	246000	0.40		2	127000	0.43
	3	776000	0.35		3	358000	0.36
	4	2890000	0.15		4	1260000	0.12
Run314	1	14100	0.08	Run317	1	11400	0.08
	2	70500	0.37		2	57200	0.37
	3	194000	0.42		3	149000	0.44
	4	705000	0.13		4	464000	0.11

[$] Experimental conditions are given in Chapter 3.

In order to discuss the temperature effect, the GPC curves of two PP samples prepared from Run38 and Run312 (see Chapter 3) and their resolutions into Flory components are shown in Figure 4.11. The M_w^{avg} of individual Flory component obtained for PP sample prepared at 70 ^oC (Run312: X = 0.00143) illustrated a shift towards high molecular part with a magnitude of factor 2 compared to the other sample (Run38: X = 0.00133). This effect can be seen from shifted GPC curve for Run312 towards the direction of arrow shown in Figure 4.11. On the contrary, from the published literature it is known that the average molecular weight of the polymer decreases with increasing polymerization temperature (for examples see Soares et al. (1996) and Soares et al. (2000) [35, 37]).

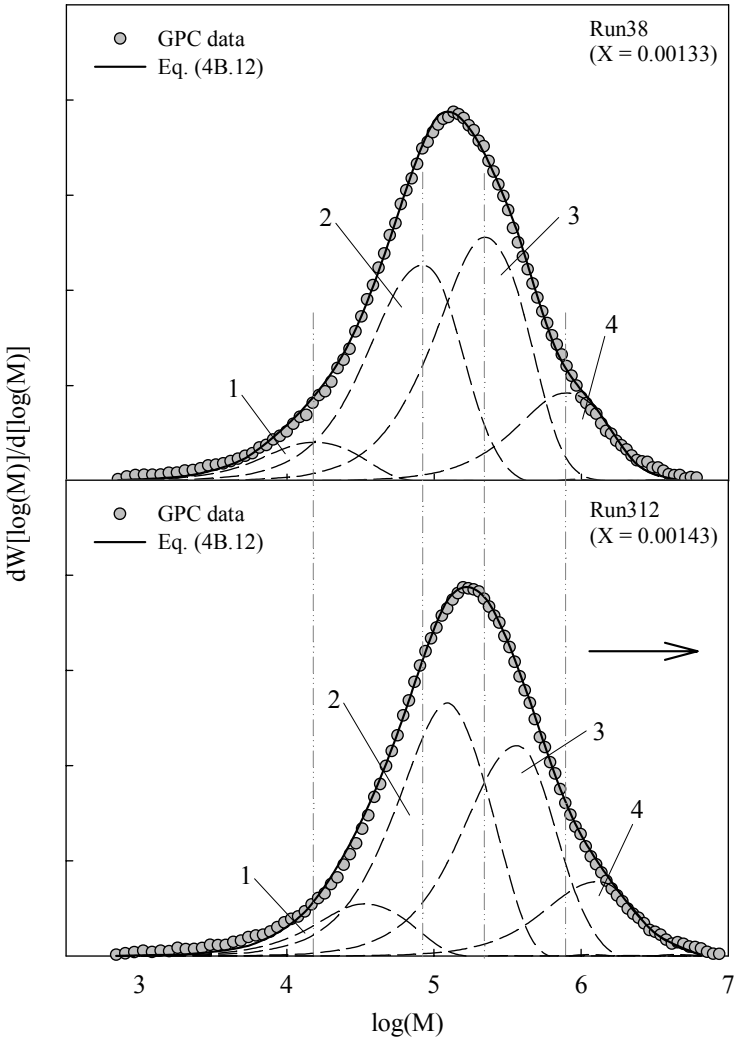

Figure 4.11: MWD data for two PP samples prepared at 60 ^oC (Run38: X = 0.00133) and 70 ^oC (Run312: X = 0.00143) with similar hydrogen concentration and their resolution into Flory components.

Al-haj Ali et al. (2006) [2] explained that this effect of temperature may occur due to the higher activation energy of the polymerization reaction compared to that of termination reaction. It is important to note here that if the stereochemistry studies developed by Chadwick et al. (1996) [13] is correct then at similar hydrogen concentration, the coupled effect of temperature and external donor (such as Silane in this case) on the molecular properties of polymer seem to play an important role in controlling the stereochemistry of active catalyst sites.

Recently, Kissin et al. (2004) [25] found that for $MgCl_2$-supported ZN catalysts in the presence of external donor, an increase polymerization temperature leads to a significant increase in the stereoregularity of isotactic fractions. According to Chadwick and his coworkers (1995 and 1996) [12, 13], this effect can be explained by an increase in the activation energy with increasing isospecificity of the active sites. The authors assumed that a 2,1-inserted center remain in the "dormant" state for a significant period of time even in the presence of hydrogen, and that the temperature increase can reduce the barrier to chain propagation after the mis-insertion. This implies that molecular weight of the isotactic fractions may increase with increasing polymerization temperature which is in line with the results obtained for Run38 and Run312 (see Table 4.8 and Figure 4.11).

The GPC curves of three PP samples and their resolution into Flory components is shown in Figure 4.12, which illustrate the influence of hydrogen on the MWD and the M_w^{avg} of individual Flory components. As expected, the molecular weight of the polymer significantly decreased when the hydrogen amount was increased during the reaction (see Chapter 3 and Table 3.3). An examination of these data shown that as the hydrogen concentration increases, M_w^{avg} values of all Flory components decreases approximately in parallel (see Table 4.8). The content of each Flory component also remained approximately the same, independent of hydrogen concentration. It is interesting to observe that an effect of hydrogen on the molecular properties of PP samples is not due to the significant change in the contribution of different Flory components to the polymer makeup, but reflects a particular kinetic effect inherent to each type of active center. This effect of hydrogen as a chain transfer agent during polymerization has been thoroughly investigated by several researches. For most polymerization conditions with $MgCl_2$-supported ZN catalysts, the molecular weight of the polymer decreases significantly with increasing concentration of hydrogen [1, 3, 20, 25, 44]. However, it has been shown that the magnitude of this change in molecular weight is dependent on the composition of this $MgCl_2$-supported ZN catalyst types. For example, Chadwick et al. (1995) [12] stated that

at a given hydrogen concentration, methoxysilanes used as an external donor typically give a higher molecular weight polymer than ethoxysilanes.

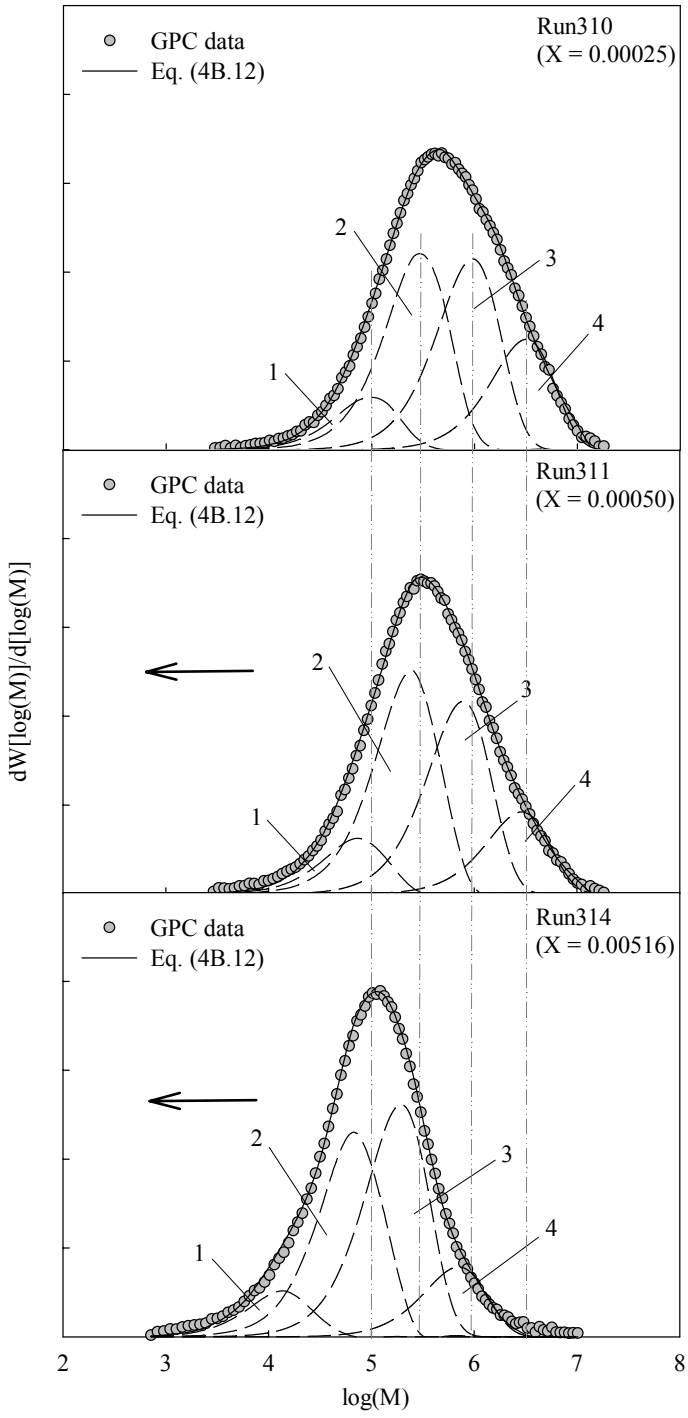

Figure 4.12: MWD data for PP samples prepared at 70 °C with different hydrogen concentration and their resolution into Flory components (see Chapter 3 Table 3.2 and Table 3.3).

Figure 4.13 illustrate the comparison between the experimental data and model prediction for the MWD of the PP sample prepared at 80 ^{o}C and X value of 0.01238. As said above, even at high temperature and hydrogen amount compared to other samples, the mass fractions of Flory components did not demonstrate any significant variation. This might reflect the influence of increasing catalyst activity with increasing polymerization temperature even at 80 ^{o}C. The activity of different active sites remained unchanged at this temperature and hydrogen concentration. As per quoted in Chapter 3, this effect may come from the completely filled batch reactor, which influenced the dynamics of active catalyst particles during the reaction.

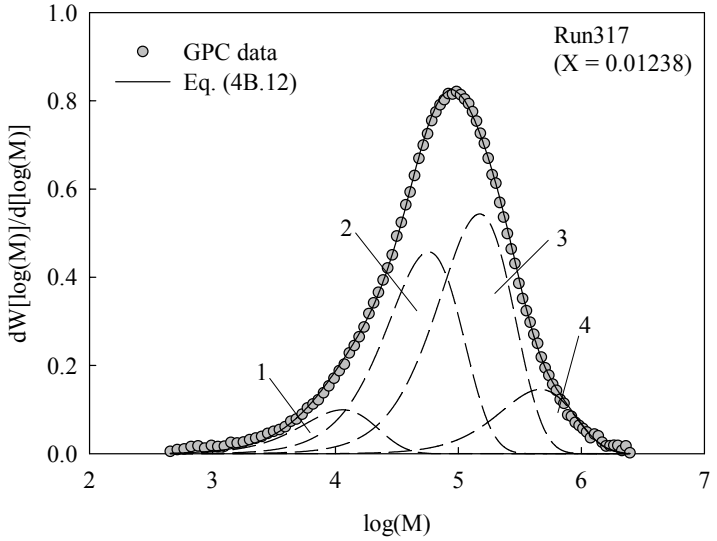

Figure 4.13: MWD data for PP sample prepared at 80 ^{o}C (Run317) and their resolution into Flory components (see Chapter 3 Table 3.2 and Table 3.3).

4.9 Conclusions

In this chapter, several kinetic peculiarities involved with the catalytic propylene polymerization has been discussed based on the experimental findings and published literature. Several kinetic schemes were derived for R_{po} and q by performing the detailed analysis of kinetic model, and were fitted with experimental data points for analyzing the hydrogen response on the catalyst activity as well as molecular properties of the polymer. The developed model for R_{po} and q exhibit the dependency on the polymerization temperature and concentrations of monomer, catalyst and hydrogen. Among all the derived schemes, Scheme I has shown good statistical agreement for the predicted values

with respect to the experimental values. The kinetic model developed in this study provided an opportunity to understand the different aspects of hydrogen during the catalytic propylene polymerization reaction. With the development of proper experimental program, it was possible to analyze the present kinetic model, qualitatively as well as quantitatively. However, one drawback of these models is their complex nature in terms of kinetics lead to the number of different constants; and these constants are derived from various individual reaction rate constants. Therefore, in future, effort should be made in generating the wide range of experimental data in terms of different process parameters. This will definitely help in optimizing the kinetic model response, qualitatively as well as quantitatively.

The catalyst activity and average molecular weights were modeled as a function of hydrogen by combining the findings observed by Natta et al. (1959) and Keii (1972) [20, 28] with the dormant site modeling approach reported by Weickert et al. (2002) [47]. The hydrogen response observed on the catalyst activity has been classified into two categories like "activation effect" at low concentration of hydrogen ($X < 0.015$) and "retardation effect" at high concentration of hydrogen ($X > 0.015$) in the reactor. The molecular weight of the produced polymer was found to be decreased with increasing amount of hydrogen. This effect on molecular weight was discussed in terms of the termination probabilities of the active polymer chains as well as deconvoluting the GPC curves.

The "improved" kinetic model applied for modeling the polymerization activity and molecular properties offered a good insight into the experimental results and can further be adapted for its extensive application in catalytic propylene polymerization. The model described here is limited with respect to the scope of this chapter. Strictly speaking, the observations made in this chapter are valid for $MgCl_2$-supported ZN catalyst type used in this work.

In this study, the catalyst decay behavior was related to the reaction rate, and found that the deactivation of catalyst increases with its increasing activity. This performance of catalyst decay was also found to be temperature independent. It was noticed that number of mathematical models can be developed to understand the "activity-dependent" catalyst decay. The GPC curves for a few PP samples were deconvoluted into the four individual Flory components. The influence of temperature as well as hydrogen on the MWD of produced PP samples was studied based on the data regarding the average molecular

weights and mass fractions of the individual Flory components. The deconvolution model developed for interpreting the MWD of PP samples provided useful information on specific kinetic effects intrinsic to each type of active centers.

Finally, the results obtained concerning the influence of hydrogen on the catalytic propylene polymerization reflects the specific kinetic effects intrinsic to the nature of catalyst site.

Appendix 4A

Brief introduction to Natta Model

In this section, the approach initially postulated by Natta (1959) [28] on hydrogen influence on the catalytic olefin polymerization is briefly introduced. Natta et al. (1959) [28] performed number of experiments for catalytic polymerization of ethylene and propylene in the presence of hydrogen. The authors were first to report the decrease in rate of polymerization upon increasing partial pressure of hydrogen during polymerization reaction. They explained this effect based on the basic kinetic mechanism consisting mainly propagation of polymer chain, termination of polymer chain due to hydrogen chain transfer and reinitiation of active sites (having metal-hydride bond) with monomer that are produced as a result of hydrogen chain transfer, and these reactions are shown below,

Polymer chain propagation:

$$Cat-P + M \xrightarrow{k_a} Cat-P(+1) \qquad (4A.1)$$

Chain transfer to hydrogen:

$$Cat-P + H_2 \xrightarrow{k_b} Cat-H + PH \qquad \text{(Similar to equation (4.3))}$$

Reinitiation of active sites (having metal-hydride bond) with monomer:

$$Cat-H + M \xrightarrow{k_c} Cat-P \qquad \text{(Similar to equation (4.4))}$$

All the assumptions used here are according to the model presented in Natta et al. (1959) [28].

The author formulated the net rate of polymerization based on above mentioned kinetic mechanism,

$$R^H = k_a \left(C_o - C_H\right) pM + k_c C_H \, pM \tag{4A.2}$$

If it is assumed that the monomer consumption due to reinitiation reaction shown in equation (4.4) is negligible, then the rate of polymerization given in equation (4A.2) can be described as,

$$R^H = k_a \left(C_o - C_H\right) pM \tag{4A.3}$$

The term C_H used in equation (4A.3) denotes the concentration of active sites, which are formed as a result of chain transfer reaction shown in equation (4.3). This term is formulated based on the balance made on its formation and consumption. Therefore,

For formation of C_H,

$$\frac{dC_H}{dt} = k_a \, k_b \left(C_o - C_H\right) pM \, f\left(pH_2\right) \tag{4A.4}$$

For consumption of C_H,

$$\frac{dC_H}{dt} = k_c \, C_H \, pM \tag{4A.5}$$

Assuming an equilibrium state, the rate of formation will be equal to rate of consumption,

$$k_a \, k_b \left(C_o - C_H\right) pM \, f\left(pH_2\right) = k_c \, C_H \, pM \tag{4A.6}$$

Rearranging equation (4A.6) for C_H will lead to the following expression,

$$C_H = \frac{k_a \, k_b \, C_o \, f\left(pH_2\right)}{k_c + k_a \, k_b \, f\left(pH_2\right)} \tag{4A.7}$$

Finally, substituting the derived term C_H from equation (4A.7) into equation (4A.3) will result in,

$$R^H = k_a C_o \, pM - \frac{pM \, k_a^{\,2} \, k_b \, C_o \, f\left(pH_2\right)}{k_c + k_a \, k_b \, f\left(pH_2\right)} \tag{4A.8}$$

The expression for net rate of polymerization shown in equation (4A.8) illustrates the dependency of catalyst activity on partial pressure of monomer and on the function representing the hydrogen partial pressure. The term presented as $f(pH_2)$ in equation (4A.8) describe the effect of hydrogen on the polymerization activity. In order to derive this function, Natta et al. (1959) [28] assumed a hypothesis in which the catalyst surface is capable of adsorbing the molecule of hydrogen. The authors presented the following preliminary mechanism for understanding the adsorption of hydrogen,

$$H_2 + L_2 \rightleftarrows H_2 L_2 \tag{4A.9}$$

$$H_2 L_2 + 2L \rightleftarrows 2HL + L_2 \tag{4A.10}$$

The term L represents here the active centers, which are capable of adsorbing the molecule of hydrogen.

Under the equilibrium condition, the dissociative adsorption of hydrogen molecule will take place according to the equation (4.6) mentioned earlier.

Applying the equilibrium condition for reactions presented by equation (4A.9) and (4A.10), the concentration of term HL can be evaluated [28],

$$\frac{\left[HL\right]^2}{pH_2 \left[L\right]^2} = K_{eq} \tag{4A.11}$$

Rearranging equation (4A.11),

$$\left[HL\right] = \kappa \sqrt{pH_2} \tag{4A.12}$$

Natta et al. (1959) [28] believed that concentration of HL found in equation (4A.12) can be characterized as a solution for term f(H_2).

Substituting the definition of f(H_2) in equation (4A.8) lead to,

$$R^H = R^o - \frac{pM\, k_a{}^2\, k_b\, C_o\, \kappa \sqrt{pH_2}}{k_c + k_a\, k_b\, \kappa \sqrt{pH_2}} \tag{4A.13}$$

where, R^o is corresponding to the rate of polymerization in the absence on hydrogen.

Rearranging equation (4A.13) will lead to final form of Natta Model shown in equation (4.1),

$$R^H = R^o - \frac{1}{\frac{A}{\sqrt{pH_2}} + B} \qquad \text{(Similar to equation (4.1))}$$

where,

$$A = \frac{k_c}{pM\, k_a{}^2\, k_b\, C_o\, \kappa} \qquad B = \frac{1}{pM\, k_a\, C_o} \tag{4A.14}$$

On the basis of kinetic mechanism proposed by Natta et al. (1959) [28], the number-average molecular weight ($M_n{}^{avg}$) can be presented as follow,

$$M_n{}^{avg} = K` \frac{k_a \left(C_o - C_H\right) pM}{k_a\, k_b \left(C_o - C_H\right) pM\, \kappa \sqrt{pH_2} + R} \tag{4A.15}$$

The R term shown in equation (4A.15) represent the rate of polymerization as per given by equation (4A.3). This definition of term R can be substituted in equation (4A.15).

Therefore, $M_n{}^{avg}$ can be written as,

$$M_n{}^{avg} = K` \frac{k_a \left(C_o - C_H\right) pM}{k_a\, k_b \left(C_o - C_H\right) pM\, \kappa \sqrt{pH_2} + k_a \left(C_o - C_H\right) pM} \tag{4A.16}$$

Further, rearranging equation (4A.16) will describe the final form of equation for M_n^{avg} as per shown by equation (4.2).

$$\frac{1}{M_n^{avg}} = a + b\sqrt{pH_2} \qquad \text{(Similar to equation (4.2))}$$

where,

$$a = \frac{1}{K`} \quad b = \frac{k_b \kappa}{K`} \qquad (4A.17)$$

Appendix 4B

Deconvolution analysis: Molecular weight distribution

It is well known that the $MgCl_2$-supported ZN catalyst show multi-site behavior. The reasons for different kinetics of various sites are multiple and not well identified. The different origins of various physical locations on the support material and possible divergent circumstances for the components during preparation will lead to a spread in the type of active sites.

In the literature, a number of techniques are available to mathematically model the MWD of polymers. Soares (2001) [38] has explained that the use of method of instantaneous distribution seem to be fully justified for most of the olefin polymerization processes. An instantaneous chain length distribution for olefin polymerization is given by a single-parameter equation known as Schulz-Flory distribution,

$$y(j) = j\,q^2\,e^{-jq} \qquad (4B.1)$$

and, an area under the curve is normalized,

$$\int_{j\geq 1}^{\infty} y(j)\,dj = 1 \qquad (4B.2)$$

The instantaneous distribution function shown in equation (4B.1) is depending on only one parameter, i.e., q. As per the assumption of "quasi-single" site made in section 4.3,

the average molecular weights data from GPC analysis could be used to determine an average q, according to following equation reported by Weickert (1997) [46],

$$q = \frac{2\,M_{mon}}{M_w^{\,avg}} = \frac{M_{mon}}{M_n^{\,avg}} \tag{4B.3}$$

The equation (4B.3) is generally only valid for single site catalysts types.

The GPC method is the most preferred technique for the measurements of M_w^{avg} and M_n^{avg} values for polyolefins. Potentially, a high-quality GPC curve contains detailed information on many aspects of polymer's MWD, and such information can be extracted from the data using computer analysis of GPC curves. Therefore, the deconvolution method is often used for the direct conversion of GPC chromatograms to the differential distribution.

However, this technique has certain limitations based on the analysis and mathematical error during the processing of GPC curves, as explained by Kissin et al. (2002) [24]. Several authors reported the application of deconvolution method for MWD analysis of different classes of polymers [22, 34, 45]. The main disadvantage found in the literature presented by these authors, is the disagreement on the number of different site types. It is observed from their work that the number of active site types is varied from 2 to 7 in MWD analysis of polyolefins prepared using heterogeneous Ziegler-Natta catalysts. However, Kissin et al. (2004) [24] showed that four active site types are sufficient to deconvolute the complete MWD.

In this section, detailed mathematical information is provided in order to represent a Schulz-Flory distribution function in terms of GPC coordinates. Further, this method is extended to 4 active site types, in which each site type produces polymer with a MWD given by Schulz-Flory distribution. The results show that the detailed GPC analysis can be used as an important tool in kinetic studies of polymerization reactions.

The principle equation of the GPC method correlates the weight distribution function of a polymer, y(j) in equation (4B.1), and an experimentally determined function H(v) which describes the height of a GPC curve as a function of an elution volume or count (v); see Altgelt et al. (1971) [4],

$$y(j) = H(v)\left[\frac{dv}{dj}\right] \tag{4B.4}$$

It is often more convenient to represent the molecular weight distribution on a semi-logarithmic plot. Let this distribution of log molecular weight be represented by W(log(M)), then,

$$W(\log(M)) = H(v)\left[\frac{dv}{d\log(M)}\right] \tag{4B.5}$$

If H(v) has already been normalized then y(j) and W(log(M)) computed from equation (4B.4) and (4B.5) are also normalized. Further, the two normalized distribution function shown in equation (4B.4) and (4B.5), respectively can be correlate as,

$$y(j)\, dj = W(\log(M))\, d\log(M) \tag{4B.6}$$

Equation (4B.6) can be rewritten using the following transformation,

$$d\log(M) = \frac{d\ln(M)}{\ln(10)} = \frac{dM}{M\ln(10)} = \frac{d(j\,M_{mon})}{(j\,M_{mon})\ln(10)} = \frac{dj}{2.3026\,j} \tag{4B.7}$$

and, thus according to equation (4B.1), (4B.6) and (4B.7),

$$W(\log(M)) = 2.3026\, j\, y(j) \qquad \text{or} \qquad W(\log(M)) = 2.3026\, j^2\, q^2 \exp\left(-j\,q\right) \tag{4B.8}$$

Equation (4B.8) can be described in terms of molecular weights, and using q definition according to equation (4B.3),

$$W(\log(M)) = 9.2104\left[\frac{M}{M_w^{\,avg}}\right]^2 \exp\left(\frac{2\,M}{M_w^{\,avg}}\right) \tag{4B.9}$$

Further, replacing M by log(M) with the following equation,

$$M = \exp\left(2.3026\log(M)\right) \tag{4B.10}$$

Substitution of equation (4B.10) into equation (4B.9) will lead to a final form of Schulz-Flory distribution function in the GPC coordinates,

$$W(\log(M)) = \frac{9.2104}{\left(M_w^{\,avg}\right)^2}\exp\left\{4.6052\log(M) - \frac{2}{M_w^{\,avg}}\exp\left(2.3026\log(M)\right)\right\} \qquad (4B.11)$$

However, equation (4B.11) can only explain the distribution of weight fraction of polymer chains produced by "quasi-single" site type of catalyst. Therefore, the final deconvolution model for the GPC curve using 4 active site types can be formulated as,

$$W(\log(M)) = \sum_{i=1}^{4} m_i \left[\frac{9.2104}{\left(M_w^{\,avg}\right)_i^2}\exp\left\{4.6052\log(M) - \frac{2}{\left(M_w^{\,avg}\right)_i}\exp\left(2.3026\log(M)\right)\right\}\right] \qquad (4B.12)$$

According to equation (4B.12), the mass fraction of each site (m_i) and weight average molecular weight of each site ($(M_w^{avg})_i$) is fitted to the experimental GPC curve for detail analysis of polymerization kinetics.

Nomenclature

a, b	: Constants used in equation (4.2)
a_1, a_2, b_1, b_2	: Constants used in equation shown in Figure 4.9
A, B	: Constants used in equation (4.1)
A_1 to A_6	: Constants used in equation (4.46)
C^H	: Concentration of active polymer chain attached to H_{ads} ($kg.m^{-3}$)
$C_o^{\,H}$	: Initial concentration of active catalyst site attached to H_{ads} ($kg.m^{-3}$)
C_o	: Initial concentration of active catalyst site ($kg.m^{-3}$)
C_H	: Hydrogen concentration used in reference [24]
C_H	: Concentration of active sites (representing metal-hydride bond), see Appendix 4A
C_j	: Concentration of active polymer chain with chain length of j ($kg.m^{-3}$)
C_j^H	: Concentration of active polymer chain attached to H_{ads} with chain length of j ($kg.m^{-3}$)

C_{max} : Maximum concentration of active sites ($kg.m^{-3}$)
C_{Pr} : Propylene concentration used in reference [24]
C_1 : Concentration of active polymer chain with chain length of 1 ($kg.m^{-3}$)
C : Concentration of active polymer chain ($kg.m^{-3}$)
Cat-H : Active site attached to hydrogen atom
Cat-P : Active site attached to polymer chain
D_j : Concentration of dead polymer chain with chain length of j ($kg.m^{-3}$)
$E_{act\ d}$: Activation energy for deactivation reaction ($J.mol^{-1}$)
H_{ads} : Concentration of adsorbed hydrogen ($kg.m^{-3}$)
H_2 : Hydrogen concentration ($kg.m^{-3}$)
H_{2o} : Initial moles of hydrogen present during reaction (mole)
H(v) : Height of GPC curve
J : Chain length
k_a : Propagation reaction rate constant shown in equation (4A.1)
k_b : Chain transfer reaction rate constant shown Appendix 4A
k_c : Reinitiation reaction rate constant shown Appendix 4A
k_{dm} : Rate constant for dormant site formation reaction ($m^3.gCat^{-1}.hr^{-1}$)
k_{d_rel} : Relative rate constant for deactivation constant (hr^{-1})
k_{do} : Arrhenius constant for deactivation reaction (hr^{-1})
k_{d1} : Constant used in equation (4.50)
k_{d2} : Constant used in equation (4.50)
k_d : Rate constant for deactivation constant (hr^{-1})
k_f : Rate constant for forward reaction of hydrogen dissociation (hr^{-1})
k_i, k_{iH} : Rate constant for initiation reaction ($m^3.gCat^{-1}.hr^{-1}$)
k_p : Rate constant for propagation reaction ($m^3.gCat^{-1}.hr^{-1}$)
k_{rm}, k_{rh} : Rate constant for dormant site reactivation reaction by monomer and molecular hydrogen ($m^3.gCat^{-1}.hr^{-1}$)
k_{rah1}, k_{rah2} : Rate constant for dormant site reactivation reaction by adsorbed hydrogen ($m^3.gCat^{-1}.hr^{-1}$)
k_{tm}, k_{th} : Rate constant for chain transfer reaction by monomer and molecular hydrogen ($m^3.gCat^{-1}.hr^{-1}$)
k_{tah1}, k_{tah2} : Rate constant for chain transfer reaction by adsorbed hydrogen ($m^3.gCat^{-1}.hr^{-1}$)
k_r : Rate constant for reverse reaction of hydrogen dissociation (hr^{-1})
k_0 to k_6 : Constants required for equation (4.35)
K_a to K_e : Constants used in equation (4.37)

K_{eq} : Equilibrium constant used in equation (4A.11)

K_H : Equilibrium constant used in equation (4.7)

K` : Constants used in equation (4A.15)

L_2 : Active metal surface capable for adsorbing molecule of hydrogen; see Natta et al. (1959) [28]

M_o : Initial concentration of monomer ($kmol.m^{-3}$)

M_{mon} : Molecular weight of monomer ($kg.kmol^{-1}$)

M_n^{avg} : Number-average molecular weight ($kg.kmol^{-1}$)

M_w^{avg} : Weight-average molecular weight ($kg.kmol^{-1}$)

M_v^{avg} : Viscosity-average molecular weight ($kg.kmol^{-1}$)

M : Concentration of monomer ($kmol.m^{-3}$) or Chain length on weight basis

p : Chain propagation probability

pH_2 : Partial pressure of hydrogen; see Natta et al. (1959) [28]

pM : Partial pressure of monomer; see Natta et al. (1959) [28]

PH : Dead polymer chain, represented in equation (4.3)

PPY_o : Initial moles of liquid propylene present during reaction (mole)

q : Chain termination probability

rS : Reaction rate for dormant sites ($kg.m^{-3}.hr^{-1}$)

rC_o^H, rC^H : Reaction rate for active site formed due to metal-hydride bond ($kg.m^{-3}.hr^{-1}$)

rC_j : Reaction rate for active polymer chain with chain length j ($kg.m^{-3}.hr^{-1}$)

rS^H : Reaction rate for dormant sites with adsorbed hydrogen ($kg.m^{-3}.hr^{-1}$)

rS_j : Reaction rate for dormant polymer chain with chain length j ($kg.m^{-3}.hr^{-1}$)

R^o : Stationary polymerization rate in absence of hydrogen; see Natta et al. (1959) [28]

R^H : Stationary polymerization rate in presence of hydrogen; see Natta et al. (1959) [28]

R_{po_rel} : Relative initial rate of polymerization ($kg.gCat^{-1}.hr^{-1}$)

R_{po} : Initial rate of polymerization ($kg.gCat^{-1}.hr^{-1}$)

R_p : Rate of polymerization ($kg.gCat^{-1}.hr^{-1}$)

S^H : Concentration of dormant polymer chain attached to H_{ads} ($kg.m^{-3}$)

S_j : Concentration of dormant polymer chain with chain length of j ($kg.m^{-3}$)

S_j^H : Concentration of dormant polymer chain attached to H_{ads} with chain length of j ($kg.m^{-3}$)

S : Concentration of dormant polymer chain ($kg.m^{-3}$)

v : Elution volume or count

W[log(M)] : Distribution of log molecular weight
X : Mole ratio of hydrogen to liquid propylene
y : Weight distribution function of a polymer (equation (4B.4))

Greek letters

α : Coefficient used in equation (4.43)
κ : Coefficient used in equation (4A.12)

Sub- and superscripts

act : Activation
ads : Adsorbed
d : Deactivation
dm : Represent dormant site formation due to monomer 2,1- insertion
eq : Equilibrium
f : Forward
i : Initiation or initial
j : Polymer chain length
mon : Monomer
o : Zero or initial
p : Propagation or polymer
rah1, rah2 : Represent dormant site reactivation reaction due to adsorbed hydrogen
rel : Relative
rh : Represent dormant site reactivation reaction due to molecular hydrogen
rm : Represent dormant site reactivation reaction due to monomer
r : Reverse
H : Adsorbed H atom
* : Active
Max : Maximum
n : Number
tah1, tah2 : Represent chain transfer reaction due to adsorbed hydrogen
th : Represent chain transfer reaction due to molecular hydrogen

tm : Represent chain transfer reaction due to monomer
v : Viscosity
w : Weight

Abbreviations

$Al(C_2H_5)_2Cl$, $AlEt_2Cl$: Diethylaluminum Chloride
$Al(C_2H_5)_3$, $AlEt_3$: Triethylaluminum
EB : Ethyl Benzoate
GPC : Gel permeation chromatography
MAO : Methylaluminoxane
$MgCl_2$: Magnesium dichloride
MWD : Molecular weight distribution
PE : Polyethylene
PP : Polypropylene
SiO_2 (PQ) : Pennsylvania Quarts Silica
TEA : Triethylaluminum
$TiCl_3$: Titanium trichloride
$TiCl_4$: Titanium tetrachloride
ZN : Ziegler-Natta

Literature

[1] Albizzati, E., Giannini, U., Collina, G., Noristi, L. and Resconi, L. (**1996**), Polypropylene Handbook, Chapter 2, 11 - 112.
[2] Al-haj Ali, M., Betlem, B., Roffel, B. and Weickert G. (**2006**), AIChE Journal, 52, 5, 1866 - 1876.
[3] Al-haj Ali, M. (**2006**), Doctorate Thesis, University of Twente, Enschede, The Netherlands.
[4] Altgelt, K. H. and Segal, L. (**1971**), Gas Permeation Chromatography, Marcel Dekker Inc., NY, 146 - 147.
[5] Blom, R. and Dahl, I. M. (**1999**), Macromol. Chem. Phys., 200 (2), 442 - 449.
[6] Blom, R., Andersen, A. and Dahl, I. M. (**2001**), Macromol. Chem. Phys., 202 (5), 726 - 733.

[7] Blom, R., Swang, O. and Heyn, R. H. (**2002**), Macromol. Chem. Phys., 203 (2), 381 - 387.

[8] Böhm, L. L. (**1978**), Polymer, 19, 545 - 552.

[9] Busico, V., Cipullo, R. and Corradini, P. (**1992**), Makromol. Chem., Rapid Commun., 13, 15 - 20.

[10] Bukatov, G. D., Guncharov, V. S., Zakharov, V. A., Dudchenko, V. K. and Sergeev, S. A. (**1994**), Kinetics and Catalysis, 35 (3), 358 - 362.

[11] Chadwick, J. C., Miedema, A. and Sudmeijer, O. (**1994**), Macromol. Chem. Phys., 195, 167 - 172.

[12] Chadwick, J. C., van Kessel, G. M. M. and Sudmeijer, O. (**1995**), Macromol. Chem. Phys., 196, 1431 - 1437.

[13] Chadwick, J. C., Morini, G., Albizzati, E., Baldontin G., Mingozzi, I. and Christofori, A. (**1996**), Macromol. Chem. Phys., 197, 2501 - 2510.

[14] Guastalla, G. and Giannini, U. (**1983**), Makromol. Chem., Rapid Commun., 4, 519 - 527.

[15] Guyot, A., Spitz, R., Dassaud, J. P. and Gomez, C. (**1993**), Journal of Molecular Catalysis, 82, 29 - 36.

[16] Hoffman, A. S., Fries, B. A. and Condit, P. C. (**1963**), Journal of Polymer Science: Part C, 4, 109 - 120.

[17] Horiuti, I. and Polanyi, M. (**1934**), Trans. Faraday Soc., 30, 1164 - 1172.

[18] Kahraman, R., Erdogan, M. and Bilgic, T. (**1996**), Journal of Applied Polymer Science, 60, 333 - 342.

[19] Keii, T., Okura, I., Soga, K. and Kojima, A. (**1970**), Journal of Polymer Science: Part A-1, 8, 2717 - 2719.

[20] Keii, T. (**1972**), Kinetics of Ziegler-Natta Polymerization, Chapman & Hill, UK.

[21] Keii, T., Doi, Y., Suzuki, E., Tamura, M., Murata, M. and Soga, K. (**1984**), Makromol. Chem., 185, 1537 - 1557.

[22] Kissin, Y. V. (**1995**), Journal of Polymer Science: Part A, Polymer Chemistry, 33, 227 - 237.

[23] Kissin, Y. V., Rishina, L. A. (**2002**), Journal of Polymer Science: Part A, Polymer Chemistry, 40, 1353 - 1365.

[24] Kissin, Y. V., Rishina, L. A. and Vizen, E. I. (**2002**), Journal of Polymer Science: Part A, Polymer Chemistry, 40, 1898 - 1911.

[25] Kissin, Y. V., Ohmishi, R. and Konakazawa, T. (**2004**), Macromol. Chem. Phys., 205, 284 - 301.

[26] Meier, G. B. (**2000**), Doctorate Thesis, University of Twente, Enschede, The Netherlands.
[27] Mori, H., Endo, M. and Terano, M. (**1999**), Journal of Molecular Catalysis A: Chemical, 145, 211 - 220.
[28] Natta, G. and Pasquon I. (**1959**), Adv. Catal., 11, 1.
[29] Pater, J. T. M. (**2001**), Doctorate Thesis, University of Twente, Enschede, The Netherlands.
[30] Pijpers, E. M. J. and Roest, B. C. (**1972**), European Polymer Journal, 8, 1151 - 1158.
[31] Samson, J. J. C., Bosman, P. J., Weickert, G. and Westerterp, K. R. (**1999**), Journal of Polymer Science: Part A, Polymer Chemistry, 37, 219 - 232.
[32] Shaffer, A. W. K. and Ray, W. H. (**1997**), Journal of Appl. Polym. Sci., 65, 1053 - 1080.
[33] Shimizu, F. (**2001**), Doctorate Thesis, University of Twente, Enschede, The Netherlands.
[34] Soares, J. B. P. and Hamielec, A. E. (**1995**), Polymer, 36 (11), 2257 - 2263.
[35] Soares, J. B. P. and Hamielec, A. E. (**1996**), Polymer, 37 (20), 4607 - 4614.
[36] Soares, J. B. P., Chu, K. J. and Penlidis, A. (**2000**), Macromol. Chem. Phys., 201, 552 - 557.
[37] Soares, J. B. P. and Penlidis, A. (**2000**), Metallocene-based Polyolefins, Edited by Scheirs, J. and Kaminsky, W., John Wiley & Sons Ltd., 237 - 267.
[38] Soares, J. B. P. (**2001**), Chemical Engineering Science, 56, 4131 - 4153.
[39] Soga, K. and Siono, T. (**1982**), Polymer Bulletin, 8, 261 - 268.
[40] Spitz, R., Bobichon, C. and Guyot, A. (**1989**), Makromol. Chem., 190, 707 - 717.
[41] Spitz, R., Masson, P., Bobichon, C. and Guyot, A. (**1989**), Makromol. Chem., 190, 717 - 723.
[42] Stern, C., Frick, A. R., Pater, J. T. M. and Weickert, G. (**2005**), Macromolecular Material and Engineering, 290, 372 - 383.
[43] Tupe, R. and Weickert, G. (**2005**), Proceedings of JICEC05, Amman, Jordon.
[44] van Putten, I. (**2004**), Doctorate Thesis, University of Twente, Enschede, The Netherlands.
[45] Vickroy, V. V., Scheinder, H. and Abbott, R. F. (**1993**), Journal of Applied Polymer Science, 50, 551 - 554.
[46] Weickert, G. (**1997**), Modellierung von Polym., Springer - Verlag Berlin Heidelberg.
[47] Weickert, G. et al. (**2002**), EC Project Report: GRD2-2000-30189 "Polyprop", Milan, Italy.

Chapter 5

Tubular reactor for liquid-phase propylene polymerization: I. Kinetics and morphology

Abstract: A novel (capillary type) tubular reactor is developed for the catalytic polymerization of liquid propylene using $MgCl_2$-supported Ziegler-Natta catalyst. The polymerization experiments were carried out with the injection of preactivated catalyst slurry into a continuous flow of liquid propylene, with a short residence time inside the reactor. The reactor behavior has been systematically analyzed by carrying out the pulse experiments with an isoperibolic reaction mode. The catalyst response with respect to temperature profile over the reactor length has been analyzed at near-industrial polymerization conditions. The obtained results in terms of catalyst activity are reported in this chapter and compared with the kinetic data evaluated for the same catalyst type from batch polymerization experiments. It is observed that the catalyst exhibit similar thermal characteristics in batch as well as in tubular reactor. This is in agreement with narrow residence time distribution assumption that has been derived from the narrow temperature distribution found when injecting separated pulses of catalyst. The initial catalyst activity determined from tubular reactor experiments shown 14 - 30 % higher values compared to the batch reactor data. A few polypropylene samples were analyzed for molecular weight distributions using GPC technique to understand the effect of hydrogen on the molecular properties of polymer. The average molecular weights of the produced polymer samples were observed to decrease with increasing hydrogen concentration. In addition, the GPC curves found to be broadened at higher hydrogen concentrations. In order to understand the effect of reactor behavior on the morphology of produced polymer samples, off line characterization techniques such as SEM, EDX, PSD and DSC were used, and relevant parameters are discussed such as temperature, hydrogen concentration and quenching agent. SEM analysis of polymer particles illustrated a smooth surface morphology of the polymer particles prepared using the present reactor concept. The analysis of normalized PSD data exhibited that the reactor dynamics has shown no significant influence on the size of polymer particles. The thermal response of the reactor observed during experiment was believed to be typical for a present reactor-catalyst-heat transfer system. The data presented here demonstrate a unique capability of a reactor for performing a “high-output” characterization of different process variables.

Keywords: kinetics (polym.), tubular reactor, quenched-flow technique, Ziegler-Natta polymerization

5.1 Introduction

The olefin polymerization process at elevated reaction temperature and pressure, using heterogeneous catalysts, is of a great commercial interest, and certainly accounts for a very active field of research and development. At present, a variety of processes and chemical reactors are used at the industrial level for the production of polyolefins. The trend of using a series of reactors for polymerization processes indicates a broader market demands for the desired product from an end-user prospective. Such process often consist of a combination of two reactor types, for example, gas-phase reactor preceded by a liquid-phase reactor as a "prepolymerization reactor" and/or a "main reactor" [5, 12].

Weickert et al. (2005) [17] recently emphasized the fact that with the help of improved experimental techniques a large number of peculiarities and phenomena involved with the olefin polymerization processes can be explored, observed and interpreted in a better way. The authors especially mentioned that a number of these phenomena are present under initial conditions, just milliseconds after the catalyst is exposed to monomer, further influencing the subsequent polymerization processes and final polymer properties strongly. McKenna et al. (2005) [8] reported that the complex interactions involved during an initial period of polymerization process is at the root of both how the material properties evolve and how the reactor behaves. Because, the heat and mass transfer at the particle scale are clearly related to phenomena taking place both at the active sites as well as at the reactor scale. Therefore, the order of magnitude of characteristic times involved with the different phases of catalytic polymerization process must be studied carefully for kinetics and morphology interpretations along with the reactor hydrodynamics. As an example, the time-scales observed for different polyolefin processes are already mentioned in Chapter 1.

A few examples have been reported in the open literature addressing the application of different techniques for investigating the kinetic and morphogenesis involved with the olefin polymerization processes [3, 4, 8, 12, 13, 14, 15, 17]. One of the techniques reported is "stopped-flow" method for investigation of polymerization kinetics at reaction time of the order of an average chain growth (let us say, typically < 1 s; see Chapter 1). For example, Busico et al. (1999) [3] performed ethylene and propylene slurry polymerization with homogeneous metallocene catalyst and Mori et al. (1999) [9] examined hydrogen influence in propylene slurry polymerization using $MgCl_2$-supported Ziegler-Natta (ZN) catalyst, using "stopped-flow" technique. An interesting application of such device has

been successfully reported by Di Martino et al. (2005) [4] for the characterization of nascent slurry polymerization of ethylene under industrial conditions. The authors noticed extremely high reaction rates obtained from the kinetic analysis at very short residence time (< 1.4 s). This indicates that such method can also be applied for the determination of initial polymerization rate. With the conventional batch reactor set-ups for polymerization, it is often difficult to estimate an initial catalyst activity immediately after its injection into the reactor mainly due to the dynamics of system and the capability of sensors used for measuring the process variables like temperature and pressure. Al-haj Ali (2006) [1] reported the different natures of kinetic rate profiles measured during the course of ZN catalyzed polymerization, exhibiting the kinetic fingerprints for a given catalyst-monomer system. One type of behavior for the rate of polymerization is schematically presented in Figure 5.1.

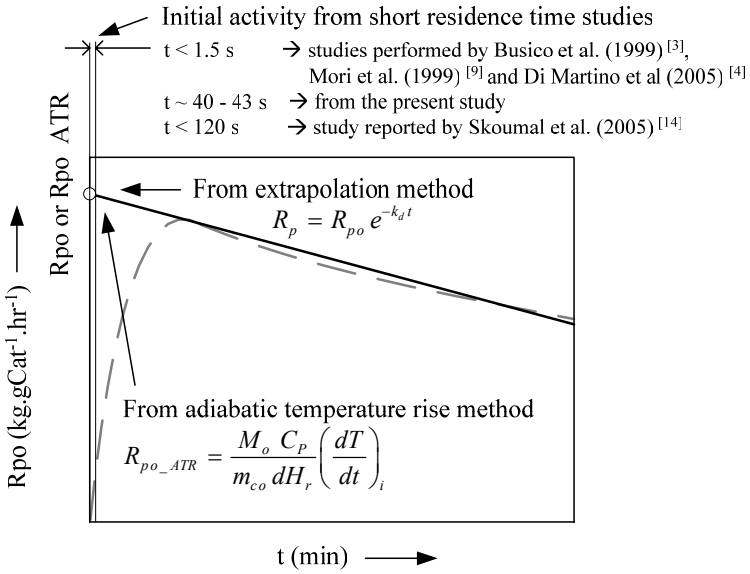

Figure 5.1: Schematic kinetic curve obtained during the propylene polymerization (for extrapolation and adiabatic temperature rise methods see Chapter 3).

As can be seen from Figure 5.1, the profile drawn in dotted lines illustrate the characteristic kinetic response of the catalyst type used in this study, in which the rate may rise very rapidly to a maximum value, depending upon the activation process with the cocatalyst, and then decreases with time. This response is derived from the measured temperature and pressure profiles during reaction, and can be affected by a composition of active catalyst and process variables. Therefore, with the magnitude of reactor and time scale, it is sometime tricky to estimate the initial activity of the catalyst. Generally,

different ways are adopted to estimate the initial polymerization rate, such as extrapolation and adiabatic temperature rise methods (discussed in Chapter 3). On the other hand, from Figure 5.1, it can be seen that the short residence time study reported here could present an excellent opportunity to estimate the initial activity of the catalyst.

Next important key issue is analysis of time-scales involved with the olefin polymerization processes developed over a past few decades for the industrial scale polymer production. The schematic of time-scales for the different processes is discussed in Chapter 1. It has been seen that these processes differ in both the physical state of the reactor media and in the mechanical operation of the unit. It is often reported that the choice of different processes is determined by economics, feedstock availability, catalyst type and desired range of polymer products to be produced, and thus mainly divided into three parts, for example,

1. Slurry-phase processes either with an inert diluent or condensed monomer (loop and continuous stirred tank reactors).
2. Gas-phase processes (such as vertical stirred bed reactor, horizontal stirred bed reactor and fluidized bed reactor).
3. Solution (multi) phase processes where the solvent temperature is high enough to dissolve the polymer material (tube and stirred tank reactors).

Several modeling approaches have been developed for these processes depending upon the scope of interest varying from single particle models to a study involving the analysis of macro scale properties of the process such as reactor hydrodynamics. These models provide some useful information related to the reactor behavior in terms of residence time distribution (RTD) of the reactor as well as in terms of particle size distribution (PSD) of the catalyst and polymer on the polymerization kinetics and polymer properties.

However, McKenna et al. (2005) [8] reported that ideally there is still need to link the phenomena taking place on the different time-scales via an “all-encompassing process model” in order to quantify how reactor conditions, polymer particle characteristics and polymerization kinetics combine to form the polymer obtained at the reactor exit. The authors suggested that such approach will provide a better control on the development of the new olefin polymerization processes and polyolefin materials with novel properties.

With this understanding, the focus of the present study is to introduce and demonstrate an experimental technique applicable for catalytic polymerization under near-industrial

conditions. On this basis, a novel (capillary type) tubular reactor has been developed especially for performing the catalytic olefin polymerization. An important objective of this work is to investigate the early stage polymerization kinetics of liquid propylene by carrying out polymerization tests with a shortened reaction time, and address its possible application as a "high-output" tool for the fast estimation of kinetics. From such tests, it will be interesting to know that,

1. What will be the effect of reactor dynamics on the reaction kinetics and morphology of the produced polymer?
2. Is it possible to reduce the reaction time for kinetic investigation from hours to minutes, ultimately speeding-up the catalyst characterization as well as monomer quality check by varying different process parameters?
3. What will be the effect of RTD on the molecular weight distribution (MWD) of the produced polymer?
4. Is it feasible to extend the understanding from the present study to a macro scale level of real polymer production and to analyze its applicability on the industrial scale as a "prepolymerization reactor" and/or a "main reactor"?

The details about the complete experimental set-up are reported in Chapter 2, which also provides information regarding chemicals, polymerization procedure, analytical techniques and their recipes used in this study. The catalyst type used here was a highly active supported catalyst of type $MgCl_2/TiCl_4$ with Phthalate as an internal donor, Silane as an external donor and Triethylaluminum (TEA) as a cocatalyst [$]. The polymerization experiments were carried out with an injection of preactivated catalyst slurry into a continuous flow of liquid propylene, with a short residence time inside the reactor. The catalyst response with respect to temperature profile over the reactor length has been analyzed at near-industrial polymerization conditions. The obtained temperature curves describing the kinetic performance of the catalyst during reaction are reported in this chapter and compared with the kinetic data evaluated for the same catalyst type from the batch polymerization experiments; see Chapter 3.

A few polypropylene (PP) samples were analyzed for MWD using GPC technique. The GPC data is reported here, especially to understand the effect of hydrogen on the molecular properties of polymer at extremely high hydrogen concentrations. At present,

[$] Details of catalyst preparation or composition are confidential; however, it is irrelevant here from the point of view of objectives involved with the present study.

comparable data on polymerization kinetics are not available in the open literature for the range of hydrogen concentration used in this study. Selected PP samples were characterized for the morphology studies using SEM, EDX, PSD and DSC techniques, and relevant investigations are discussed with respect to the different process parameters such as temperature, hydrogen concentration and quenching agent.

5.2 Reactor behavior

The experimental results obtained from selected catalytic liquid propylene polymerization tests performed in a tubular reactor are discussed in this section. The schematic of reactor system is given in Figure 5.2, and the complete reactor set-up is discussed in Chapter 2. The kinetic experiments reported here were carried out with the injection of preactivated catalyst into a continuous flow of liquid propylene at reaction temperature of 70 ^{o}C and pressure of 65 bar. A 2.70 kg.hr^{-1} of mass flow rate for liquid propylene was used while performing the polymerization experiments, yielding an average axial velocity of 14 cm.s^{-1}. This axial velocity is constantly maintained over the period of reaction in order to avoid the flow disturbances caused due to the changing properties of the reaction mixture. As the polymerization reaction proceeds further, the reactive plug travelling along the different zones of tubular reactor will contain a mixture of liquid propylene with density of 438.3 kg.m^{-3} and a polymer phase having density of 900 kg.m^{-3}.

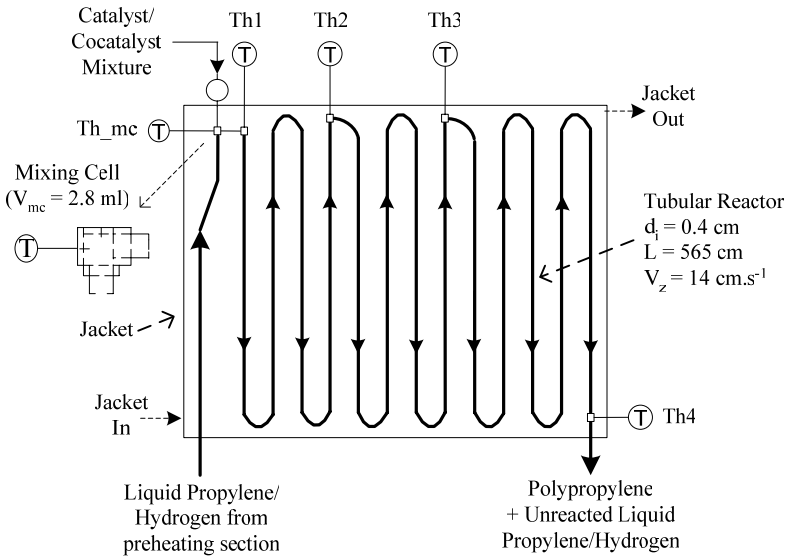

Figure 5.2: Schematic of tubular reactor set-up (for details see Chapter 2).

For preactivation, the weight ratio of cocatalyst and external donor to catalyst was kept constant at 10 $mg.mg^{-1}$ and 1 $mg.mg^{-1}$, respectively. The preactivated catalyst was injected in a pulse mode into the reactor. These pulses were created using a pulsating valve with the stroke rate and stroke length of 42 $strokes.min^{-1}$ and 1.2 cm, respectively [‡‡‡]. With such specification of pulsating valve, a 0.1 ml of catalyst slurry was injected into the reactor with the every stroke having an injection period of 1.45 $s.stroke^{-1}$. A single pulse of catalyst was created by immediate injections of few strokes (therefore allows varying amount of catalyst with every pulse). In case of hydrogen experiments, the mass flow of hydrogen and propylene was maintained constantly over the period of experiment, and hydrogen was believed to be completely dissolved in the liquid propylene due to over-pressurized (completely filled) reactor system. At the exit of the reactor, the reactor mixture was expanded into the quenching agent.

The temperature profiles with respect to time and axial coordinates were measured using five thermocouples placed along the reactor length. They are shown in Figure 5.2 as different thermocouple sections like Th_mc, Th1, Th2, Th3 and Th4 and located in axial direction at 0, 0.1, 1.88, 3.57 and 5.65 m positions, respectively [§§§]. The accuracy of temperature measurement is in the order of 0.01 K. The reactor pressure was measured using two pressure sensors placed at the inlet and exit of the reactor (not shown in Figure 5.2). These pressure sensors were used to monitor the plugging inside the reactor by following the pressure drop over the reactor length. Several experiments were carried out to standardize the polymerization test with respect to the catalyst loading and flow conditions of monomer. However, due to the present specification of HPLC pump the liquid propylene flow rate was kept at its maximum volumetric flow rate of 90 - 95 $ml.min^{-1}$, and resulted in an average Reynolds number (Re) of ≈ 3700.

It indicates that it is vital to analyze the mixing behavior of the freshly injected catalyst pulse after being in contact with liquid propylene. As can be seen from Figure 5.2, the catalyst pulse was injected into a so-called “Mixing Cell” with a volume of 2.8 ml, installed especially to enhance a mixing of catalyst mixture with the liquid propylene. The mixing pattern inside this cell will certainly be influenced by the amount of catalyst

[‡‡‡] The stroke rate of pulsating pump differs from one pump to another, and it is advisory to check before its operation. For example, a pump with stroke rate 30 $strokes.min^{-1}$ will have an injection period of 1.98 $s.stroke^{-1}$.

[§§§] The length was calculated according to catalyst injection point, which is the “Mixing Cell” shown in Figure 5.2.

being injected, the flow velocity of liquid propylene and the subsequent particle dynamics of an active catalyst due to the reaction, ultimately changing the thermal balance of the cell. Thus, the developed mixing behavior inside the "Mixing Cell" will definitely have consequences on the temperature profile along the reactor length.

With the present set-up design, the characteristic of "Mixing Cell" was possible to analyze by measuring the temperature rise inside the cell after injection of an active catalyst pulse. The experiments were performed to see the effect of catalyst amount by means of injecting different pulses of catalyst slurry via varying the catalyst quantity from 0.06 mg in 1 stroke to 0.24 mg in 4 strokes with the injection period of 1.45 s.stroke^{-1}. The obtained thermal response inside the "Mixing Cell" is shown in Figure 5.3. The observed temperature distribution was believed to be due to the exothermic nature of polymerization reaction initiated after the addition of active catalyst particles into the continuous flow of liquid propylene. Figure 5.3 compare the temperature dynamic measured from the "Mixing Cell" and from the CSTR model. The temperature distribution observed in Figure 5.3 can be assumed as a function representing the RTD of active catalyst particles, and exhibit a RTD of near perfectly mixed CSTR. From Figure 5.3, it is also noticed that with the increasing amount of catalyst loading, the RTD of active catalyst particles is found to be more dispersed.

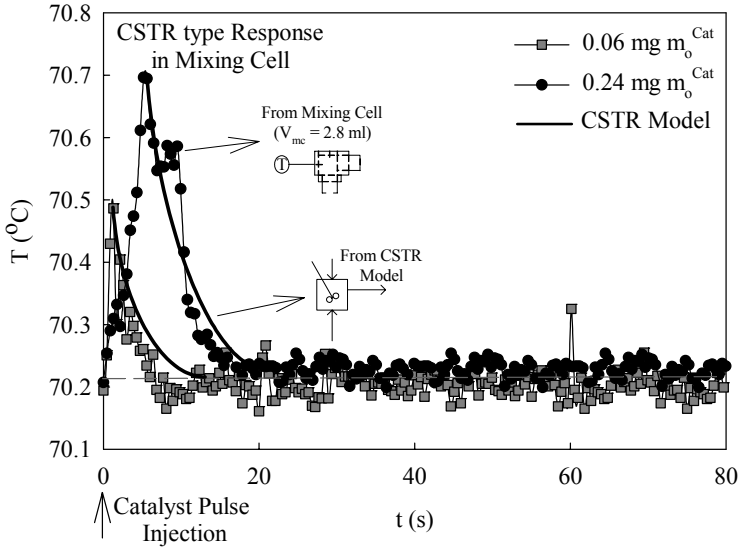

Figure 5.3: Thermal response in mixing cell
(experiment performed with the procedure reported above and with X value of 0.0219).

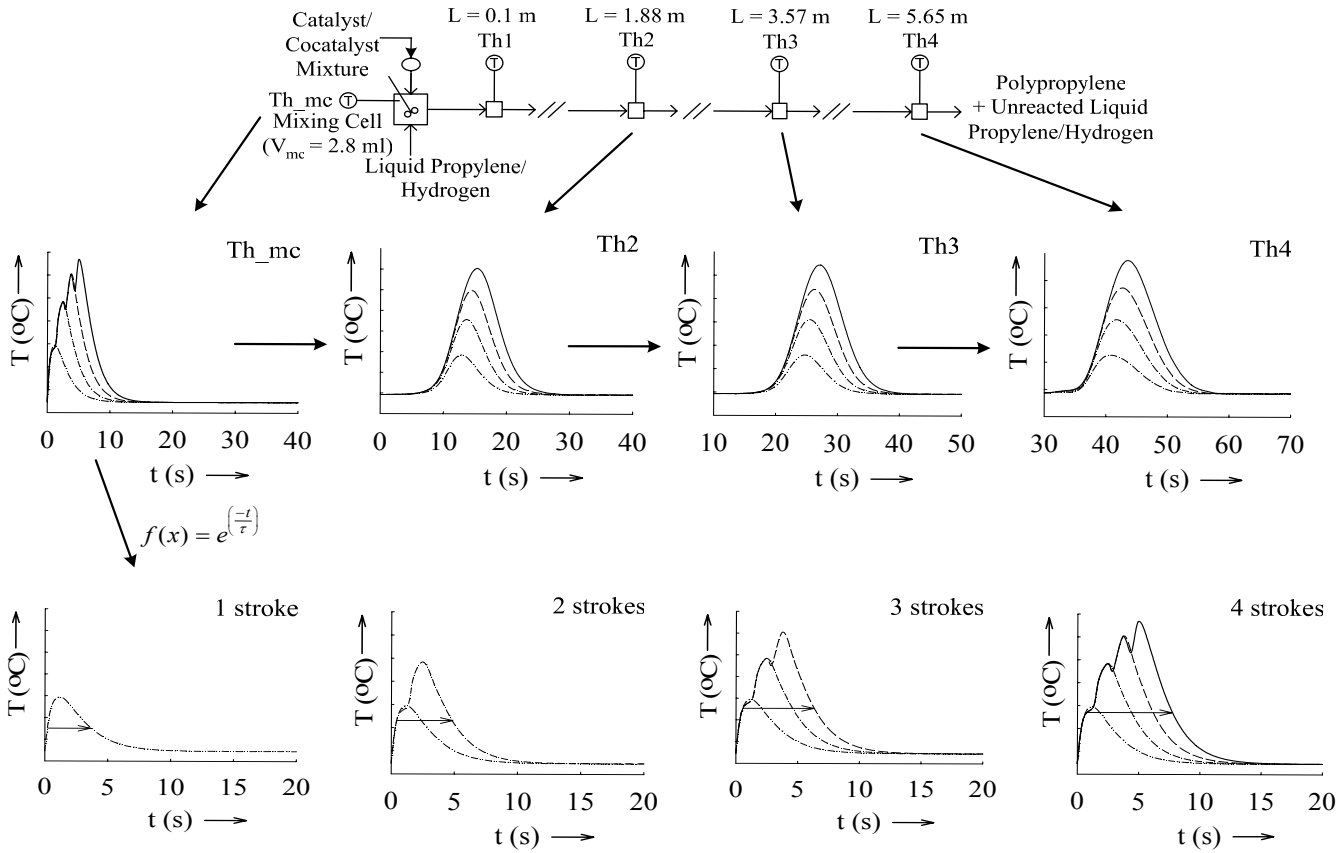

Figure 5.4: Schematic of temperature profile along the reactor length obtained after the injection of different active catalyst pulses into a continuous flow of liquid propylene(−·−·−·−·−1 stroke, −·−·−·−·− 2 strokes, −−−−−−3 strokes, ——— 4 strokes) [****].

[****] The case study presented in Figure 5.4 is simulated using a developed mathematical model for the reactor system used in this work (see Chapter 6). The parameters used for simulation are T_o = 70 ^oC, P_o = 54 bar, m_{fr}^M = 2.71 $kg.hr^{-1}$, catalyst amount per stroke = 0.06 mg, X = 0.0 and axial velocity = 14 $cm.s^{-1}$. In Chapter 6, the dynamic behavior of present reactor set-up is discussed in detailed together with mathematical reactor model.

The question arises now how will these different pulses with different RTD's take a shape along the reactor length. Theoretically, it can be easy to check by developing the mathematical model according to the present reactor specifications and considering the reactor model as a CSTR followed by the tubular reactor; see Figure 5.4. The complete mathematical model is developed and evaluated in Chapter 6. The temperature profiles shown in Figure 5.4 were obtained by simulating the reactor performance for injection of different number of strokes (thus varying the catalyst quantity). It was observed that with increasing number of strokes the dispersion of temperature distribution (representing RTD) estimated at each thermocouple section was enhanced. Similar to Figure 5.3, the CSTR type response of "Mixing Cell" is highlighted in Figure 5.4, depicting the broadening of temperature profile with increasing number of strokes. Moreover, it is also noticed that the "degree of change" in dispersion in case of individual catalyst pulse moving along the reactor length is not very significant, and thus showing a narrow temperature distribution in axial direction (see Figure 5.4).

In order to check the hypothesis presented in Figure 5.4, few polymerization runs were carried out with the injection of different pulses of catalyst slurry. The catalyst amount was varied as 0.12 mg, 0.18 mg and 0.24 mg with catalyst amount per stroke of 0.06 $mg.stroke^{-1}$ and injection period of 1.45 $s.stroke^{-1}$. These experiments were performed in the absence of hydrogen in order to have a mild catalyst activity and therefore controlling the temperature rise inside the reactor. Mainly, because the catalyst used in this work exhibits high activity in presence of hydrogen, and can be seen from the batch reactor data reported in Chapter 3.

Figure 5.5 represent the thermal response of the reactor measured from these experiments. As per mentioned earlier, after injection, the catalyst-cocatalyst system initiates an exothermic polymerization reaction with a continuous flow of monomer. The polymerization reaction generates a temperature profile over the reactor length indicating catalyst activity and accordingly polymerization rate; see Figure 5.5. This way, for the first time, the thermal response of the catalyst was noted at the time-scale of early stage polymerization with near-industrial polymerization conditions. The history of these temperature profiles will depend on,

1. Reaction kinetics (heat production).
2. Heat transfer to the cooling media.
3. Mixing dynamics of reactor fluid.

(a)

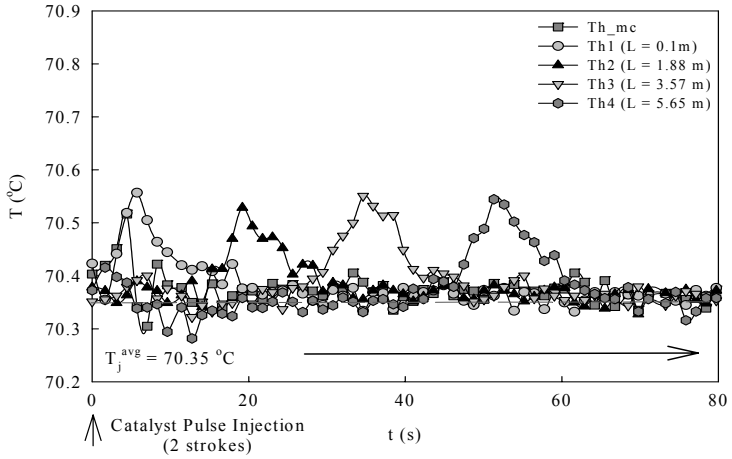

(b)

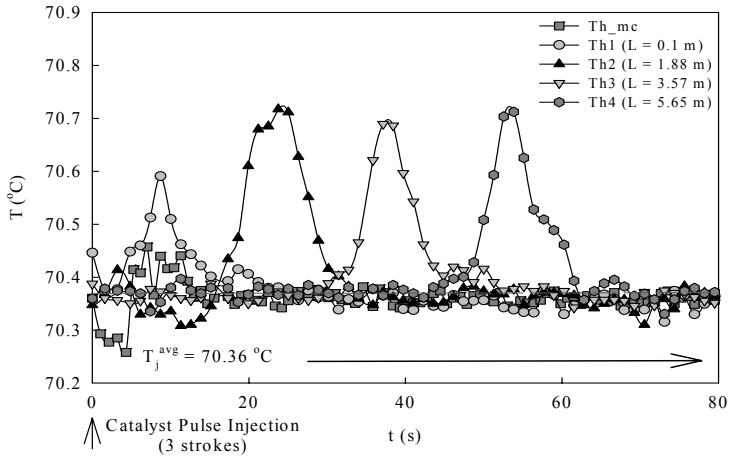

(c)

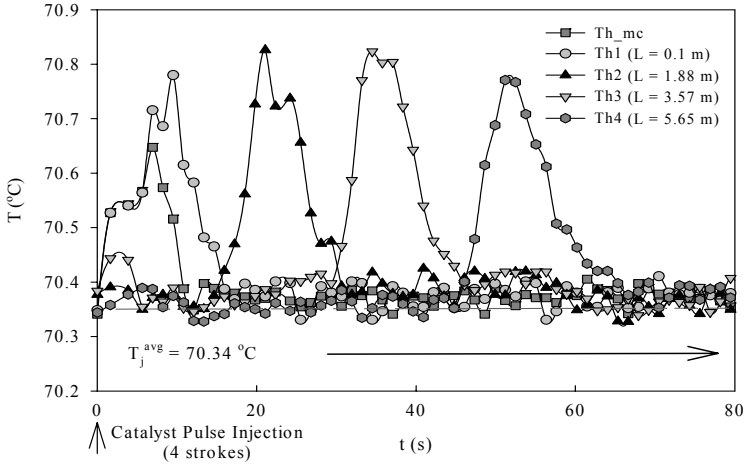

Figure 5.5: Observed temperature profile after injection of a preactivated catalyst pulse into a flow of liquid propylene; (a) m_o^{Cat} = 0.12 mg, (b) m_o^{Cat} = 0.18 mg and (c) m_o^{Cat} = 0.24 mg (X = 0.0, injection period = 1.45 s.stroke^{-1}).

For instance, an intense release of heat during the initial stages of polymerization, caused by the high initial catalyst activity, could unfavorably influence the formation and stability of active sites [17]. The impact on such temperature profiles might also come from the instantaneous heat transfer from the reactor to jacket. However, with the present design of the reactor system all experiments were carried out in an isoperibolic mode by keeping the jacket temperature constant, which allowed measuring the "quasi-adiabatic temperature rise" inside the reactor.

The effect of catalyst loading on the release of heat is well observed from the Figure 5.5; however, its intensity is low due to the low initial activity of the catalyst especially in the absence of hydrogen. The increase in maximum temperature of first thermocouple section (Th1) was found to be increased by factor 2 with the increase in mass of catalyst from 0.12 mg to 0.24 mg. The maximum temperature of other three thermocouple sections (Th2, Th3 and Th4) showed a constant value indicating a quasi steady state. The average value of maximum temperature for thermocouple section Th2, Th3 and Th4 showed increment of 0.2 K, 0.32 K and 0.45 K with increasing catalyst amount of 0.12 mg, 0.18 mg and 0,24 mg, respectively (see Figure .5.5). This effect is obvious as with the increasing amount of catalyst the probability that number of active particles will grow due to polymerization is increased thus enhancing the heat release.

As can be seen from Figure 5.5, with increasing number of strokes the dispersion of temperature distribution measured at thermocouple sections Th1, Th2, Th3 and Th4 is found to be enhanced. The effect observed here is similar to the simulation studies shown in Figure 5.4. However, the broadening of temperature distribution obtained at individual thermocouple section is not consistent. Such in-homogeneity in the dispersion of temperature profile observed experimentally can be explained based on "stochastic" of the active catalyst particle dynamics injected into the reactor.

This suggests that it is essential to know, what happens to a particle of a supported catalyst when it is injected into an olefin polymerization reactor. Just to get an idea, Figure 5.6 present a simplified schematic of the reactive plug created inside the reactor after an injection of different amount of active catalyst. Figure 5.6 illustrate the different factors influencing the characteristics of the reactive plug, such as,

1. Increasing particle clouds with increasing number of strokes.
2. Pressure fields acting on the boundaries of the plug.
3. The movement of the upward and downward flow of the plug.

4. The changing physical properties of the bulk liquid-phase affecting the mixing and heat transfer dynamics of the plug.

In addition, Figure 5.6 also exhibit that the interaction between these factors will change with the increasing concentration of active catalyst particles as well as with the proceedings of polymerization reaction. The hydrodynamics of this reactive plug may alter with the increasing population of particles when injected into a constant flow of liquid propylene, and may influence the local interaction between the particles.

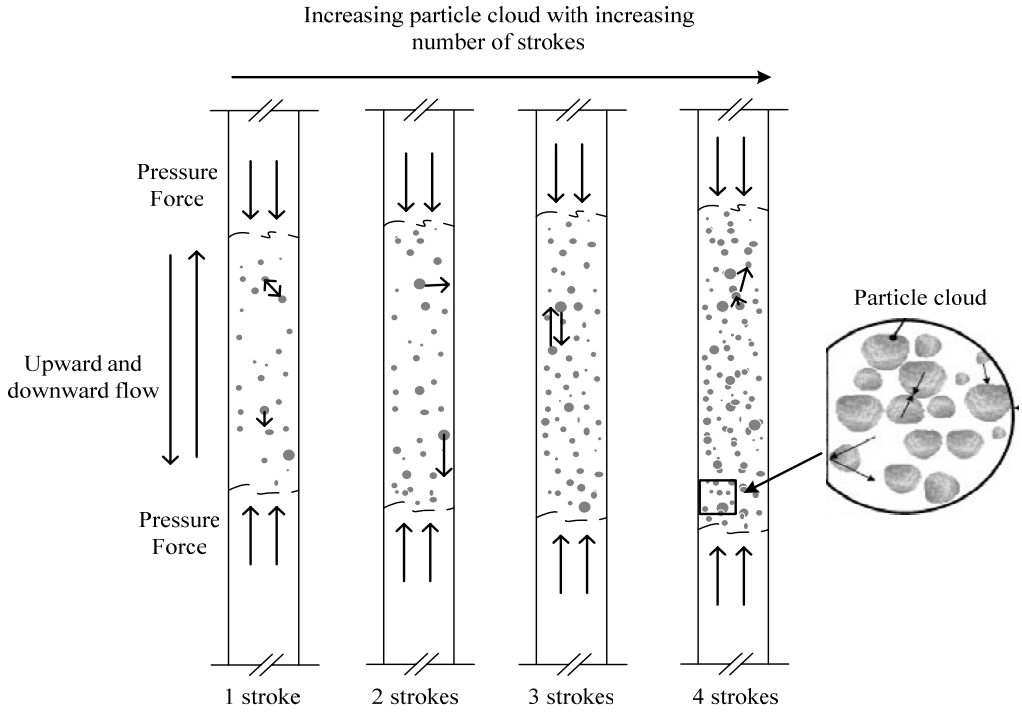

Figure 5.6: Schematic of an increasing population of active catalyst particles inside the reactive plug created by injection of different number of strokes.

Furthermore, immediately after the injection, the porous catalyst particles will follow several extremely important phenomena taking place during olefin polymerization. The occurrence of these phenomena will be influenced by several factors such as,

1. Reactor flow pattern.
2. Reaction conditions.
3. Concentrations of reactive species.
4. Phase present in the reactor: “Influencing mixing”.
5. Movement of the particles: “Sedimentation behavior” - changing RTD.

6. Initial morphology of an active catalyst particle.
7. Effect of inter- and intra - particle mass and heat transfer in the presence of changing degree of particle clouds ††††.

Therefore, it is important to understand the interactions between different phenomena that are taking place on a large number of length scales in order to describe correctly the role of particle dynamic, reaction kinetics, and development of product properties along with the reactor hydrodynamics. One of such phenomena often reported in literature is the "fragmentation step" describing the rapid process of rupture and expansion due to the particle growth of 2 - 5 times to its original size in only 2 - 3 s, ultimately determines the morphology of the particle.

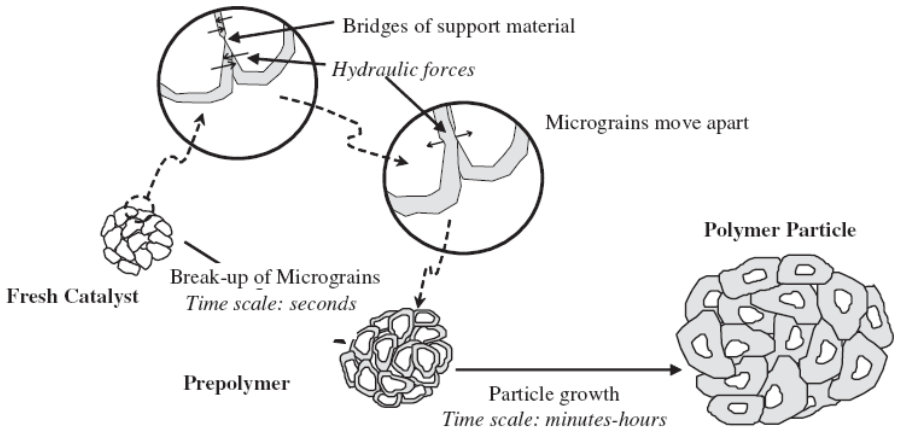

Figure 5.7: A schema of the particle fragmentation, growth and the evolution of particle morphology suggested by McKenna et al. (2005) [8].

Figure 5.7 show the scheme of the particle fragmentation, growth and the evolution of particle morphology recently reported by McKenna et al. (2005) [8]. Figure 5.7 explains, what happens to a particle of a supported catalyst when it is injected into an olefin polymerization reactor. In Figure 5.7, the authors highlighted few interesting phenomena that are taking place during the course of polymerization reaction,

1. After injecting the porous catalyst particle into the reactor, instantaneously the monomer begins to diffuse into the pores, and a layer of polymer forms on the active sites located on the pore walls.

†††† Particle cloud: Ratio representing the number of particles present per unit volume of reactor space.

2. The build-up of polymer will lead to a rupture of support material after a few seconds of reaction.
3. If the catalyst particle is well engineered, it will remain its original form due to entanglement of the polymer molecules; otherwise, it can either sinter, leading to fines or not fragment at all.

From the observed experimental findings, it is clear that the present reactor operating conditions and flow behavior has certainly played a role in controlling the temperature distribution along the reactor length. The constant dispersion of these distributions may have occurred due to the,

1. Reactor operating under high pressure of liquid propylene (40 - 65 bar).
2. Upward and downward motion of reactor flow controlling the sedimentation of active growing particles [‡‡‡‡].
3. Uniform change in the local "particle - particle" interaction in a given reactive plug flowing along the reactor length over the period of reaction time.

However, it should be remembered that the catalyst activity in the absence of hydrogen is very low and might exhibit a limited influence of reaction kinetics at the early stage of polymerization.

Therefore, it is interesting to know that how will the active catalyst particles perform when injected into the reactor in the presence of hydrogen. As noted earlier, the catalyst type used here exhibit higher polymerization activity in the presence of hydrogen. Furthermore, the higher activity indicate that the process of fragmentation for an active catalyst particle might take place at much faster rate in comparison to the low catalyst activity observed during the polymerization tests carried out in the absence of hydrogen. In order to observe the thermal response of the catalyst at its high initial activity, selected propylene polymerization experiments were performed in the presence of hydrogen with a 0.0219 mole ratio of hydrogen to liquid propylene (X). Figure 5.8 (a) and (b) represent the obtained temperature profiles from these tests carried out in the presence of different concentrations of active catalyst.

[‡‡‡‡] The upward and downward motion is obtained due to the vertical assembly of tubular reactor; see Figure 5.2. The sedimentation behavior of the growing polymer particles is characterized based on its terminal settling velocity, and can be estimated from the standard correlation. These correlations are presented in Chapter 6.

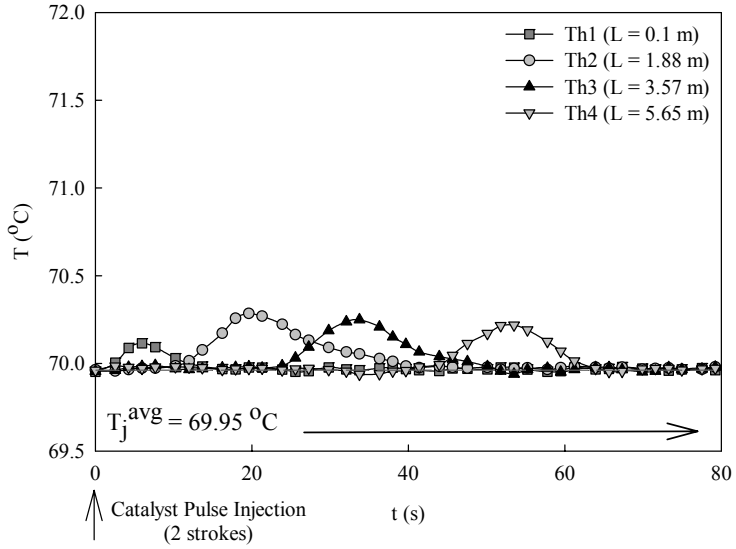

(a) Experiment performed with X = 0.0219, diluted catalyst slurry, m_o^{Cat} = 0.06 mg, injection period = 1.45 s.stroke^{-1}.

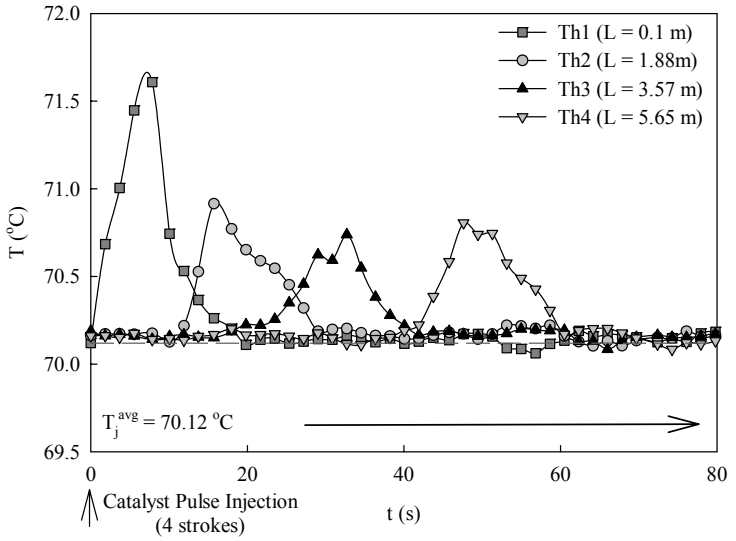

(b) Experiment performed with X = 0.0219, concentrated catalyst slurry, m_o^{Cat} = 0.24 mg, injection period = 1.45 s.stroke^{-1}.

Figure 5.8: Observed temperature profile after injection of a preactivated catalyst pulse into a flow of liquid propylene.

Injection of much diluted catalyst pulse (m_o^{Cat} = 0.06 mg) generated a limited rise of 0.17 K in temperature of Th1 section and showing increment of 0.3 K in maximum temperatures of other three thermocouple sections; see Figure 5.8 (a). On the other hand, from Figure 5.8 (b), it is observed that the injection of concentrated catalyst slurry resulted to a temperature rise of 1.55 K in Th1 section and descending to average maximum temperature value of 0.8 K in other three thermocouple sections.

Additionally, it is also observed that the dispersion of obtained temperature distribution is higher for the polymerization tests performed in the presence of hydrogen in comparison to the experiments carried out in the absence of hydrogen.

As can be seen from Figure 5.8 (a) that the catalyst activity observed to be still increasing until 20 s of reaction time. The similar trend was also observed for catalyst activity measured from the test performed in absence of hydrogen. On the other hand, Figure 5.8 (b) shows a rapid decrease in activity to a level of 50 % of the starting value over a period of first 20 s, and after this, catalyst activity becomes much more stable. Skoumal et al. (2005) [15] described this behavior as a characteristics of the high activity catalysts exhibiting high initial polymerization rates, with a very fast initiation period, followed by polymerization rate deceleration. Pimplapure et al. (2005) [13] interpreted such initial drop in the catalyst activity because of the growing polymer layer around the active sites leading to an "encapsulation effect" (also see Weickert et al. (2005) [17]).

This exhibits that the degree of increment in temperature might be depending on the,

1. Changing concentrations of chemical constituents present in a reactive plug of the reactor: especially the "dilution effect".
2. Nature of the active sites present on the catalyst particle and their distribution on the support material.
3. Stochastic of the fragmentation process of catalyst particle after became in contact with the liquid propylene under given process conditions.
4. Dynamics of the complex relation between kinetic reaction rates, polymer properties, and particle fragmentation.

The reactor behavior discussed here showed a unique "opportunity" and "potential" for analyzing kinetic performance of the catalyst by systematically varying the polymerization conditions. With the ease in changing the reactor dimensions as well as process parameters, the fast characterization of catalyst is possible to execute with a reduced reaction time. An importance of this tool for investigation of reaction kinetics

and subsequent off-line characterization of produced polymer is demonstrated in the following sections.

5.3 Kinetic analysis

Table 5.1 show the experimental recipes for number of polymerization runs carried out to study the effect of different process parameters on the reaction kinetics along with the performance of tubular reactor. These experiments were performed with multiple pulse injections of preactivated catalyst into the reactor. The amount of catalyst injected with a single pulse is optimized in order to avoid any operational problems such as "reactor plugging". In the present study, quite often, the plugging phenomena in tubular reactor have been observed due to the injection of concentrated preactivated catalyst slurry, yielding a pressure drop (ranging from 4 to 30 bar) over the reactor length. It was noticed that the pressure drop usually either caused due to an incomplete washing out of the active catalyst particle or because of the accumulation of agglomerates (large polymer particles) at the back pressure valve placed at the end of the reactor.

Figure 5.9 shows two distinct regions for the selection of amount of catalyst per number of strokes. A linear relationship was observed between the catalyst amount and the number of strokes. This linearity predicts the mixing behavior inside the catalyst vessel, and evident the effect of continuous bubbly flow of helium through the vessel, which restrict the sedimentation of catalyst particles.

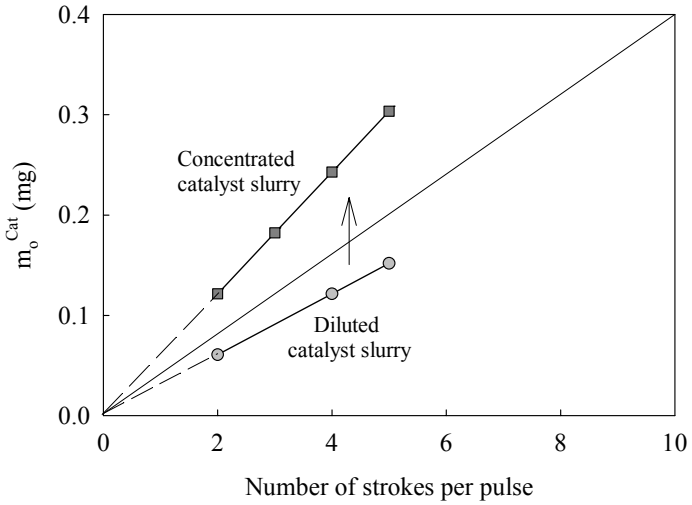

Figure 5.9: Amount of preactivated catalyst injected with different number of strokes.

Table 5.1: Experimental conditions for all the tests performed with a tubular reactor to study the catalytic polymerization of liquid-phase propylene [$]

Experiment Code	T_o (^oC)	P_o (bar)	m_{fr}^M ($kg.hr^{-1}$)	m_o^{Cat} † (mg)	X ($molH_2o.molPPYo^{-1}$)	Quenching Agent
Run51	40.0	40.0	2.68	3.20	0.0	EtOH
Run52	50.0	43.8	2.69	6.32	0.0	EtOH
Run53	50.0	40.0	2.68	2.71	0.0	EtOH
Run54	70.0	43.8	2.69	2.67	0.0	EtOH
Run55	70.0	43.5	2.69	2.46	0.0	EtOH
Run56	70.0	43.5	2.69	2.29	0.0	EtOH
Run57	70.0	65.0	2.73	0.76	0.0219	EtOH
Run58	70.0	54.0	2.71	0.77	0.0219	CO_2 + EtOH
Run59	70.0	54.5	2.71	0.73	0.0219	CO_2 + 1N HCl
Run510	70.0	54.0	2.71	0.20	0.0219	CO_2 + EtOH
Run511	70.0	54.0	2.71	0.77	0.0219	CO_2 + EtOH
Run512	70.0	54.0	2.71	0.50	0.0219	CO_2 + EtOH
Run513	70.0	53.0	2.71	0.55	0.0219	CO_2 + EtOH
Run514	70.0	54.5	2.71	0.73	0.0219	CO_2 + 1N HCl
Run515	70.0	55.0	2.71	3.31	0.0510	CO_2 + EtOH
Run516	70.0	55.0	2.71	3.20	0.0981	CO_2 + EtOH
Run517	80.0	48.6	2.70	2.89	0.0	EtOH

[$] The weight ratio of cocatalyst to catalyst was 10 $mg.mg^{-1}$ and external donor to catalyst was 1 $mg.mg^{-1}$. The jacket temperature was always maintained at the initial reaction temperature (for isoperibolic mode).
† The m_o^{Cat} values reported here, represents the total amount of catalyst injected in pulse mode over the period of reaction.

The overall summary of experimental results, presenting the activity, yield, molecular properties and average particle size ($d_p(0.5)$) of produced PP samples are given in Table 5.2. The activity data obtained from these experiments was estimated from the polymer yield and average residence time of the tubular reactor. The yield, for each experiment, was calculated based on the amount of PP produced (g) per amount of injected preactivated catalyst into the reactor (gCat). The average residence time of tubular reactor was measured to be 40 - 43 s based on the mass flow rate of liquid propylene. Therefore, the activity obtained from tubular reactor could be referred as an "initial polymerization rate" due to the short residence time (see Figure 5.1).

Table 5.2: Tubular reactor data for activity, yield, molecular weights and particle size

Experiment Code	Activity ($kg.gCat^{-1}.hr^{-1}$)	Yield ($g.gCat^{-1}$)	M_v^{avg} ($kg.kmol^{-1}$)	M_w^{avg} ‡ ($kg.kmol^{-1}$)	PDI	$d_p(0.5)$ (μm)
Run51	5.0	63.2	2131000	*3122000*	-	66.7
Run52	8.7	107.0	2040000	*2990000*	-	79.0
Run53	9.3	114.7	2110000	*3092000*	-	-
Run54	24.2	262.2	2200000	*3224000*	-	107.5
Run55	22.5	243.9	2298000	*3367000*	-	-
Run56	23.6	255.5	2102000	*3080000*	-	-
Run57	129.3	1437.9	58000	73000	7.3	166.7
Run58	130.6	1407.5	-	-	-	-
Run59	128.8	1421.7	-	-	-	-
Run510	131.8	1424.7	-	-	-	-
Run511	130.6	1407.5	60000	-	-	168.1
Run512	131.0	1445.2	58000	-	-	-
Run513	129.5	1427.1	-	-	-	-
Run514	128.8	1421.7	-	-	-	-
Run515	86.0	948.9	47000	64000	8.6	155.6
Run516	61.5	679.2	30000	43000	9.5	140.2
Run517	32.2	330.3	2019000	*2960000*	-	116.5

‡ M_w^{avg} values shown in italic are estimated using M_v^{avg} with a standard correlation.

The reproducibility of (active) catalyst injection has been tested by repeating the standard experiment at 70 ^oC; see Table 5.1 and Table 5.2. The catalyst performance at different reaction temperatures can be seen from Table 5.1 and Table 5.2. A known amount of catalyst was injected into the reactor at different reactor temperatures, and reaction was carried out under an isoperibolic reaction condition. It appears that the catalyst activity is strongly influenced by temperature, and shows an increment of factor 1.5 to 2 with every 10 ^oC rise in temperature. The increasing trend in "initial" catalyst activity with increasing reaction temperature is shown in Figure 5.10. The effect observed in tubular reactor was comparable to the batch experiments data; see Chapter 3. Interestingly, the decreasing effect in the initial catalyst activity above 70 ^oC was also not observed in the present study, and thus can be confirmed that experiments done with a completely filled reactor has an influence on the dynamics of active catalyst particles during the reaction, and may vary from one catalyst type to another. It was interesting to note that activity in

tubular reactor is higher by approximately 14 to 30 % in comparison with batch reactor data; see Figure 5.11. The high activity can be judged on the basis of two factors, one with respect to the dynamic behavior of tubular reactor in terms of mixing and heat transfer and another with regard to the influence of "early stage" processes on the subsequent polymerization reaction; see Weickert et al. (2005) [17].

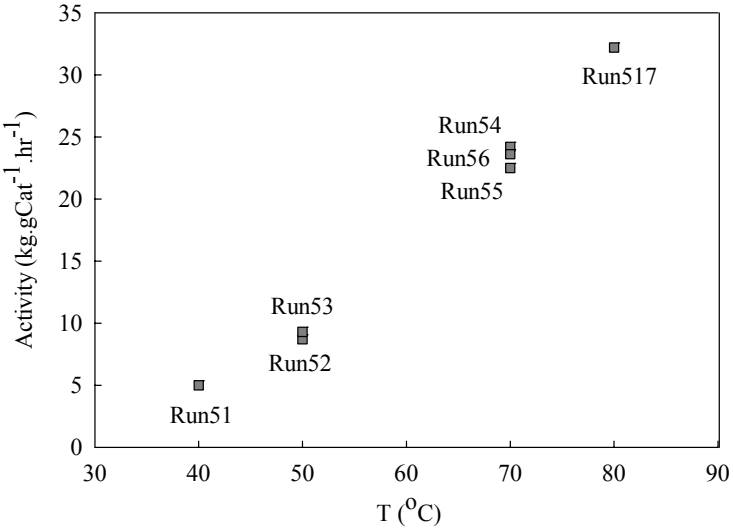

Figure 5.10: Catalyst activity obtained from tubular reactor experiments as a function of reaction temperature.

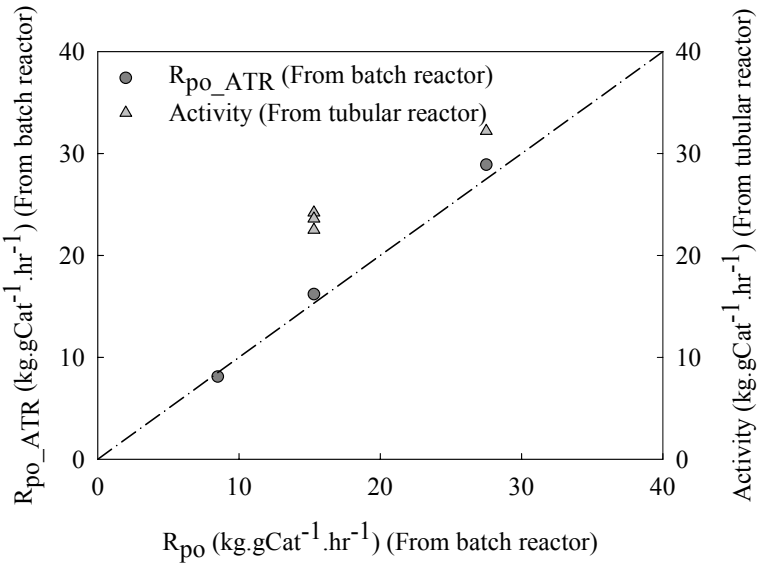

Figure 5.11: Comparison of polymerization activity obtained from tubular reactor with batch reactor data.

An Arrhenius plot for (polymerization) activity is given in Figure 5.12, enabling the estimation of apparent activation energy for propagation reaction (E_p) together with the Arrhenius constant (k_{po}). In general, the similar experimental studies performed with the "quenched-flow" technique seem to give a higher value of propagation constant (k_p). For instance, Keii et al. (1987) [7] observed such high value of k_p for the slurry polymerization of propylene using MgCl2-supported ZN catalyst type, and Busico et al. (1999) [3] found the similar finding for slurry polymerization of ethylene using metallocene catalyst in comparison with k_p obtained from the conventional slurry polymerization process. According to the literature reviewed in Chapter 1, the reason for such finding was believed to be mainly due to the differing time (polymerization yield) pertaining to the particular methods. For the first the time the high value of k_p (by a factor of 1.6) was observed in case of a liquid-phase propylene polymerization performed in the tubular reactor over a short residence time as compared to the k_p observed from the batch reactor kinetic data (see Figure 5.12).

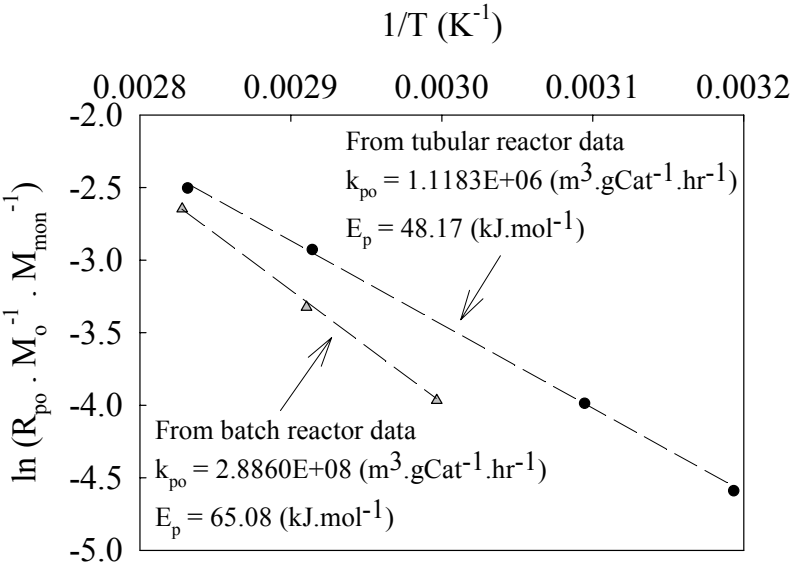

Figure 5.12: Comparison of Arrhenius plot obtained for the activity from tubular reactor as well as from batch reactor experiments (see Chapter 3 for batch reactor data).

The effect of hydrogen on the reaction kinetics as well as on the molecular properties of the polymer was studied from the experiments performed at X values ranging from 0.0219 to 0.0981. The polymerization activity and molecular property data obtained from these experiments has already been analyzed with the batch experiment data; see Chapter 3 and Chapter 4.

According to the previous discussions, it is noticed that using a batch polymerization reactor, the hydrogen response on the catalyst activity is studied only up to a critical value of X. However, with the help of tubular reactor used in this work, a unique opportunity is created to study the influence of hydrogen over a wide range. As per data shown in Chapter 3 and Chapter 4, the tubular reactor has been used to perform the polymerization reaction with the X values of 0.0219, 0.0510 and 0.0981. The overall influence of hydrogen on the activity of catalyst is shown in Figure 5.13, wherein the data obtained on the initial reaction rate from batch and tubular reactor experiments is combined together. For batch reactor experiments, the initial activity of the catalyst showed an accelerating effect upon increasing the value of X up to 0.01. From tubular reactor experiments with high values of X, it appeared that above 0.0219 value of X the retardation period was observed for catalyst activity (see Figure 5.13), and similarly can be seen from Table 5.1 and Table 5.2, the activity decreases to 86 and 61.5 ($kg.gCat^{-1}.hr^{-1}$) at the X values of 0.05 and 0.1, respectively.

To the author's knowledge, for the first time, the influence of hydrogen over a wide range was investigated for liquid-phase propylene polymerization, and modeled with the help of improved kinetic mechanisms. The detailed analysis of this kinetic model for catalyst activity and average probability of chain termination (q; representing inverse of average molecular weights) has already been discussed in Chapter 4.

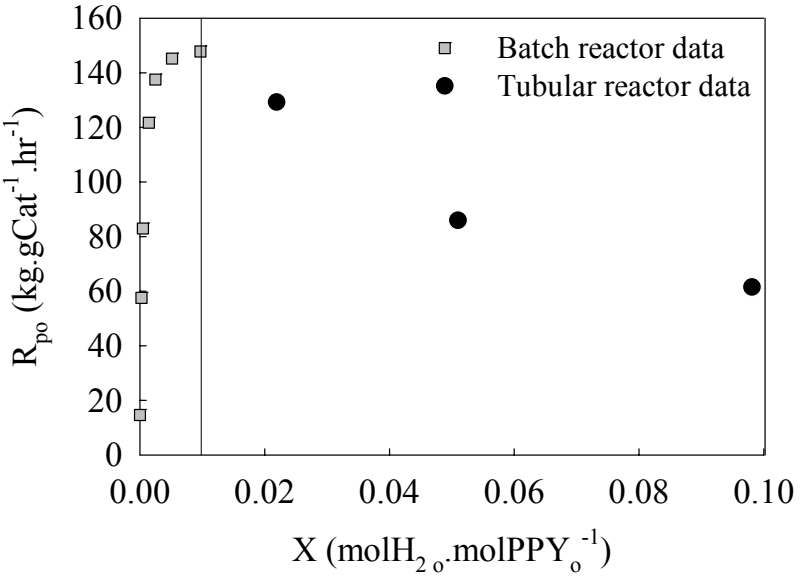

Figure 5.13: Hydrogen influence on "initial" catalyst activity.

The molecular weight data for selected PP samples is reported in Table 5.2. The part of weight-average molecular weights (M_w^{avg}) values reported in Table 5.2, were estimated using the viscosity-average molecular weights (M_v^{avg}) measured by the intrinsic viscometry. The usual effect of hydrogen on the molecular weights can be seen for the M_w^{avg} values obtained for Run57, Run515 and Run516 (see Table 5.2), and appeared to be decreasing linearly with increasing values of X. This effect can also be seen from the estimated values of q, shown in Figure 5.14. Similar to Figure 5.13, Figure 5.14 presents the overall influence of hydrogen on the average probability of chain termination. The q values observed from the tubular reactor experiments did not show a steep increase with increment in X value from 0.0219 to 0.0981. This effect can very well be judged in accordance with the reduced activity of catalyst observed in this range of X values, thus limiting the hydrogen response on the chain transfer of active polymer chains during polymerization. The behavior of q is important to check over the wide range of hydrogen concentration, especially for the end-use application of produced polymer.

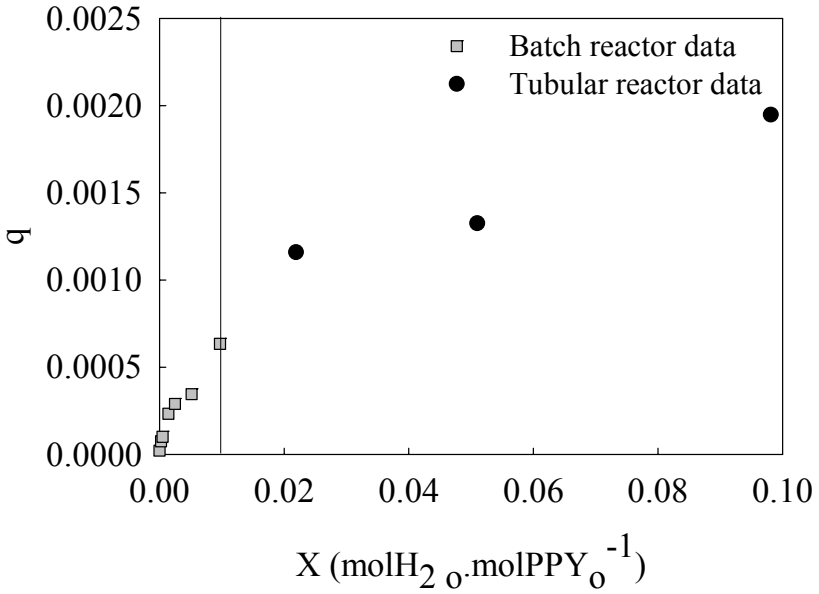

Figure 5.14: Hydrogen influence on average probability of chain termination.

The broadness in the MWD represented by polydispersity index (PDI) was influenced by hydrogen. The PDI data for selected PP samples is shown in Table 5.2. With the increase in X value from 0.0219 to 0.0510 and 0.0981, the PDI values for PP samples prepared with Run515 and Run516 found to be increased by 18 % and 30 % with respect to Run57. Such broadness in MWD with the increasing concentration of hydrogen can be seen from the GPC curves of the studied polymer samples. The GPC curves of three PP samples

prepared from Run57, Run515 and Run516 are shown in Figure 5.15. As expected, the MWD curves of PP samples were shifted towards the low molecular weight region with the increasing value of X from 0.0219 to 0.0981. The detailed characteristics of these curves were evaluated using the deconvolution method.

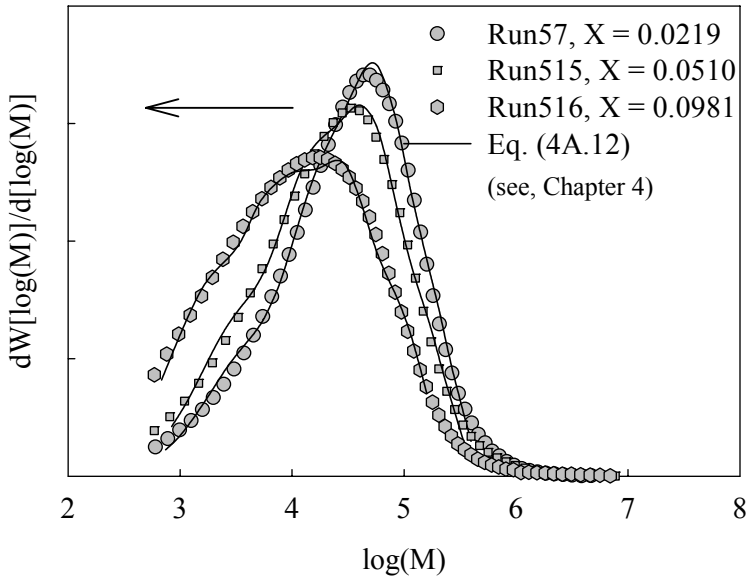

Figure 5.15: MWD data for PP samples prepared at 70 °C with different hydrogen concentration.

Table 5.3: Hydrogen effect on molecular weights and contents of Flory components in propylene polymerization reactions

Experiment Code	Center	M_w^{avg} (kg.kmol^{-1})	Fraction	Experiment Code	Center	M_w^{avg} (kg.kmol^{-1})	Fraction
Run57	1	2660	0.09	Run515	1	2400	0.12
	2	12300	0.21		2	10400	0.25
	3	45300	0.43		3	38000	0.40
	4	135000	0.27		4	120000	0.23
Run516	1	1400	0.16				
	2	5600	0.27				
	3	22000	0.34				
	4	75000	0.23				

The GPC curves shown in Figure 5.15 were deconvoluted using a "four site" model and according to the procedure described in Chapter 4. It was found that the Four Flory components (1 - 4 in order of increasing molecular weight) described the MWD of these polymers in a satisfactory manner. The data regarding molecular weights and mass fractions for individual Flory component is given in Table 5.3.

Inevitably, the individual M_w^{avg} values of different sites was observed to decrease by an average factor of 1.2, mainly due to the increase in X value from 0.0219 to 0.0510, and it decreased by factor 2 for the X value increment from 0.0219 to 0.0981. These results reflect the particular kinetic response intrinsic to each type of active sites, and exhibit a constant change in their performance with increasing values of X.

At high hydrogen concentration, the mass fraction of polymer originating from different families of active sites found to be enhanced especially for the low molecular weight part. For the number of MWD curves presented in Chapter 4, the influence of hydrogen on the mass fraction of different Flory components seem to be very limited. Therefore, these fractions can be represented by the average values for all the MWD curves obtained for the X values below 0.01. However, at high concentration of hydrogen (i.e., $0.01 < X < 0.1$), this effect was not observed. It seems that the mass fractions of Flory components representing the lower molecular part are very sensitive in the region of high hydrogen concentrations.

For instance, mass fractions of site type 1 and 2 increased by 70 % and 28 %, respectively, for Run516 in comparison with the values estimated for Run57. This clearly represents the sensitivity of different sites in the presence of hydrogen. These results indicated the involvement of hydrogen in the reactivation process of dormant sites, and further enhancing the termination probability of the active polymer chains. However, as per discussed in Chapter 4, the changes in the behavior of different active centers may partly be dependent on the nature of the hydrogen present during the reaction.

Next important point is analyzing the obtained morphology of PP samples prepared from the present reactor having short residence time. Few PP samples were characterized using different analytical tools, and results are discussed based on essential process parameters. The link presented here between the reaction kinetics and off line characterization of polymer samples is important from the point of understanding the reactor behavior.

5.4 SEM and EDX observations

SEM investigation was made to inspect the surface and cross-sectional morphology of PP samples prepared from the tubular reactor experiments. EDX technique was used to analyze the amount of element C.

(a) Run51, 40 °C, X = 0.0

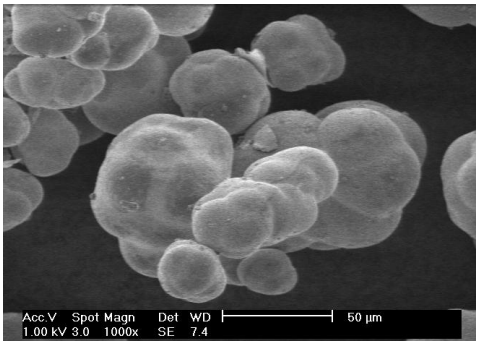

(b) Run52, 50 °C, X = 0.0

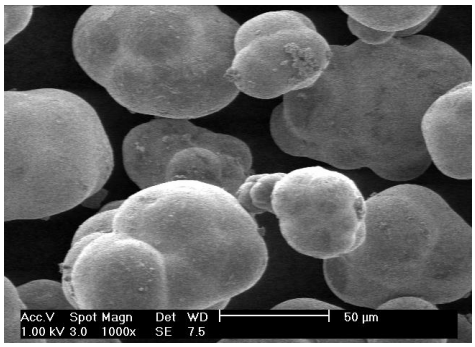

(c) Run517, 80 °C, X = 0.0

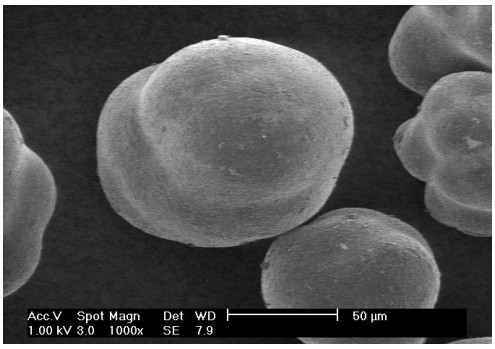

(d) Run57, 70 °C, X = 0.0219

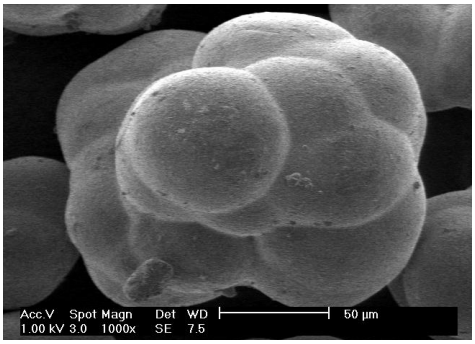

(e) Run515, 70 °C, X = 0.0510

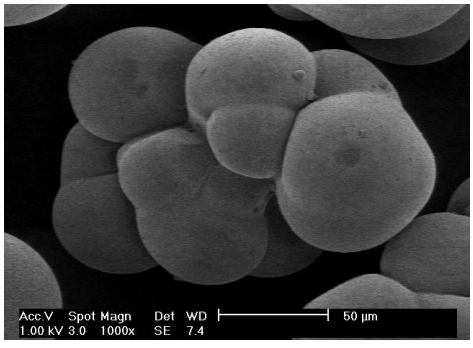

(f) Run516, 70 °C, X = 0.0981

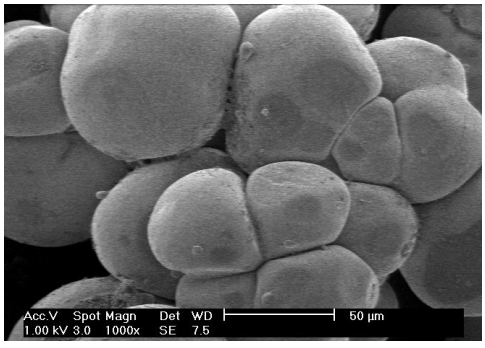

Figure 5.16: Particle geometry of liquid-phase polymerized PP powder observed by SEM.

(a) Run51, 40 °C, X = 0.0

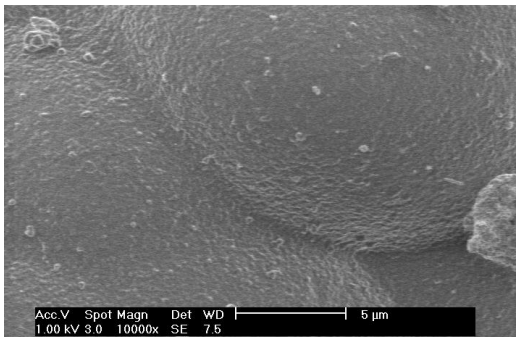

(b) Run52, 50 °C, X = 0.0

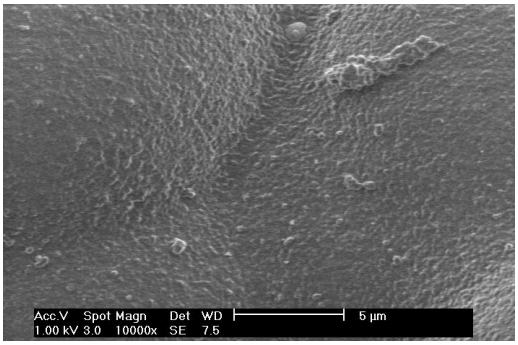

(c) Run57, 70 °C, X = 0.0219

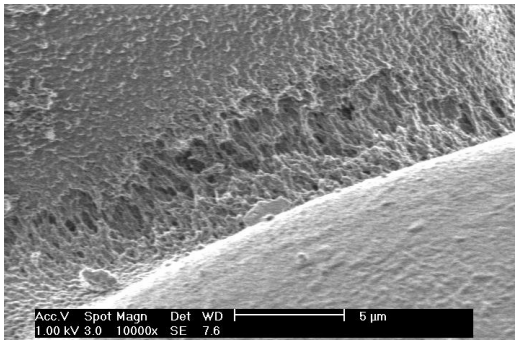

(d) Run58, 70 °C, X = 0.0219

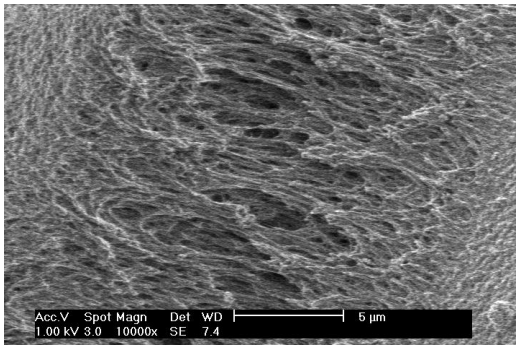

(e) Run515, 70 °C, X = 0.0510

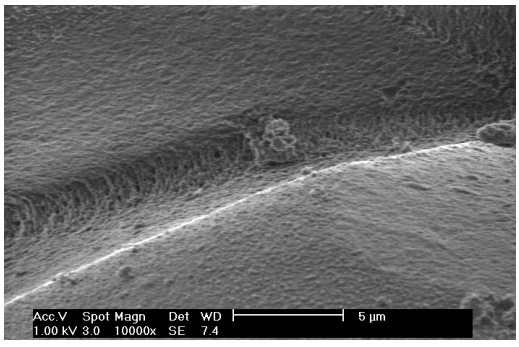

(f) Run516, 70 °C, X = 0.0981

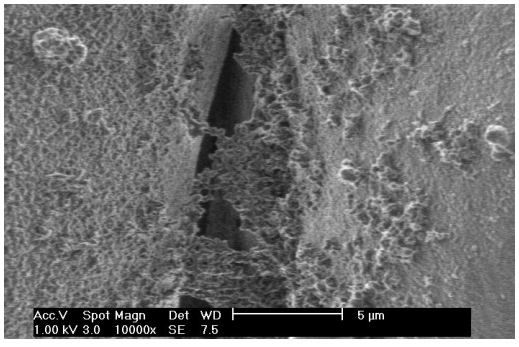

Figure 5.17: Expansion effect of the reaction mixture at the reactor exit on the particle geometry of (liquid-phase polymerized) PP samples observed by SEM.

Figure 5.16 illustrate the PP particle structures having smooth surface morphology developed during the polymerization reaction with an average residence time of 40 - 43 s. It seems that the polymer particles tend to replicate the shape and texture of the catalyst, and the extent of its replication depends on the reaction rate. It can be observed that with the proceeding of polymerization reaction the support material (here $MgCl_2$) begin to

fragment and the polymer grows to a particle around each fragment. This phenomenon can be seen from the surface morphology of the PP samples shown in Figure 5.16. The most striking effect found here is even under such severe polymerization conditions the polymer particles have developed their structure with unique degree of replication (after observing several particles, SEM pictures are not presented here). This finding suggests that the morphology of polymer particle is well controlled, which is very important from the industrial point of view. The expansion effect of reactor fluid at the reactor exit on the morphology of PP particles was also analyzed and shown in Figure 5.17. It appears that the polymer layer around the fragments was "stretched" due to the sudden expansion of liquid propylene from 40 - 60 bar of reactor pressure to a 1 bar into the expansion vessel. However, this "stretching" effect was negligible in case of the PP particles having high molecular weight (which were prepared in absence of hydrogen, for example, see Run51 and Run52), and kept the polymer morphology intact. The samples (Run57, Run58, Run515 and Run516) with low molecular weights demonstrated this influence of expansion (especially the evaporation of liquid propylene to gas) on the particle morphology. The "stretching" phenomenon was more pronounced for these samples creating a "fibril" structure around the edges of fragments; however, this fact did not affect the molecular properties of PP samples.

(a) Run51, 40 °C, X = 0.0

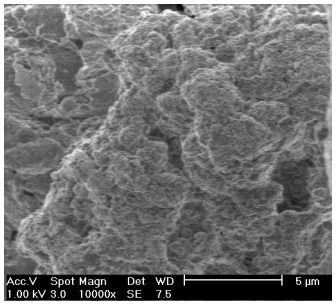

(b) Run57, 70 °C, X = 0.0219

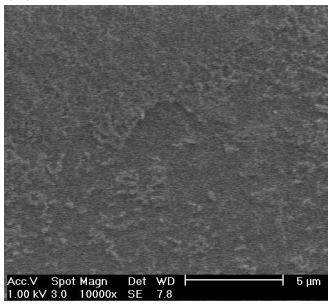

(c) Run58, 70 °C, X = 0.0219

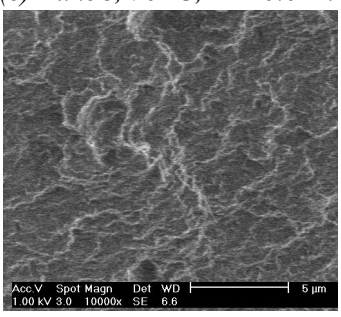

(d) Run59, 70 °C, X = 0.0219

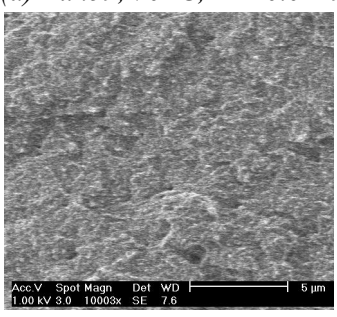

Figure 5.18: Cross-sectional SEM observation of PP samples.

Figure 5.18 shows the cross-section of PP particles prepared from liquid-phase propylene polymerization. The results indicated that the polymer forms as a continuous phase in which the catalyst fragments are distributed homogeneously [12]. This also suggests that under such high polymerization rate the "phase-transition" phenomenon inside the growing polymer particle is already achieved within a short residence time ∅. This result was also confirmed from EDX characterization of polymer sample showing maximum amount of element C; see Figure 5.19. Obviously, the time-scale for the "phase-transition" depends on the monomer concentration and initial propagation frequency.

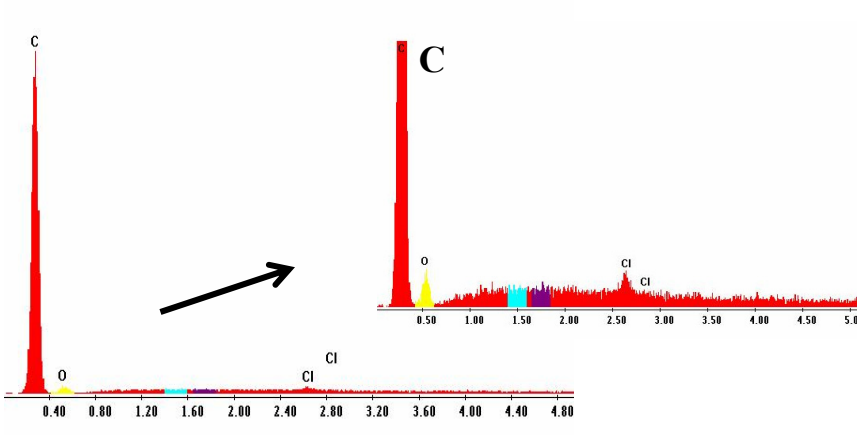

(a) Run58, 70 °C, X = 0.0219, QA(CO_2 + EtOH)

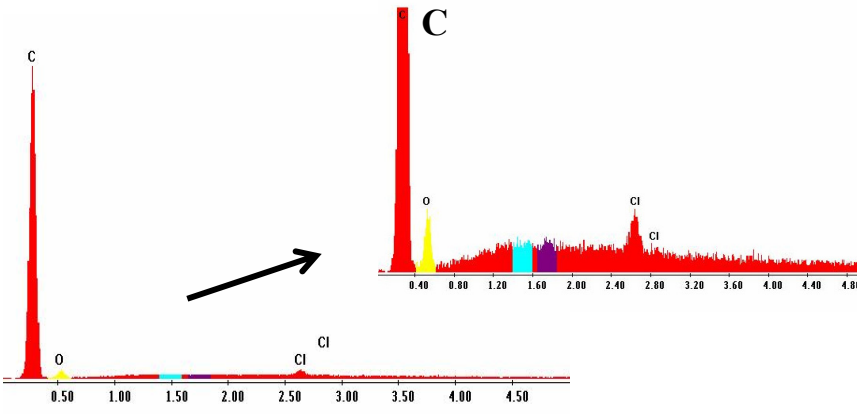

(b) Run59, 70 °C, X = 0.0219, QA(CO_2 + 1N HCl)

Figure 5.19: EDX analysis of liquid-phase polymerized PP samples.

∅ The "phase-transition" phenomenon has been discussed earlier in Chapter 1.

5.5 PSD analysis

The PSD analysis of selected PP samples was performed to study the effect of process parameters and the tubular reactor performance on the geometry of polymer particles. The PSD curves shown in Figure 5.20 were normalized based on the polymer yield [▽].

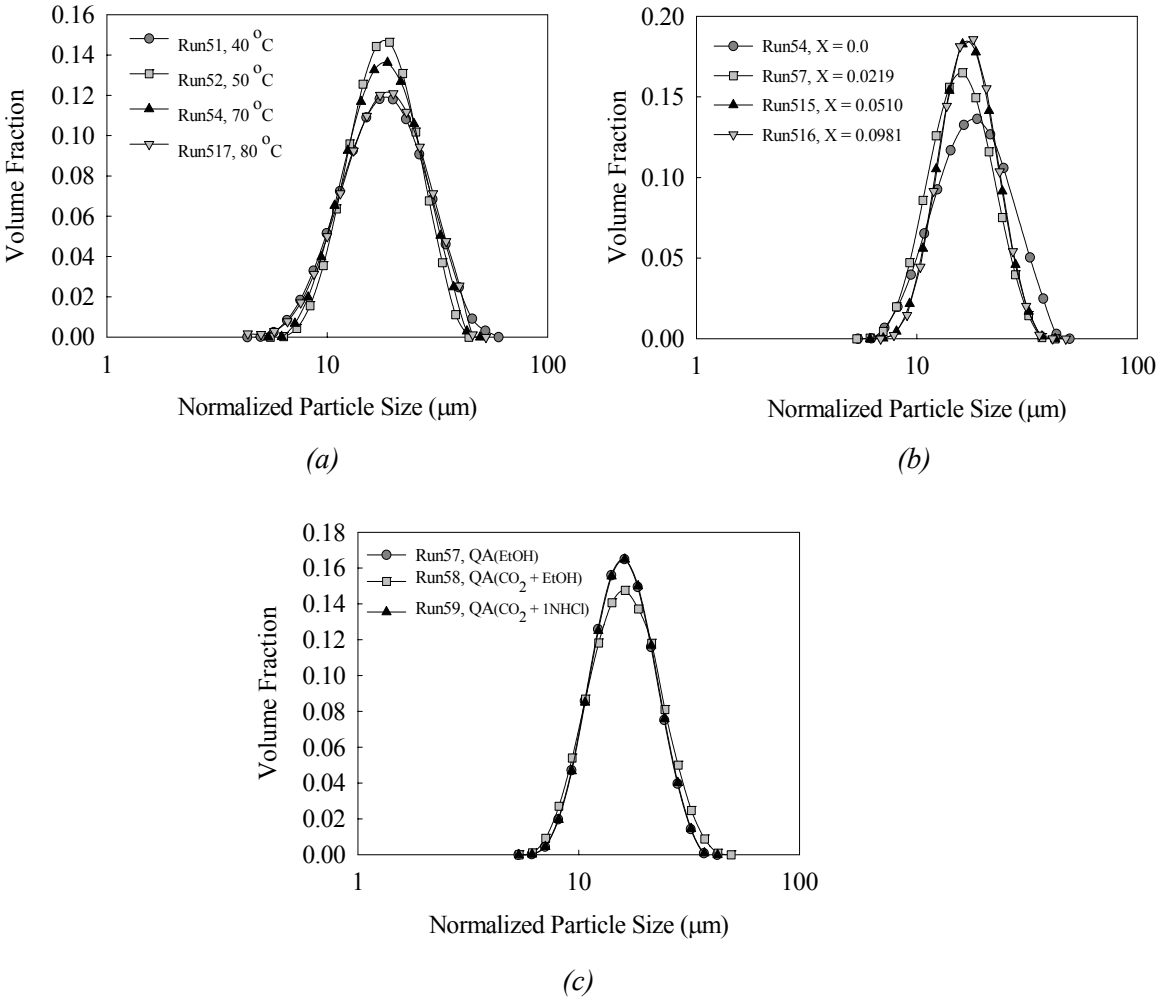

Figure 5.20: PSD curves for selected PP samples prepared with different (a) reaction temperatures, (b) hydrogen amount and (c) quenching agents.

[▽] It is generally accepted that the primary polymer particles grow surrounding the primary catalyst crystallites [7]. When this view is valid, an average diameter of the primary polymer particles ($d_p(0.5)$) can be calculated using following equation,

$$d_p(0.5) = d_c(0.5)\left[\frac{\rho_c}{\rho_p}(Y+1)\right]^{\frac{1}{3}} \tag{5.1}$$

From Figure 5.20, it is interesting to see that the different polymerization condition have not shown any influence on the PSD curves plotted for the normalized particle size. Even in the presence of high polymerization rate at high concentration of hydrogen, the PSD of the PP samples did not exhibit any significant influence of such extreme reaction conditions as compared to the PSD data of PP samples obtained at low reaction rate (for example Run54).

The results presented here also suggest that the morphology of polymer particles is intact and no problem of fines formation or particle agglomeration. In other words, the catalyst particles are well engineered, and its original form is retained due to entanglement of polymer molecules. This might be a one of the good criteria in applying the tubular reactor as a "prepolymerization reactor tool".

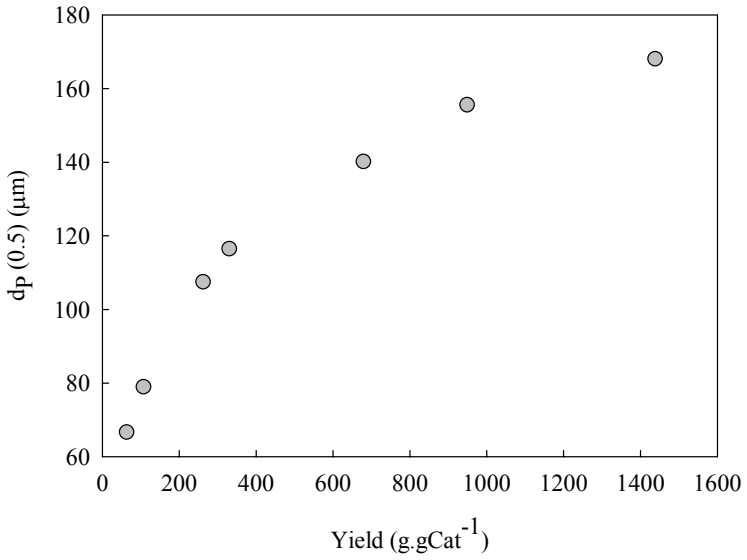

Figure 5.21: Relationship between $d_p(0.5)$ and polymer yields in propylene polymerization.

The increasing trend in $d_p(0.5)$ was observed with increasing polymer yield (Table 5.2 and Figure 5.21). Generally, the particle growth phenomena is explained based on the following steps [6],

1. At an initial stage of polymerization, the catalyst crystallites are dispersed uniformly within the polymer particles.
2. After a certain extent of polymerization time, the polymer subparticles containing some catalyst crystallites are formed.

3. As the polymerization proceeds further, the polymer subparticles disintegrate to the primary polymer particles containing a catalyst crystallite, which grow with the proceedings of polymerization.

5.6 DSC analysis

DSC measurements were carried out for different PP samples to study the heating and cooling behavior of an individual sample. The complete DSC scans for two heating cycles and one cooling cycle are shown in Figure 5.22 and Figure 5.23, representing the effect of reaction temperature, hydrogen concentration and quenching agent on the thermal history of the produced PP. The black line showed in the figures is an assistance line to highlight the variation in the peak maximum and minimum location of the melting and cooling range, respectively.

The selected DSC data are summarized in Table 5.4. The height to width ratio (HWR) of the melting peaks reported in Table 5.4 described qualitatively the crystallite size distribution of a semi-crystalline material [16]. The melt enthalpy (H_f) representing the crystallinity of PP sample was estimated by integrating the melting curve in the temperature range from 90 to 190 ^oC using a linear baseline.

Table 5.4: DSC data for different PP samples prepared from tubular reactor

Experiment Code	1st Heating			1st Cooling	2nd Heating		
	T_{m1} (^oC)	HWR ($W.g^{-1}.^oC^{-1}$)	H_{f1} ($J.g^{-1}$)	T_{c1} (^oC)	T_{m2} (^oC)	HWR ($W.g^{-1}.^oC^{-1}$)	H_{f2} ($J.g^{-1}$)
Run51	162.5	0.0995	67.4	116.8	160.7	0.3032	90.2
Run52	162.2	0.0949	70.1	117.7	160.9	0.3580	95.1
Run54	162.5	0.0938	73.8	116.3	161.3	0.3828	94.1
Run57	160.1	0.1683	85.9	119.7	158.4	0.5889	114.1
Run58	160.1	0.1774	81.8	118.6	158.8	0.5585	110.0
Run59	158.7	0.1548	80.9	114.3	155.8	0.3960	107.4
Run515	158.1	0.1520	87.1	116.6	155.5	0.6045	111.2
Run516	156.2	0.1162	91.8	118.0	153.2	0.3484	110.2
Run517	163.4	0.0856	81.3	117.1	162.8	0.3592	91.2

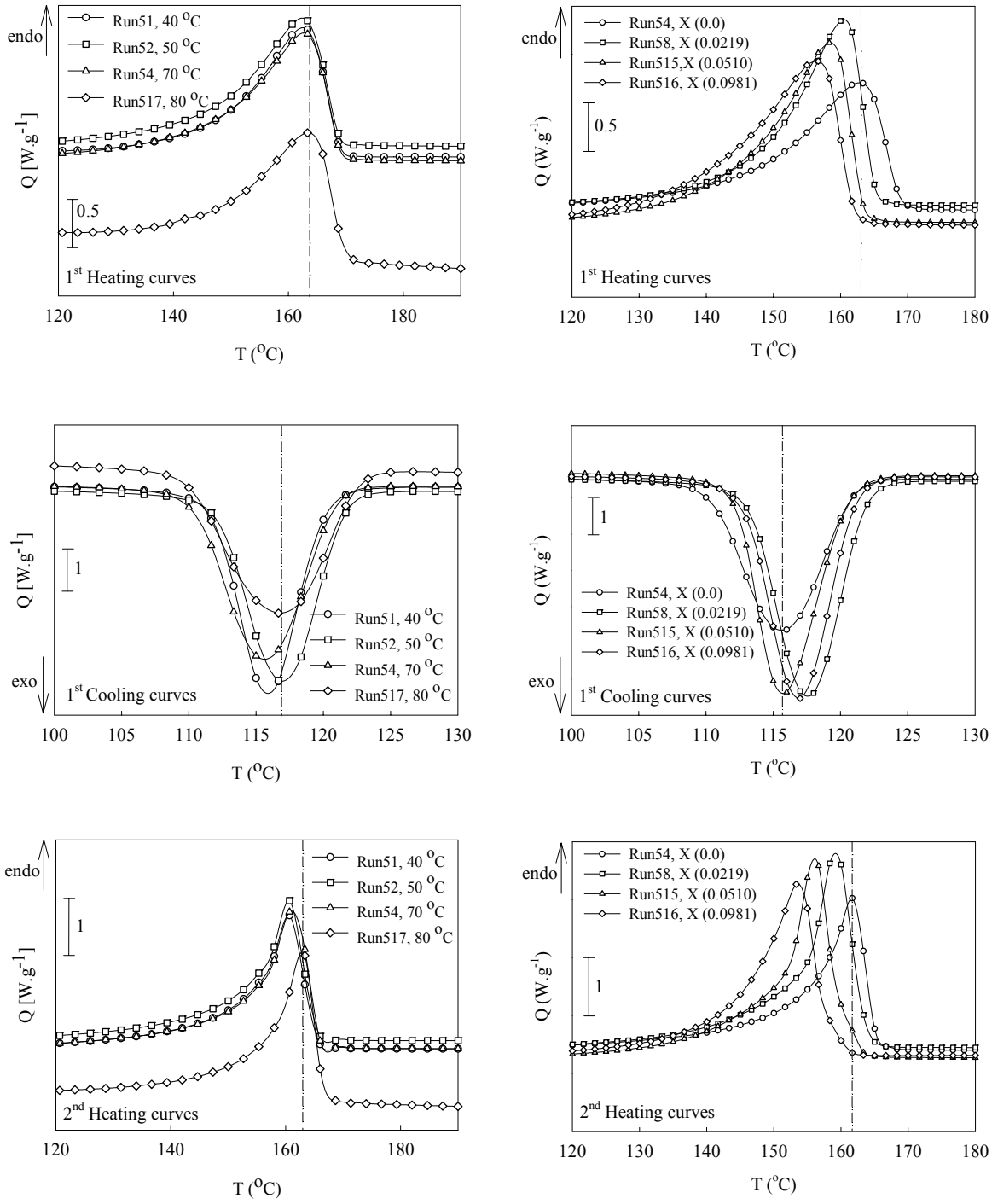

(a) *(b)*

Figure 5.22: DSC scans for PP samples prepared from tubular reactor (a) at different reaction temperature and (b) with different hydrogen amount represented by X at 70 °C.

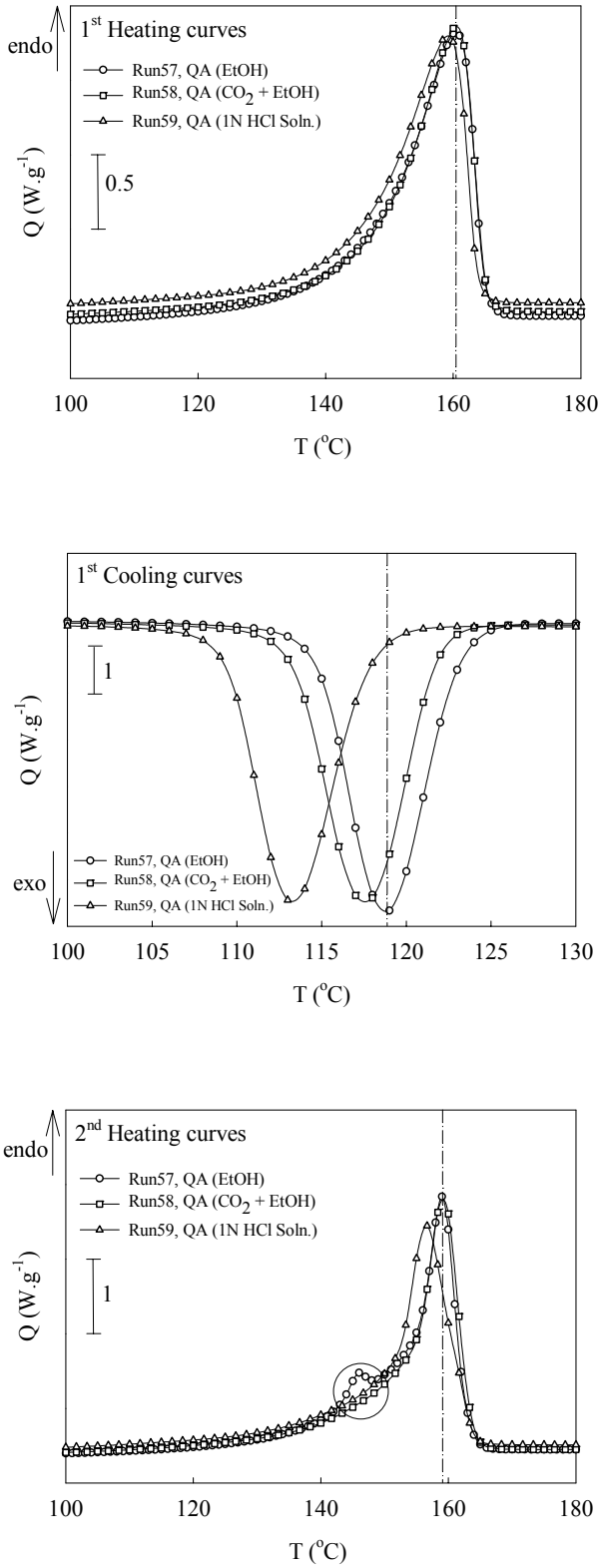

Figure 5.23: DSC scans for PP samples prepared from tubular reactor: effect of quenching agent.

From the DSC data presented Figure 5.22 (a) and Table 5.4, a very limited effect of reaction temperature was noticed on the melt temperature (T_m) and H_f of PP, prepared in the absence of hydrogen. Ideally, at similar reaction conditions, a temperature increase leads to the decrease in molecular weight, which allow polymer chains to fold easier, and thus enhancing the crystallization process [5]. However, in this study, the observed change in the molecular weights with respect to reaction temperature was not enough to have a significant influence on the melt temperature especially for the M_w^{avg} values > 2000000; see Table 5.2. A number of authors have confirmed such phenomena, for example, see Nieto et al. (2001) [10] and Eriksson (2005) [5].

The influence of hydrogen on the molecular weights clearly exhibits the improvement in the crystallization process. The melting peak of the lower molecular weight PP samples prepared from Run58, Run515 and Run516 (adding high hydrogen concentration during polymerization) shifted to a lower temperature as compared to the PP sample prepared from Run54 where no hydrogen was added during its polymerization. This effect can also be observed from the H_f values shown in Table 5.4. The H_f value decreases as the molecular weight increases, for instance, PP prepared from Run54 has a minimum H_f value of 73.8 and 94.1 $J.g^{-1}$ estimated from 1st and 2nd heating cycle, respectively, in comparison with the polymer samples prepared from Run58, Run515 and Run516.

The expansion effect on PP samples into the different quenching agents showed that the degree of orientation of polymer chains upon degassing exhibits non-uniformity in the chain mobility during the crystallization process, which might show a delayed response; see Figure 5.23. A second endothermic peak was observed during the 2nd heating cycle for the PP sample, which was expanded in ethanol (Run57). This effect may be observed after the successive crystallization where the spherulites formed did not appeared at the same position in the lattice [1].

Furthermore, the H_f values of all PP samples, at the 2nd heating, were higher than at the 1st heating. This indicates that the crystallization capability of polymer chains has improved after the 1st heating cycle. Such crystallization enhancement was also studied by determining the % crystallinity for the PP samples. In order to estimate the % crystallinity, the H_f values measured from 1st and 2nd heating scans were divided by the H_f^{100} value of PP sample having 100 % crystalline phase. Here, a 209 $J.g^{-1}$ value of H_f^{100} was used for calculations (this value is reported by Pater et al. (1999) [11]). Figure 5.24 shows the % crystallinity data as a function of M_w^{avg}. The % crystallinity for all PP

samples was found to be increased by an average of 20 %. Similar to H_f values, the % crystallinity was decreasing with increasing molecular weight of PP samples. These results indicate the transfer of polymer chain units from amorphous or disoriented phase to the crystalline phase after the 1st heating and cooling cycle.

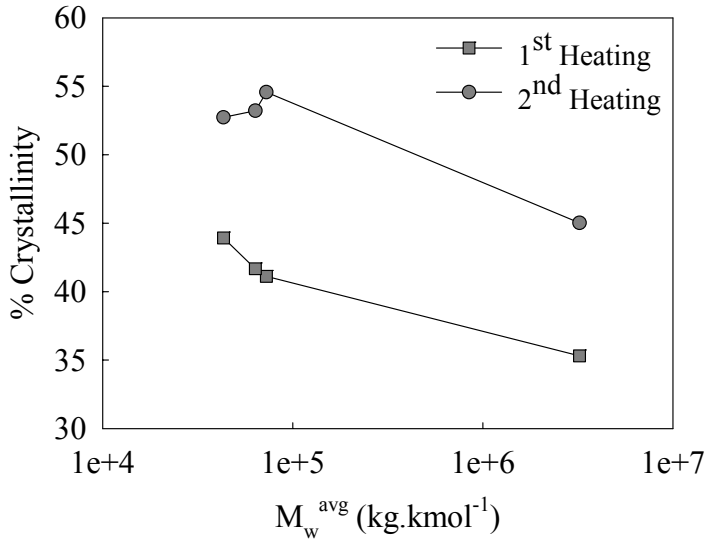

Figure 5.24: % Crystallinity versus M_w^{avg} for liquid-phase PP samples.

Stern et al. (2005) [16] studied the DSC data of PP samples prepared from the batch polymerization experiments for liquid propylene using the same catalyst type as used in this study, and observed the similar behavior of thermal history for polymer. More importantly, the authors reported the similar range of values for H_f and HWR.

It is interesting to see that the dynamics of tubular reactor does not show any significant influence on the crystallization ability of the polymer chains in comparison with the DSC data of PP sample prepared from batch reactor experiments. In addition, the high H_f values estimated from 2nd heating cycle certainly tell that the folding of polymer chains to crystallites inside the reactor is not as good as in the melt state.

Another observation made from the higher values of HWR for 2nd heating cycle indicates that the PP samples seem to have achieved the narrow crystallite size distribution and therefore represented a more homogeneous crystallinity, and can be seen from the DSC scans presented above.

5.7 Conclusions

The tubular reactor set-up built in this work has been successfully analyzed for the polymerization kinetics and polymer morphology studies by performing different interesting experiments of liquid propylene polymerization using highly active $MgCl_2$-supported ZN catalyst type. The catalyst performance observed during the reaction in tubular reactor was compared with the batch reactor data, and found in good agreement with respect to the kinetic response of the catalyst. These results evident the effect of reactor dynamics on the reaction kinetics as well as on the morphology of produced polymer.

On the other hand, the effect of reactor dynamics and reaction conditions along with the "early stage" polymerization processes were examined from the high catalyst activity compared to batch polymerization process. The flexibility of varying the different process parameter allowed understanding the overall behavior of the catalyst. Especially, the possibility of performing the experiments with a wide range of hydrogen concentrations, thus, enabling to analyze its influence on catalyst activity and molecular properties of produced polymer.

The present tubular reactor set-up demonstrated the possibility of performing the polymerization experiments with reduced reaction time, and ultimately speeding-up the characterization of different catalyst types as well as the quality check of different process chemical constituents such as monomer.

Therefore, the emphasis of the present work has put mainly on achieving high-output by investigating reaction kinetics and polymer morphology based on the performed experiments. Combined with off line polymer characterization analyses, it was possible to generate experimental data on the morphology evolution of macroparticle. From the analysis of SEM and PSD data of produced PP particles, this reactor exhibit the potential in extending its application to a macro scale level of polymer production at least in the form of "prepolymerization reactor tool".

To conclude, the temperature profiles in tubular reactor was believed to be typical for a given reactor-catalyst-heat transfer system and can be used as a "high-output" tool for characterization of both catalyst and monomer quality.

Nomenclature

C_p : Specific heat ($kJ.kg^{-1}.K^{-1}$)

d_i : Inside reactor diameter (cm)

$d_c(0.5)$: Mean diameter of catalyst particle (μm)

$d_P(0.5)$: Mean diameter of polymer particle (μm)

dHr : Heat of reaction ($kJ.kg^{-1}$)

E_p : Activation energy for propagation reaction ($kJ.mol^{-1}$)

H_f : Heat of fusion ($J.g^{-1}$)

H_{2o} : Initial moles of hydrogen present during reaction (mole)

k_d : Rate constant for deactivation constant, (hr^{-1})

k_{po} : Arrhenius constant for propagation reaction ($m^3.gCat^{-1}.hr^{-1}$)

k_p : Rate constant for propagation reaction ($m^3.gCat^{-1}.hr^{-1}$)

L : Tubular reactor length (cm)

m_{co}, m_o^{Cat} : Mass of (preactivated) catalyst (mg)

m_{fr}^{M} : Mass flow rate of liquid propylene ($kg.hr^{-1}$)

M_{mon} : Molecular weight of monomer ($kg.kmol^{-1}$)

M_v^{avg} : Viscosity-average molecular weight ($kg.kmol^{-1}$)

M_w^{avg} : Weight-average molecular weight ($kg.kmol^{-1}$)

M_o : Initial concentration of monomer ($kmol.m^{-3}$)

M : Molecular weight of monomer used in GPC curves ($kg.kmol^{-1}$)

P_o : Reactor pressure (bar)

PPY_o : Initial moles of liquid propylene present during reaction (mole)

Q : Heat flow ($W.g^{-1}$)

Re : Reynolds number

R_{po} : Initial rate of polymerization ($kg.gCat^{-1}.hr^{-1}$)

R_{po_ATR} : Initial rate of polymerization from ATR ($kg.gCat^{-1}.hr^{-1}$)

t : Reaction time (s or min)

T_o : Reference or initial temperature (^oC)

T_{avg} : Average reactor temperature (^oC)

T_c : Crystallization temperature for polymer (^oC)

T_m : Melting temperature for polymer (^oC)

Th_mc : Thermocouple placed at catalyst injection point

Th1 to Th4 : Thermocouple used in tubular reactor set-up

T : Temperature (^oC)

V_{mc} : Volume of "Mixing Cell" (ml)
V_z : Axial velocity ($cm.s^{-1}$)
W[log(M)] : Distribution of log molecular weight
X : Mole ratio of hydrogen to liquid propylene
Y : Polymer yield ($kg.gCat^{-1}$)

Greek letters

ρ_c : Density of catalyst particle ($kg.m^{-3}$)
ρ_p : Density of polymer particle ($kg.m^{-3}$)

Sub- and superscripts

avg : Average
c, Cat : Catalyst or crystallization
d : Deactivation
i : Inside
mc : "Mixing Cell"
mon : Monomer or melting
o : Zero or initial
p : Propagation or polymer
v : Viscosity
w : Weight
z : Representing the axial direction

Abbreviations

ATR : Adiabatic temperature rise
CO2 : Carbon dioxide
CSTR : Continuous stirred tank reactor
DSC : Differential scanning calorimetry
EDX : Energy dispersive X-ray spectrometry

EtOH : Ethanol
GPC : Gel permeation chromatography
1N HCl : 1N Hydrochloric acid
HPLC : High pressure liquid compression
HWR : Height to weight ratio
$MgCl_2$: Magnesium dichloride
MWD : Molecular weight distribution
PDI : Polydispersity index
PP : Polypropylene
PSD : Particle size distribution
RTD : Residence time distribution
SAXS : Small-angle X-ray scattering
SEM : Scanning elector microscopy
TEA : Triethylaluminum
$TiCl_4$: Titanium tetrachloride
WAXD : Wide-angle X-ray diffraction
QA : Quenching agent
ZN : Ziegler-Natta

Literature

[1] Al-haj Ali, M. (**2006**), Doctorate Thesis, University of Twente, Enschede, The Netherlands.
[2] Boenig, H. V. (**1966**), Polyolefins: Structure and Properties, Elsevier, New York.
[3] Busico, V., Cipullo, R. and Esposito, V. (**1999**), Macromol. Rapid Commun., 20 (3), 116 - 121.
[4] Di Martino, A., Broyer, J. P., Spitz, R., Weickert, G. and McKenna, T. F. (**2005**), Macromol. Rapid Commun., 26, 215 - 220.
[5] Eriksson, E. (**2005**), Doctorate thesis, LCPP - CNRS/ESCPE, Lyon, France.
[6] Kakugo, M., Sadatoshi, H., Sakai, J. and Yokoyama, M. (**1989**), Macromolecules, 22, 3172 - 3177.
[7] Keii, T., Terano, M., Kimura, K. and Ishii K. (**1987**), Makromol. Chem. Rapid Commun, 8, 583 - 587.
[8] McKenna, T. F., Soares, J. B. P. and Simon, L. C. (**2005**), Macromolecular Material and Engineering, 290, 507 - 510.

[9] Mori, H., Endo, M., Tashino, K. and Terano, M. (**1999**), Journal of Molecular Catalysis A: Chemical, 145, 153 - 158.

[10] Nieto, J., Oswald, T., Blanco, F., Soares, J. B. P. and Monrabal, B. (**2001**), Journal of Polymer Science Part B: Polymer Physics, 39, 1616 - 1628.

[11] Pater, J. T. M. and Kopmels M. (**1999**), Polymerization of liquid propylene using Zeigler- Natta catalyst system, Project Report, University of Twente, Enschede, The Netherlands.

[12] Pater, J. T. M. (**2001**), Doctorate Thesis, University of Twente, Enschede, The Netherlands.

[13] Pimplapure, M., Zheng, X., Loos, J. and Weickert, G. (**2005**), Macromol. Rapid Commun., 26, 1155 - 1158.

[14] Ruddick, V. J. and Badyal, J. P. S. (**1998**), J. Phys. Chem., 102, 2991 – 2994.

[15] Skoumal, M., Cejpek, I. and Cheng, C. P. (**2005**), Macromol. Rapid Commun., 26, 357 - 360.

[16] Stern, C., Frick, A. R., Pater, J. T. M. and Weickert, G. (**2005**), Macromolecular Material and Engineering, 290, 372 - 383.

[17] Weickert, G., Pimplapure, M., Al-haj Ali, M., Tupe, R. and Banat, Y. A. I. (**2005**), Proceedings of ECOREP III, Lyon, France.

Chapter 6

Tubular reactor for liquid-phase propylene polymerization: II. Model development and validation

Abstract: In this work, a mathematical model for the catalytic polymerization of liquid propylene in a tubular reactor is presented. The "Axial Dispersion Model" was applied to describe the flow characteristics of the reactor, and the modified heat transfer model was used to explain the heat transfer phenomena of the reactor. The reactor model analysis has been carried out based on the selected experimental data obtained from the polymerization tests. The predicted profiles of reactor temperature and the experimental one are found to be in good agreement. The model predictability for reaction rates, polymer yield and average molecular weights was also evaluated with the experimental data, and observed to be in well accordance with the reactor performance. The "early stage" kinetic experiments together with the reactor model enabled to characterize the catalyst performance over a reduced time of reaction. This indicates the model capability in elaborating the reactor behavior with respect to varying process variables and parameters during polymerization reaction. For instance, the reactor model was simulated for different reactor lengths. With the increasing reactor length, the influence of polymerization temperature and hydrogen concentration on the catalyst activity was analyzed using the predicted reactor temperature profiles and the dynamics of moving reactive plug. In addition, it is demonstrated that based on the model predictions, the optimal process conditions can be developed for catalytic polymerization reactions using the present tubular reactor concept. On the basis of simulation study performed using the validated reactor model, it was observed that the broad experimental analysis could be designed to explore the capability of tubular reactor from the point of view of industrial applications.

Keywords: axial dispersion, catalytic olefin polymerization, heat transfer, modeling, tubular reactor

6.1 Introduction

It is apparent that the liquid-phase propylene polymerization is one of the most important industrial processes in polypropylene (PP) manufacture. Such process became vital especially after the remarkable developments in the high performance catalysts for olefin polymerization both in terms of improved activity and stereospecificity, further stimulating the new reactor design capable of achieving corresponding improvements in the process technology.

In this context, the tubular reactor appeared as a very attractive option because of economic and technological advantages. For example, tubular systems closed in a loop (called as "Loop Reactor") are industrially used for the polymerization of olefins in both diluent-slurry and bulk slurry processes. Furthermore, in Chapter 5, the novel study consisting of catalytic liquid propylene polymerization in a capillary type tubular reactor has also been demonstrated experimentally, and it certainly exhibited the unique effect of mixing and heat transfer behavior on the reactor performance (which has shown the effect on reaction kinetics as well as on the product morphology). This undoubtedly opened a door for different new ideas (with respect to the applications of tubular reactor as a "high-output" tool and as a "prepolymerization reactor prior to the main polymerization reactor"; see Chapter 5) and challenges involved in understanding the reactor behavior. For example, some limitations originate not only in the particular complexity of the reacting system but in the severe operating conditions as well. For instance, the reproduction of certain extreme conditions in a laboratory set-up makes any study on the thermodynamic compatibility of the reaction mixture, the elucidation of the kinetic mechanism or the measurement of kinetic and transport parameters very difficult. This might be one of the reasons that many researchers have analyzed the tubular reactor behavior by constructing a mathematical framework of the complete process along with the number of practical assumptions. This fact can be well evident from the published literature reporting, "the modeling of a particular reactor system is an important tool in gaining the sound knowledge about different challenges, and could help in maintaining the comprehensive understanding of the process".

Modeling of tubular reactor is not a new issue and plenty of published articles are available describing the unique applications of tubular reactor for specific fields, and one of them is polymerization process. It is believed that the tubular reactor have become

interestingly attractive due to the degree of freedom involved with its process operation such as,

1. Unique ability of heat removal.
2. Flexibility in altering the mixing patterns.
3. Able to control the residence time distribution of the components.

Despite such uniqueness, to the best of the author's knowledge, not a single literature is available on focusing the function of tubular reactor for catalytic polymerization of liquid-phase propylene, except the work published by Zacca et al. (1993) [15] and Reginato et al. (2003) [11] on the modeling of "Loop Reactors" for catalytic liquid-phase propylene polymerization. On the contrary, Di Martino et al. (2005) [3] did publish the study representing the catalytic ethylene polymerization at industrial conditions using a tubular reactor as a "stopped-flow" technique. However, the focus of their work was on understanding the morphology of the polymer during the "early stages" of polymerization and not on applying such method as a competitive reactor process. Unfortunately, it seems that the advantages of tubular reactor process for catalytic olefin polymerization became overwhelmed due to the fact of reactor fouling and reactor plugging. Nevertheless, the results reported in Chapter 5 definitely highlight the significance of such reactor type in broadening the understanding in the field of catalytic olefin polymerization; and certainly, constructing the mathematical model for such process would help in building-up the thoughtful considerations for the future research activities, such as developing an optimal design criteria and operation policies.

In this chapter, a developed mathematical model is presented to describe the polymerization process performed in a tubular reactor for liquid propylene using $MgCl_2$-supported Ziegler-Natta (ZN) catalyst. Particular attention is given to study the macroscopic properties of the process, such as dynamics of the reactor unit and average properties of the polymer. The model is based on the fundamental equations of mass and energy balance, and makes use of comprehensive kinetic model (see Chapter 4). Emphasis was put on keeping the equations as general and detailed as possible, aiming for an intrinsic description of the reactor in terms of mixing and heat transfer effects. The model reliability analyses in terms of these effects were performed by comparing the dynamic reactor performance with the experimental data, and thus enabling the estimation of kinetic information such as rate profiles and polymer yield at the time-scale involved with such reactor process. Furthermore, the model was simulated for different

reactor designs and process parameters, and explained the potential involved with such process in the field of liquid-phase propylene polymerization.

6.2 Process model

6.2.1 Brief description

Figure 6.1 shows the schematic of tubular reactor process similar to that shown in Chapter 2. The capillary type tubular reactor (d_i = 0.4 cm) folded up in the vertical sections was submerged in a cylindrical jacket. The feed stream to the main reactive section of the tubular reactor was preheated to the reaction temperature with the help of preheating section shown in Figure 6.1. After attaining the stable reactor temperature, the reactor pressure was maintained constantly with the help of back pressure valve (represented by number 2 in Figure 6.1). Therefore, the reactor was kept filled with liquid propylene. Once the stable operating conditions have been achieved, the catalyst previously activated with the cocatalyst and external donor was fed into the reactor after mixing with a main stream of liquid propylene and hydrogen in a "Mixing Cell" (represented by number 1 in Figure 6.1). The catalyst slurry was injected with the specific volume and injection period (values are mentioned in Chapter 2 and Chapter 5).

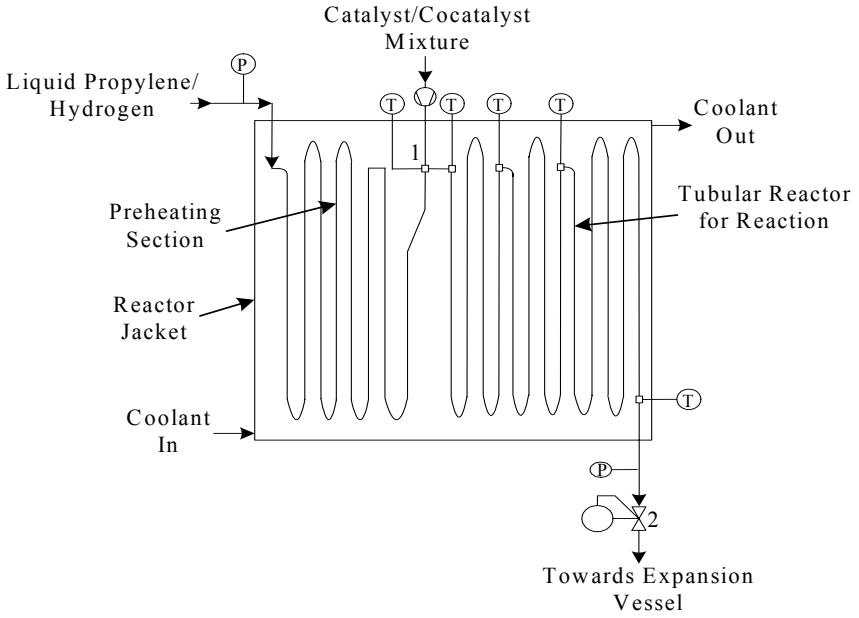

Figure 6.1: Schematic of tubular reactor set-up for liquid-phase propylene polymerization (for details, see Chapter 2).

The polymerization reactions are highly exothermic in nature. Therefore, the produced heat was removed by means of cooling jacket that works isoperibolically. That means the jacket temperature during the reaction was maintained constant. All the inlet flow rates and reactor pressure were measured along with the reactor and jacket temperatures. Off-line measurements were made for the average molecular weights of polymer samples. The experimental data obtained from this process has been used in comparison with the model predictions to understand the reactor performance in detail.

6.2.2 Programming environment

The entire mathematical model presented in this chapter is a system of non-linear partial differential and algebraic equations. The model framework was set-up in the programming environment "gPROMS" as a distributed model in which the tubular reactor was distributed over an axial direction with a specific number of grids using different discretisation method provided by the software. In this case, an "Orthogonal Collocation" method was selected to discretise the tubular reactor in the axial direction. In order to construct the mathematical framework in a simplified way, the complete process was modeled in three different sections and these sections were connected accordingly to exhibit the real process pattern. These three sections can be seen in Figure 6.2, and are mentioned below:

1. "Mixing Cell" section - the inlet zone: depicting the behavior of Continuously Stirred Tank Reactor (CSTR), pointed out by section 1 [†].
2. Tubular reactor section: highlighting only the important junction of thermocouple connections, pointed out by section 2.
3. Reactor jacket section: pointed out by section 3.

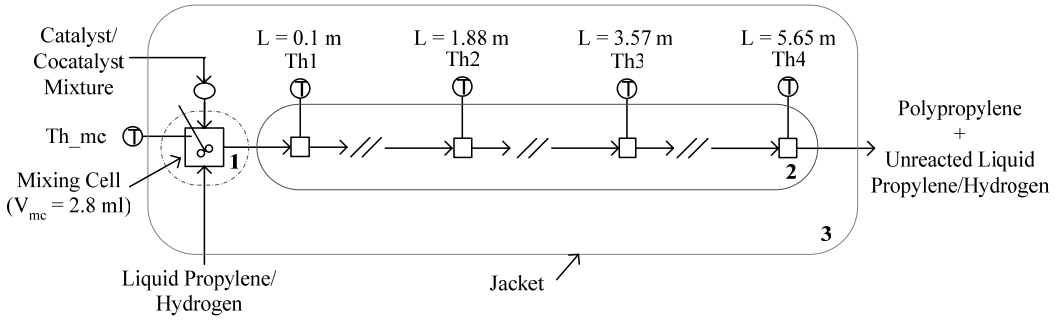

Figure 6.2: Simplified schematic of tubular reactor set-up for model construction.

[†] The response of "Mixing Cell" has already been discussed in Chapter 5.

6.2.3 Basic assumptions

The fundamental assumptions were employed during the development of model and they are described as follows:

1. The "Mixing Cell" (the so-called inlet zone) is modeled as a CSTR [4].
2. The tubular reactor is described according to the "Axial Dispersion Model" [4].
3. In the present case, the thermal capacitance due to the reactor metal wall and its influence on the thermal dynamics of the reactor is assumed to be negligible (however, it should depend on the ratio of outside to inside tube diameter, and it should be checked while constructing a mathematical model; see Melo et al., 2001 [9].
4. Due to the present reactor design and flow conditions, the tubular reactor is always filled with liquid propylene and no gas-phase is present inside the reactor.
5. In this work, it is also assumed that the tubular reactor contains mainly two-phases:
    - A liquid monomer phase consists of liquid propylene monomer with dissolved hydrogen (when hydrogen is used during experiments).
    - A polymer phase consists of semicrystalline polymer particles.
6. The flow regime found in the present reactor is on the verge of turbulent region (Re = 3700). Even so, the assumption of turbulent flow is made in order to have further simplifications:
    - No velocity, concentration or temperature gradients in the radial directions are considered [2] ⊗.
    - A global axial dispersion coefficient, identical for all the species can be used.
    - No inter-particle gradients are considered.
7. The liquid-phase velocity is assumed to be sufficiently high that the catalyst particles are carried along at the liquid-phase velocity and the sedimentation of the particles can be neglected. This assumption always needs to be checked in order to verify that there is no particle deposition in the reactor.

⊗ This assumption will vary from one polymerization reactor process to other. For example, in a specific case study performed by Kleinstreuer et al. (1987) [6] on styrene polymerization, it was found that a tube of radius up to 2 cm could be effectively used for continuous flow polymerization with a turbulent flow conditions. In addition, the authors mentioned that below this critical radius, thermal runaway, channeling and very large radial gradients in temperature and conversion might not develop.

8. The concentrations of different chemical constituents are always considered as a bulk concentration present inside the reactor.
9. The assumptions made for reaction kinetics in Chapter 4 are also applicable here.
10. The cooling jacket used in the present set-up, to promote the heat removal from reaction media, has a large volume compared to the tubular reactor, and enable to dissipate the heat quite instantaneously. The jacket temperature is controlled by a thermostat and the temperatures measured at different positions in the jacket found to be uniform. Therefore, the jacket temperature is considered to be constant ($T_j = T_{j\_sp}$).

6.2.4 Model equations

In this section, the detailed mathematical equations describing the tubular reactor process are presented. This includes the mass and energy balances, heat transfer equations, reaction kinetics, physical properties equations and other auxiliary equations.

6.2.4.1 Inlet zone ("Mixing Cell")

As described above, the "Mixing Cell" was modeled as a perfectly mixed tank with capacity (V_{mc}) which could be specified as a small fraction of the volume correspondent to the tubular reactor section. Unsteady-state mass balance for a generic component "k" was derived considering an inlet zone as a perfectly mixed zone •,

$$\frac{\partial C_k}{\partial t} = \frac{\phi_{mc\_in}}{V_{mc}} C_{k\_in} - \frac{\phi_{mc\_out}}{V_{mc}} C_{k\_out} + R_k \tag{6.1}$$

For condensed system, it is reasonable to assume that enthalpy is not a function of pressure. Then the energy balance of a perfectly mixed zone can be written according to the following equation,

$$\rho_{mix} C_{p\,mix} \frac{\partial T}{\partial t} = \rho_{mix\_in} C_{p\,mix\_in} \frac{\phi_{mc\_in}}{V_{mc}} T_{in} - \rho_{mix} C_{p\,mix} \frac{\phi_{mc\_out}}{V_{mc}} T + \left(dH_r\right) R_p - \frac{4 h_{mc} \left(T - T_{w1}\right)}{d_i} \tag{6.2}$$

• The "Mixing Cell" volumetric flow was calculated using liquid monomer pump flow rate.

6.2.4.2 Tubular reactor section

Unsteady-state mass balance for a generic component "k" was derived considering that the tubular reactor section is modeled using "Axial Dispersion Model", and shown in equation (6.3),

$$\frac{\partial C_k}{\partial t} = D_{mz}\,\frac{\partial^2 C_k}{\partial z^2} - v_z\,\frac{\partial C_k}{\partial z} + R_k \tag{6.3}$$

In the present work, the boundary conditions were applied only at an inlet of the tube [□]. Therefore, in a tube with closed inlet boundary, Wen et al. (1975) [12] stated that the so-called "Dankwerts" boundary can be applied.

$$\text{At z} = 0, \quad C_k = C_{k\_in} + \frac{D_{mz}}{v_z}\frac{\partial C_k}{\partial z} \tag{6.4}$$

As per the simplifications of neglecting the work of expansion, viscous heating, external field effects, radiation, heat transfer associated with diffusion and heat of mixing, the differential equation of energy in one special dimension can be written as,

$$\rho_{mix}\,C_{pmix}\,\frac{\partial T}{\partial t} = \rho_{mix\_in}\,C_{pmix\_in}\,D_{tz}\,\frac{\partial^2 T}{\partial z^2} - \rho_{mix}\,C_{pmix}\,v_z\,\frac{\partial T}{\partial z} + \left(dH_r\right)R_p - \frac{4\,h_i\left(T - T_{w1}\right)}{d_i} \tag{6.5}$$

By making the analogy between mass and energy transfer, the energy boundary condition results,

$$\text{At z} = 0, \quad T = T_{in} + \frac{D_{tz}}{v_z}\frac{\partial T}{\partial z} \tag{6.6}$$

[□] The influence of boundary condition at the reactor exit has been analyzed and observed no impact on the dynamic behavior of the present reactor concept.

The velocity profiles in the tubular reactor section can be obtained by means of a volume balance performed over an arbitrary fixed volume of the reactor (V_r). As the reaction proceeds, the velocity of the reaction mixture (v_z) changes with axial position. By corresponding the total fluid volume change with reaction, Zacca et al. (1993) [15] derived the final velocity profile equation,

$$\frac{\partial v_z}{\partial z} = \sum_{k=1}^{NC} \frac{R_k \, MW_k}{\rho_k} + \frac{dT}{dt} \sum_{k=1}^{NC} C_k \, MW_k \, \frac{d}{dT}\left(\frac{1}{\rho_k}\right) \tag{6.7}$$

Equation (6.7) allows the calculation of the bulk average axial velocity profiles in the tubular reactor section at any position and for any instant of time. The following boundary condition is applied for velocity profile,

$$\text{At z} = 0, \quad v_z = v_{z\_in} = \frac{\phi_{mc\_out}}{A_f} \tag{6.8}$$

As mentioned earlier, the reaction medium used in this study is consisting of liquid-phase as a monomer and solid-phase as a polymer. Even though it is assumed that the sedimentation of the solid particles is negligible, it always needs to be checked quantitatively from one process scheme to another. This is important because the sedimentation of particles in the reactor is a highly undesirable event, which risks safety and lowers production and operability of process plants. It is noted for the "Loop Reactors" that the liquid-solid system in high velocity "Loop Reactors" can be considered as a "Pseudo-Homogeneous" system. Liang et al. (1996) [8] checked this hypothesis experimentally and presented the quantitative nature of this hypothesis. The authors stated that in the liquid-solid two-phase system, the relationship between the liquid and solids velocity can be represented by following the generalized fluidization theory, such as ‡,

$$v_{z\_s} = v_z - v_t \left(1 - \phi_s\right)^n \tag{6.9}$$

‡ In the present case study, the liquid-phase velocity was considered to be similar to bulk average fluid velocity.

The authors explained that in the high velocity "Loop Reactors", the terminal settling velocity (v_t) of the particle is very small compared with either liquid or solids velocity, so that the difference between the liquid and the solids velocities becomes insignificant. Therefore, the system can be treated as "Pseudo-Homogeneous".

It indicates that an estimation of terminal settling velocity of the particle is critical. As per suggested by the published literatures, the following relationship can be used for the estimation of the terminal velocity of the solid particles in the liquid medium,

For $Re_p < 0.4$,
$$v_t = \frac{g_c (dp)^2 (\rho_p - \rho_l)}{18 \eta_l} \tag{6.10}$$

For $0.4 < Re_p < 500$,
$$v_t = \left(\frac{4 (g_c)^2 (\rho_p - \rho_l)^2}{225 \eta_l \rho_l} \right)^{\frac{1}{3}} (dp) \tag{6.11}$$

For $Re_p > 500$,
$$v_t = \left(\frac{6.2 g_c \left(\frac{dp}{2} \right) (\rho_p - \rho_l)}{\rho_l} \right)^{\frac{1}{2}} \tag{6.12}$$

where, Re_p is the particle Reynolds number and defined as,

$$Re_p = \frac{dp\, v_t\, \rho_l}{\eta_l} \tag{6.13}$$

6.2.4.3 "Mixing Cell" and tubular reactor wall effects

In order to understand the reactor wall effect, the energy balance equations were framed for the metal wall considering the "n" set of layers with a uniform layer temperature, and they are discussed below. Cross-section of the metal wall depicting the individual layers is shown in Figure 6.3. From the reactor liquid medium to the first wall layer the internal heat transfer coefficient controls the heat transfer to and from the reactor wall. The

different resistances for heat transfer exist due to the wall layers were estimated using the physical properties of the wall materials. The surface temperature of the metal wall was assumed to be same as jacket temperature.

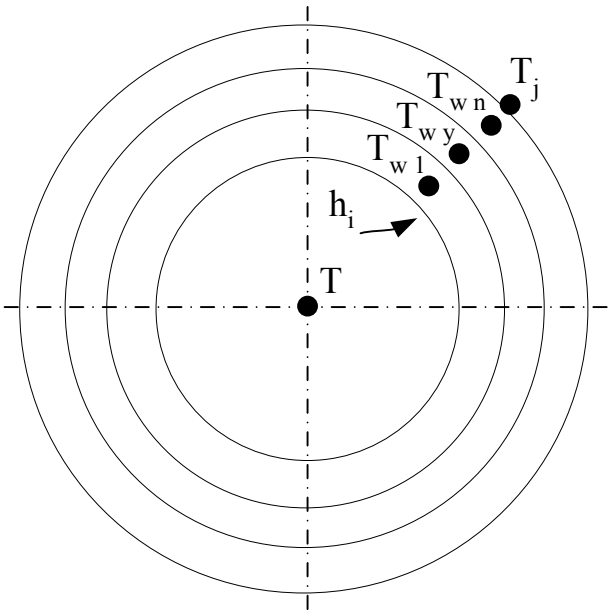

Figure 6.3: Cross-section of the metal wall having "n" set of layers.

The energy balance for an inside wall layer of "Mixing Cell" is,

$$\rho_{w1} C_{pw1} V_{w1} \frac{\partial T_{w1}}{\partial t} = h_i A_{mc} \left(T - T_{w1} \right) - K_{w1} d_{w1} \left(T_{w1} - T_{w2} \right) \tag{6.14}$$

For "y" number of layers,

$$\rho_{wy} C_{pwy} V_{wy} \frac{\partial T_{wy}}{\partial t} = K_{wy} d_{wy} \left(T_{wy-1} - T_{wy} \right) - K_{wy+1} d_{wy+1} \left(T_{wy} - T_{wy+1} \right) \tag{6.15}$$

For "n^{th}" layer,

$$\rho_{wn} C_{pwn} V_{wn} \frac{\partial T_{wn}}{\partial t} = K_{wn} d_{wn} \left(T_{wn-1} - T_{wn} \right) - K_{wn} d_o \left(T_{wn} - T_j \right) \tag{6.16}$$

Similar to the tubular reactor, the wall of the reactor was equally discretised. The thermal dispersion coefficient for the wall layers was also estimated using the physical properties of wall materials.

The energy balance for an inside wall layer of tubular reactor section is,

$$\rho_{w1} C_{pw1} A_{fw1} \frac{\partial T_{w1}}{\partial t} = \rho_{w1} C_{w1} D_{tz\_w} \frac{\partial^2 T_{w1}}{\partial z^2} + h_i \pi d_i \left(T - T_{w1}\right) - K_{w1} 2\pi \left(T_{w1} - T_{w2}\right) \quad (6.17)$$

For "y" number of layers,

$$\rho_{wy} C_{pwy} A_{fwy} \frac{\partial T_{wy}}{\partial t} = \rho_{wy} C_{wy} D_{tz\_w} \frac{\partial^2 T_{wy}}{\partial z^2} + K_{wy} 2\pi \left(T_{wy-1} - T_{wy}\right) - K_{wy+1} 2\pi \left(T_{wy} - T_{wy+1}\right) \quad (6.18)$$

For "n^{th}" layer,

$$\rho_{wn} C_{pwn} A_{fwn} \frac{\partial T_{wn}}{\partial t} = \rho_{wn} C_{wn} D_{tz\_w} \frac{\partial^2 T_{wn}}{\partial z^2} + K_{wn} 2\pi \left(T_{wn-1} - T_{wn}\right) - K_{wn} 2\pi \left(T_{wn} - T_j\right) \quad (6.19)$$

6.2.4.4 Reaction kinetics

For the energy balance, the assumption was made that the contribution of heat production due to reaction comes only from the propagation reaction. It was considered that the propagation step was the only important step in determining the heat of polymerization. The final polymerization rate expression was derived based on the kinetic mechanism presented in Chapter 4, and also based on the kinetic assumptions made in Chapter 3 and Chapter 4, respectively. The kinetic model structure (especially the hydrogen response) and parameters, were validated through the batch-scale liquid-phase propylene polymerization experiments, which were described earlier in Chapter 3 and Chapter 4. Therefore, equation (4.37) derived in Chapter 4 for the final form of rate of

polymerization (R_p) with Arrhenius temperature dependence of propagation reaction rate constant has been used here (which also represent Scheme I for R_{po}; see Table 4.2, Chapter 4).

Besides the propagation reaction, the catalyst deactivation is also an important reaction step in the polymerization kinetics. The catalyst deactivation rate (R_d) expressed in the mass balance of catalyst assumed the catalyst decay is of the first order (see Chapter 3 and Chapter 4). The rate of catalyst deactivation can be described according to the following equation,

$$R_d = - k_d C^* \tag{6.20}$$

From the batch-scale polymerization experiments, the deactivation reaction rate for catalyst was evaluated as a function of reaction temperature and hydrogen concentration. In recent studies, Al-haj Ali (2006) [1] reported the final form of equation for deactivation reaction rate constant (k_d) for the same type catalyst as used in this study, and it has shown in equation (4.50) in Chapter 4. The similar equation was adopted in describing the behavior of k_d during the course of polymerization reaction in a tubular reactor.

6.2.4.5 Weight-average molecular weight

The so-called instantaneous weight-average molecular weight of polymer was estimated using the equation derived for average probability of chain termination (q) based on the assumption of "quasi-single" site [▽]. The final form of termination probability for average chain length has already been derived in Chapter 4, and it has shown in equation (4.46) (which also represents Scheme I for q; see Table 4.3, Chapter 4). The similar equation was used here along with the reactor dynamic model to estimate the average molecular weight of the polymer.

The average molecular weight produced over the length of the tubular reactor is then calculated using the following expression,

$$M_{wr}^{\ avg} = \frac{\sum R_p M_w^{\ avg}}{\sum R_p} \tag{6.21}$$

[▽] Equation (4.46) is generally only valid for single site catalyst type.

6.2.4.6 Auxiliary equations

Axial dispersion coefficient

For the tubular reactor operating in turbulent flow, an axial dispersion coefficient (D_{mz}) can be estimated using the semi-empirical equation proposed by Wen et al. (1975) [12]. The correlation shown in equation (6.22) is also valid for transition flow regimes, and compensates for the bends in reactor; see equation (6.23) and (6.24).

$$D_{mz} = \left[\left(\frac{3x10^{7}}{\mathrm{Re}^{2.1}} + \frac{1.35}{\mathrm{Re}^{0.125}}\right)\left(1 + \frac{2\,N_t\,l_{eq}}{L}\right)\right]\left(v_z\,d_i\right) \tag{6.22}$$

For "90°" bend, $l_{eq} = 30\,d_i$ (6.23)

For "U" bend, $l_{eq} = 50\,d_i$ (6.24)

Under turbulent conditions, an analogy between heat and mass transfer is usually assumed such that the thermal and mass diffusivity are supposed to be the same [2].

Heat transfer coefficient

The overall heat transfer coefficient (U) changes along the reactor length because of the changes in the physical properties of the reaction medium, as well as due to the possible changes in macroscopic mixing patterns. It is therefore important to model this coefficient as a distributed parameter along the reactor length. Yao et al. (2004) [13] stated that the U can be described according to the equation (6.25),

$$U^{-1} = h_i^{-1} + h_w^{-1} \tag{6.25}$$

where, h_i is the heat transfer coefficient on reaction side, and h_w represents the film coefficient for the metal wall, reactor jacket, and fouling effect.

The fouling resistance and the resistance to the jacket were neglected. The total wall thermal resistance is the sum of n layers resistances. The h_i coefficient employed for all

flow regime was obtained from the conventional heat exchanger design correlations found in Perry et al. (1997) [10], and it is described as,

$$h_i = \left[\left(\frac{\frac{f_r}{2}\left(\mathrm{Re} - 1000\right)\mathrm{Pr}}{1 + 12.7\sqrt{\frac{f_r}{2}}\left(\mathrm{Pr}^{0.66} - 1\right)} \right) \left(1 + \left(\frac{d_i}{z} \right)^{c_1} \right) \right] \left(\frac{K_{mix}}{d_i} \right) \tag{6.26}$$

where, the term f_r is representing as a "Fanning" friction factor, and can be describe in the case of smooth tubes according to the following equation,

$$f_r = 0.25\left(1.82\log\left(\mathrm{Re}\right) - 1.64\right)^{-2} \tag{6.27}$$

Particle average growth factor

This quantity is defined as the ratio between the average diameter of the polymer particle (dp) and the original catalyst particle (dc). This factor is important in the evaluation of the particle settling-out effects. By keeping track of the amounts of catalyst and produced polymer in the system, it is possible to describe this factor using following expression (see also equation (5.1) in Chapter 5),

$$dx = \frac{dp}{dc} = \left\{ \frac{\rho_p}{\rho_c}\left(Y + 1\right) \right\}^{\frac{1}{3}} \tag{6.28}$$

The additional necessary and important equations and special tasks used with the reactor model are reported in Appendix 6A, and they are divided in following sub-parts,

- Physical properties.
- Reactor connectivity.
- Catalyst injection task.
- Miscellaneous equations.

Model parameters

The following model parameters were used for performing model simulations,

A_1:A_6	:= Constants reported in Chapter 4	
$C_{p\,w}$	:= 0.51	($kJ.kg^{-1}.K^{-1}$)
c_1	:= 0.6667	(-)
d_c	:= 0.000035	(m)
d_i	:= 0.004	(m)
d_o	:= 0.006	(m)
d_{mc_i}	:= 0.008	(m)
d_{mc_o}	:= 0.022	(m)
dHr	:= 2033	($kJ.kg^{-1}$)
$E_{act\,d}$	:= - 20	($kJ.gmol^{-1}$)
$E_{act\,p}$	:= 48.17	($kJ.gmol^{-1}$)
g_c	:= 9.81	($m.s^{-2}$)
h_{mc}	:= 0.45023	($kJ.m^{-1}.K^{-1}.s^{-1}$)
k_{do}	:= 0.00017	(hr^{-1})
k_{d1}	:= 0.00000838	($kg.kg^{-1}$)
k_{d2}	:= 288.2	(hr^{-1})
k_{po}	:= 301560	($m^3.kg^{-1}.s^{-1}$)
k_1, k_2	:= Constants reported in Chapter 4	(-)
K_a:K_e	:= Constants reported in Chapter 4	(-)
l_{eq}	:= 50 d_i	(m)
L_{mc}	:= 0.056	(m)
L	:= 5.65	(m)
m_o^{Cat}	:= 0.06E-6	(kg)
MW_m	:= 42.10	($kg.kmol^{-1}$)
n	:= 1	(-)
N_t	:= 15	(-)
P_{in}	:= 54	(bar)
R_g	:= 0.008213	($kJ.gmol^{-1}.K^{-1}$)
t_{inj}	:= 0.02	(s)
T_{in}	:= 343.15	(K)
T_j	:= 343.15	(K)
X ©	:= 0.0219	(-)
ϕ_{v_HPLC}	:= 1.5E-6	($m^3.s^{-1}$)
ρ_w	:= 7980	($kg.m^{-3}$)

© The "X" value was varied according to the required amount of mole ratio of hydrogen to liquid propylene, for particular experiment.

6.3 Model analysis

In this section, a number of representative calculations obtained using the simulation model are discussed, and the results are compared with experimental data measured from the pilot-scale tubular reactor system. The basic parameters used for simulating the reactor model for different process parameters, are reported in section 6.2.4.6. The initial conditions for reaction temperatures and reactor pressures were set as per the required operating conditions.

The difficulty in predicting an operational behavior of the tubular reactor and the final polymer properties arises from the strong interaction between the polymerization reactions and the fluid dynamics of the reactor. In order to understand such interaction with the help of reactor model, the pulse experiments analyzed in Chapter 5 are chosen here for model verification and predictions.

The simulated temperature profiles along the tubular reactor length for the pulse experiments are shown in Figure 6.4 together with the on-line measurements. Figure 6.4 compares the effect of different amount of catalyst injection on the reactor thermal response. During the polymerization experiments, the known preactivated catalyst amount of 0.12 mg, 0.18 mg and 0.24 mg, respectively, was injected into a continuous flow of liquid-phase propylene with an average axial velocity of 0.14 $m.s^{-1}$. The catalyst amount was injected in a stroke mode with injection period of 1.45 $stroke.s^{-1}$. All the experiments shown in Figure 6.4 were carried out in the absence of hydrogen.

The agreement between the mathematical reactor model and the experimental data illustrated a good predictability of the model. The model could able to estimate the thermal profile of the reactor initiated as a results of exothermic nature of the polymerization reaction.

It can be seen that the “Axial Dispersion Model” applied in this study was found to be an useful tool in describing the typical features of tubular reactor especially in terms of the sensitivity of the temperature profiles with respect to the heat transfer, dynamics of reactor fluid mixing and heat production (kinetics). The models selected to represent these three phenomenons were found to be valid for the overall experimental conditions mentioned in this chapter. The influence of these models on the reactor behavior is analyzed in further discussions.

(a)

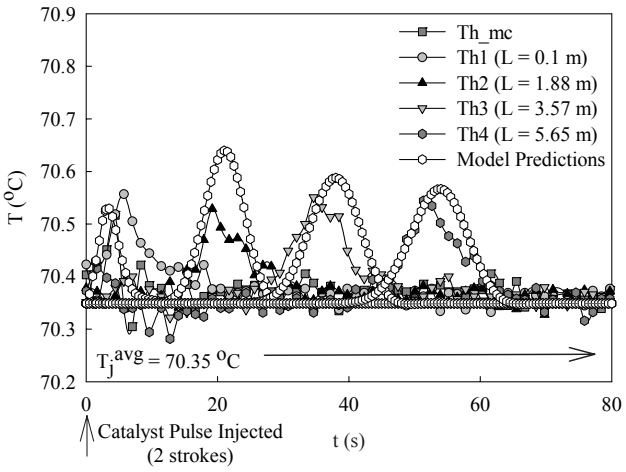

(b)

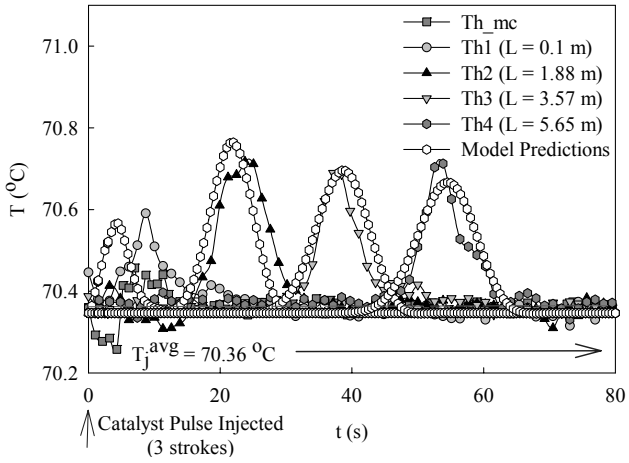

(c)

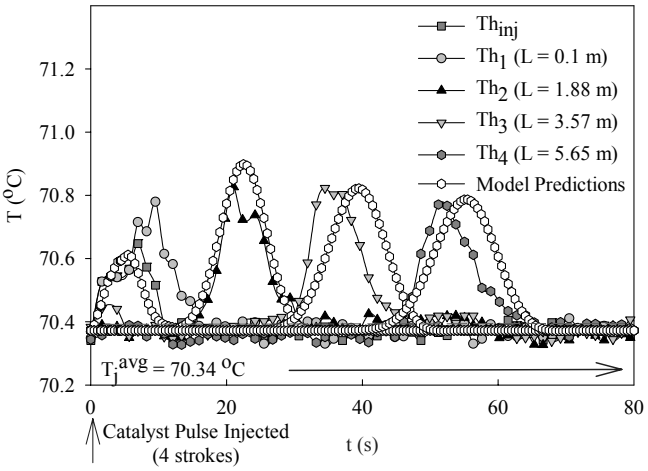

Figure 6.4: Comparisons of measured and model predictions of temperature profile after injection of a preactivated catalyst pulse into a flow of liquid propylene; (a) m_o^{Cat} = 0.12 mg, (b) m_o^{Cat} = 0.18 mg and (c) m_o^{Cat} = 0.24 mg (T_o = 70 °C, P_o = 54 bar, X = 0.0, injection period = 1.45 s.stroke^{-1}).

The first important factor to understand is the heat transfer capability of the present tubular reactor concept. Thanks to the in-depth analysis reported on the heat transfer coefficients in the open literature that can apply for the high-pressure tubular polymerization reactor and tubular reactor in general [7, 10, 11, 14]. From different published literature, several predictive and validated heat transfer model can be found. This allowed researchers to exchange and develop number of models with validity over the broad flow regimes. In addition, it certainly helped in building-up the sense for adopting the proper heat transfer model for the tubular reactor presented in this study (see equation (6.26) and (6.27)), and therefore, keeping the model as simple as possible.

Equation (6.26) exhibit a dependency of h_i coefficient on the physical properties of the reaction mass. The influence of different catalyst injection on h_i coefficient was estimated to be very limited and resulted in an average value of 0.33 $kJ.m^{-2}.K^{-1}s^{-1}$ (on the basis of model predictions carried out for the experimental conditions shown in Figure 6.4). It is important to note here that the reactor is appeared to be in a constant heat flux mode for the heat transfer from reactor to jacket during the different amount of catalyst injections at constant reaction conditions.

This effect was quite obvious from the point that the rate of polymerization upon injection of different amount of preactivated catalyst was similar at constant initial reaction conditions, i.e., at 70 ^oC temperature and 54 bar pressure, and thus shown an unvarying change in the physical properties of the reaction medium. According to the comparison presented in Figure 6.4, it is understood that the characteristics of the reactive pulse created from the different amount of catalyst injections is mainly dependent on the concentrations of the reactive species and the movements of the particles with the changing degree of particle clouds. However, from the operational point of view, it is important to study the combined effect reaction kinetics and varying fluid dynamics on the heat transfer phenomena of the reactor to the cooling jacket.

Figure 6.5 illustrate the predicted temperature profiles generated at different reaction temperatures after addition of 0.24 mg of preactivated catalyst amount into the continuous flow liquid propylene (with an average axial velocity of 0.14 $m.s^{-1}$). All the predicted results shown in Figure 6.5 were simulated for the 0.0 mole ratio of hydrogen to liquid propylene (X).

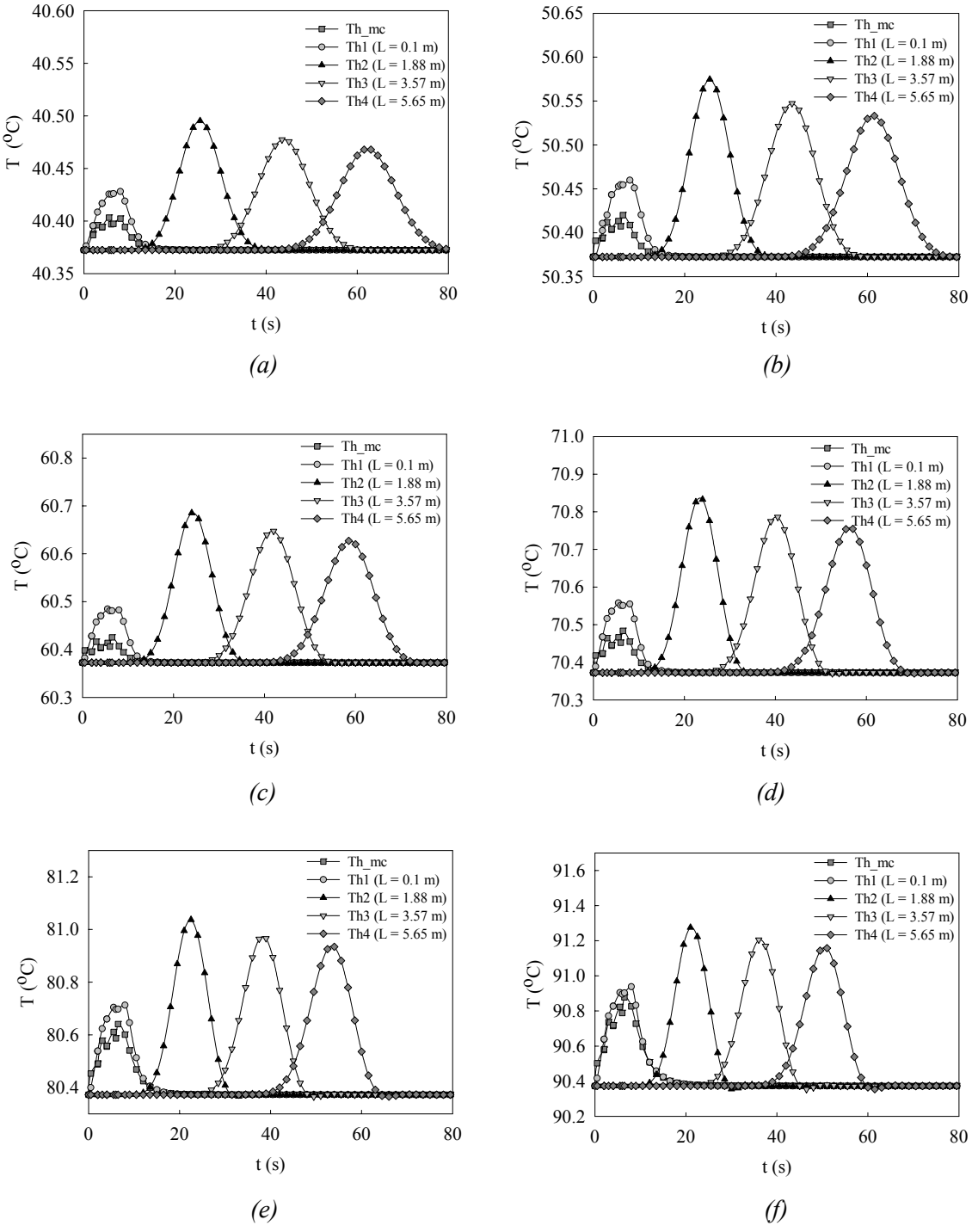

Figure 6.5: Predicted temperature profile after injection of a preactivated catalyst pulse into a flow of liquid propylene; (a) 40 °C, (b) 50 °C, (c) 60 °C, (d) 70 °C, (e) 80 °C and (f) 90 °C (P_o = 54 bar, m_o^{Cat} = 0.24 mg, X = 0.0, injection period = 1.45 s.stroke^{-1}).

The case study presented in Figure 6.5 would be an appropriate way to discuss the influence of varying reaction kinetics and physical properties of the reaction medium on the heat transfer as well as on the dynamics of fluid mixing. Firstly, as discussed in Chapter 3, the rate of polymerization approximately doubles with every 10 ^{o}C increase in the temperature, and thus, might present the similar impact on the rate of heat generation upon initiation of polymerization reaction with increasing reaction temperature. Secondly, the physical properties of the main reaction medium, i.e., liquid propylene as well differ with changing reactor temperature. For instance, for an increase in reaction temperature from 40 ^{o}C to 90 ^{o}C, the density and viscosity of liquid propylene dropped by 25 % and 45 %, respectively.

Therefore, the interaction between an enhanced degree of heat generation and the reduced physical properties of liquid propylene should show an impact on the resistance for the heat transfer from reactor to jacket. In order to understand the cumulative influence of these two parameters on the heat transfer resistance at the reaction side, the average predicted values of h_i coefficient are plotted as a function of increasing reaction temperatures; see Figure 6.6.

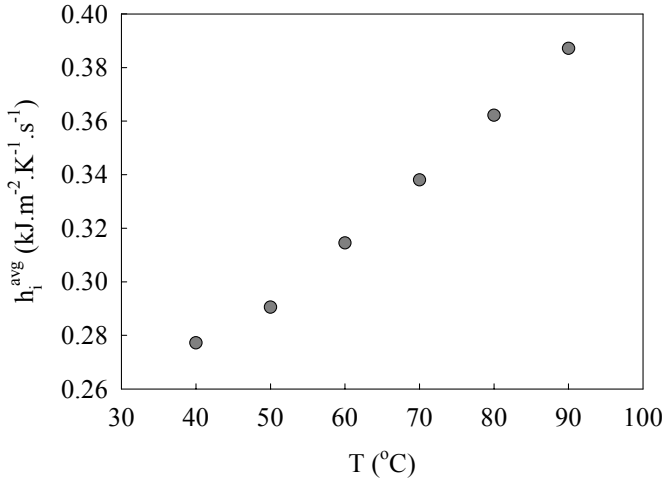

Figure 6.6: Predicted values of an average h_i coefficient at different reaction temperatures (experimental conditions are same as reported in Figure 6.5).

Figure 6.6 show that an average h_i coefficient increases linearly with increasing reaction temperature. This linear dependency is well in accordance with the linear relationship

observed for the rate of polymerization (discussed in Chapter 3) and physical properties of the liquid monomer (based on the estimated properties as an only function of temperature), with the reaction temperature. However, it should be noted that this effect might be applicable only for the specific range of reaction temperatures that are mentioned in Figure 6.6.

It is also interesting to see from Figure 6.6 that the reduction in physical properties of liquid monomer with increasing temperature helped in enhancing the heat exchange capacity at the reaction side, and thus assisted in controlling the thermal response of the reactor at higher rate of polymerization (and can be observed from Figure 6.5).

Another essential factor to analyze is the behavior of flow pattern present in the currently used tubular reactor system. One way to understand this factor is by estimating the "Peclet (Pe)" number at different reaction conditions, for instance, at different reaction temperatures as per shown in Figure 6.5. The estimated values of Pe numbers shown in Figure 6.7 are found to be very large, and thus, depicted the "Plug Flow" behavior for the reactor. The Pe number was calculated using the axial dispersion coefficient equation (6.30), which is reported in section 6.2.4.6 ⊕.

Zheng et al. (2002) [17] studied the influence of Pe number (in the range of 0.01 to 500) on the tubular reactor performance for "Living" free-radical polymerization and for the polymer properties. The authors stated that the key issue in designing a tubular reactor to have a narrow residence time distribution is to achieve good radial mixing and have a sufficiently large value of Pe number.

They suggested that one can design a tubular reactor with a narrow residence time distribution by using static mixers, helical coils, or sufficiently frequent bends in the tube. The tubular reactor concept designed for the present study does provide sufficiently frequent bends in the tube (see Figure 6.1).

⊕ The Pe number was estimated using following equation [17],

$$Pe = \frac{v_z L}{D_{mz}} \tag{6.29}$$

The values of Pe numbers shown in Figure 6.7 were merely based on the predicted values of D_{mz}, which were calculated using equation (6.22).

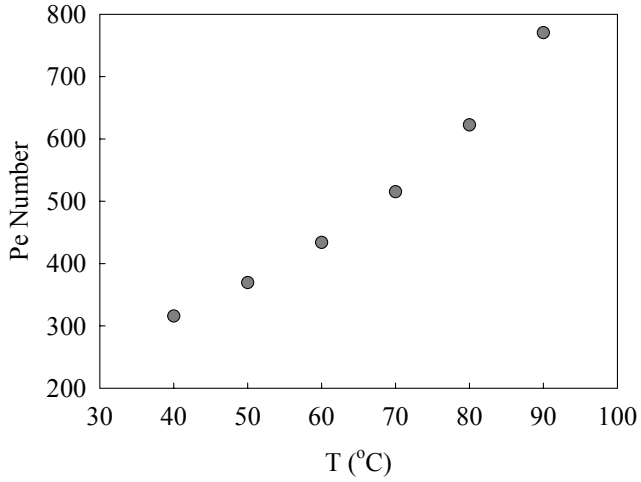

Figure 6.7: Predicted values of the "Pe" number at different reaction temperatures (experimental conditions are same as reported in Figure 6.5).

The temperature profiles so far discussed above are the measure for the thermal response of the catalyst at an early stage of polymerization, and certainly shown that the history of these profiles depend on the interaction between heat transfer to the jacket, flow pattern for mixing and reaction kinetics. The last factor to discuss is the reaction kinetics, as the rate of heat generation plays an important role in (ultimate) understanding of the reactor behavior too.

As per kinetic data discussed in the precious chapters for the catalyst used in this work, the activity in the absence of hydrogen was very low, and mainly affects the development of an initial morphology of the catalyst after being injected into the bulk of liquid monomer. This might be one of the reasons that the maximum rise in peak temperature was observed at the second thermocouple section (could be seen from the profiles shown in Figure 6.4 and Figure 6.5), explaining the delayed activating effect for some fraction of injected catalyst amount. The model predictions reported here indicate that the elaborative kinetic model developed for the catalytic liquid propylene polymerization can very well be used along with the reactor model to describe the tubular reactor performance.

One of the examples is presented in Figure 6.8 for analyzing the predictability of the kinetic model. Figure 6.8 explains the comparison between model prediction and experimental data for the temperature profile obtained during the polymerization test

performed in the presence of hydrogen with the X value of 0.0219. This profile was generated after addition of 24 mg of preactivated catalyst into the continuous flow reaction medium with an average axial velocity of 0.14 $m.s^{-1}$.

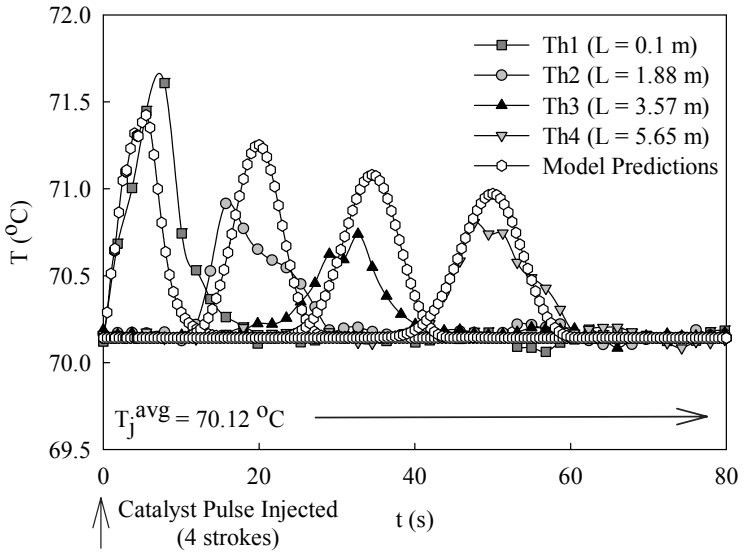

Figure 6.8: Comparison of measured and model predictions of temperature profile after injection of a preactivated catalyst pulse into a flow of liquid propylene (experiment performed with T_o = 70 °C, P_o = 65 bar, X = 0.0219, concentrated catalyst slurry, m_o^{Cat} = 0.24 mg, injection period = 1.45 s.stroke^{-1}.

The comparison made in Figure 6.8 did demonstrate an ability of the kinetic model in judging the characteristics of catalyst type. The model predictions for temperature profiles plotted in Figure 6.8 also explain the sensitivity of hydrogen function (described in section 6.2.4.4) towards the prediction of polymerization rate. Similar to the experimental findings reported in Chapter 5, the kinetic model along with reactor dynamic model did describe the high activity nature of catalyst type in the presence of hydrogen exhibiting enhanced polymerization rate, with rapid initiation period, followed by rate deceleration.

Furthermore, in order to extrapolate an ability of kinetic model, a number of temperature profiles were simulated for different amount X values used during polymerization runs. Figure 6.9 represent the three temperature profiles generated after injection of 24 mg of preactivated catalyst into the reactor with X values varying from 0.0, 0.0510 and 0.0981,

respectively. The model predictions shown in Figure 6.9 are found to be in-line with the experimental observations discussed in the previous chapters about the hydrogen influence on the reaction rates. Just to revise, at 0.0219 values of X, the catalyst activity exhibited the so-called retardation effect during liquid propylene polymerization. The plausible reason mentioned in Chapter 4 for this reduction in the catalyst activity at higher hydrogen concentration was the distinct nature of hydrogen present during the reaction affecting the nature of the active sites strictly produced due to the chain transfer reactions with hydrogen. This could explain the drop in temperature at X value of 0.0981 shown in Figure 6.9.

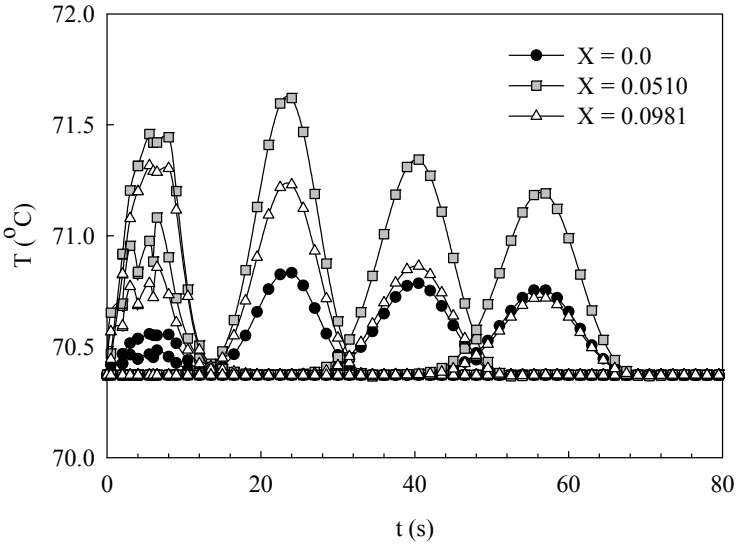

Figure 6.9: Predicted hydrogen influence on the temperature profile after injection of a preactivated catalyst pulse into a flow of liquid propylene (T_o = 70 °C, P_o = 65 bar, m_o^{Cat} = 0.24 mg and injection period = 1.45 s.stroke^{-1}).

Until now, the reactor behavior was understood by analyzing the characteristics of reactive pulses based on the information derived from the proper heat transfer and mixing model along with the well-characterized kinetic model. On the other hand, a simplified attempt was made by calculating the pulse area and pulse height to width ratio (HWR), for judging the pulsed tubular reactor behavior.

The variations in pulse area and HWR according to reaction temperatures and different X values are shown in Figure 6.10 (a) and (b), respectively. The four points shown in Figure 6.10 (a) and (b) were determined at different thermocouple sections placed at 0.1 m 1.88

m, 3.57 m and 5.65 m, along the tubular reactor length. An interesting phenomenon observed from these figures is that the pulse area seems to exhibit an indirect relationship with the reaction rate, because the pulse areas are increasing with increasing reaction temperature meaning with increasing rate of polymerization, and they could also able to illustrate the response of hydrogen on the catalyst activity.

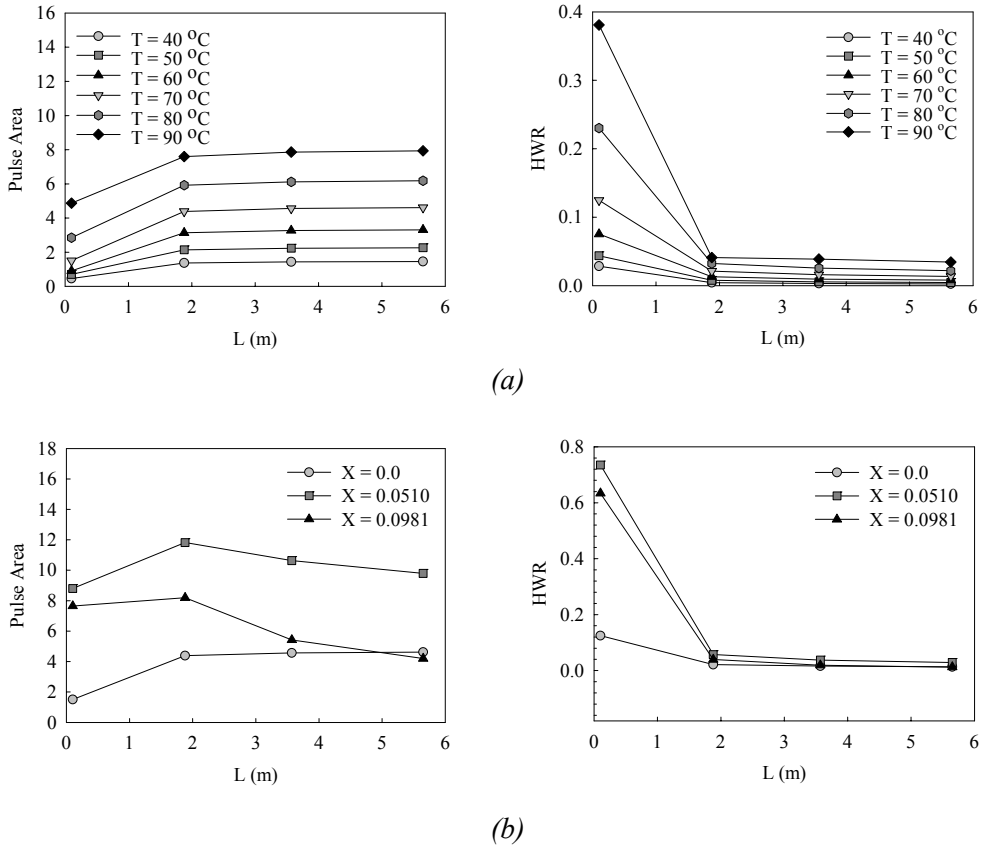

Figure 6.10: Estimated pulse areas and HWR values from reactor model simulated for different (a) reaction temperatures and (b) hydrogen concentrations.

The estimated values of HWR shown in Figure 6.10 (a) and (b) describe the dynamic behavior of the pulse travelling along the reactor length. The high values of HWR obtained at the inlet of tubular reactor indicate the response of reactor connectivity, wherein the "Mixing Cell" and tubular reactor connected in series. However, this response gets dampen over the remaining length of tubular reactor, and can be seen from the constant values of HWR at 1.88 m, 3.57 m and 5.65 m section of the reactor; see Figure 6.10 (a) and (b). The HWR values observed along the reactor length also supports the Pe number theory in describing the "Plug Flow" behavior of the reactor.

One of the main advantages of the proposed model is its capability in predicting the kinetic rate profiles. Applying the appropriate assumptions made earlier on the kinetic as well as reactor model and using the mass balances for chemical constituents, the profiles for rate of polymerization during an early stage of polymerization can be simulated for different process parameters.

For example, the simulated rate profiles at different reaction temperatures are plotted in Figure 6.11, using the same parameters reported in section 6.2.4.6. The quantitative nature of the rate profiles could very well describe the experimental data given in Chapter 5. For instance, instantaneous maximum values of polymerization rate estimated for different reaction temperatures and at different location along the reactor length, shown in Figure 6.11, were in good agreement with the measured initial rate of polymerization data discussed in Chapter 5. The profiles plotted in Figure 6.11 shows a negligible decrease in the reaction rate, which could be well understood from the low decay rate of the catalyst for such short residence time experiments [].

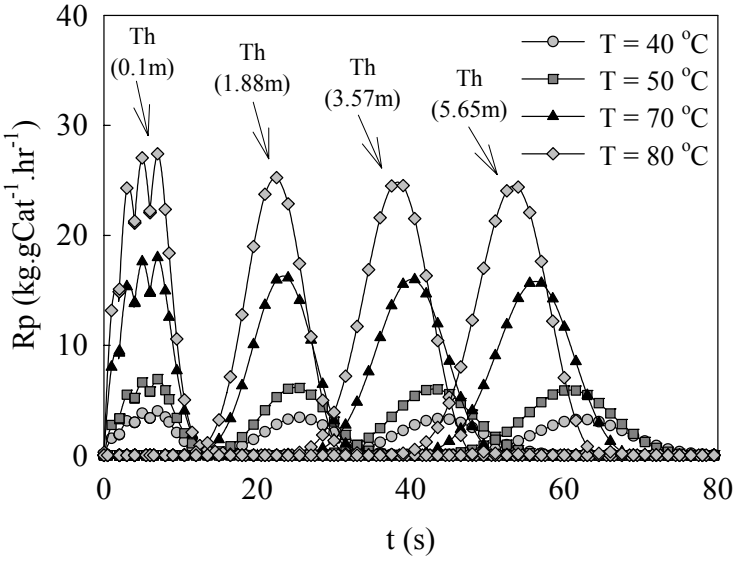

Figure 6.11: Estimated rate of polymerization at different reaction temperatures used during the polymerization of liquid propylene (P_o = 55 bar, m_o^{Cat} = 0.24 mg and injection period = 1.45 s.stroke^{-1}).

[] The decay rate for catalyst was estimated using equation (6.20) reported in section 6.2.4.4, which explains the dependency of catalyst deactivation on reaction temperature as well as on different hydrogen concentrations.

The sensitivity of reactor model towards the heat transfer and dynamics of mixing can also be tested by analyzing the catalyst performance at different process parameters during the polymerization reaction. Principally, the effect of these two factors on the performance of the catalyst can be observed by estimating the "cumulative" polymer yield at the end of the reaction ♦. The comparison between measured and predicted yield values at different reaction temperatures and X values is shown in Figure 6.12 (a) and (b), respectively.

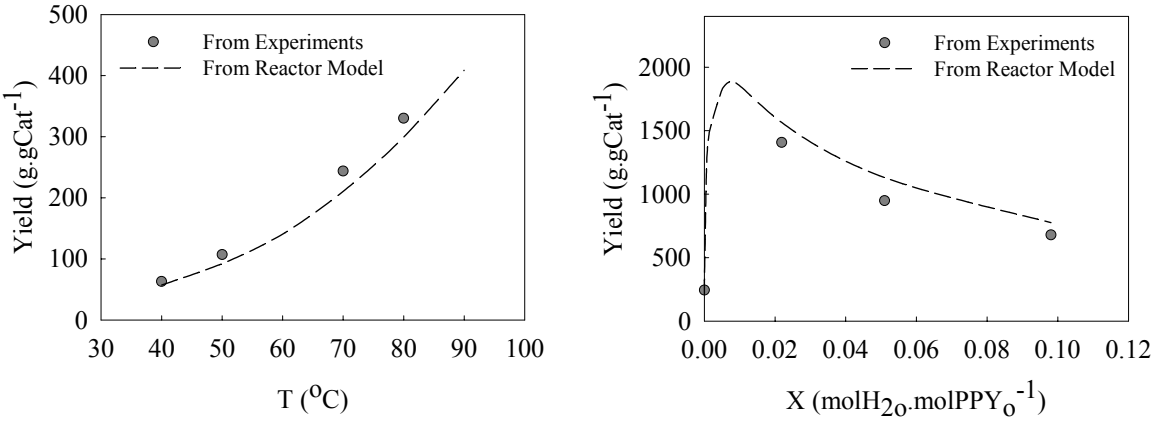

Figure 6.12: Comparison of measured and model predictions of polymer yield obtained during the polymerization of liquid propylene in a tubular reactor (a) at different reaction temperature and (b) at different values of X.

The better predictions of polymer yield shown in Figure 6.12 (a) and (b) exhibit two "art-effects" of the present tubular reactor process ◊,

♦ Yield of the polymer was calculated using following formula [16],

$$Yield = \int_0^{\tau} Rp \, d\tau \tag{6.30}$$

◊ The predicted values of polymer yield were found to be deviating within the range of 15 % from the experimental data points. This deviation however was considered within the range of reproducibility of the experiments.

1. Ability of liquid-phase reaction to remove the heat of polymerization from the polymer particles during reaction, thus, avoiding any kind of catalyst deactivation due to overheating or thermal runway. This heat transfer capability of the present process is already discussed above on the basis of internal h_i coefficients affecting the thermal response of tubular reactor.
2. The "Plug Flow" nature of the reactor flow, controlling the average residence time of the active catalyst particles. This character of the flow is judged based on the model prediction discussed above, and could also be seen from the normalized PSD data shown in Chapter 5.

The simulation model presented in this chapter can predict the weight-average molecular weight (M_w^{avg}) of the polymer samples produced from the tubular polymerization reactor. Figure 6.13 show the comparison of M_w^{avg} calculations using the simulation model versus the off line GPC measurements of the polymer samples. The predicted values of average molecular weight (M_{wr}^{avg}) demonstrate a good agreement with the GPC measurements of polymer samples, and suggest that a simplified "q" model assuming a "quasi-single" site approach can be used to predict the average molecular weight property of the polymer [Θ].

The M_{wr}^{avg} values shown in Figure 6.13 illustrate the influence of hydrogen on the molecular weight with two distinct regions,

1. One is at low hydrogen concentration, i.e., at X values of <= 0.01, exhibiting a steep decrease in average molecular weight explaining a chain transfer ability of hydrogen.
2. Another is at high hydrogen concentration, i.e., at X values of > 0.01, exhibiting a very limiting and linear decrease in average molecular weight with increasing hydrogen amount. Such limited decrease is similar to the influence of hydrogen observed on the termination probability of the active polymer chain, and could be noticed from the Figure 4.7 shown in Chapter 4.

[Θ] However, this approach is generally not valid for the ZN catalyst type, which contains multiple active sites. The multiplicity in number of active sites for the catalyst type used in the present study has been discussed in detail in Chapter 4. The "four site" model was developed for understanding the behavior of molecular weights and its distribution. This model can be elaborated and used along with the reactor model presented here, with the specific objective of molecular weight distribution modeling.

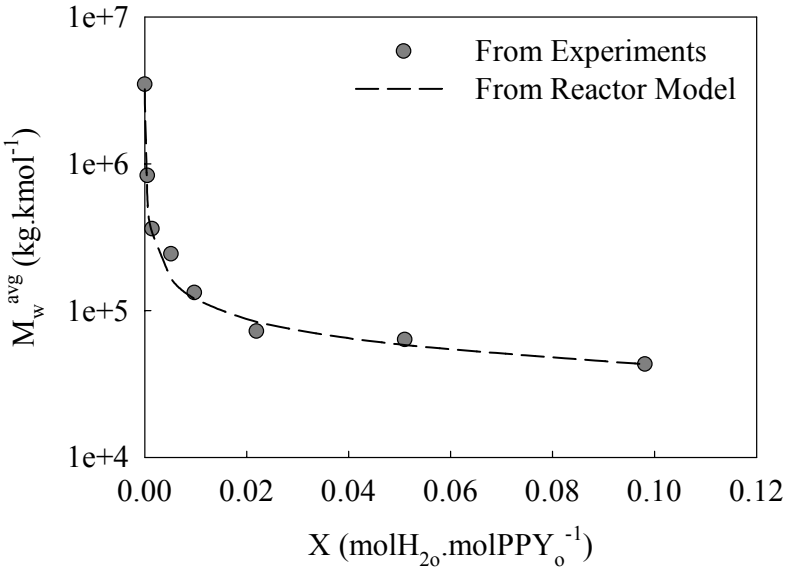

Figure 6.13: Comparison of measured and model predictions of M_{wr}^{avg} obtained during the polymerization of liquid propylene in a tubular reactor.

So far, the model presented above was validated and simulated for the reactor design used in the present work. Next, the attempt is made to study the extensive applications of the tubular reactor for catalytic olefin polymerization. The tube dimension play the most important role in analyzing the broad prospects of tubular reactor for catalytic polymerization, especially its,

1. Flexibility in providing the operational simplicity and varying process conditions, and thus elaborating an applicability of reactor as a "high-output" tool.
2. Possibility of using as a "prepolymerization reactor" at an industrial scale, allowing the production of polymer of comparable quality from economic considerations.

However, by keeping in mind the focus of this chapter on the "high-output" tool, the first preliminary approach is discussed here, in which, more importantly, the effect of different reactor length on the monomer conversion in terms of polymer yield is studied. On the other hand, the utility of the tubular reactor as a "prepolymerization or main polymerization reactor" on the industrial scale is described in the next chapter based on the dynamic reactor model and on the validated kinetic response of the catalyst.

The reactor lengths were varied in identical proportion so that the residence time (τ) would change by an equal factor. By keeping the same inside tube diameter (d_i = 0.004 m) and flow conditions as used in the above model (v_z = 0.14 $m.s^{-1}$), the reactor length was varied from 5.65 m, 11 m, 17 m and 23 m, allowing the τ values of 40 s, 80 s, 120 s and 160 s, respectively. All other parameters used for the simulations were same as shown in section 6.2.4.6. The predicted values of polymer yield obtained at different reaction temperatures and hydrogen concentration, are plotted as a function of different reactor lengths; see Figure 6.14 (a) and (b).

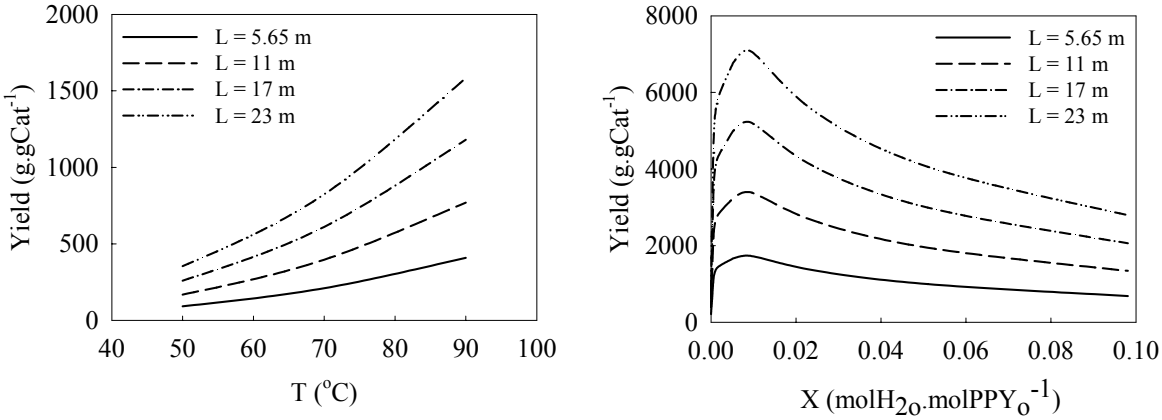

Figure 6.14: Predicted polymer yield obtained during the polymerization of liquid propylene in a tubular reactor with different reactor length (a) at different reaction temperature and (b) at different values of X.

The polymer yield observed from Figure 6.14 (a) and (b) illustrates a proportional increase with an increasing value of τ of an active catalyst particle (from 40 s to 160 s) inside the reactor. This yield enhancement is known to be a function of catalyst deactivation rate and τ. The deactivation rate for the catalyst used in this study was very low and thus did not show any significant effect on the polymer yield. With the "Plug Flow" character of the tubular reactor, the effect of increasing residence time of the catalyst particles on the polymer yield was trivial.

This way, a number of simulations can be performed using the validated reactor model, and can be able to explore the unique opportunity of such set-up in carrying out kinetic experiments with the reduced reaction time. The aim at this point is to propose pragmatic

strategies on the basis of the flexibilities involved with “capillary type” tubular reactor as well as with reactor model, in generating quality of kinetic data at an “early stage” of polymerization.

The policies discussed below can be used as an objective for the future research work, and they are as follows,

1. A sufficiently long length of capillary tube with vertical mounting can be used for the pulsed catalytic polymerization experiments. The flow conditions should be maintained properly to have a “Plug Flow” reactor characteristic, which will help in evaluating the dynamics of an individual pulse. The reactor jacket must be designed for an isoperibolic mode experiments in order to analyze the “non-isothermal” reactor behavior as a result of “quasi-adiabatic” temperature rise due to an exothermic polymerization reaction.
2. In order to broaden the operating window of the process, the multiple injection system can be used for different chemical constituents along the reactor length. In this way, number of polymerization tests can be performed over a short period of reaction time, which allow to generate a wide range of data on monomer quality, catalyst performance (with respect to various process conditions), fast estimation of reaction kinetics for different catalyst type having different activating procedures.
3. Most importantly, the long reactor length can be divided into similar sections with the help of separate reactor jacket that will enable to maintain the different reaction conditions. This could assist in developing some unique polymer products with enhanced end-use properties.
4. Lastly, the “high-output” expansion system should be developed for the degassing and polymer collection from the multiple experiments.

6.4 Conclusions

A complete mathematical model has been developed for the dynamic simulation of a pilot-scale tubular reactor for catalytic polymerization of liquid-phase propylene. The reactor model and kinetic model has been validated with a good agreement for the temperature dynamics of the reactor measured from the selected polymerization tests performed with the pulse injections of preactivated catalyst into a reactor.

The model could able to explain the influence of heat removal, mixing dynamics and reaction kinetics on the appearance of the temperature profiles generated during the polymerization experiments, which were performed using different process parameters. The selected heat transfer correlation and semi-empirical axial dispersion model published in the open literatures were found to be very useful in analyzing the several interesting heat transfer phenomena associated with the macroscopic heat transfer and axial dispersion.

The detailed kinetic model developed in Chapter 4 could illustrate the catalyst performance in the tubular reactor. The main advantage of the present model was in predicting the polymerization rate profiles at an "early stage" of polymerization process by taking into consideration the hydrodynamics of the reactor. For example, the polymer yield calculated from the reactor model shown a good comparison with the experimental values. As a simplified approach, the "quasi-single" site assumption in modeling the M_w^{avg} of the polymer as a function of different hydrogen concentrations was quite practical, and can be seen from the predicted and experimental values of M_w^{avg}. To conclude, the accurate predictions of catalytic liquid-phase polymerization were attained using a non-isothermal and non-adiabatic axially dispersed "Plug Flow" model of the reactor.

Furthermore, the model predictability was extended to explore the applicabilites of the tubular reactor for catalytic polymerization of liquid propylene. The experimental results reported in Chapter 5 and the model predictions demonstrated in this chapter certainly explain the key importance of the reactor concept.

Appendix 6A

Physical properties

The calculation of the physical properties of reaction mixtures requires basically the definition of a mixing rule and the specification of a relationship between the phases involved. The basic assumptions employed in this work are,

1. Mass additivity of specific masses and specific heats.
2. Contributions other than monomer and polymer are considered to be negligible.
3. The density of produced polymer is assumed to be constant.

The physical properties of monomer were estimated using the polynomial equations derived as a function of pressure and temperature along the reactor length. These equations were modeled based on the thermophysical properties database provided by "National Institute of Science and Technology (NIST)" [$]. These equations were valid accurately for the following range of conditions: Pressure = 10 - 250 bar and Temperature = 293 - 363 K.

Density

Using the mixing rule of mass additivity, the density of reaction medium can be calculated using following expression,

$$\rho_{mix} = \rho_m \left(1 - X_m\right) + \rho_p \left(X_m\right) \tag{6A.1}$$

The density of the liquid propylene (with P in bar),

$$\rho_m = \frac{\rho_{T1} + \rho_{T2} P}{\left(1 + \rho_{T3} P\right)^2} \tag{6A.2}$$

where the constants are estimated from following equations (with T in K),

$$\rho_{T1} = 426.54975 - 3.9648742\,T + \left(1.3098731E-2\right)T^2 - \left(1.4580818E-5\right)T^3 \tag{6A.3}$$

$$\rho_{T2} = -3.5534637 + \left(4.7812216E-2\right)T - \left(2.0039163E-4\right)T^2 + \left(2.7062122E-7\right)T^3 \tag{6A.4}$$

$$\rho_{T3} = -\left(1.658065E-1\right) + \left(2.187214E-3\right)T - \left(9.0610047E-6\right)T^2 + \left(1.2131313E-8\right)T^3 \tag{6A.5}$$

Specific heat

As per the assumption made above, the specific heat of reaction medium can be calculated using following expression,

$$C_{pmix} = C_{pm}\left(1 - X_m\right) + C_{pp}\left(X_m\right) \tag{6A.6}$$

[$] For more information please see this website: http://webbook.nist.gov/chemistry/fluid/

The specific heat of the liquid propylene (with P in bar),

$$C_{pm} = \frac{C_{pT1} + C_{pT2}\,P}{\left(1 + C_{pT3}\,P\right)^2} \tag{6A.7}$$

where the constants are estimated from following equations (with T in K),

$$C_{pT1} = 10154.0054384501 - 130.791087219449\,T + \left(6.31549045998E - 1\right)T^2 - \left(1.354759329E - 3\right)T^3 + \left(1.089388E - 6\right)T^4 \tag{6A.8}$$

$$C_{pT2} = 833.909087758304 - 10.746202327803\,T + \left(5.1907483705E - 2\right)T^2 - \left(1.11389246E - 4\right)T^3 + \left(8.9604E - 8\right)T^4 \tag{6A.9}$$

$$C_{pT3} = 552.311843145278 - 7.117022994947\,T + \left(3.4375570491E - 2\right)T^2 - \left(7.3762975E - 5\right)T^3 + \left(5.9333E - 8\right)T^4 \tag{6A.10}$$

The specific heat of the PP is estimated from the assumed linear relationship (with T in K),

$$C_{pp} = 0.002881T + 1.020333 \tag{6A.11}$$

Viscosity

Zacca (1991) [14] assumed the most common approximation while estimating the reaction medium viscosity that the total viscosity is only a function of the viscosity of the liquid-phase ($\mu_{m)}$ and of the solids volume fraction (ϕ_v), and can be described as,

$$\mu_{mix} = \mu\left(\mu_m, \phi_v\right) \tag{6A.12}$$

The author also reported a generic expression for estimating the viscosity of reaction medium [Δ],

[Δ] The constants used in equation (6A.13) were obtained from Zacca (1991) [14] and they are as follows, μ_0 = 1.0, μ_1 = 0.5, μ_2 = 0.0, μ_3 = 0.0, μ_4 = 1.0, μ_5 = –2.0, μ_6 = 1.0, μ_7 = 0.0 and μ_8 = 0.0.

$$\mu_{mix} = \left[\frac{\mu_0 + \mu_1 \phi_v + \mu_2 \phi_v^{\,2} + \mu_3 \phi_v^{\,3}}{\mu_4 + \mu_5 \phi_v + \mu_6 \phi_v^{\,2}} + \mu_7 e^{\mu_8 \phi_v} \right] \mu_m \tag{6A.13}$$

The viscosity of the liquid propylene (with P in bar),

$$\mu_m = 0.001\left(\mu_{T1} + \mu_{T2} P - \mu_{T3} P^2 + \mu_{T4} P^3 - \mu_{T5} P^4 \right) \tag{6A.14}$$

where the constants are estimated from following equations (with T in K),

$$\begin{aligned} \mu_{T1} = {} & 33.435433 - \left(3.9947527E-1\right)T + \left(1.7921347E-3\right)T^2 \\ & - \left(3.5609391E-6\right)T^3 + \left(2.6358625E-9\right)T^4 \end{aligned} \tag{6A.15}$$

$$\begin{aligned} \mu_{T2} = {} & -1.1158682 + \left(1.3646602E-2\right)T - \left(6.2314104E-5\right)T^2 \\ & + \left(1.2586234E-7\right)T^3 - \left(9.480488E-11\right)T^4 \end{aligned} \tag{6A.16}$$

$$\begin{aligned} \mu_{T3} = {} & -\left(1.2903578E-2\right) + \left(1.5838961E-4\right)T - \left(7.2648841E-6\right)T^2 \\ & + \left(1.4751363E-9\right)T^3 - \left(1.1182122E-12\right)T^4 \end{aligned} \tag{6A.17}$$

$$\begin{aligned} \mu_{T4} = {} & -\left(6.0246215E-5\right) + \left(7.4122487E-7\right)T - \left(3.4087538E-9\right)T^2 \\ & + \left(6.9424933E-12\right)T^3 - \left(5.2813663E-15\right)T^4 \end{aligned} \tag{6A.18}$$

$$\begin{aligned} \mu_{T5} = {} & -\left(9.8346553E-8\right) + \left(1.2117614E-9\right)T - \left(5.5819415E-12\right)T^2 \\ & + \left(1.390182E-14\right)T^3 - \left(8.683922E-18\right)T^4 \end{aligned} \tag{6A.19}$$

Thermal conductivity

The thermal conductivity of reaction medium is most commonly correlated as a function of the thermal conductivity of the two phases, mainly liquid propylene and polymer (K_m and K_p), and of the polymer volume fraction (ϕ_v).

Zacca (1991) [14] reviewed a few thermal conductivity correlations and used a “Maxwell and Tareef” correlation for thermal conductivity for their modeling study on “Loop Reactors” for catalytic olefin polymerization.

The similar correlation is used here,

$$K_{mix} = \left[\frac{2\frac{K_m}{K_p} + 1 - 2\phi_v\left(\frac{K_m}{K_p} - 1\right)}{2\frac{K_m}{K_p} + 1 + 2\phi_v\left(\frac{K_m}{K_p} - 1\right)} \right] K_m \tag{6A.20}$$

The thermal conductivity of the liquid propylene (with P in bar),

$$K_m = 0.001\left(K_{T1} + K_{T2}\,P - K_{T3}\,P^2 + K_{T4}\,P^3 - K_{T5}\,P^4\right) \tag{6A.21}$$

where the constants are estimated from following equations (with T in K),

$$K_{T1} = 5.5777035 - \left(6.36469178E-2\right)T + \left(2.757934E-4\right)T^2 - \left(5.266667E-7\right)T^3 + \left(3.6702255E-10\right)T^4 \tag{6A.22}$$

$$K_{T2} = -\left(1.9034867E-1\right) + \left(2.2963721E-3\right)T - \left(1.029789E-5\right)T^2 + \left(2.0302718E-7\right)T^3 - \left(1.4789616E-11\right)T^4 \tag{6A.23}$$

$$K_{T3} = -\left(2.1550819E-3\right) + \left(2.6275321E-5\right)T - \left(1.1935199E-7\right)T^2 + \left(2.3903768E-10\right)T^3 - \left(1.777056E-13\right)T^4 \tag{6A.24}$$

$$K_{T4} = -\left(9.871243E-6\right) + \left(1.2109769E-7\right)T - \left(5.540828E-10\right)T^2 + \left(1.1194561E-12\right)T^3 - \left(8.4137036E-16\right)T^4 \tag{6A.25}$$

$$K_{T5} = -\left(1.5851541E-8\right) + \left(1.9523947E-10\right)T - \left(8.974557E-13\right)T^2 + \left(1.8231021E-15\right)T^3 - \left(1.379261E-18\right)T^4 \tag{6A.26}$$

The thermal conductivity of the PP is estimated from the assumed linear relationship (with T in K),

$$K_p = 0.000122 + \frac{0.000161}{1 + e^{\left(\frac{T - 409.65}{-10.116}\right)}} \tag{6A.27}$$

Reactor connectivity

As can be seen from Figure 6.2, the "Mixing Cell" and the tubular reactor models were connected in series, and thus, the input conditions for both the models has to be set properly. The input conditions for "Mixing Cell" were set as follows,

At t = 0, $C_k = C_{k\_in}$ (6A.28)

$T = T_{in}$ (6A.29)

$P = P_{in}$ (6A.30)

The outlet stream from the "Mixing Cell" was connected as an input to the tubular reactor system. The "STREAM" function in gPROMS has been used to perform this task, and it is explained in Figure 6A.1, wherein the two streams were created as "Outlet" and "Inlet".

MODEL: Reactor

```
Unit
    PFR   AS    TubularReactor

STREAM
    Outlet      IS    PFR.MC.STREAM_Source_Connect
    Inlet       IS    PFR.STREAM_Connect

EQUATION
    Outlet      IS    Inlet
```

Figure 6A.1: "STREAM" function in gPROMS.

Catalyst injection task

During the polymerization experiments, the injection of preactivated catalyst slurry was carried out in two modes, such as pulse mode and continuous mode. This task was modeled using a "TASK" function provided with the gPROMS. Figure 6A.2 shows the overall structure of the "TASK" declaration, in which, the sequential execution of the series of tasks was specified by enclosing them within a "SEQUENCE" structure. The execution of a "SEQUENCE" structure was complete when the execution of the last task

in the structure has terminated. This way the number of strokes could be created for the injection of preactivated catalyst slurry. The three time constants t_1, t_2 and t_3 shown in Figure 6A.2 have used to control the injection period of the catalyst for a particular experiment.

TASK: Start_Injections

```
PARAMETER
    Reactor      AS    MODEL Reactor
    NoStroke     AS    INTEGER

VARIABLE
    Stroke       AS    INTEGER

SCHEDULE
    SEQUENCE
        Stroke := 1;
        While Stroke <= NoStroke DO
            SEQUENCE
                RESET
                Reactor.PFR.MC.mCat := "x1" amount
                END    # RESET
                CONTINUE FOR "t1"
                RESET
                Reactor.PFR.MC.mCat := 0.0
                END    # RESET
                CONTINUE FOR "t2"
                Stroke := Stroke + 1;
            END    # Sequence
        END    # Sequence
        CONTINUE FOR "t3"
    END    # Sequence
```

Figure 6A.2: "TASK" function in gPROMS.

Miscellaneous equation

The following miscellaneous equations were used along with the reactor model discussed above.

Flow area for tubular reactor,

$$A_f = \frac{\pi d_i^{\,2}}{4} \tag{6A.31}$$

Flow area for tubular reactor wall layers,

$$A_{fwy} = \frac{\pi\left(d_{wy+1} - d_{wy}\right)^2}{4} \tag{6A.32}$$

Area for "Mixing Cell",

$$A_{mc} = \frac{\pi d_{mc\_i}^{\,2}}{4} \tag{6A.33}$$

Injected preactivated catalyst amount [⊗],

$$C^*_{in} = \frac{m_o^{Cat}}{\phi_{mc\_in}\, t_{inj}} \tag{6A.34}$$

Tubular reactor wall thickness,

$$d_w = d_i + \Delta d \tag{6A.35}$$

Heat dispersion inside reactor metal wall,

$$D_{tzw} = \frac{K_w}{\rho_w C_{pw}} \tag{6A.36}$$

Thermal conductivity of the reactor metal wall,

$$K_w = 0.000013 T_j + 0.011449 \tag{6A.37}$$

Prandtl number

$$\mathrm{Pr} = \frac{C_{pmix}\,\mu_{mix}}{K_{mix}} \tag{6A.38}$$

[⊗] The injection period "t_{inj}" for catalyst addition was similar to the time constant, "t_1" shown in Figure 6A.2.

Reynolds number

$$\mathrm{Re} = \frac{d_i \, v_z \, \rho_{mix}}{\mu_{mix}} \tag{6A.39}$$

"Mixing Cell" volume,

$$V_{mc} = \frac{\pi \, d_{mc\_i}{}^2 \, L_{mc}}{4} \tag{6A.40}$$

Volume of "Mixing Cell" metal wall,

$$V_{mc\_w} = \frac{\pi \left(d_{mc\_w\,y+1} - d_{mc\_w\,y} \right)^2 L_{mc}}{4} \tag{6A.41}$$

Monomer conversion,

$$X_m = \left(1 - \frac{M}{M_{in}} \right) \tag{6A.42}$$

Polymer volume fraction [∅],

$$\phi_v = \frac{\rho_{mix}}{\rho_p \, X_m} \tag{6A.43}$$

Nomenclature

A_f	: Flow area for reaction mixture (m^2)
$A_{fw\,n}$	: Flow area for reactor wall layer n (m^2)
A_{mc}	: Flow area for "Mixing Cell" (m^2)
A_1 to A_6	: Constants used in equation (4.46) in Chapter 4
C_{k_in}	: Inlet concentration of generic component "k" in tubular reactor ($kg.m^{-3}$)
C_k	: Concentration of generic component "k" in tubular reactor ($kg.m^{-3}$)

[∅] The solid volume fractions (ϕ_s) and polymer volume fractions (ϕ_v) were considered to be same.

$C_{p\ mix}$: Specific heat of reaction mixture ($kJ.kg^{-1}.K^{-1}$)

$C_{p\ mix\_in}$: Specific heat of reaction mixture at inlet reactor conditions ($kJ.kg^{-1}.K^{-1}$)

$C_{p\ m}$: Specific heat of monomer ($kJ.kg^{-1}.K^{-1}$)

$C_{p\ p}$: Specific heat of polymer ($kJ.kg^{-1}.K^{-1}$)

$C_{p\ T1}$ to $C_{p\ T3}$: Constants used in equation (6A.7)

$C_{p\ w}$: Specific heat of reactor wall ($kJ.kg^{-1}.K^{-1}$)

$C_{p\ w\ n}$: Specific heat of reactor wall layer n ($kJ.kg^{-1}.K^{-1}$)

C_{in}^{*} : Inlet concentration of preactivated catalyst ($kg.m^{-3}$)

C^{*} : Concentration of preactivated catalyst ($kg.m^{-3}$)

c_1 : Constants used in equation (6.26)

d_i : Inside reactor diameter (m)

d_{mc_i} : Inside diameter of "Mixing Cell" (m)

d_{mc_wn} : Wall thickness of "Mixing Cell" for layer n (m)

d_o : Outside reactor diameter (m)

$d_{w\ n}$: Wall thickness of reactor for layer n (m)

dHr : Heat of reaction ($kJ.kg^{-1}$)

dc : Catalyst particle diameter (m)

dp : Polymer particle diameter (m)

dT : Temperature difference (^{o}C)

dx : Ratio between polymer particle and catalyst particle.

D_{mz} : Axial dispersion coefficient for tubular reactor ($m^2.s^{-1}$)

D_{tz_w} : Thermal dispersion coefficient for tubular reactor wall ($m^2.s^{-1}$)

D_{tz} : Thermal dispersion coefficient for tubular reactor ($m^2.s^{-1}$)

E_{act_d} : Activation energy for deactivation reaction ($kJ.mol^{-1}$)

E_{act_p} : Activation energy for propagation reaction ($kJ.mol^{-1}$)

f_r : Friction factor coefficient

$f(H_2)$: Hydrogen response function

g_c : Gravitational force ($m.s^{-2}$)

h_i : Internal heat transfer coefficient (for reactor side) ($kJ.m^{-2}.K^{-1}.s^{-1}$)

h_{mc} : Internal heat transfer coefficient (for "Mixing Cell") ($kJ.m^{-2}.K^{-1}.s^{-1}$)

h_w : Heat transfer coefficient (for metal wall, reactor jacket and fouling effect) ($kJ.m^{-2}.K^{-1}.s^{-1}$)

H_{2o} : Initial moles of hydrogen present during reaction (mole)

k_{do} : Arrhenius constant for deactivation reaction (s^{-1})

k_d : Rate constant for deactivation constant (s^{-1})

k_{d1}, k_{d2} : Constants used in equation (4.50) in Chapter 4

k_{po} : Arrhenius constant for propagation reaction ($m^3.kgCat^{-1}.hr^{-1}$)

k_p : Rate constant for propagation reaction ($m^3.kgCat^{-1}.hr^{-1}$)

k_1, k_2 : Constants used in equation (4.37) and (4.46) in Chapter 4

K_a to K_e : Constants used in equation (4.37) in Chapter 4

K_{mix} : Thermal conductivity of reaction mixture ($kJ.m^{-1}.K^{-1}.s^{-1}$)

K_m : Thermal conductivity of monomer ($kJ.m^{-1}.K^{-1}.s^{-1}$)

K_p : Thermal conductivity of polymer ($kJ.m^{-1}.K^{-1}.s^{-1}$)

K_{T1} to K_{T5} : Constants used in equation (6A.21)

$K_{w\,n}$: Thermal conductivity of reactor wall material of layer n ($kJ.m^{-1}.K^{-1}.s^{-1}$)

K_w : Thermal conductivity of reactor wall material ($kJ.m^{-1}.K^{-1}.s^{-1}$)

l_{eq} : Equivalent length (m)

L_{mc} : "Mixing Cell" length (m)

L : Tubular reactor length (m)

m_o^{Cat}, mCat : Mass of (preactivated) catalyst (mg)

M_{wr}^{avg} : Cumulative weight-average molecular weight ($kg.kmol^{-1}$)

M_w^{avg} : Weight-average molecular weight ($kg.kmol^{-1}$)

MW_k : Molecular weight of generic component "k" ($kg.kmol^{-1}$)

MW_m : Molecular weight of monomer ($kg.kmol^{-1}$)

M_{in} : Inlet monomer concentration in tubular reactor ($kg.m^{-3}$)

M : Monomer concentration in tubular reactor ($kg.m^{-3}$)

N_t : Number of turns for tubular reactor

Pe : Peclet number

P_o : Initial reactor pressure (bar)

P : Reactor pressure (bar)

P_{in} : Reactor pressure at inlet reactor condition (bar)

P_r : Prandtl number

PPY_o : Initial moles of liquid propylene present during reaction (mole)

R_d : Rate of catalyst deactivation ($kg.m^{-3}.s^{-1}$)

Re : Reynolds number

Re_p : Particle Reynolds number

R_g : Universal gas constant ($kJ.mol^{-1}.K^{-1}$)

R_k : Reaction rate for generic component "k" ($kg.m^{-3}.s^{-1}$)

R_{po} : Initial rate of polymerization ($kg.m^{-3}.s^{-1}$)

R_p : Rate of polymerization ($kg.m^{-3}.s^{-1}$)

t_{inj} : Catalyst injection time (s)

t : reaction time (s)

T_o : Initial reactor temperature (^oC)
T_j : Jacket Temperature (^oC)
T_{in} : Temperature at inlet reactor condition (^oC)
$T_{w\,n}$: Temperature for reactor wall layer n (^oC)
T : Temperature (^oC)
Th_mc : Thermocouple point at "Mixing Cell"
Th1 to Th4 : Different thermocouple points along the reactor length
U : Overall heat transfer coefficient ($kJ.m^{-2}.K^{-1}.s^{-1}$)
v_t : Particle terminal settling velocity ($m.s^{-1}$)
v_{z_in} : Initial axial velocity ($m.s^{-1}$)
v_{z_s} : Axial velocity for solid component ($m.s^{-1}$)
v_z : Axial velocity ($m.s^{-1}$)
V_{mc_w} : Volume of "Mixing Cell" wall (m^3)
V_{mc} : Volume of "Mixing Cell" (m^3)
Vr : Volume of tubular reactor (m^3)
$V_{w\,n}$: Volume of tubular reactor wall layer n (m^3)
X_m : Monomer conversion
X : Mole ratio of hydrogen to liquid propylene
Y : Polymer yield ($g.gCat^{-1}$)
z : Varying point location on reactor length (m)

Greek letters

η_l : Viscosity of liquid medium ($kg.m^{-1}.s^{-1}$)
η_{mix}, μ_{mix} : Viscosity of reaction mixture ($kg.m^{-1}.s^{-1}$)
μ_m : Viscosity of monomer ($kg.m^{-1}.s^{-1}$)
μ_{T1} to μ_{T5} : Constants used in equation (6A.14)
μ_0 to μ_8 : Constants used in equation (6A.13)
ϕ_{mc_in} : Inlet volumetric flow rate to "Mixing Cell" ($m^3.s^{-1}$)
ϕ_{mc_out} : Outlet volumetric flow rate from "Mixing Cell" ($m^3.s^{-1}$)
ϕ_v : Solid volume fraction
ρ_c : Density of catalyst particle ($kg.m^{-3}$)
ρ_k : Density of polymer particle ($kg.m^{-3}$)
ρ_l : Density of liquid medium ($kg.m^{-3}$)

ρ_{mix} : Density of reaction mixture ($kg.m^{-3}$)
ρ_{mix_in} : Density of reaction mixture at inlet reactor conditions ($kg.m^{-3}$)
ρ_{m} : Density of monomer ($kg.m^{-3}$)
ρ_{p} : Density of polymer ($kg.m^{-3}$)
ρ_{T1} to ρ_{T3} : Constants used in equation (6A.2)
ρ_{w} : Density of reactor wall ($kg.m^{-3}$)
$\rho_{w\,n}$: Density of reactor wall layer n ($kg.m^{-3}$)
τ : Average residence time (s)

Sub- and superscripts

act : Activation
c : Catalyst
d : Deactivation
eq : Equivalent
f : Flow
g : Gas
i, in : Initial or inlet or inside
j : Jacket
k : Representing generic component
l : Liquid
mc_in : At “Mixing Cell” inlet
mc_out : At “Mixing Cell” outlet
mc : “Mixing Cell”
m : Monomer or mass
mix : Mixture
mix_in : Mixture at inlet reactor conditions
n : Representing number of wall layers or number
o : Initial or outside
p : Polymerization or polymer or particle
r : Reactor
s : Solid
t : Tube or thermal or terminal
v : Volume

w : Wall or weight
y : Representing number of wall layers
z : Representing the axial direction

Abbreviations

gPROMS : general PROcess Modeling Systems
GPC : Gel Permeation Chromatography
NC : Number of components

Literature

[1] Al-haj Ali, M. (**2006**), Doctorate Thesis, University of Twente, Enschede, The Netherlands.
[2] Bird, R. B., Stewart, W. E. and Lightfoot, E. N. (**1960**), Transport phenomena, Wiley, NY.
[3] Di Martino, A., Broyer, J. P., Spitz, R., Weickert, G. and McKenna, T. F. (**2005**), Macromol. Rapid Commun., 26, 215 - 220.
[4] Fogler, S. H. (**1999**), Elements of chemical reaction engineering, Prentice Hall PTR, NJ.
[5] Husain, A. and Hamielec, A. E. (**1976**), AIChE Symposium Series, 72, 160, 112 - 127.
[6] Kleinstreuer, C. and Agarwal, S. S. (**1987**), Int. J. Engng. Sci., 25, 5, 597 - 607.
[7] Lacunza, M. H., Ugrin, P. E., Brandolin, A. and Capiati, N. J. (**1998**), Polymer Engineering and Science, 38, 6, 992 - 1013.
[8] Liang, W., Jin, Y., Yu, Z., Wang, Z., Zhu, J. and Chen, J. (**1996**), The Chemical Engineering Journal, 63, 181 - 188.
[9] Melo, P. A., Biscaia Jr., E. C. and Pinto, J. C. (**2001**), Chemical Engineering Science, 56, 6793 - 6800.
[10] Perry, R. H. and Green, D. W. (**1997**), Perry's Chemical Engineers' Handbook, 6th edition, McGraw-Hill, NY.
[11] Reginato, A. S., Zacca, J. J. and Secchi, A. R. (**2003**), AIChE Journal, 49, 10, 2642 - 2654.

[12] Wen, C.Y. and Fan, L.T. (**1975**). Models for flow systems and chemical reactor, Marcel Dekker Inc., NY.

[13] Yao, F. Z., Lohi, A., Upreti, S. R. and Dhib, R (**2004**), International Journal of Chemical Reactor Engineering, 2, A16.

[14] Zacca, J. J. (**1991**), Master's Thesis, University of Wisconsin, Madison, USA.

[15] Zacca, J. J. and Ray, H. (**1993**), Chemical Engineering Science, 48, 22, 3743 - 3765.

[16] Zacca, J. J., Debling, J. A. and Ray, H. (**1996**), Chemical Engineering Science, 51, 21, 4859 - 4886.

[17] Zheng, M. and Ray, H. (**2002**), Journal of Applied Polymer Science, 86, 1047 - 1056.

Chapter 7

Model based analysis of scale-up tubular reactor for liquid-phase propylene polymerization

Abstract: The scale-up tubular reactor for catalytic liquid-phase propylene polymerization is investigated based on the selected simulation runs performed using the developed mathematical reactor model. The purpose of the present analysis is to demonstrate the theoretical strategy in studying the response of the tubular reactor at industrial scale. The reactor behavior has been predicted in terms of the reactor thermal response, varying concentration of chemical constituents like active catalyst and hydrogen and the polymer properties mainly the molecular weights and their distributions. Strictly speaking, the predictions reported in this chapter are based on the kinetic peculiarities of the catalyst type discussed in the previous chapters. The thermal response of the reactor was studied using the three dependent process variables such as ΔT, ΔP and overall conversion. The maximum overall conversion was constrained to 30 % allowing a limited solid content of the reactor and thus, providing a better process operation. The magnitude of ΔT increases with increasing the catalyst loading and consequently, increases the overall conversion. Therefore, the catalyst concentration was optimized to have the ΔT in the range of 10 - 14 ^{o}C and the overall conversion value up to 30 %. The optimum predicted annual production capacity of the tubular reactor was found to be 214 kton.yr^{-1}, with the overall conversion limit of 30 % and with an inside reactor diameter of 0.1 m resulting into the reactor volume of 39 m^3. The tubular reactor dynamics for different concentrations of hydrogen during the polymerization is also been investigated based on the influence of hydrogen on the catalyst productivity as discussed in the previous chapters. The nature of the profile predicted for cumulative polymer yield, average molecular weights and polydispersity index as a function of hydrogen amount were found to be similar and intrinsic to the type of the catalyst used throughout this study. The multiple injection of hydrogen along the reactor length enabled to modify the molecular weight distributions of the polymer produced. The nature of the predicted molecular weight distributions demonstrated the so-called “Bimodal” distribution containing a relatively high molecular weight fraction and a relatively low molecular weight fraction. The polydispersity indexes of the predicted “Bimodal” molecular weight distributions were ranging from 34.1 to 70.2.

Keywords: catalytic olefin polymerization, modeling, molecular weight, molecular weight distribution, scale-up tubular reactor

7.1 Introduction

After looking at the past fifty years, the growth in polyolefin industry is a result of an enhancement taking place in the catalyst development, process advancement and product development and its demand. For example, processes initially used for the manufacture of polypropylene (PP) were designed to accommodate the limitations of the early Ziegler-Natta (ZN) catalyst types, see Keii (2004) [6]. Removal of the catalyst from the polymer and separation of the nonstereoregular atactic fraction were required to produce a marketable product, however, with limited production capacity. Moreover, as the demand for PP increased, the continuous polymerization processes were employed, replacing the batch polymerization vessels by a series of stirred vessels.

Further, the commercialization of high yield, high stereospecificity fourth generation catalysts enabled the development of processes in which the removal of catalyst and atactic polymer were unnecessary. These processes also eliminate the use of hydrocarbon diluent by either using liquid or gaseous monomer as a polymerization medium. The reduction in capital and operating costs achieved by these new processes has both promoted the expansion of PP production and established the high yield process products as the industry standards. Virtually all new PP capacity installed since the mid 1980s has utilized high yield, high stereospecificity catalysts. Due to the rationalization and merging process carried on by the industry, the major technology providers and process licensors are now: Basell (Spheripol), Dow (Unipol), NTH (Novolen), Mitsui (Hypol), Borealis (Borstar) and BP (Innovene) [8]. Their technology is used in most new facilities. Additionally, the processes using liquid monomer as a polymerization medium are often divided into two categories: those using continuous stirred reactors and those using loop reactors.

Such scenario definitely motivate the idea of developing new high yield processes combining the liquid monomer as a polymerization medium and novel reactor types (for example, tubular reactor) and keeping the broad focus on the manufacturing novel polymer products. As a high yield process, the use of liquid propylene as a polymerization medium maximizes the rate of the polymerization reaction by providing high monomer concentration. Similar to other processes, the concept of tubular reactor with liquid reaction medium process could be used to produce homopolymer PP and random copolymers with less than 5 % ethylene. In addition, for producing the impact-modified copolymers, the tubular reactor with liquid-phase propylene can be used with a

hybrid process consisting of homopolymerization in the liquid-phase followed by copolymerization in gas-phase. This also suggests the application of tubular reactor as a "prepolymerization reactor" with optimum reactor dimensions and residence time. However, the main objective of using the tubular reactor technology would be to make use of the advantage of axial mixing and heat removal on developing the unique polymer properties, as well as reducing the reaction time compared to the conventional process without altering the standard polymer properties. Along with the degree of freedom reported in the previous chapter, the tubular reactor with inside diameters (d_i) in the range of 0.06 - 0.1 m should also provide the operational simplicity avoiding the requirement of special fabrication technique, thus reducing the operational costs.

In order to understand the performance of the scale-up tubular reactor for catalytic liquid-phase propylene polymerization, the accomplishment of a useful model is essential for further work on development of optimal design criteria and operation policies. The purpose of the present investigation is to demonstrate the theoretical strategy in analyzing the response of the tubular reactor at industrial scale. The reactor behavior is predicted in terms of

- Thermal response.
- Varying concentrations of chemical constituents such as catalyst and hydrogen.
- Polymer properties.

Strictly speaking, the predictions presented in this chapter are based on the data reported in the previous chapters on the kinetic characteristics of the ZN catalyst as well as on the properties of the produced polymer. However, the methodology discussed in this chapter is generic, and can be applied to another catalyst type and reaction medium having authentic kinetic information for speculating the tubular reactor performance.

7.2 Reactor model

The mathematical model used in this chapter is the same as the model presented in Chapter 6. The system considered here was a "Plug Flow" model with axial dispersion. The generic model assumptions reported in Chapter 6 are also applied here. The model framework was set-up in the programming environment "gPROMS" as a distributed model in which the tubular reactor was distributed over an axial direction with a specific number of grids using different discretisation method provided by the software. In this case, a "Backward Finite Difference" method was selected to discretise the tubular

reactor in the axial direction. However, in this case, for simplifying the model analysis, the tubular reactor was modeled without having the "Mixing Cell" as an inlet zone. The simplified schematic of scale-up tubular reactor is shown in Figure 7.1, wherein the reactor is mounted in the vertical axial position [∇]. The liquid propylene, preactivated catalyst and hydrogen (as a chain transfer agent) are continuously fed into the reactor [∀]. For the present case, the shell and tube configuration is envisaged (see Figure 7.1); in which the jacket temperature is controlled by a thermostat and assumed to be uniform in any given section. This assumption is based on the well-mixed flow situation in the jacket having a quick response compared to the mean residence of the reactants in the reactor. Upon exiting the tubular reactor, the reaction mixture and PP is depressurized and flashed, which enable the recycling of liquid monomer. The temperature and pressure profiles with respect to time and axial coordinates can be measured using sensors placed along the reactor length.

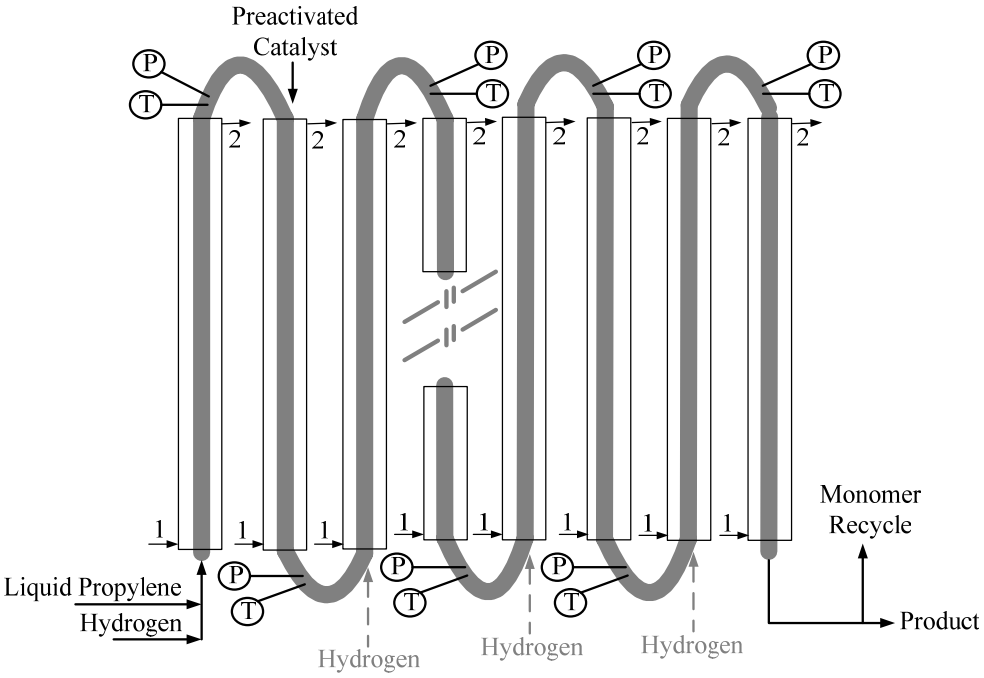

Figure 7.1: Simplified schematic of scale-up type tubular reactor for catalytic liquid-phase propylene polymerization (1: Coolant in and 2: Coolant out).

[∇] In another polymerization system, a typical high pressure tubular reactor for low-density polyethylene (LDPE) production is consist of spiral-wrapped, jacketed metallic pipe.

[∀] Similar to hydrogen, the comonomer such as ethylene can also be fed to the reactor continuously or in with a multiple injections (not shown in Figure 7.1).

For industrial high pressure tubular reactor (used in LDPE polymerization studies), the length-to-diameter ratio (L/d_i) of the pipe is very large depicting a broad range varying from 250:1 to 60000:1, and using very high axial velocities, ranging from 3 to 22 $m.s^{-1}$ [2, 10, 11]. The overall conversion for these reactors ranges from 9 - 29 % depending on the final product specification, reactor configuration, and the catalyst type used.

In this study, the tubular reactor behavior was predicted using an inside diameter of 0.1 m and with the maximum reactor length of 5000 m. The axial velocity was chosen in such a way that the average residence time (τ) inside the reactor was 1000 s, enabling to operate the reactor in turbulent flow regime (Re >> 200000). The operating conditions used during the simulations were typically in the range of 60 to 80 ^oC reactor temperature and 50 to 200 bar of reactor pressure □. The reactor response was simulated for maximum overall conversion of 30 % to limit the solid content of the reactor. The model framework was set in such a way that the multiple injections of the chemical constituents can be possible at different positions along the reactor length, especially to study the influence of hydrogen on the molecular weights of the polymer.

For the present case, the momentum balance has been reduced to the axial component of the equation of motion in cylindrical coordinates. The application of the modeling assumptions reported in Chapter 6 result in the following equation ◊, which could be used for calculating the pressure drop across the tubular reactor section.

$$\frac{\partial P}{\partial z} = \left(-0.00001\,\rho_{mix} \left(\frac{\partial v_z}{\partial t} + v_z \frac{\partial v_z}{\partial z} + \frac{2 v_z^{\,2} f_r}{d_i} \right) + \frac{4}{3} \frac{\eta_{mix}}{\rho_{mix}} \frac{\partial^2 v_z}{\partial z^2} + \rho_{mix}\, g_c \right) \tag{7.1}$$

The following boundary condition was applied for pressure drop profile,

$$P = P_{in} \tag{7.2}$$

where, f_r, is the "Fanning" friction factor, and can be describe in the case of smooth tubes according to the equation (6.27) described in Chapter 6.

□ Operating pressures in excess of 30 bar were required to maintain propylene in the liquid-phase at polymerization temperatures of 60 to 80 ^oC.

◊ The complete derivation of the momentum balance for depicting the pressure drop across the tubular reactor section has been reported by Zacca (1991) [11].

The overall heat transfer coefficient (U) is the result of the combination of all thermal resistances present between the reactor contents and the coolant, can be represented in the same manner as it was shown by equation (6.25) in Chapter 6. The internal tube (reaction side) heat transfer coefficient (h_i) was calculated for all flow regime and obtained from the conventional heat exchanger design correlations found in Perry et al. (1997) [9] Δ,

$$h_i = 0.0265\ R_e^{0.8}\ \mathrm{Pr}^{0.3}\ \left(\frac{\mu_{mix}}{\mu_{mix\ w}}\right)^{0.14} \tag{7.3}$$

The reaction kinetics, molecular weights, its distribution, and all other auxiliary equations used for simulating the present case study are the same as reported in section 6.2.4 of Chapter 6. The molecular weight distribution (MWD) predicted here was based on the four site model discussed in Chapter 4. The final form of Deconvolution model for GPC curves given by equation (4B.12) in Chapter 4 has been used to predict the MWD.

The following basic model parameters were used for performing model simulations,

A_1:A_6	:= Constants reported in Chapter 4	
$C_{p\,w}$	:= 0.51	($kJ.kg^{-1}.K^{-1}$)
d_c	:= 0.000035	(m)
d_i	:= 0.1	(m)
d_o	:= 0.112	(m)
dHr	:= 2033	($kJ.kg^{-1}$)
$E_{act\,d}$	:= - 20	($kJ.gmol^{-1}$)
$E_{act\,p}$	:= 67.22	($kJ.gmol^{-1}$)
g_c	:= 9.81	($m.s^{-2}$)
k_{do}	:= 0.00017	(hr^{-1})
k_{d1}	:= 0.00000838	($kg.kg^{-1}$)
k_{d2}	:= 288.2	(hr^{-1})
k_{po}	:= 1.7778E+8	($m^3.kg^{-1}.s^{-1}$)
k_1, k_2	:= Constants reported in Chapter 4	(-)
K_a:K_e	:= Constants reported in Chapter 4	(-)
l_{eq}	:= 50 d_i	(m)
L	:= 5000	(m)
MW_m	:= 42.10	($kg.kmol^{-1}$)
N_t	:= 200	(-)

Δ However, from the analysis of series of simulation runs, it was observed that the term representing the ratio of viscosity in the equation (7.3) did not exhibit any significant change in the temperature profiles predicted along the axial direction of the reactor.

P_{in}	:= 200	(bar)
R_g	:= 0.008213	($kJ.gmol^{-1}.K^{-1}$)
T_{in}	:= 343.15	(K)
T_j	:= 343.15	(K)
X [©]	:= 0.0025	(-)
ρ_w	:= 7980	($kg.m^{-3}$)

7.3 Simulation results and analysis

The simulation results of the developed model for the scale-up tubular reactor for catalytic liquid-phase propylene polymerization are discussed in this section. A number of simulations were performed to predict the influence of reactor dynamics on its thermal response upon continuous injection of preactivated catalyst into the reactor, on its production capacity with varying different process parameters and variables, and on the properties of the produced polymer (in this case the molecular weights of the polymer and their distributions). The basic parameters used for simulating the reactor model for different process parameters, are reported in section 7.2. The initial conditions for reaction temperatures and reactor pressures were set as per the required operating conditions.

Table 7.1 shows the recipes and obtained data for several simulation runs carried out to study the influence of reaction temperature on the dynamics of the tubular reactor. The three temperatures, 60, 70 and 80 ^oC were chosen for this case study, which represents the standard range of operating conditions used for industrial scale reactors; see part (a), (b) and (c) in Table 7.1.. Another sub-parameter varied was the catalyst amount. The amount of catalyst was selected based on the overall conversion of the reactor. The maximum boundary for catalyst amount was set according to the maximum acceptable conversion of < 30 %. The amount of hydrogen used during these simulation runs was kept constant with an initial value of 0.0025 of mole ratio of hydrogen to liquid propylene (X). The overall simulation data reported in Table 7.1 represent the maximum change in the reactor temperature and pressure, the cumulative yield, the annual production capacity, and polymer properties in terms of weight-average molecular weight (M_w^{avg}) and polydispersity index (PDI). Based on these data, the effect of temperature on the tubular reactor performance was analyzed.

[©] The "X" value was varied according to the required amount of mole ratio of hydrogen to liquid propylene, for particular experiment.

Table 7.1: Simulation runs carried out to study the thermal response of the scale-up tubular reactor for catalytic liquid-phase propylene polymerization [*]

Simulation Code	T_o (°C)	$[M]_o$ (kg.m^{-3})	$[Cat]_o$ (kg.m^{-3})	X (molH$_2$o.molPPYo^{-1})	ΔT [#] (°C)	ΔP [$] (bar)	Overall Conversion (%)	Yield (kg.gCat^{-1})	Annual Production (kton.yr^{-1})	M_w^{avg} (kg.kmol^{-1})	PDI
(a)											
Run71			0.0019		1.70	29.94	5.7	17.6	40	208600	6.3
Run72	60.0	506.2	0.0032	0.0025	3.22	29.22	10.7	19.6	75	212000	6.2
Run73			0.0060		9.62	26.53	30.0	30.0	200	227000	6.0
(b)											
Run74			0.0010		1.83	28.73	6.1	37.0	44	250000	5.9
Run75	70.0	492.9	0.0019	0.0025	4.04	27.77	13.2	42.1	94	253000	5.8
Run76			0.0032		9.75	25.48	29.7	57.4	204	260000	6.0
(c)											
Run77			0.0005		1.67	27.71	5.3	68.5	42	279000	6.1
Run78	80.0	479.8	0.0010	0.0025	3.77	26.86	11.7	77.1	90	276000	6.3
Run79			0.0019		10.27	24.48	28..9	101.7	214	272000	7.3

[*] All the simulations were performed at P_o = 200 bar, v_z = 5 m.s^{-1} with tubular reactor having d_i = 0.1 m and L = 5000 m, and yielding a τ value of 1000 s. The jacket temperature was always maintained at the initial reaction temperature. [#] ΔT is the difference between reactor maximum temperature and the initial temperature. [$] ΔP is the difference between the reactor pressures estimated at the inlet and outlet position.

From Table 7.1, it is observed that the maximum temperature difference (ΔT) estimated over the reactor length is proportionally increasing with increasing catalyst loading. Simultaneously, the increasing amount of catalyst loading was decreasing the pressure drop (ΔP) over the complete reactor length. This effect was obvious as the solid content of the reactor was increasing with increment in the catalyst concentration and subsequently the polymer yield, which might limit the probable instability of the flow characteristics due to the excess amount of polymer particles along with the exothermic nature of the polymerization reaction. This indicates that the optimized catalyst loading is very important to control these three dependent process variables like ΔT, ΔP and overall conversion for better process operation.

It was interesting to notice that at constant amount of active catalyst the magnitude of drop in the reactor pressure was estimated to be similar for increasing reaction temperature from 60 to 80 ^{o}C, which might be the result from insignificant change in the density of liquid propylene with temperature especially at high reactor pressures.

Now, let us discuss the influence of increasing conversion on the temperature profile of the reactor along the axial direction. Figure 7.2 shows the reactor temperature profiles that are scaled by the initial temperature inside the reactor. These profiles illustrate an average steady state response of the reactor upon continuous injection of an active catalyst into a continuous flow of liquid propylene and at varying initial reaction conditions (in this case 60, 70 and 80 ^{o}C). The change in the reactor temperature with respect to the reference initial temperature in axial direction is a clear function of the dynamics of active catalyst particles. As can be seen from Figure 7.2, the increasing magnitude of ΔT with increasing catalyst loading (or increasing overall conversion) exhibited the growth in the production rate of tubular reactor. Therefore, to conclude, such influence can be evaluated with the help of two main factors,

1. The active catalyst concentrations, those are available inside the reactor for polymerization (for example see Table 7.1).
2. The extremely high monomer concentrations in liquid-phase reaction give the process the highest production rates (assuming the same catalyst intrinsic activity).

On the other hand, the aspects of hydrogen involved with the catalyst activity cannot be eliminated and has to be considered as an important point in optimizing the reactor throughput, too.

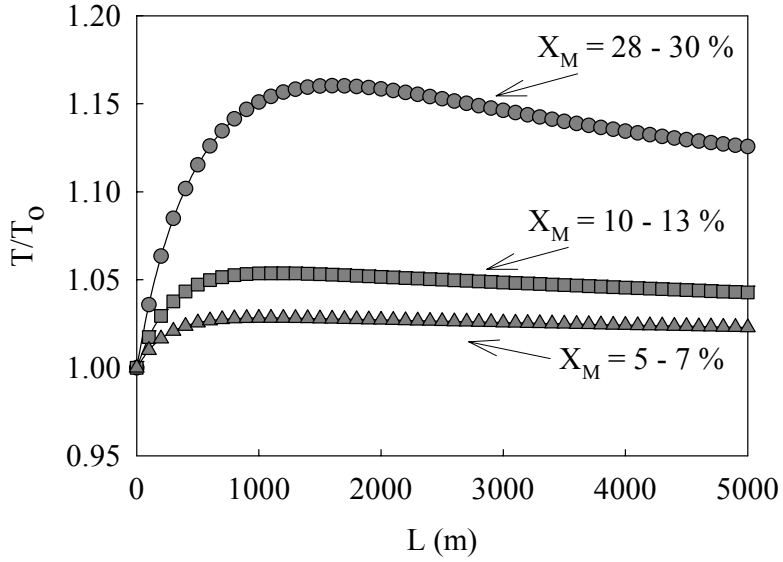

Figure 7.2: Scaled temperature profile in the tubular reactor predicted at different conversion level (profile reported here are estimated at 36000 s of reaction time, and other simulation conditions are same as reported in Table 7.1).

The range of temperature reported in Table 7.1 is the optimal temperature of operation in terms of catalytic activity, which is only approximately 10 - 30 ^{o}C below the critical temperature of liquid propylene. Therefore, the temperature control system for the reactor must be designed to be very fast and robust. In this sense the most important characteristics of the tubular reactor is very useful, i.e., its heat transfer capability. Figure 7.3 show the high values of heat transfer coefficients that can be achieved in this kind of the reactor. The profile for U illustrated in Figure 7.3 was simulated from Run76; see Table 7.1. The higher values of U (0.90 - 0.94 kJ.m^{-2}.s^{-1}.K^{-1}) in the first half of the reactor represent the influence of higher flow rates at the inlet of the reactor, which increased the heat exchange capacity of the reactor and generated a more uniform temperature distribution along the reactor length [⊗].

[⊗] The values of U estimated here were based on the heat transfer equations and assumptions used along with the reactor model. The high values of U can be achieved for high flow rates of bulk fluid yielding a Reynolds (Re) number >> 200000. In case of the tubular reactor arranged in loop geometry used for catalytic liquid propylene polymerization, Zacca et al. (1993) [12] estimated an average U value of 3.25 KJ.m^{-2}.s^{-1}.K^{-1}, which is 3.5 fold higher than the value shown in Figure 7.3. According to the authors, the stirred tanks, in general, would provide from half to one fourth of that heat exchange capacity for the same degree of agitation.

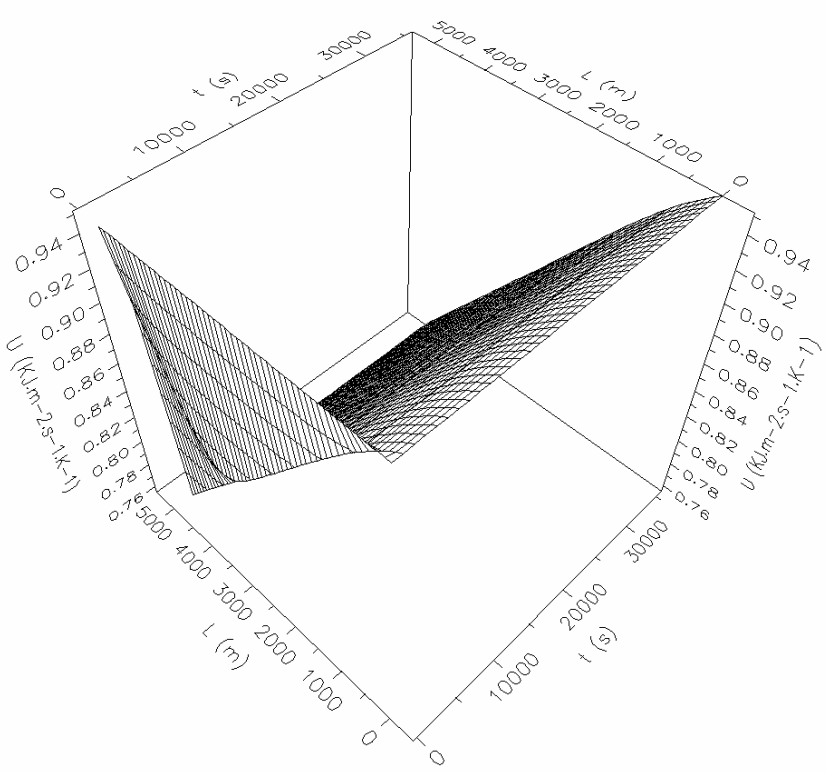

Figure 7.3: Overall heat transfer coefficient along the reactor (simulation conditions are same as for Run76 reported in Table 7.1).

Figure 7.3 also demonstrate the variations in the U as per the changing properties of the reaction mixture. The U was observed to be decreased by 20 % at the end of the reactor. This may be a result of increasing solid content of the reactor along the axial direction, thus changing the mixing behavior of the reaction mixture.

Now, the question will arise that how the reactor will behave if the catalyst concentration increases above its maximum allowable limit. Let us take a simulation case study same as Run76 but with higher amount of catalyst loading. Figure 7.4 show the reactor temperature profile predicted for catalyst concentration of 0.0040 $kg.m^{-3}$ and with other simulation parameters same as Run76; see Table 7.1. The nature of the profile seen from Figure 7.4 indicate the possible risk of "run-away" polymerization, as the increase in ΔT is very high (> 130 ^{o}C), and it is reported to be inherent in large sized tube.

Husain et al. (1976) [5] reported that the risk of "run-away" polymerization appear due to the higher throughput of the larger size tube, which is often associated with an additional complex problem of heat dissipation. This is quite possible as for the 60 ^{o}C of

temperature rise in the reactor the overall conversion reaches > 70, which ultimately increases the solid content of the reactor.

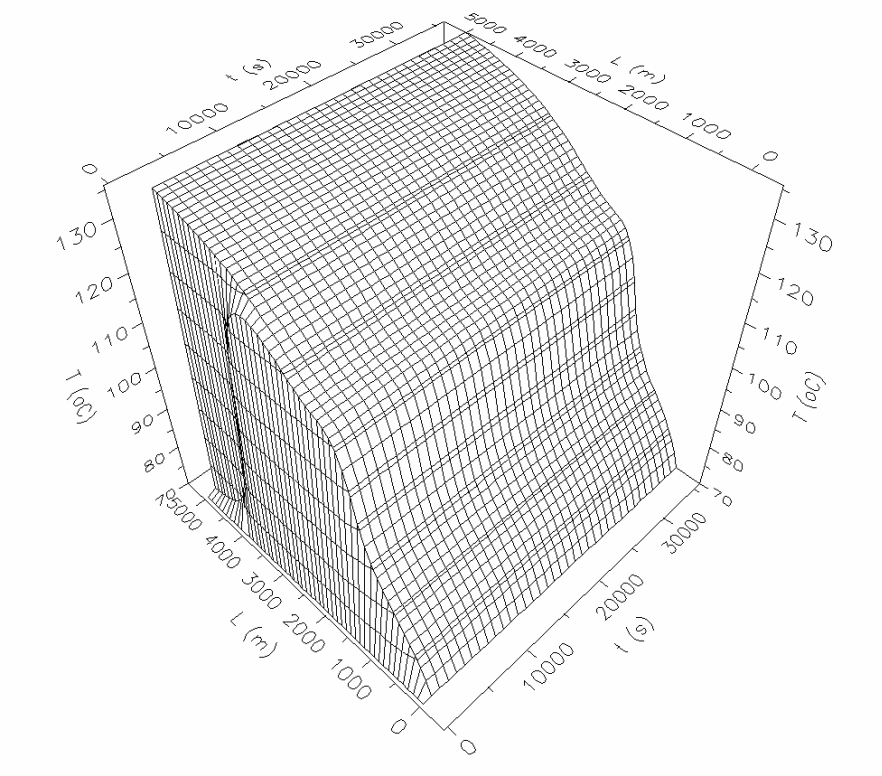

Figure 7.4: Predicted temperature profile in the tubular reactor: runaway response ($[Cat]_o$ = 0.0040 kg.m^{-3}; other simulation conditions are same as for Run76 reported in Table 7.1).

With such a high conversion inside the tubular reactor, the physical properties of the reactor changes dramatically along the axial direction, and does create the operational problems. One of the problems involved is the heat transfer capability of the tubular reactor.

The variation in the U for the "run-away" polymerization can be seen from the Figure 7.5. The value of U was estimated to be dropped by 90 % over the reactor length, which indicates that the heat accumulation inside the reactor was increased with the increasing reactor temperature, which affects the mixing characteristics of the reaction mixture. This large change in the reactor fluid properties will influence the dynamics of the growing polymer particle in the axial direction.

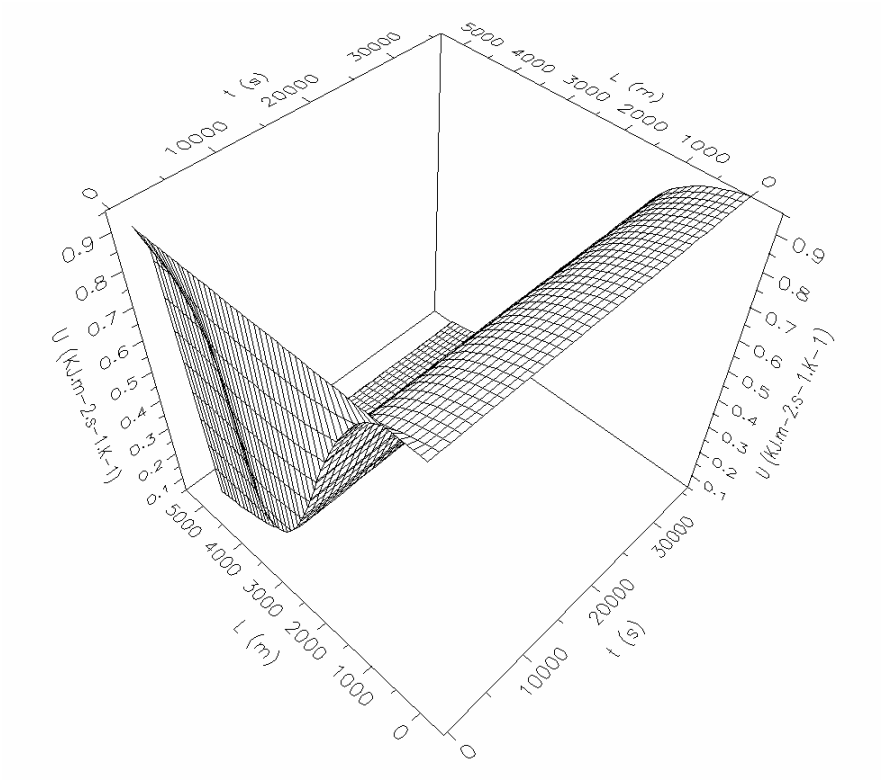

Figure 7.5: Predicted profile for U along the reactor length: runaway response ($[Cat]_o$ = 0.0040 $kg.m^{-3}$; other simulation conditions are same as for Run76 reported in Table 7.1).

From the findings discussed above, the preactivated catalyst concentration must be optimized for an individual process in order to achieve the maximum production rate and less operational problems. Zacca et al. (1996) [13] mentioned an important issue that the catalyst yields should not be insufficient; otherwise, the residue content in the end product might be too high.

To summarize the thermal response of the tubular reactor, the optimum conditions must be reached to have an efficient process technology without sacrificing the demands at industrial scale. One of such requirement from industrial plant is to have a maximum production capacity of the polymer to meet the demand of the end-user market. The simulation examples reported in Table 7.1 give an idea of increasing the production capacity of the plant. It can be noted that optimizing the process operating parameters and variables, a production capacity of industrial scale could be achieved with the present reactor concept. For example, with 30 % of overall conversion, a maximum annual production capacity in the range of 200 - 214 $kton.yr^{-1}$ could be obtained with the tubular

reactor, which is in fact comparable to the currently available processes for catalytic liquid-phase propylene polymerization [8] ∅.

Next important point to study is the influence of thermal dynamics of the reactor on the properties of polymer especially their average molecular weights and its distribution. Table 7.1 provides a data regarding M_w^{avg} and PDI at different reaction temperature and as a function of overall conversion (i.e., with increasing magnitude of ΔT). The M_w^{avg} of polymer was increased by 12 % for increasing reaction temperature from 60 to 70 ^oC. Further, the % increase in M_w^{avg} was dropped to 5 % for increasing temperature from 70 to 80 ^oC. From Table 7.1, it can be observed that the model used to estimate the average molecular weight enable to predict the temperature dependency of the molecular weight. These influences of temperature on the average molecular weight have already been discussed in Chapter 4, and the similar findings are observed here.

At 60 and 70 ^oC of initial temperature conditions, the PDI values for polymer samples decreases with increasing magnitude of ΔT. The PDI values estimated for the polymer sample were in agreement with the results described in Chapter 3. As per the results discussed in Chapter 4, Chadwick and his coworkers (1995 and 1996) [3, 4] explained the decreasing PDI effect as a result of increasing isospecificity of the active sites. On the other hand, at 80 ^oC reaction temperature, the PDI value was increasing with increasing magnitude of ΔT. Such broadening in MWD above 80 ^oC was also observed in the investigations performed by Kissin et al. (2004) [7]. The authors concluded that the "steric perfectness" of the material with the highest isotacticity decreases above 80 ^oC of polymerization temperature. This might be the reason that PDI value for Run79 was enhanced by 15 % as compared to the value estimated for Run78.

Figure 7.6 displays the predicted cumulative MWD for three polymer samples obtained from the simulation runs performed at 60, 70 and 80 ^oC, respectively. These three samples were selected based on the maximum magnitude in the ΔT; see Table 7.1. Similar to the findings observed for M_w^{avg} and PDI at different reaction temperature, the MWD seem to be shifted towards the higher molecular weight part with increasing polymerization temperature. The MWD of polymer sample simulated at 80 ^oC was found to be stretched at the tail representing the lower molecular part, and thus showed a broad

∅ It should be noted here that the obtained production capacity was based on the kinetics of the catalyst used in this study.

MWD in comparison with the other two samples. The overall influence of higher temperature > 80 ^{o}C on the molecular properties of the polymer could possibly be derived on the basis of sensitivity of the active centers during the polymerization reaction with the changing reactor circumstances towards the supercritical condition of the propylene.

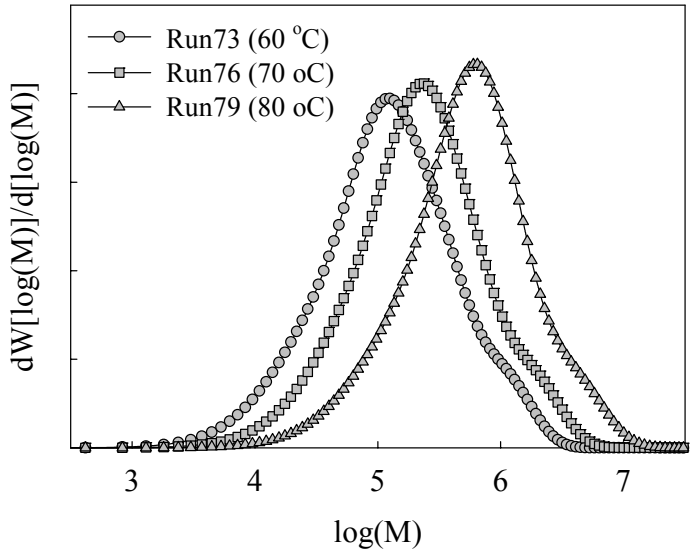

Figure 7.6: Predicted cumulative MWD data for three PP samples simulated at 60 ^{o}C (Run73), 70 ^{o}C (Run76) and 80 ^{o}C (Run79) with similar hydrogen concentration (other simulation conditions are reported in Table 7.1).

As pointed out above, the features of hydrogen on the catalyst activity as well as on the properties of the polymer is very important and has to be analyzed thoroughly together with the thermal dynamics of reactor in order to improve the reactor performance. If one look at the recent literature the know-how about the catalyst response to hydrogen has been improved very much, see for example Al-haj Ali et al. (2006) [1].

In addition, the work presented in this thesis report the broad art-effects of the hydrogen on the catalyst productivity and on the average molecular weight properties of the polymer. Such imperative information was useful in deriving the proper output of the scale-up reactors. Few simulations were performed to understand the dynamics of the presence of hydrogen during the polymerization reaction carried out in the scale-up tubular reactor. The overall summary of simulation conditions and results is reported in Table 7.2.

Table 7.2: Simulation runs carried out to study the hydrogen response on the catalytic productivity and average molecular weights of the polymer samples [∀]

Simulation Code	$[Cat]_o$ ($kg.m^{-3}$)	X ($molH_2o.molPPYo^{-1}$)	ΔT [#] (^oC)	ΔP [$] (bar)	Overall Conversion (%)	Yield ($kg.gCat^{-1}$)	Annual Production ($kton.yr^{-1}$)	M_n^{avg} ($kg.kmol^{-1}$)	M_w^{avg} ($kg.kmol^{-1}$)	PDI
Run710	0.0110	0.00005	9.25	26.02	26.2	13.3	165	291200	1990000	6.8
Run711	0.0050	0.00050	9.50	25.54	30.6	32.3	197	107000	651000	6.1
Run712	0.0036	0.00140	9.38	25.58	29.6	45.3	199	60800	358000	5.9
Run713	0.0030	0.00500	10.16	25.43	29.3	62.0	207	28300	180000	6.3
Run714	0.0030	0.00971	9.54	25.78	26.3	57.1	192	18700	130000	7.0
Run715	0.0088	0.09810	10.13	26.72	17.4	20.0	203	4300	43000	10.0
Run716	0.0120	0.14000	10.16	27.04	15.0	15.2	212	3500	36000	10.2
Run717	0.0183	0.21900	9.54	27.6	11.4	10.3	222	2600	28000	10.7
Run718	0.0530	0.50000	10.04	28.84	7.7	4.5	287	1300	16000	12.9

[∀] All the simulations were performed at $T_o = 70\ ^oC$, $[M]_o = 492.9\ kg.m^{-3}$, $P_o = 200$ bar, $v_z = 5\ m.s^{-1}$ with tubular reactor having $d_i = 0.1$ m and $L = 5000$ m, and yielding a τ value of 1000 s. The jacket temperature was always maintained at the initial reaction temperature. [#] ΔT is the difference between reactor maximum temperature and the initial temperature. [$] ΔP is the difference between the reactor pressures estimated at the inlet and outlet position.

The hydrogen influence studied here is in very broad range, and represented in terms of X, which is varying from 0.00005 to 0.5; see Table 7.2. The catalyst loading used for simulating the reactor performance was selected in a way that the maximum rise in temperature would not increase > 10 ^{o}C (see ΔT in Table 7.2). This also allowed to keep the overall conversion of monomer <= 30 %. Let us first analyze the influence of hydrogen on the productivity of catalyst. This can be judged from the cumulative polymer yield given in Table 7.2 for increasing values of X. This data is plotted in Figure 7.7 ♦. The response of catalyst yield for increasing values of X is similar to the results discussed in Chapter 4.

Therefore, if the gas- and liquid-phase data on hydrogen influence is compared for the catalyst type used here, then the catalyst response shown in Figure 7.7 is inherent to the nature of the catalyst. However, the magnitude of this response varies from one scale of the process to another.

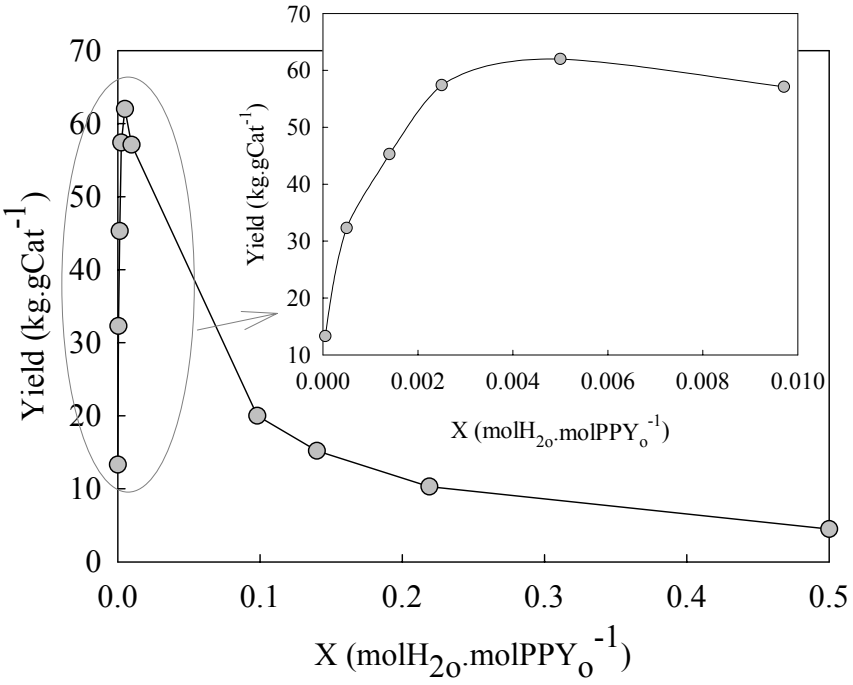

Figure 7.7: Predicted cumulative yield as a function of X (other simulation conditions are reported in Table 7.2).

♦ Until now, the data shown in the previous chapters on the catalyst activity was evaluated only up to the X value of 0.1.

The in-depth kinetic analysis of this influence has already been discussed in Chapter 4. Therefore, the two important findings are concluded here for Figure 7.7,

1. At low values of X (< 0.01), the "activation effect" of hydrogen on the catalyst should indeed reveal from the reactivation of dormant sites in the presence of hydrogen.
2. At high values of X (> 0.01), the so-called "retardation effect" on catalyst activity during propylene polymerization was noticed. This illustrates that the nature of the hydrogen plays an important role in producing the different types of active sites, which may further act as a rate determining step.

As per the objective of the present study, the scale-up reactor should be used with the proper operational policy, which could maximize the reactor throughput. In this sense, it is practical to design the value of X for homopolymerization of liquid propylene in the range of higher productivity, and with the optimum amount of catalyst loading. From the data shown in Table 7.2, it was apparent to select the X values between 0.0005 and 0.005. For example, the annual production capacity for Run711 to Run713 was on average 197 - 207 kton.yr^{-1} and it was in-line with the conventional processes. On the other hand, the higher annual production capacity estimated for higher values of X (> 0.09810) cannot be chosen as efficient and economical operational policies because the catalyst loading for these runs was very high.

Another key issue is the response of hydrogen on the average molecular weights of the produced polymer. The function of hydrogen as a chain transfer agent is well known, and therefore controlling the chain length of polymer in the presence of hydrogen is very important. The M_w^{avg} and number-average molecular weight (M_n^{avg}) of the produced PP from the scale-up tubular reactor are reported in Table 7.2. The PDI values of the modeled MWD of the PP samples are also given in Table 7.2. Figure 7.8 shows the data regarding M_n^{avg}, M_w^{avg}, and PDI as a function of X. The decreasing trend in M_n^{avg} and M_w^{avg} values was found to be similar up to the X value of 0.00971. It can be seen from the insignificant change in the PDI values estimated for the X values < 0.00971. At high values of X (> 0.00971), the decrease in M_n^{avg} values was 1.9 - 2 folds higher than the M_w^{avg}. This resulted in a broad MWD of a polymer sample. The PDI value for Run715 was increased by 44 % as compared to Run714. It shows that the catalyst site types representing the lower molecular region are more sensitive towards the high hydrogen concentration, and probably controlling the broadness of the MWD.

(a)

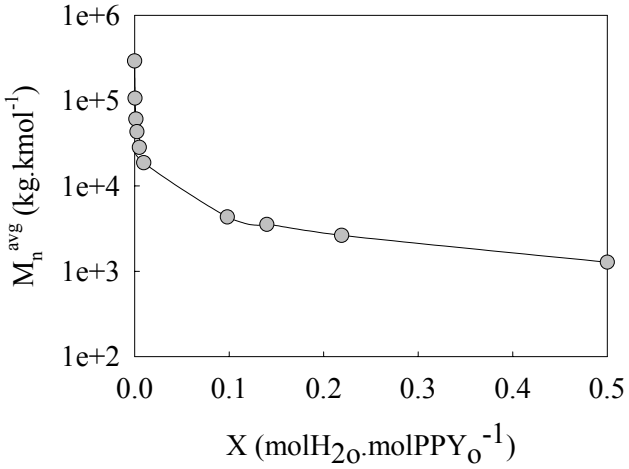

(b)

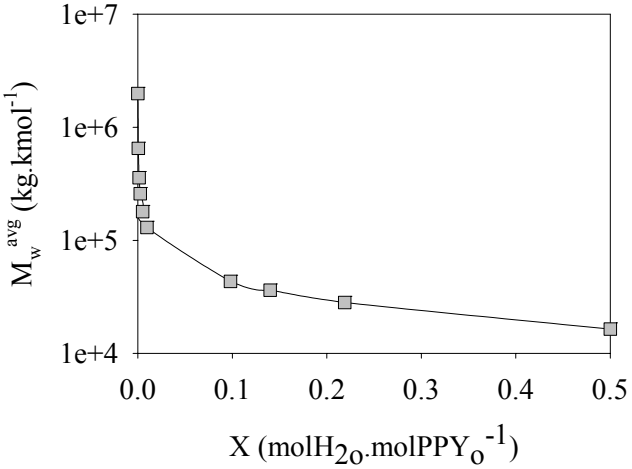

(c)

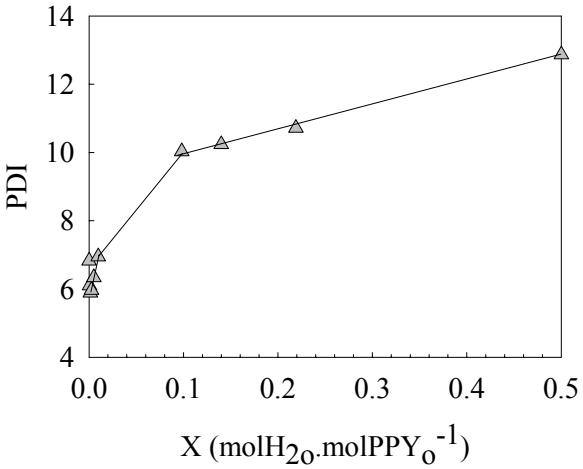

Figure 7.8: Predicted values of (a) M_n^{avg}, (b) M_w^{avg} and (c) PDI as a function of X (other simulation conditions are reported in Table 7.2).

The variations in the PDI values above X value of 0.14 were found to be linear; see Table 7.2 and Figure 7.8 (c). The broadness in the MWD observed from the PDI values might exhibit the individual kinetic response of the active sites present on the catalyst. Furthermore, it was cleared that optimizing the action of hydrogen in controlling the broadness of MWD was very important, which could further facilitate in targeting the production of different characteristics of the PP samples to meet the demand of wide end-user market. The changes in the MWD of PP samples with increasing hydrogen concentration are illustrated in Figure 7.9. As expected, the predicted MWD's shown a shift towards a lower molecular part. The shift observed in Figure 7.9 may vary from one process conditions to another, as the catalyst performance is dependent on the reaction temperature, pressure, catalyst composition, monomer concentration, hydrogen amount, etc. Therefore, while designing a new process concept, only modeling a dynamic response of reactor is not sufficient but combining the reactor model with the complete kinetic characteristics of the catalyst is a critical point, especially in judging the performance of the reactor for throughput and product properties. This fact recalls the selection made above for the most favorable range of the process conditions, i.e., from Run711 to Run713. For these runs, the annual production capacity is in the range of the conventional processes and seems to be economical too. Also from Figure 7.8 (a) and (b), and Figure 7.9, the average molecular weights and their distribution for these runs are in good agreement with the standard polymer properties.

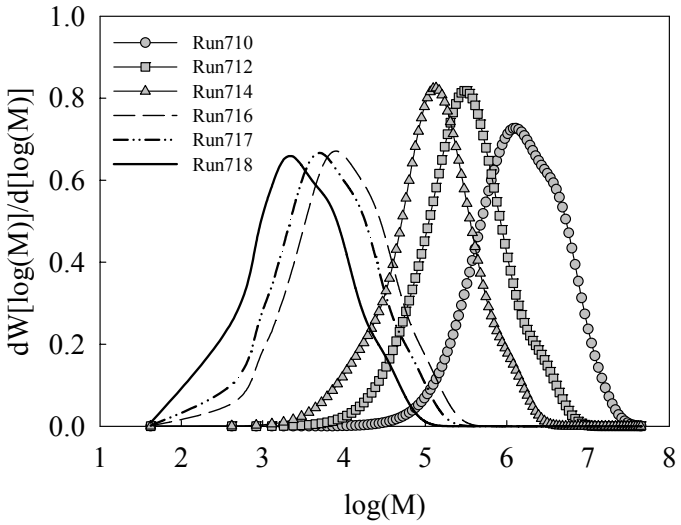

Figure 7.9: Predicted cumulative MWD data for selected PP samples simulated at 70 ^{o}C with increasing hydrogen concentration (other simulation conditions are reported in Table 7.2).

From the above discussion it must be cleared that the molecular weight is the key selection element of the product for the conversion technologies, being directly related to the processing characteristics of the material and, therefore, to the overall processability requirements that widely differ from technology to technology. The influence of molecular weights on the processing properties of the polymeric material can be quantified based on the stereoregularity aspects of the catalyst and the MWD of the produced polymer.

Most importantly, the MWD is characteristic and unique for each catalytic type. In general, a given catalyst type produces its own typical MWD. Therefore, it is very important to control the molecular properties of the polymer over the period of polymerization reaction. Pasquini (2005) [8] reviewed two distinct facts:

1. As molecular weight increases, there is a positive effect on impact properties, with a corresponding decrease in elastic modulus, which is a direct result caused by a reduction in crystallinity.
2. As molecular weight decreases, the MWD tends to narrow, limiting the broad aspects of material processing.

This put forwards that the combined analysis of intrinsic catalyst property and the dynamic response of the reactor concept during the polymerization reaction is vital in balancing the final polymer properties.

Presently, it becomes a common practice to control the MWD of the polymer through the selection of appropriate parameters in polymerization. For instance, the adoption of a split mode polymerization of different molecular weights in a multistep process allows a broadened MWD to be produced.

This mode of polymerization can be performed with the present concept of tubular reactor. In a tubular reactor, the multiple injections of important process chemical components, like comonomer or chain transfer agent, can be injected along the length of reactor. For example, hydrogen, a very important component in controlling the molecular weight, can be feed at different locations over the reactor length; see Figure 7.1. To highlight and demonstrate this point, specific simulations were performed by increasing the concentration of hydrogen along the reactor length and predicted the reactor dynamics with respect to its thermal response and the MWD of the produced polymer. The simulation data and predicted data are presented in Table 7.3.

Table 7.3: Simulation runs carried out to study the hydrogen response on the broadening of MWD of produced polymer [Ξ]

Simulation Code	$[Cat]_o$ ($kg.m^{-3}$)	X ($molH_2o.molPPYo^{-1}$)			ΔT [#] (°C)			ΔP [$] (bar)	Yield ($kg.gCat^{-1}$)	Annual Production ($kton.yr^{-1}$)	M_w^{avg} ($kg.kmol^{-1}$)	PDI
		L_0	L_1	L_2	L_0	L_1	L_2					
(a)												
Run719	0.00400	0.00005	0.00140	0.140	2.21	14.78	0.66	26.72	42.3	199	463000	36.4
Run720	0.00400	0.00005	0.00140	0.219	2.21	14.82	0.25	26.80	42.1	199	464000	46.5
Run721	0.00400	0.00005	0.00140	0.500	2.21	14.95	0.02	26.86	42.0	199	495000	70.1
(b)												
Run722	0.00325	0.00005	0.00500	0.140	1.75	14.81	0.52	26.72	49.7	190	283000	34.1
Run723	0.00325	0.00005	0.00500	0.219	1.75	14.81	0.21	26.78	49.5	190	296000	43.2
Run724	0.00325	0.00005	0.00500	0.500	1.75	14.81	0.01	26.84	49.3	190	320000	64.5
(c)												
Run725	0.00340	0.00005	0.00971	0.140	1.85	14.91	0.52	26.59	49.6	199	250000	34.5
Run726	0.00340	0.00005	0.00971	0.219	1.85	14.91	0.19	26.65	49.4	198	262000	43.2
Run727	0.00340	0.00005	0.00971	0.500	1.85	14.91	0.01	27.07	49.2	198	284000	64.4

[Ξ] All the simulations were performed at T_o = 70 °C, $[M]_o$ = 492.9 $kg.m^{-3}$, P_o = 200 bar, v_z = 5 $m.s^{-1}$ with tubular reactor having d_i = 0.1 m and L = 5000 m, and yielding a τ value of 1000 s. The predicted overall conversion for these simulations is ranging from 18 - 21 %. The jacket temperature was always maintained at the initial reaction temperature. The locations at which the hydrogen concentration is increased are: L_0 = Inlet, L_1 = 1000 m and L_2 = 3000 m, respectively.

[#] ΔT is the difference between reactor maximum temperature and the initial temperature and estimated at different location along the reactor length.

[$] ΔP is the difference between the reactor pressures estimated at the inlet and outlet position.

In the simulation runs shown in Table 7.3, a polymerization reaction was initiated with a small concentration of hydrogen (X = 0.00005) and it was kept constant to all simulations. Further, the concentration of hydrogen was changed in two steps over the reactor length, for example, at 1000 m and 3000 m of reactor length. However, these injection locations can be changed to predict the dynamic behavior of the reactor during the polymerization reaction. Few combinations made in the variation of X values at L_0, L_1 and L_2 are categorized in (a), (b) and (c); see Table 7.3. Similar to the case studies presented in Table 7.1 and 7.2, the catalyst loading was optimized to maintain the same maximum magnitude of ΔT in the reactor. The activity of active catalyst will change with the changing concentration of hydrogen and with the increasing time of reaction. Therefore, it will be interesting to know the dynamics response of the reactor for multiple injections of hydrogen into a continuous flow of liquid propylene carrying active catalyst particles. As an example, a predicted temperature profile obtained from simulation Run719 is shown in Figure 7.10.

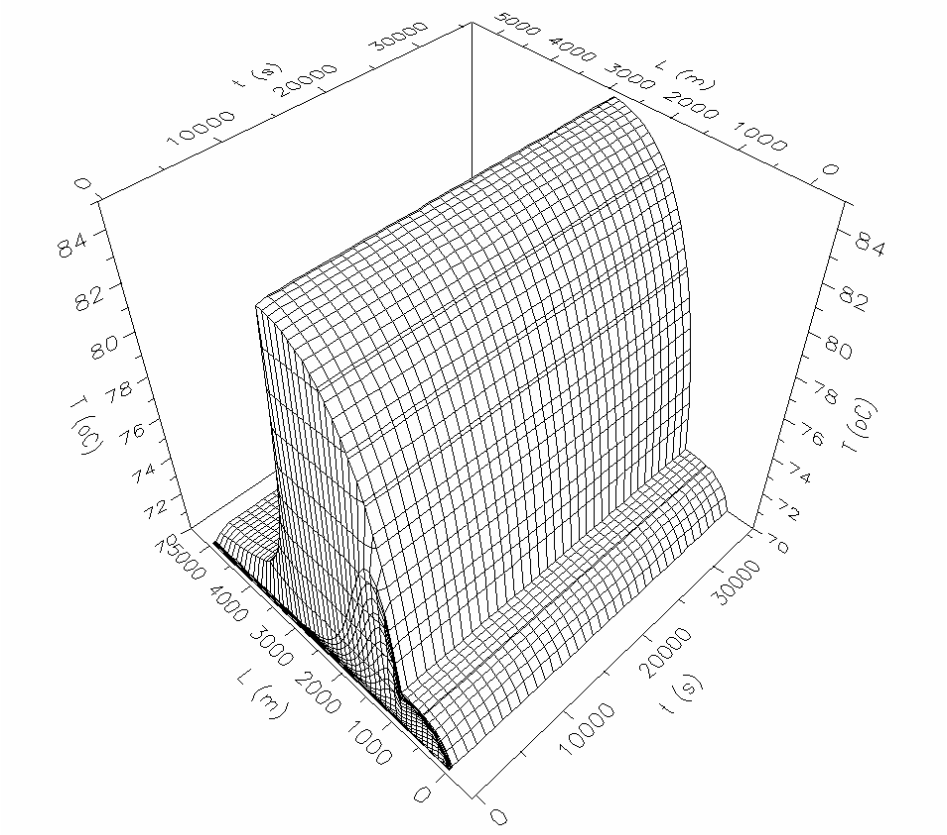

Figure 7.10: Predicted temperature profile in the tubular reactor for Run719 (other simulation conditions are reported in Table 7.3).

From Figure 7.10, it is appeared that the multiple injection of hydrogen at different location of reactor did change the activity of the catalyst during the course of polymerization reaction. The magnitude of ΔT varying along the reactor length could be evidenced based on the specific influence of hydrogen interpreted above for the productivity of the active catalyst over a broad range of X values. The changes in the magnitude of ΔT with increasing hydrogen concentration are reported in Table 7.3.

For a constant loading of catalyst, a rise in the reactor temperature at low value of X (0.00005) and very high value of X (ranging from 0.14 to 0.5) was very limited, which in fact reflect the low activity of the catalyst in this range of X (see also Figure 7.10). However, the maximum rise (ranging from 14.78 to 14. 95) in the ΔT was predicted when the X value has increase by factor 28, 100 and 190.4, respectively, at reactor location L_1 with respect to the X value of 0.00005 used within the first section of the reactor (length between reactor inlet and L_1).

An interesting effect of varying temperature profile on the polymer yield can be noted from the Table 7.3. The cumulative polymer yield measured for the τ value of 1000 s was decreased by average values of 7 %, 20 % and 13 % for the simulation runs shown in category (a), (b) and (c), respectively, compared to the yield noted for Run712, Run713 and Run714 in Table 7.2. This clearly indicates the consequence of the low polymer yield obtained at low X value of 0.00005 and at high X values above 0.14. More importantly, the annual production capacity of the reactor estimated using the simulation conditions shown in Table 7.3 did not decrease significantly compared to the production capacity reported in Table 7.1 and 7.3. This influence has been found to be more impressive from the point of view carrying out the split mode polymerization. The production capacity of the reactor for the operating conditions shown in Table 7.3 was based on the optimized loading of active catalyst. From the various simulation runs, it was observed that the behavior of the reactor in terms of its thermal response was very sensitive to a small change in the catalyst injection.

The main impact of the split mode polymerization can be observed from the cumulative MWD of the produced polymer. The combined influence of varying reactor temperature and hydrogen concentration in the axial direction may produce a distinct effect on the different nature of active sites, which ultimately control the MWD of the polymer. However, the changes in MWD may differ from one catalyst type to another, and may be

difficult to generalize. Therefore, the results discussed here are strictly based on the kinetic peculiarities of the catalyst type used during the present reactor modeling.

Figure 7.11 display the predicted MWD curves for individual simulation run reported in Table 7.3. These curves are presented in three categories based on the changing values of X in the last section of the tubular reactor, i. e., L_2; see Table 7.3. Figure 7.11 also compare the cumulative MWD curve obtained from the multiple injection of the hydrogen with the MWD predicted from the simulation runs performed using a constant values of X.

The MWD data shown in Figure 7.11 did exhibit that the broad MWD for a produced polymer could be achieved using a multiple injection of hydrogen in the axial direction of the tubular reactor. In general, as the X value increases from 0.14 to 0.219 and 0.5 at section L_2 the broadness in the MWD was found to be enhanced by 21 % and 47 %, respectively, for all other values of X used at section L_0 and L_1. It revealed that a very large change in the hydrogen concentration at the tail section of the reactor tend to control the broadness of MWD.

A nature of the MWD observed from Figure 7.11 is the so-called “Bimodal” distribution, which content a relatively high molecular weight fraction and a relatively low molecular weight fraction. The contribution of these two fractions to the complete MWD is very crucial from the processing view point of the material. The increasing broadness in the MWD of the PP improves its processability and widens its end-use applications. This may be the result of the following two facts related to the PP having “Bimodal” distribution,

1. Improved processability of the material due to the low molecular weight part.
2. Increased melt strength of the material due to the high molecular weight part.

Therefore, it is important to recognize that the balance between the low molecular weight part and the high molecular weight part must be controlled during the polymerization step. Figure 7.11 suggest that the low molecular weight content of the MWD is increasing with the increasing hydrogen concentration at section L_2. It can be seen from the shifting of MWD curve towards the low molecular weight regime. The predicted MWD also indicate that the higher the step change in the values of X over the reactor length the more distinct difference can be obtained between the two modes of the distribution. This effect can be judged from the higher values of PDI obtained for Run721, Run724 and Tun727.

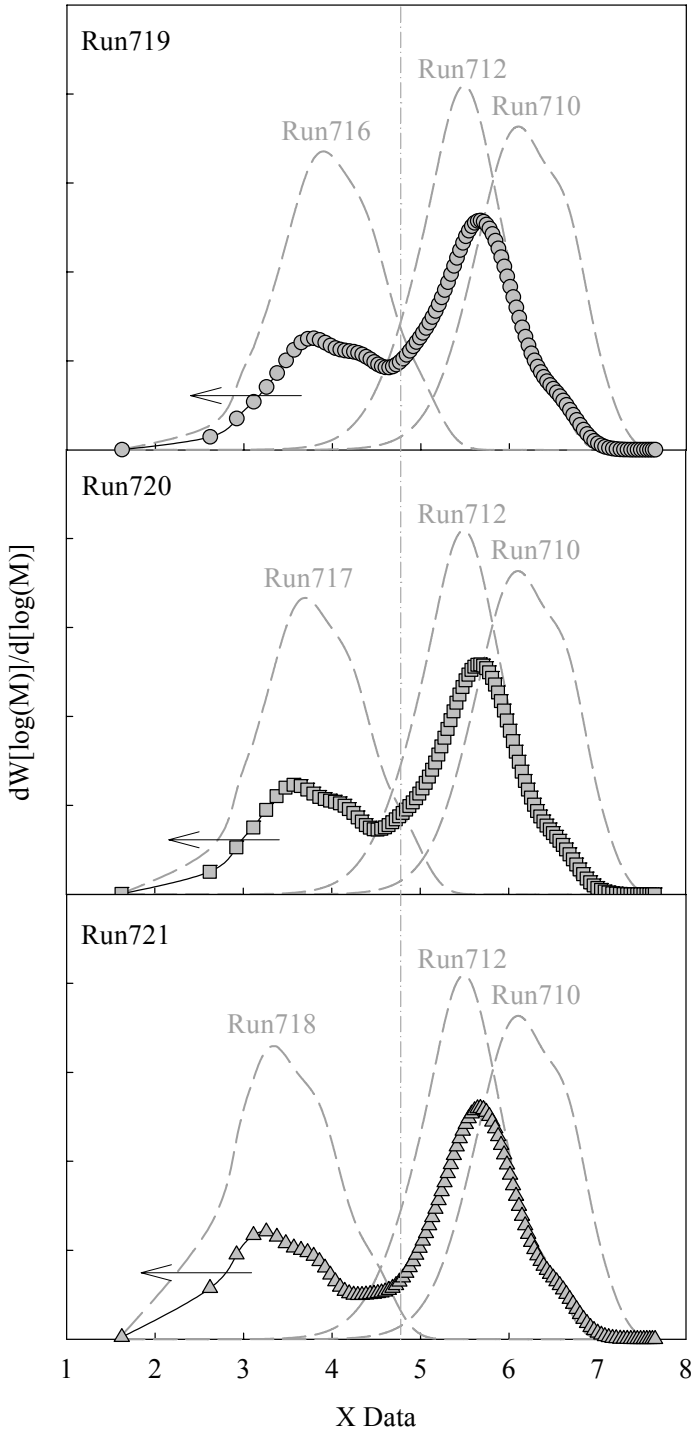

(a)

Figure 7.11: Predicted cumulative MWD data for PP samples simulated at 70 °C with multiple injection hydrogen concentration (other simulation conditions are reported in Table 7.3).

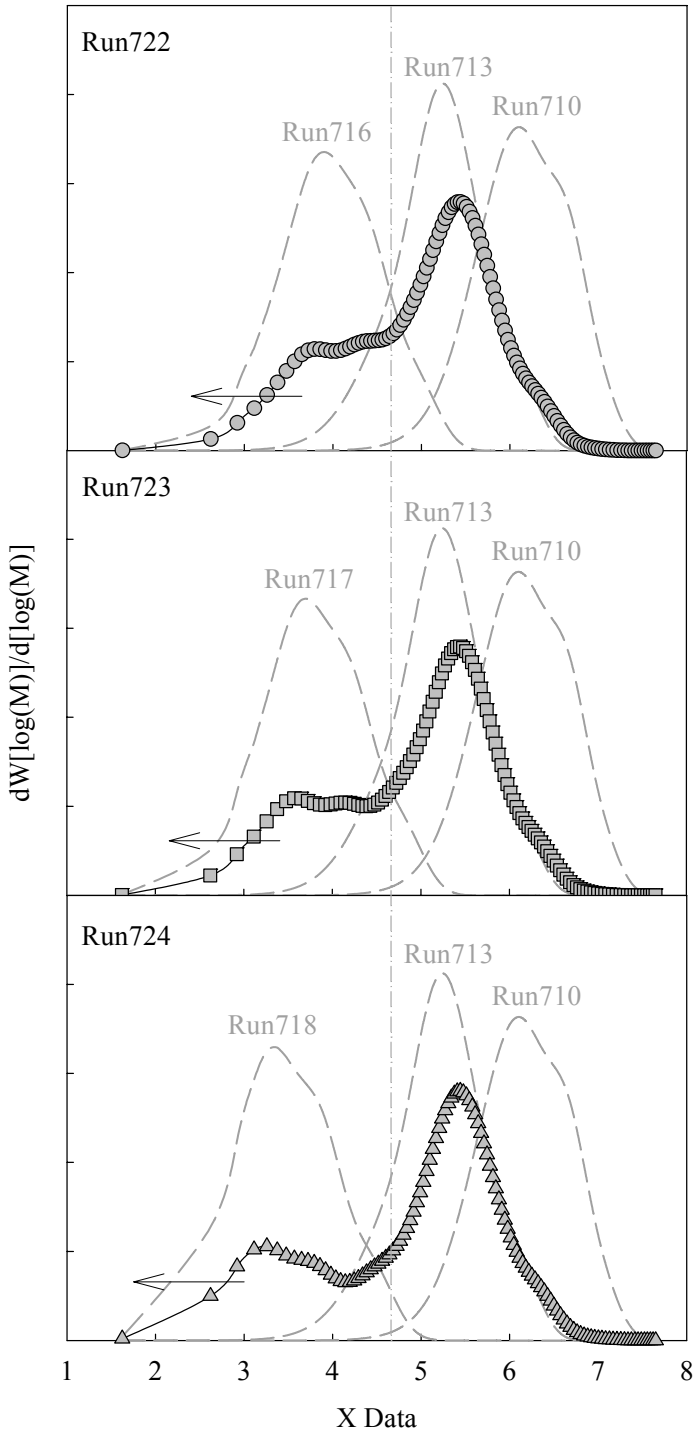

(b)

Figure 7.11: Continue…

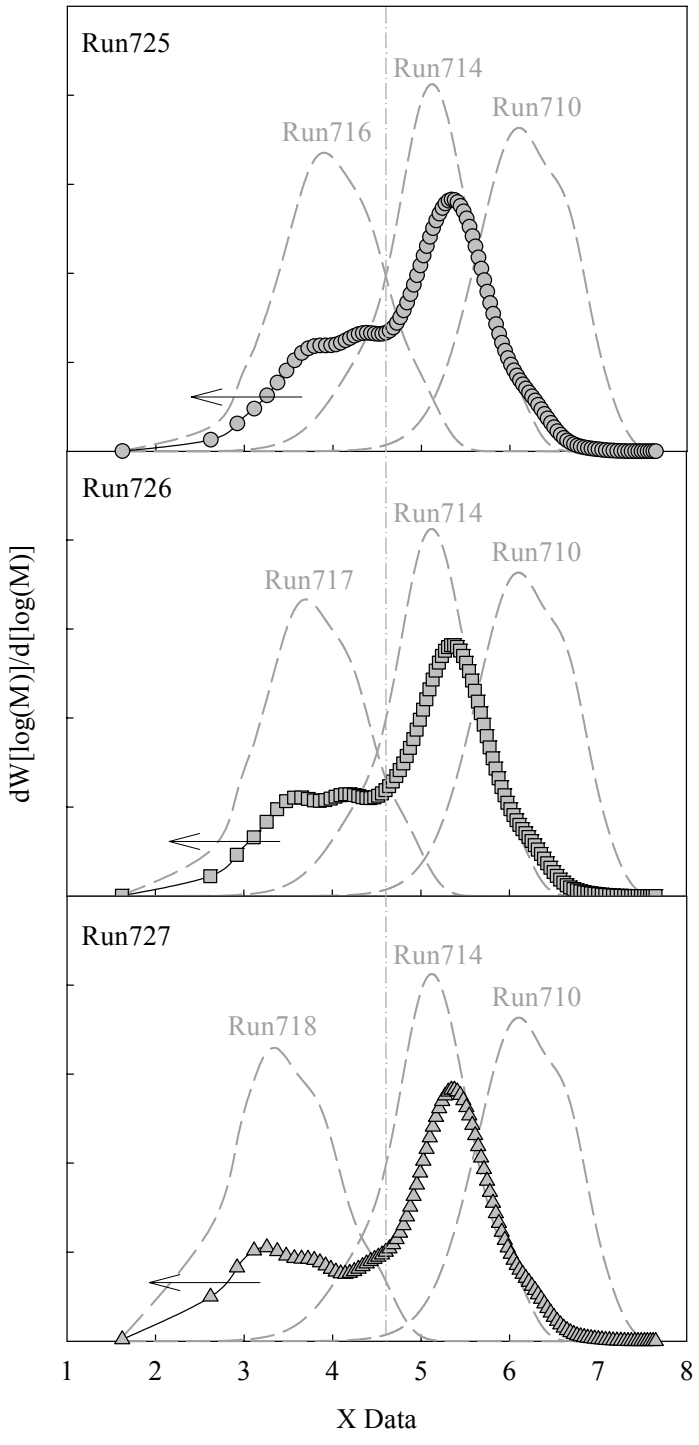

(c)

Figure 7.11: Continue…

7.4 Conclusions

The performance of the scale-up tubular reactor for catalytic liquid-phase propylene polymerization has been analyzed based on the pseudo-steady state mathematical model of the reactor. The model framework developed in this work was constructed using the kinetically characterized catalyst type and average molecular weights of the polymer as a function of reaction temperature and hydrogen concentration. The reactor dimensions used for simulating the response of tubular reactor were selected within the range reported in the open literature. The speculations discussed in this chapter did illustrate the importance of applying the tubular reactor concept for catalytic liquid-phase propylene polymerization at the industrial scale.

The key points in achieving the high-output from the tubular reactor are,

1. Optimum loading of active catalyst allowing to run the process in a stable and safe manner, and increasing the output economically.
2. Proper balancing of the operating conditions enabling to manufacture the polymer product with broad end-use properties.

In addition, the characteristic advantages of the present reactor concept would play major role in advancing its process technology. Few important characteristics are presented here,

1. Unique capability of heat removal in axial direction.
2. Dynamic motion of the active catalyst particles travelling along the reactor axis with changing degree of mass and heat transfer allowing to develop a unique morphology of the polymer product within a short period of reaction.
3. Ability to perform the polymerization reaction with reduced reaction time (this depends on the proper selection of the process parameters as well as on the requirement of the reactor output).
4. Flexibility in varying the operating parameter and variable along the reactor length (such as concentration, temperature, pressure, etc.), thus permitting to create different section of the reactor through which the active reaction mixture is travelling during the course of polymerization.
5. Able to produce the polymer product with broad processing features.

More importantly, the output of the tubular reactor in terms of its production capacity and product properties were comparable with respect to the available license technology for the catalytic liquid-phase propylene polymerization in the market. For example, the

optimum annual production capacity of the present reactor process has been predicted as 214 kton.yr^{-1}, with the overall conversion limit of 30 % and with an inside reactor diameter of 0.1 m resulting into the reactor volume of 39 m^3. The thermal response of the tubular reactor did demonstrate the philosophy in enhancing the capability of the reactor in running the process efficiently as well as economically. The limiting boundary on the overall conversion (<= 30 %) for the reactor found to be reasonable in achieving the comparable production capacity according to the conventional processes. The detailed kinetic response of the catalyst type studied in previous chapters has been very helpful in predicting the know-how of the scale-up reactor for process variable and operating conditions. The utility of the tubular reactor in producing the broad MWD of PP has been investigated by applying a multiple injection of hydrogen along the reactor length. On the basis of combinations made in the variation of X values at L_0, L_1 and L_2, the predicted nature of the MWD did demonstrate the "Bimodal" distribution containing a relatively high molecular weight fraction and a relatively low molecular weight fraction.

The speculations presented on the scale-up performance of the tubular reactor in this chapter and the detailed experimental and model analysis of the plot-scale tubular reactor discussed in Chapter 5, Chapter 6 and Appendix I will help the industrial professionals to open the doors for the future investigations on this reactor concept.

Nomenclature

A_1 to A_6 : Constants used in equation (4.46) in Chapter 4
$C_{p\,w}$: Specific heat of reactor wall (kJ.kg^{-1}.K^{-1})
$[Cat]_o$: Initial concentration of preactivated catalyst (kg.m^{-3})
d_i : Inside reactor diameter (m)
d_o : Outside reactor diameter (m)
dc : Catalyst particle diameter (m)
dHr : Heat of reaction (kJ.kg^{-1})
E_{act_d} : Activation energy for deactivation reaction (kJ.mol^{-1})
E_{act_p} : Activation energy for propagation reaction (kJ.mol^{-1})
f_r : Friction factor coefficient
g_c : Gravitational force (m.s^{-2})
h_i : Internal heat transfer coefficient (for reactor side) (kJ.m^{-2}.K^{-1}.s^{-1})
H_{2o} : Initial moles of hydrogen present during reaction (mole)

k_{do} : Arrhenius constant for deactivation reaction (s^{-1})

k_d : Rate constant for deactivation constant (s^{-1})

k_{d1}, k_{d2} : Constants used in equation (4.50) in Chapter 4

k_{po} : Arrhenius constant for propagation reaction ($m^3.kgCat^{-1}.hr^{-1}$)

K_a to K_e : Constants used in equation (4.37) in Chapter 4

l_{eq} : Equivalent length (m)

L : Tubular reactor length (m)

M_n^{avg} : Weight-average molecular weight ($kg.kmol^{-1}$)

M_w^{avg} : Weight-average molecular weight ($kg.kmol^{-1}$)

MW_m : Molecular weight of monomer ($kg.kmol^{-1}$)

$[M]_o$: Initial monomer concentration in tubular reactor ($kg.m^{-3}$)

N_t : Number of turns for tubular reactor

P_{in}, P_o : Initial reactor pressure (bar)

P_r : Prandtl number

PPY_o : Initial moles of liquid propylene present during reaction (mole)

P : Reactor pressure (bar)

ΔP : Difference between the reactor pressures estimated at the inlet and outlet position (bar)

Re : Reynolds number

R_g : Universal gas constant ($kJ.mol^{-1}.K^{-1}$)

t : reaction time (s)

T_o : Initial reactor temperature (^oC)

T_j : Jacket Temperature (^oC)

T_{in} : Temperature at inlet reactor condition (^oC)

T : Temperature (^oC)

ΔT : difference between reactor maximum temperature and the initial temperature and estimated at different location along the reactor length (^oC)

U : Overall heat transfer coefficient ($kJ.m^{-2}.K^{-1}.s^{-1}$)

v_z : Axial velocity ($m.s^{-1}$)

X : Mole ratio of hydrogen to liquid propylene

z : Varying point location on reactor length (m)

Greek letters

η_{mix}, μ_{mix} : Viscosity of reaction mixture ($kg.m^{-1}.s^{-1}$)
$\mu_{mix\ w}$: Viscosity of reaction mixture near the reactor wall ($kg.m^{-1}.s^{-1}$)
ρ_{mix} : Density of reaction mixture ($kg.m^{-3}$)
ρ_{w} : Density of reactor wall ($kg.m^{-3}$)
τ : Average residence time (s)

Sub- and superscripts

act : Activation
c : Catalyst
d : Deactivation
eq : Equivalent
g : Gas
i, in : Initial or inlet or inside
j : Jacket
m : Monomer or mass
mix : Mixture
n : Number
o : Initial or outside
p : Polymerization or polymer or particle
r : Reactor
t : Tube or thermal or terminal
w : Wall or weight
z : Representing the axial direction

Abbreviations

gPROMS : general PROcess Modeling Systems
GPC : Gel Permeation Chromatography
LDPE : Low density polyethylene
MWD : Molecular weight distribution

PDI : Polydispersity index
PP : Polypropylene
ZN : Ziegler-Natta

Literature

[1] Al-haj Ali, M. (**2006**), Doctorate Thesis, University of Twente, Enschede, The Netherlands.
[2] Bokis, C. P., Ramanathan, S., Franjione, J., Buchelli, A., Call, M. L. and Brown, A. L. (**2002**), Ind. Eng. Chem. Res., 41, 1017 - 1030.
[3] Chadwick, J. C., van Kessel, G. M. M. and Sudmeijer, O. (**1995**), Macromol. Chem. Phys., 196, 1431 - 1437.
[4] Chadwick, J. C., Morini, G., Albizzati, E., Baldontin G., Mingozzi, I. and Christofori, A. (**1996**), Macromol. Chem. Phys., 197, 2501 - 2510.
[5] Husain, A. and Hamielec, A. E. (**1976**), AIChE Symposium Series, 72, 160, 112 - 127.
[6] Keii, T. (**2004**), Heterogeneous Kinetics, Kodansha Ltd. and Springer-Verlag Berlin Heidelburg.
[7] Kissin, Y. V., Ohmishi, R. and Konakazawa, T. (**2004**), Macromol. Chem. Phys., 205, 284 - 301.
[8] Pasquini, N. (**2005**), Polypropylene Handbook, Carl Hanser Verlag, Munich.
[9] Perry, R. H. and Green, D. W. (**1997**), Perry's Chemical Engineers' Handbook, 6th edition, McGraw-Hill, NY.
[10] Yao, F. Z., Lohi, A., Upreti, S. R. and Dhib, R (**2004**), International Journal of Chemical Reactor Engineering, 2, A16.
[11] Zacca, J. J. (**1991**), Master's Thesis, University of Wisconsin, Madison, USA.
[12] Zacca, J. J. and Ray, H. (**1993**), Chemical Engineering Science, 48, 22, 3743 - 3765.
[13] Zacca, J. J., Debling, J. A. and Ray, H. (**1996**), Chemical Engineering Science, 51, 21, 4859 - 4886.

Appendix I

Some remarks on the non-ideal behavior of the tubular reactor

Abstract: The experimental analysis was demonstrated for predicting the non-ideal behavior of a scaled-up tubular reactor suitable for catalytic polymerization reactions. A tubular reactor of 5.6 times the volume of the "capillary type" reactor used previously was used. The ratio of the tubular reactor's internal diameter to that of the capillary-type reactor was 5.3, while the reactor's length ratio was 0.2. The polymerization experiments were carried out in the tubular reactor through injecting of an active catalyst into a continuous inlet flow of liquid propylene with frequent opening of pulsating exit valve in order to control the reactor pressure. The flow disturbances in the tubular reactor were created by the continuous cycle of pressurization and expansion. The reactor response, in terms of reactor temperature and pressure profiles over the reactor length, to catalyst injection was analyzed at near-industrial polymerization conditions. The design of the pilot plant set-up and the data acquisition was found to be very successful in performing the catalytic polymerization experiments. It was observed that the flow field of a reactive mass in a reactor undergoing a polymerization reaction was strongly determined by mass and heat transfer processes, and predominately via the dependency of the fluid properties on molecular weight. This effect was noticed from the low yield of active catalyst even in the presence of hydrogen. The characteristic performance of the reactor was discussed based on the detected region of nonlinear transport and thermal response of the reactor during reaction. According to the thermal characterization, the crystallinities of the produced polymer samples were very low and were found to decrease drastically with the presence of hydrogen in the polymerization medium. It is believed that the investigations presented in this chapter are very important in understanding the relation between reaction kinetics and the dimensions of the tubular reactor.

Keywords: catalytic olefin polymerization, mass and heat transfer, non-ideal reactor behavior, plugging, run-away reactor, thermal instability, tubular reactor

Introduction

The simplified concept of a tubular reactor for catalytic polymerization reactions observed so far from the published literature, is that a pure monomer enters at one end and leaves as a reaction mixture of monomer and polymer at the other end. The applications of such tool are often reported to be very attractive because of certain advantages, like its simplicity, elimination of product variations, large heat transfer area, and potentially low cost. On the other hand, on a real industrial scale, the process disturbances may arise due to the flow uncertainties during polymerization reaction. This certainly indicates that an analysis of the fluid dynamics (which is strongly influenced by the coupled heat and mass transfer and variations in system properties) is important to understand the causes of the flow restrictions and to improve the reactor performance.

In this regard, a number of published articles can be found describing the experimental and modeling studies pertaining to the tubular reactor performance for different chemical reactions. While dealing with tubular reactor process, most of the theoretical investigations assumed a fully developed Poiseuille Flow or a uniform velocity profile (i.e., Plug Flow), in order to concentrate more easily on the stability aspects, reactor optimization, or multiple reaction kinetics. Very few authors have reported speculations and in-depth analysis in describing the non-ideal behavior of a tubular reactor system. Some of these studies are presented in Table AI.1.

Hamer et al. (1986) [2] reported that due to the non-ideal response of the system, it is sometimes difficult to maintain the practical challenge of operating the reactor to it's maximize throughout while retaining the desire conversion and molecular weight, without exceeding the pressure drop limitations of the equipment. The authors explained this fact for the case of free-radical solution polymerization process using tubular reactor by means of following two cases,

1. Increasing temperature may decrease the pressure drop, owing to decreased solution viscosity, or increase it, owing to increased conversion.
2. Similarly, increasing the flow rate can decrease the pressure drop, owing to decreased conversion, or increase it, owing to increased shear rate.

Table AI.1: Selected literature studies reporting the non-ideal aspects of tubular reactor processs[◊].

References	Research theme	Targets
A. Polymerization studies:		
Hamer et al. (1986) [2] →	Analysis of tubular reactor model for free-radical solution polymerization.	Discussed a complete "*Transport Model*" by adding the "*Radial Convection Term*" and improving the "*Radial Diffusion*" description, while analyzing the tubular reactor process.
Kleinstreuer et al. (1987) [5] →	Fluid dynamics of a tubular polymerizer for styrene polymerization.	Comprehensive analysis of the effects of variable system properties on the fluid flow field.
Palma et al. (2003) [6] →	Flow analysis of oscillatory-flow tubular reactor for emulsion polymerization.	Analyzed a reactor behavior for the non-ideal mixing patterns.
B. Non-polymerization studies:		
Agrawal et al. (2001) [1] →	Modeling of a coiled tubular chemical reactor.	Compared the flow behavior of curved tubular reactor with "*Plug Flow*" and laminar flow tubular reactors.
Ujhidy et al. (2003) [9] →	Fluid flow in tubes with helical elements.	Demonstrated the effect of laminar flow conditions on the flow behaviors in the "*Coiled Tubes*" as well as in the tubes with "*Twisted Tapes Inserts*".
Joye (2003) [3] →	Pressure drop correlation for laminar, mixed convection, aiding flow heat transfer in a vertical tube.	Developed a predictive equation for reactor pressure drop in vertical, internal, aiding flow situations with constants wall temperatures.

In another study, Kleinstreuer et al. (1987) [5] reported a comprehensive analysis highlighting the effects of variable system properties on the fluid flow field, which their

◊ The literature on catalytic liquid-phase propylene polymerization in tubular reactors is very limited.

in turn affect the process stability and reactor performance. According to the author prospective, the tubular reactor geometry and inlet flow conditions must be carefully chosen to avoid thermal instability and non-linear transport fields.

Recently, Palma et al. (2003) [6] mentioned a number of different causes that can lead to the deviation from the ideal "Plug Flow" behavior of the tubular reactor,

1. The presence of stagnant regions (dead zones).
2. The presence of regions, which offer little resistance to flow (channeling, by-passing, or short circuit).
3. Additional secondary mechanisms that may cause mixing, such as,
    - Molecular and turbulent diffusion in both the radial and axial direction.
    - Non-flat velocity profiles.
    - Dispersion of particles due to differences in terminal velocities.
    - Flow maldistribtution inside the reactor.

Therefore, without the aid of a detailed simulator or a devoted experimental program, understanding the response of the system and guessing at optimal conditions can be very difficult.

In this appendix, however, the focus is kept on executing a variety of experiments on the catalytic polymerization of liquid-phase propylene using a scaled-up tubular reactor. The attempt made here is to recognize the non-linear relation between the polymerization chemistry and the reactor behavior on the basis of different catalytic polymerization experiments, which are performed under rarely used or observed flow conditions in laminar regimes and with having different "art-effects" from the reactor configuration. The main motivation in carrying out the present study is to judge the unpredictive behavior of such a reactor because any reactor of this type has many non-ideal parameters in terms of mixing and heat transfer, which cannot be extrapolated easily.

Set-up details

The tubular reactor used for the present study has an internal diameter (d_i) of 2.1 cm and a length (L) of 115.5 cm. The reactor is jacketed from the outside using a concentric cylindrical pipe with d_i of 4.23 cm. The reactor pressure and flow rate are maintained with the help of a "Pulsating Valve" mounted at the exit of the reactor. This scaled-up

tubular reactor is used together with the same hardware infrastructure that was constructed for the "capillary type" of tubular reactor. The scaled-up tubular reactor was placed in a vertical position, and only replacing the "capillary type" reactor and its jacket. The scaling-up factors between the "capillary type" and scaled-up type of tubular reactor are illustrated in Figure AI.1, and they are characterized based on ratios of d_i, L and reactor volume (V_r) of these two reactors. The scaling-up factors for d_i (y_{di}), L (y_L) and V_r (y_{Vr}) are 5.3, 0.2 and 5.6, respectively.

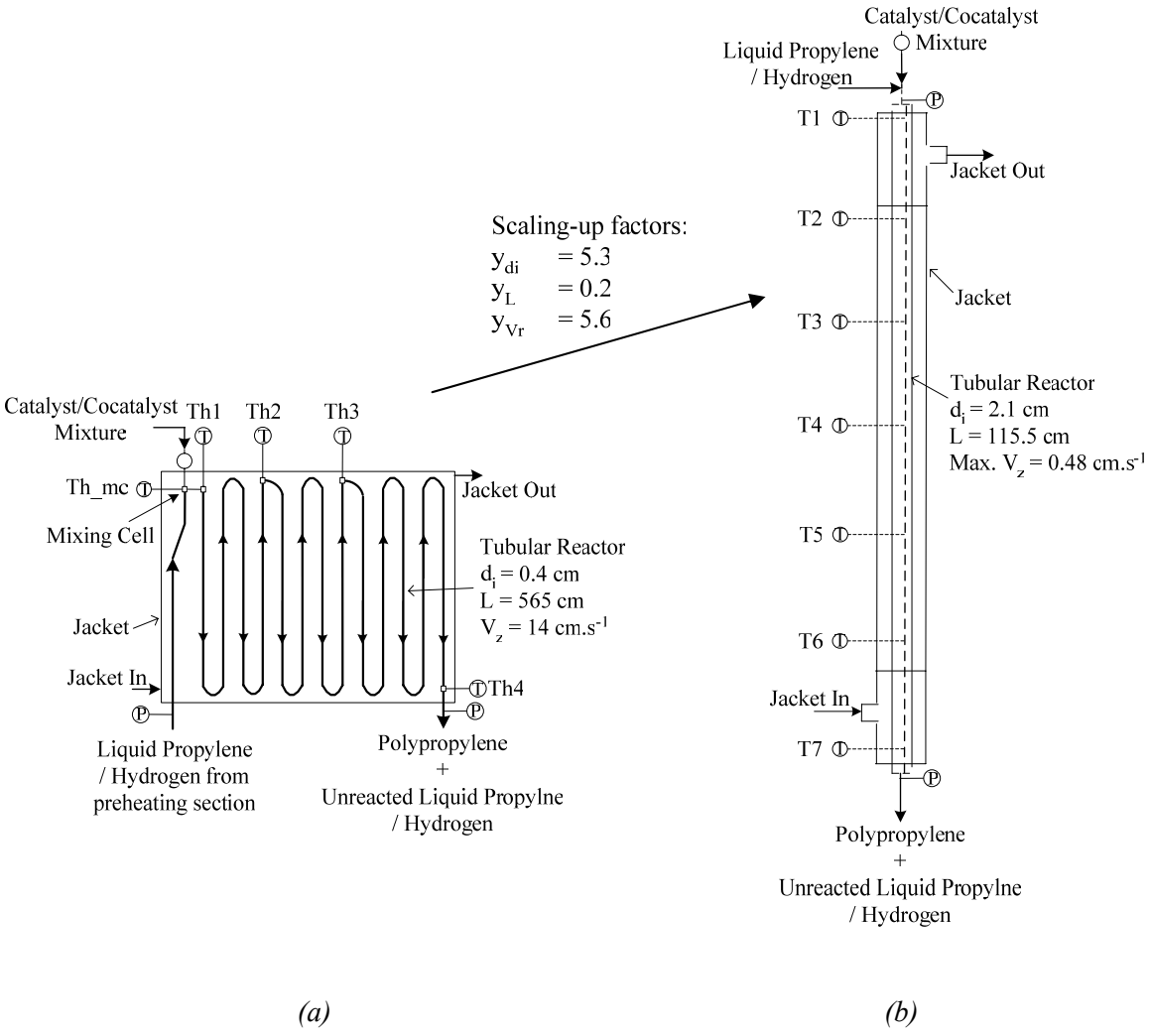

Figure AI.1: Schematic of two different tubular reactors design, (a) "capillary type" and (b) scale-up type.

The details about the complete experimental set-up are reported in Chapter 2, which also provides information regarding chemicals, polymerization procedure, analytical

techniques used in this study. The polymerization experiments were carried out through injecting a preactivated catalyst (slurry phase) into a continuous flow of liquid propylene. The catalyst type used here was a highly active supported catalyst of type $MgCl_2/TiCl_4$ with Phthalate as an internal donor, Silane as an external donor, and Triethylaluminum (TEA) as a cocatalyst [$].

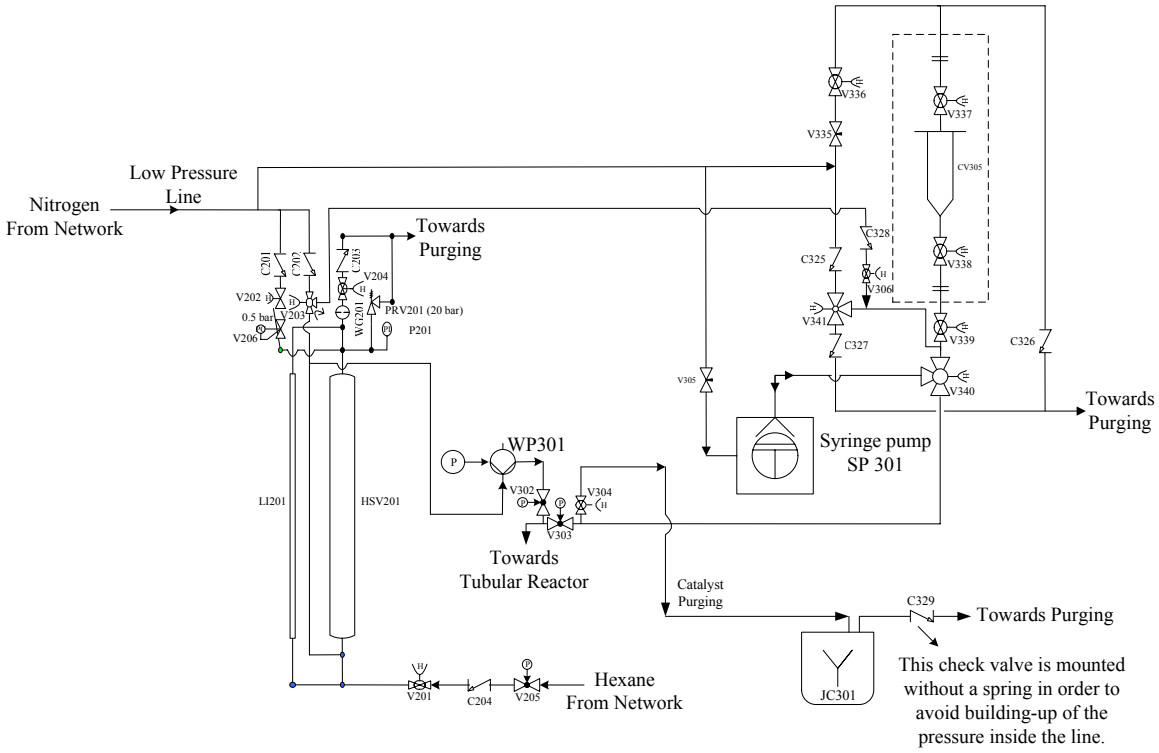

Figure AI.2: Schematic of catalyst injection system used for performing polymerization experiments using a scaled-up tubular reactor.

Unlike the "capillary type" reactor set-up, a syringe pump is used for the injection of the preactivated catalyst mixture, which can handle a sufficient amount of preactivated catalyst mixture to carry out a polymerization test for longer reaction time. The required amount of catalyst/cocatalyst/external donor mixture was prepared as described in Chapter 2. Then it is transferred to a catalyst vessel with a volume of 75 ml; see CV305 in Figure AI.2. However, the reaction time used in this work makes it impractical to suspend the catalyst in a low-viscous n-hexane. Therefore, the catalyst slurry was prepared using light mineral oil. After connecting the CV305 to the injection system, the

[$] Details of catalyst preparation or composition are confidential; however, it is irrelevant here from the point of view of the objectives involved with the present study.

tubes of the injection systems were flushed with a stream of nitrogen. In the next step, the catalyst mixture was injected into a syringe pump; see SP301 in Figure AI.2. The pump (Isco pump model 500D) has a variable speed with a stainless steel syringe with a capacity of 500 ml. The pump action was controlled via communication through the serial port (RS232) connected to the PC.

The basic preparation for the experiment is similar to that for "capillary type" of tubular reactor presented in Chapter 2. Only, a pulsating exit valve was set to constant degree of opening instead of back pressure. Then the propylene and hydrogen flow were started with the required set-point to the reactor. When the reactor pressure and temperature attained stable fluctuations, the preactivated catalyst was injected using the syringe pump. At the exit of the reactor, the reactor mixture was expanded into the high-pressure expansion vessel in the presence of CO_2, which was used as a quenching agent.

After the experiment, the hydrogen flow was stopped and the reactor was depressurized. The HPLC pump was stopped and the reactor cleaned with a continuous flow of nitrogen. The catalyst vessel and syringe pump were purged and cleaned with n-hexane and nitrogen. The produced polymer was removed from the expansion vessel and washed with i-propanol. The solution was mixed for an hour and filtrated over a glass filter. The powder was dried for four hours at 50°C in a vacuum oven.

The next important issue is analyzing the effect of a "Pulsating Valve" on the fluid dynamics of the reactor. The pulsating motion of the exit valve is controlled by certain reactor pressure, which means that once the reactor pressure reached a certain set-point, the pulsating exit valve opens for a short period of time depending on the degree of its opening. Further, with the closed exit valve, the reactor pressure increases again to its set -point due to the continuous inlet flow of liquid propylene.

The cycle of pressurizing and depressurizing the reactor takes place in a continuous pattern. The stable patterns of these cycles make it possible to estimation of average residence time (τ) of reaction medium inside the reactor. This is based on the volume of liquid propylene added to the reactor in order to keep the pressure constant and on the time required to reach constant pressure set-point (t_{Pr_rec}).

However, the t_{Pr_rec} will certainly get influenced from the different process parameters attached to the reactor flow dynamics and exit valve, such as,

1. The degree of the exit valve opening.
2. The mass flow rate of liquid propylene into the reactor.
3. The variations in the physical properties of the reaction medium due to the polymerization reaction.

In this section, only the effect of the exit valve opening and mass flow rate liquid propylene (m_{fr}^{M}) on the t_{Pr_rec} is discussed. The influence of varying physical properties due to the reaction on the t_{Pr_rec} is described elaborately in the next section.

Figure AI.3 ♦ show the dependency of t_{Pr_rec} on the opening of the reactor exit valve, evaluated at a different degrees of the valve opening and a different amount of m_{fr}^{M}. The estimated values of t_{Pr_rec} are shown in Figure AI.3 and appeared to be constant for both of these factors over a considerable period of time.

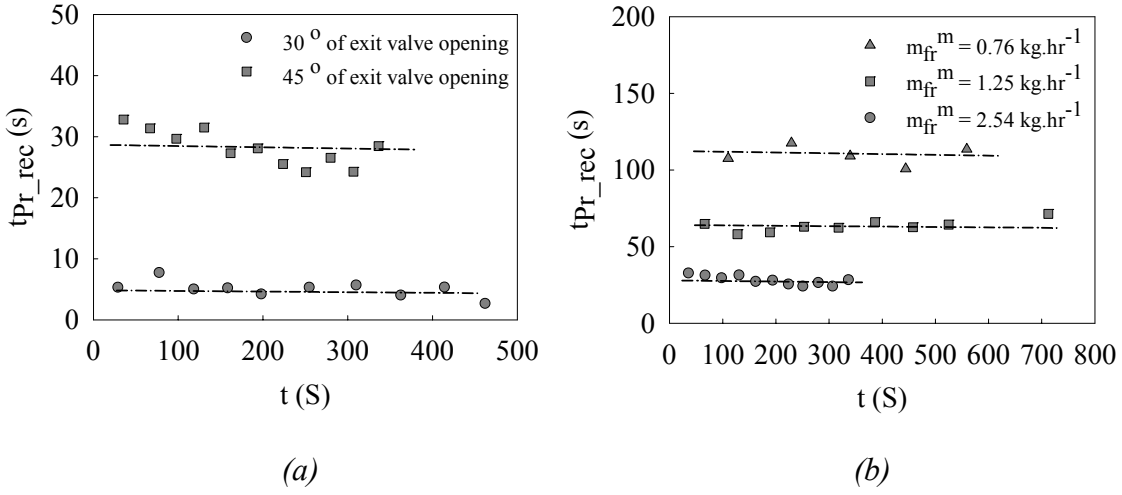

Figure AI.3: Dependence of reactor pressure recovery on the opening of reactor exit valve, estimated at (a) 2.54 kg.hr^{-1} of liquid propylene flow and (b) 45^{o} opening of reactor exit valve.

Figure AI.3 (a) clearly shows that with increasing the degree of the exit valve from 30 ^{o} to 45 ^{o} at same value of m_{fr}^{M} (2.54 kg.hr^{-1}), the value of t_{Pr_rec} increases 3 folds. This indicates that the higher amount of liquid propylene is expanding at an increased degree

♦ The effects shown in Figure AI.3 were obtained for the blank experiments without injection the preactivated catalyst slurry. The set reactor pressure for these experiments was 60 bar.

of the exit valve opening, thus needing a longer time for the reactor to be pressurized again to its original set values.

Figure AI.3 (b) illustrates the influence of different values of m_{fr}^{M} on the t_{Pr_rec} at constant degree of the exit valve opening (45 ^{o}). The average values of t_{Pr_rec} are found to be increased by factor 2 for an every step increase in the m_{fr}^{M} value from 0.76 to 2.54 kg.hr^{-1}. The increase in the amount of m_{fr}^{M} demonstrates a proportional impact on the variation of $t_{Pr\_rec.}$ For instance, for every step increase of m_{fr}^{M} value from 0.76, 1.25 to 2.54 kg.hr^{-1}, the average value of t_{Pr_rec} increases from 30.8, 62.6 to 109.5 s, respectively. However, these effects will definitely be dependent on the properties of the liquid propylene present during the experiment.

The overall influence of the exit valve opening on the average time for the recovery of reactor pressure can be seen from Figure AI.4 •, which explains the combined effect of degree of the exit valve opening and m_{fr}^{M} on recovery time for reactor pressure. It can be seen that with the increasing the degree of exit valve opening and with low amount of m_{fr}^{M}, the average value of t_{Pr_rec} could reach up to 500 s and above. These data are very useful from the point of view of designing the proper τ value for the polymerization experiments.

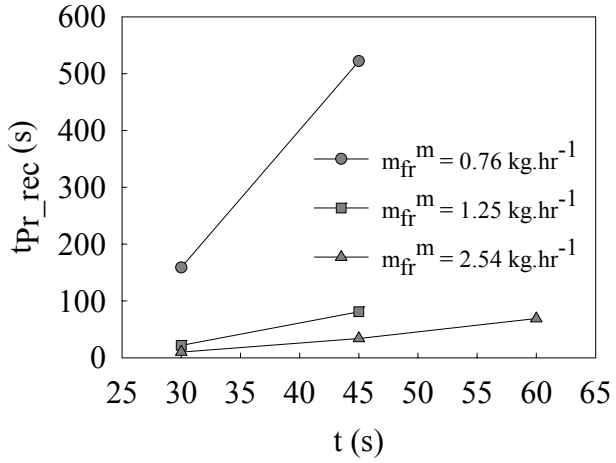

Figure AI.4: Overall effect of reactor exit valve opening on the average recovery of reactor pressure.

• The effects shown in Figure AI.4 were obtained for the blank experiments without injection the preactivated catalyst slurry. The set reactor pressure for these experiments was 60 bar.

Reactor performance

The catalytic liquid propylene polymerization experiments performed in scaled-up type tubular reactor are discussed in this section. Table AI.2 and Table AI.3 show the experimental recipes for a number of polymerization runs carried out to study the effect of different process parameters on the reaction kinetics along with the performance of tubular reactor. As given in Table AI.2 and Table AI.3, few experiments were carried out with a pulse mode injection of a preactivated catalyst. These pulses were created by opening a syringe pump for a required amount of time. The temperature profiles with respect to time and axial coordinates were measured using seven thermocouples placed along the reactor length and located in the axial direction at 17, 33, 49, 65, 81, 97 and 113 cm positions; see Figure 7.1 (b) [∅]. The reactor pressure was measured using two pressure sensors placed at the inlet and exit of the reactor (see Figure 7.1 (b)). These pressure sensors were used to monitor the plugging inside the reactor by following the pressure drop over the reactor length.

Table AI.2: Experimental recipe

Experiment Code	T_o [‡] (^oC)	P_{set} [†] (bar)	m_{fr}^{M} ($kg.hr^{-1}$)	m_{fr}^{Cat} ($kg.hr^{-1}$)	Catalyst Injection Mode	X ($molH_2o.molPPYo^{-1}$)
Run71	70.0 ± 2.5	62.0	2.54	0.030	Single Pulse injection with injection period of 3 to 6 s	0.0
Run72	70.0 ± 2.5	62.0	2.54	0.045	Single Pulse injection with injection period of 5 to 6 s	0.0
Run73	70.0 ± 2.5	60.0	1.25	0.045	Single Pulse injection with injection period of 5 to 6 s	0.0
Run74	70.0 ± 2.5	62.0	1.26	0.045	Single Pulse injection with injection period of 10 s	0.0
Run75	70.0 ± 2.5	60.0	1.26 / 0.76	0.002	Continuous injection	0.0
Run76	70.0 ± 2.5	50.0	1.26	0.002	Continuous injection	0.002

‡ Initial reactor mass temperature before addition of active catalyst.
† P_{set} values shown in table represent the reactor pressure at which the reactor exit valve is open.

[∅] The length was calculated according to the inlet connection of the tubular reactor (see Figure AI.1 (b)).

Table AI.3: Additional experimental parameters and polymer yield [⊕]

Experiment Code	$v_z^{(avg)}$ ($cm.s^{-1}$)	$\tau^{(avg)}$ (s)	$Re^{(avg)}$	Yield ($g.gCat^{-1}$)
Run71	0.48	242	662	6.7
Run72	0.48	242	677	-
Run73	0.24	480	342	136.0
Run74	0.24	480	340	-
Run75	0.24 / 0.14	480 / 800	340 / 204	-
Run76	0.24	480	341	33.7

Run71 is the first preliminary experiment performed in the scaled-up tubular reactor. This experiment was particularly aimed at analyzing the complete hardware design as well as the data acquisition and control unit of the reactor system. The experiment was carried out for an extremely low yield of polymer. This criterion was applied especially to avoid any kind of high risk involved during reaction, such as the high influence of "run-away" behavior on the reactor heat transfer, or the effect of high polymerization rate on increasing the viscosity of the reaction medium mainly at high temperatures.

The maximum achievable value of m_{fr}^{M} (2.54 $kg.hr^{-1}$) and pulse mode of injection for a preactivated catalyst was used while performing the experiment. The reactor flow conditions and the exit valve settings yield the τ value of 242 s. The reactor dynamics in terms of temperature and pressure were measured using the on-line sensors.

Figure AI.5 (a) and (b) show the profiles of the reactor temperature and pressure measured during the polymerization experiment. The influence of the pulsating exit valve can be clearly seen from the fluctuating profiles of temperature and pressure. The exit valve was set to open at a reactor pressure of 60 bar with 30 ^{o} of opening. More importantly, the fluctuations observed in the reactor temperature did not show any

[⊕] The weight ratio of cocatalyst to catalyst was 5 $mg.mg^{-1}$ and external donor to catalyst was 1 $mg.mg^{-1}$. The jacket temperature was always kept constant for isoperibolic mode. The estimated tubular reactor volume is 400 ml. All the experiments were performed in the laminar flow regime. The reaction mixture was expanded into the expansion vessel in the presence of CO_2.
For Run71: No external donor has been used during the preparation of catalyst activation with cocatalyst.
For Run75: Volumetric flow rate of liquid propylene has been changed during the polymerization reaction from 50 ml/min to 30 ml/min

influence on the jacket temperatures. The jacket temperatures were found to be constant at an average value of 73 ^{o}C.

The points denoted by 1 and 2 in the Figure AI.5 (a) show the number of pulse injections for preactivated catalyst. It was observed that the injection of an activated catalyst did not show any significant increase in the reaction temperature, and the fluctuation in the profiles measured along the reactor length remained unchanged. This effect is expected for the low yield experiment. However, the dynamics of the solid phase did show an impact on the reactor pressure.

As can be seen from Figure AI.5 (b), after the reaction time of 400 s, the accumulation of the polymer phase and the constant flow of liquid propylene increase the compressibility of the fluid within the reactor, yielding an increase in the reactor set pressure from 60 bar to 100 bar.

Part of these profiles highlighted by "A" is shown in Figure AI.6. The frequency of fluctuations for temperature and pressure was observed to be relatively constant over the period of reaction time. The pressure profiles display the cycles of pressurizing and depressurizing as a result of the exit valve opening and closing.

It can be seen from Figure AI.6 (b) that a pulse opening of the exit valve dropped the reactor pressure by 20 bar, showing a consequential effect on the reactor temperature with the drop in the temperature by 3 to 5 ^{o}C (can be seen from Figure AI.6 (a)). This drop was observed at all of the junctions of the thermocouples placed along the reactor length. This evidently illustrates that the heat wave generated due to the expansion and compression of the liquid propylene propagates very rapidly along the reactor length.

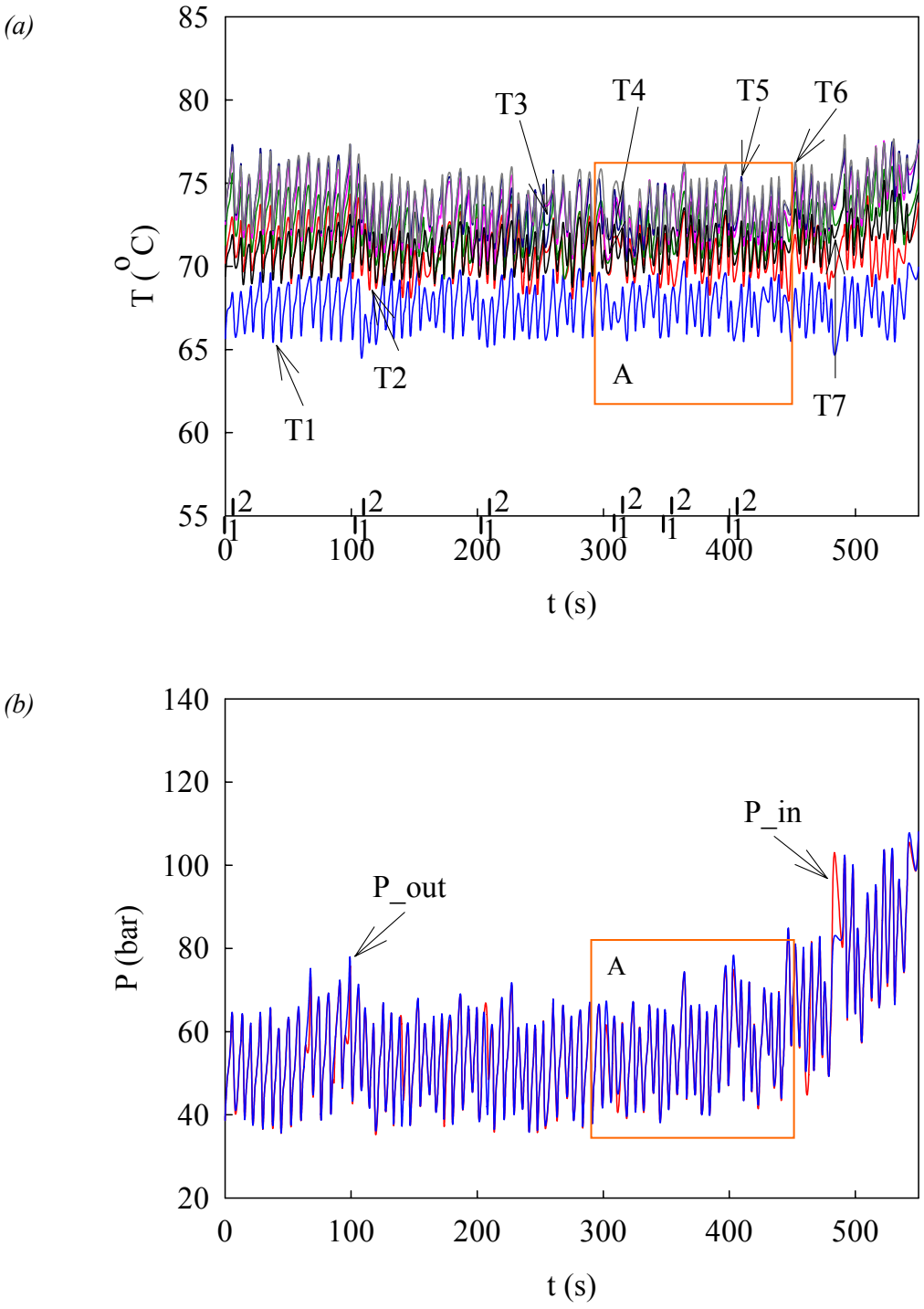

Figure AI.5: Measured profiles for an extremely low yield polymerization run, (a) reactor temperature profiles and (b) reactor pressure profiles (for experimental condition, see Table AI.2 and Table AI.3, Run71,1: Catalyst injection started and 2: Catalyst injection stopped).

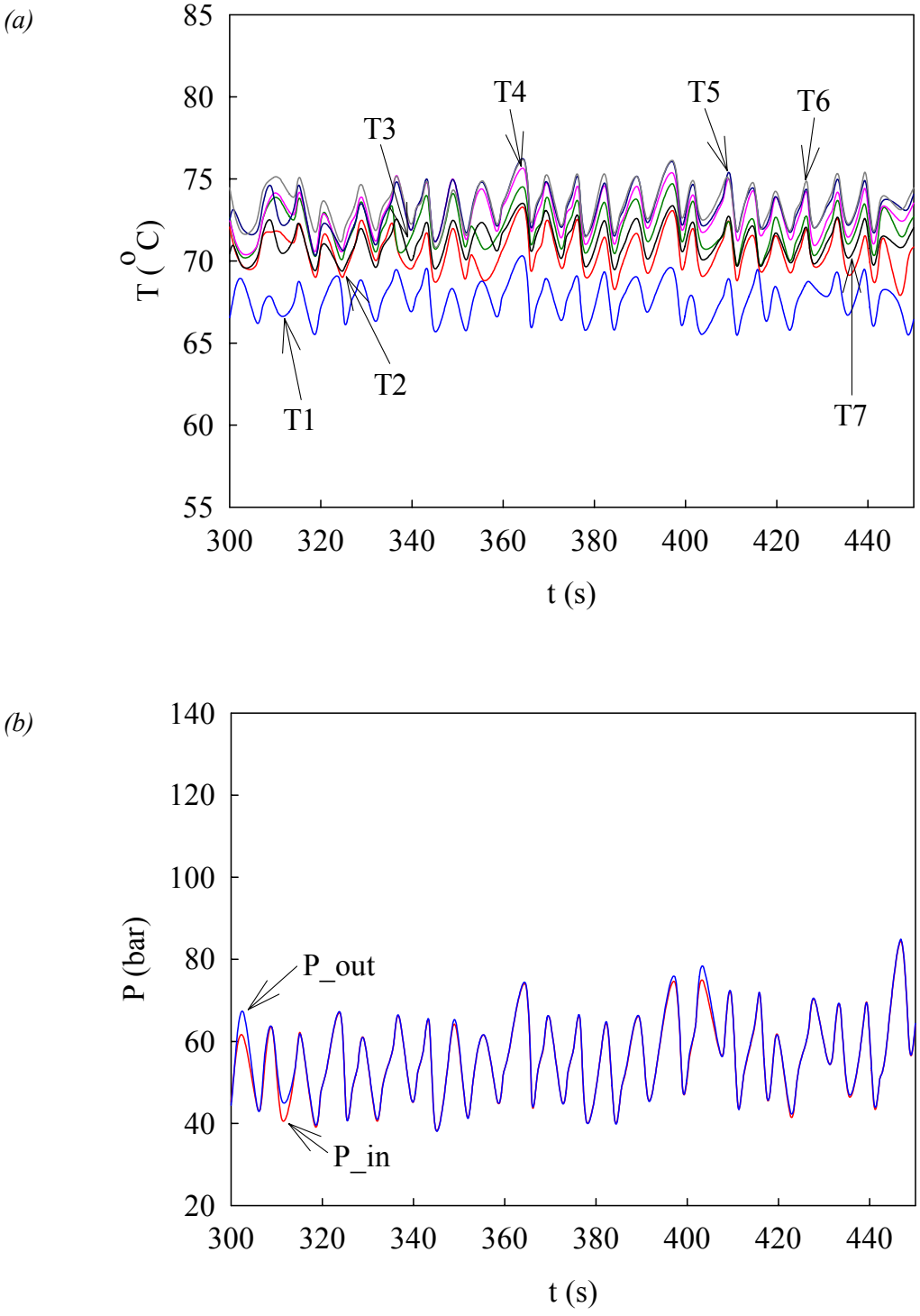

Figure AI.6: Magnification of Part "A" showed in Figure AI.5, (a) reactor temperature profiles and (b) reactor pressure profiles (for experimental condition, see Table AI.2 and Table AI.3, Run71,).

So far, the influence of frequent fluctuation in temperature and pressure on the reactor behavior has been evaluated. The characteristics of an individual fluctuation representing the pressurization and depressurization cycle can be quantified using different process parameters. This quantification can be judged based on the data presented in the previous section. For instance, the time interval between two successive cycles can be varied either using a different degree of the exit valve opening or a different amount of m_{fr}^{M}. One of the examples given above is Run71, in which, the m_{fr}^{M} of 2.54 $kg.hr^{-1}$ and 30 ^{o} exit valve opening resulted in very fast frequencies of pressurization and depressurization cycle. The ratio between the pressurization time and depressurization time (t_c) was very small and thus did not show a distinct effect on the jacket temperature as well as on the catalyst injection. Now, the question arises regarding what influence there be on these process variables when the ratio, t_c increases. In order to check the effect of this parameter, Run72 was carried out by keeping the same amount of m_{fr}^{M}, but increasing the exit valve opening to 45 ^{o}. The measured profiles of temperatures, pressures, and the volume of the injected catalyst (slurry phase) are shown in Figure AI.7 (a), (b), and (c), respectively. The catalyst was injected in a pulse mode over the duration of the reaction. The points denoted by 1 and 2 in Figure AI.7 (a) show the number of pulse injections for the preactivated catalyst. The catalyst activity observed for this experiment was quite limited. Only a slight rise in temperature was noticed immediately after the injection of the preactivated catalyst pulse, for part “A” and “B”, shown in Figure AI.7 (a). It was observed that for Run72, the ratio, t_c increased by factor 3 as compared to the value estimated for Run71. This increase indicates that the reactor required more time for pressurization. The rise in reactor pressure was found to be exponential and showed a uniform pattern over the reaction period; see Figure AI.7 (b). This exhibits different compression behavior as compared to the pressure rise phenomenon noticed for Run71. The most striking influence of compression is perceived from the profile of the injected catalyst slurry volume; see Figure AI.7 (c). During the experiment, similar amounts of catalyst pulses were injected. However, from Figure AI.7 (c), it is identified that different volumes of catalyst slurry were injected. This clearly indicates the effect of different timing of the pulse injections along the exponential pathway of a pressure rise. Such as, the catalyst pulse injected during the steep increase of the reactor pressure will have more impact on the compression; for instance, see the first and fourth stroke shown on the time scale of Figure AI.7 (a) and the corresponding values of the injected volume from Figure AI.7 (c). On the other hand, the catalyst pulse injected immediately after the expansion of the reactor pressure will have less impact of the compression, and it could be seen from the data of last injected catalyst pulse, from Figure AI.7.

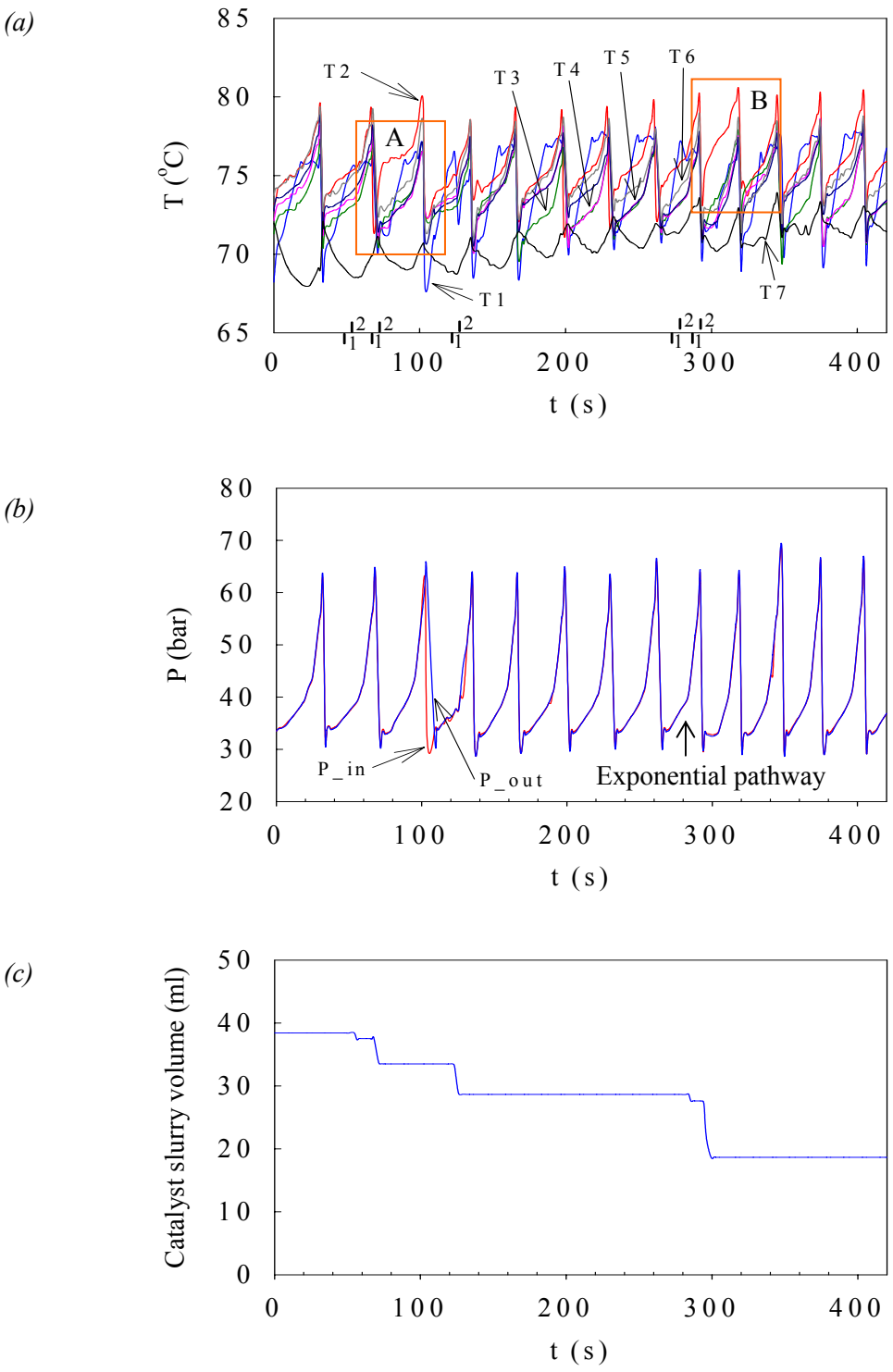

Figure AI.7: Influence of compression and expansion on the catalyst pulsing, (a) reactor temperature profiles, (b) reactor pressure profiles and (c) injection volume for catalyst slurry (for experimental condition, see Table AI.2 and Table AI.3, Run72,1: Catalyst injection started and 2: Catalyst injection stopped).

The next experiment is aimed to analyze the influence of high catalyst activity during a polymerization reaction on the thermal response of a reactor. This experiment was carried out using a single pulse of active catalyst into the reactor with m_{fr}^{M} of 1.25 $kg.hr^{-1}$. The reduced amount of m_{fr}^{M} would increase the residence time of active catalyst mass to 480 s. The amount of catalyst mass for a single pulse injection was estimated based on the m_{fr}^{Cat} and on the injection period of the pulse. The required recipe of the experiment is provided in Table AI.2 and Table AI.3; see Run73. The 1.25 $kg.hr^{-1}$ of m_{fr}^{M} and 45 ^{o} of exit valve opening were used to avoid any impact of reactor compression on the catalyst injection. In addition, the required amount of overpressure was kept on the syringe pump while injecting the active catalyst pulse. With these settings of m_{fr}^{M} and exit valve opening, the reactor took 62.6 s of time for pressurizing, which ultimately increased the ratio, t_c. The profiles of reactor temperature and pressure measured along the reactor length are shown in Figure AI.8 (a) and (b), respectively. Figure AI.8 (a) clearly explains the consequences of an active catalyst injection on the thermal response of reactor. This effect is well viewed from the maximum temperature rise of 17 ^{o}C at the second thermocouple point (T2), which was placed at 33 cm of the axial length from the inlet of reactor. This suggests that the catalyst pulse was dispersed initially up to a length of 33 cm, which might be due to the impact of the force used by the syringe pump during the injection of catalyst pulse into the reactor operating under laminar flow condition. Because with the average Reynolds number (Re) of 342, the dispersion of the catalyst pulse in the axial direction is very limited. On the other hand, the frequent expansion of the reactor did show an influence on the axial dispersion of the reactive catalyst pulse, and it could be seen from the dynamic of temperature profile shown in Figure AI.8 (a). It was observed that after the first expansion of reactor mass, the reactive catalyst pulse was spread over 50 % of the reactor's length, which resulted in a slight temperature change at the thermocouple points T3 and T4. Furthermore, after the second expansion of reactor mass, an unexpected behavior was observed from the temperature rise at thermocouple points T2 and T6, which were placed 64 cm apart from each other. This indicates that the reactive catalyst pulse was separated into two parts having different residence time inside the reactor. The pulse residing at the exit of the reactor will have a τ value of 180 s and the other pulse observed at 30 % of the reactor length will definitely have a τ value higher than 180 s. Interestingly, such non-ideal behavior of fluid dynamics did not exhibit any significant influence on the reactor pressure. From Figure AI.8 (b), no pressure difference was monitored over the reactor length and uniform fluctuations in the pressure profiles were noticed. This certainly specifies that the reactive solid phase was completely washed out of the reactor leaving no residuals.

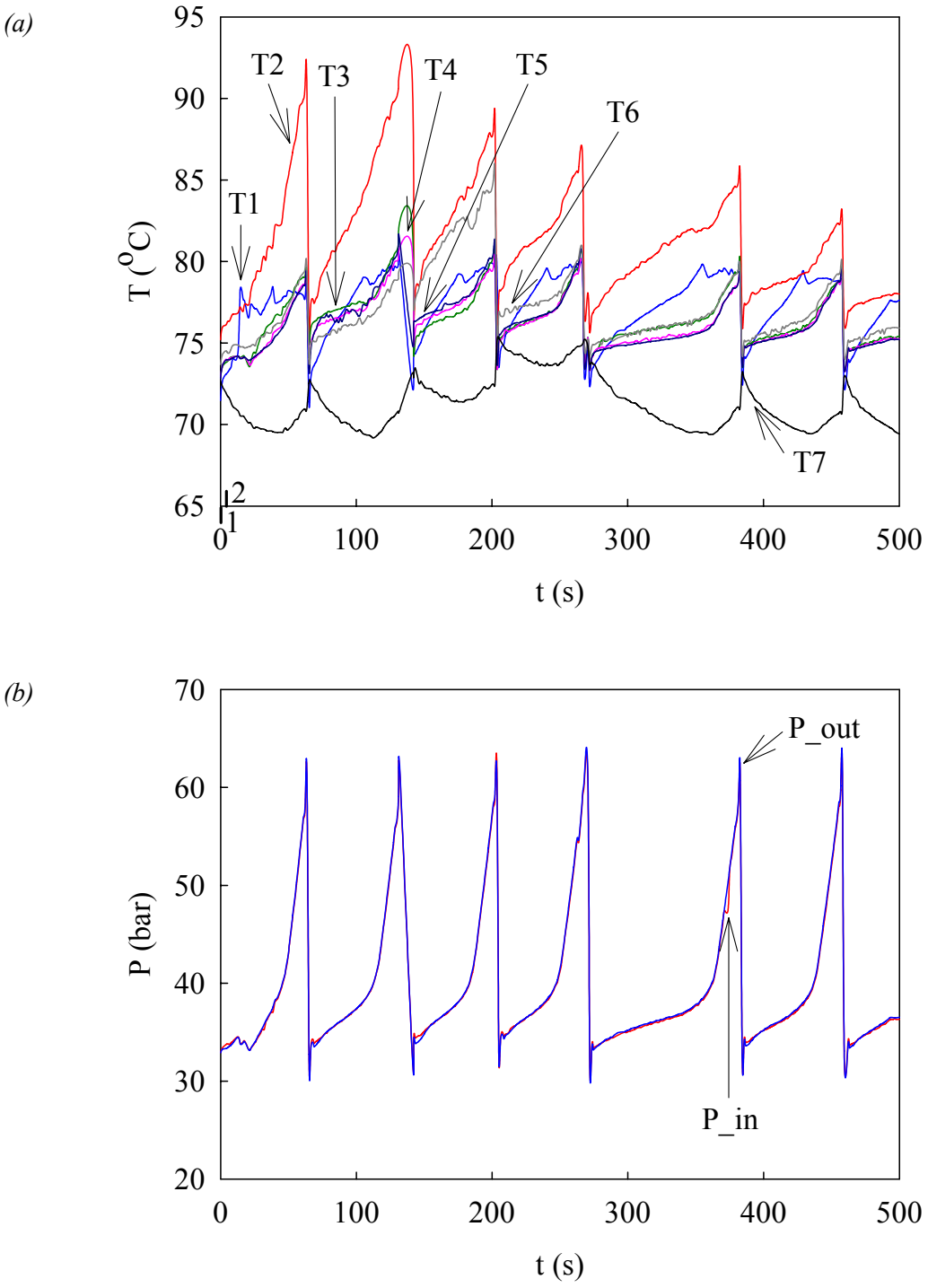

Figure AI.8: Measured profiles for the polymerization test carried out with a single pulse of preactivated catalyst, (a) reactor temperature profiles, (b) reactor pressure profiles, (for experimental condition, see Table AI.2 and Table AI.3, Run73, 1: Catalyst injection started and 2: Catalyst injection stopped).

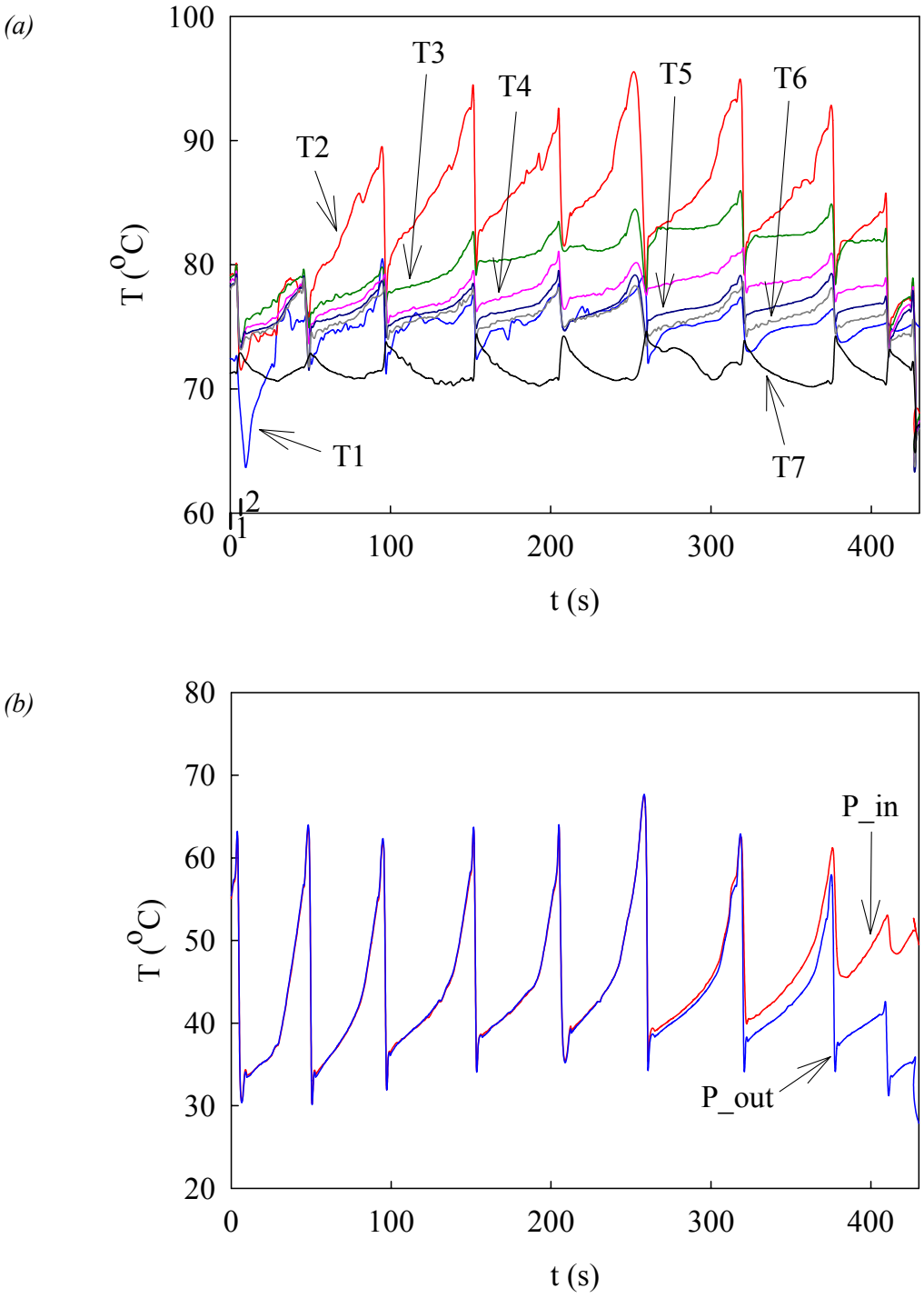

Figure AI.9: Measured profiles for the polymerization test carried out with a single pulse of preactivated catalyst, (a) reactor temperature profiles, (b) reactor pressure profiles, (for experimental condition, see Table AI.2 and Table AI.3, Run74, 1: Catalyst injection started and 2: Catalyst injection stopped).

Figure AI.9 illustrates the measured temperature and pressure profiles, which were obtained from the experiment Run74. This experiment was also performed by injecting a single pulse of active catalyst into the reactor with the similar amount of m_{fr}^{M} as used in Run73. The amount of catalyst used for Run74 was increased by injecting the pulse for an injection period of 10 s, as compared to Run73; see the data given in Table AI.2 and Table AI.3. From Figure AI.9 (a), the initial mixing pattern observed for the injected catalyst pulse is unlike to what has been examined in the case of Run73; see Figure AI.8 (a). The temperature rise noted at junction T2 was seen after the first cycle of pressurization and expansion. It seems that the injected mass of catalyst is faced towards a different characteristic of mixing that resulted in the delayed response of the active catalyst. It is monitored from Figure AI.9 (a) that as the polymerization reaction progressed, the reactive catalyst pulse was dispersed over 50 % of the reactor's length. The temperature rise measured at thermocouple junctions T2, T3 and T4 appears to be constant over the period of the reaction. This advocates that the reactive pulse was most probably stagnant in the region where it was dispersed. Such a stagnant pocket could lead to undesirable event of reactor plugging. This phenomenon could be seen from Figure AI.9 (b), wherein the pressure difference was observed after the 315 s of reaction time. The magnitude of this pressure difference increased from 2 bar to 10 bar with increasing reaction time from 315 s to 420 s, which merely an effect of increasing conversion of the active catalyst inside the stagnant zone, and thus blocking the axial flow of reaction medium upon expansion. Until now, the performance of the present tubular reactor set-up has been analyzed for the polymerization experiments performed with the pulse injection of active catalysts, and different aspects of non-ideal reactor behavior have been evaluated based on these experiments. These observed features have been found to be unpredictable and appeared to show a random influence of the various process operating conditions on the reactor know-how. Such characteristics of the process often motivate one to recognize the number of challenges involved in analyzing the non-ideality of the system. One of such challenges is to evaluate the performance of a reactor by carrying out the polymerization experiment using continuous injection of active catalyst. It will be interesting to know from these experiments about the dynamics of the reactor in terms of mass and heat transfer. One of the examples is presented in Figure AI.10, which describes the measured profiles of temperature, pressure and the values of t_{Pr_rec} obtained during the experimental Run75. This polymerization run was performed with the continuous injection of active catalyst into the reactor with an initial m_{fr}^{M} of 1.26 $kg.hr^{-1}$, resulting in an initial τ value of 480 s and Re value of 340 (see Table 7.2). A very low amount of m_{fr}^{Cat} was used in order to avoid any possibilities of plugging or polymer accumulation

inside the reactor. The points denoted by 1 and 2 on the Figure AI.10 (a) show the complete injection period of active catalyst. During the polymerization reaction, after 9.4 min of reaction time, the initial m_{fr}^{M} of 1.26 kg.hr^{-1} was changed to 0.76 kg.hr^{-1}. The reason for this change could be seen from Figure AI.10 (a), for the initial value of m_{fr}^{M} and with m_{fr}^{Cat} value of 0.002 kg.hr^{-1}, the thermal response of reactor did not change, showing the uniform fluctuations in the temperature over a complete reactor length. Figure AI.10 (b) shows a similar response in the pressure fluctuations. It is believed that in the "initial-phase" of the reaction and in the presence of a low amount of catalyst for polymerization to initiate, the heat accumulated inside the reactor is dissipated due to the frequent expansion of the reactor mass. This enables maintaining the thermal balance of the reactor for τ value of 480 s and Re value of 340. This effect is also supported from the constant values of t_{Pr_rec} shown in Figure AI.10 (c), indicating a low conversion of monomer during the reaction, exhibiting no significant influence on the reactor dynamics. The thermal response of reactor was amended immediately after increasing the τ value to 800 s by reducing the m_{fr}^{M} to 0.76 kg.hr^{-1}. As shown in Figure AI.10 (a), the reactor temperatures along the axial direction increased with the proceeding of the polymerization reaction. This increase in temperature is obvious as the conversion of propylene increases with the increasing residence time of the active catalyst. The maximum rise in temperature measured at thermocouple junction, T2, was 30 ^{o}C. The effect of temperature rises on the reactor pressure was observed from the pressure fluctuations shown in Figure AI.10 (b). The drop in the reactor pressure upon expansion decreased with the increasing reactor temperature. From Figure AI.10 (b), it could be seen that for a temperature rise of 30 ^{o}C, the reactor pressure drops from its set pressure of 60 bar to 40 bar instead of 32 bar. Furthermore, the recovery time for reactor pressure was also found to be increased by 30 %; see Figure AI.10 (c). According to the estimation presented above, the t_{Pr_rec} should have the value of 109.5 s for m_{fr}^{M} of 0.76 kg.hr^{-1}. However, as a consequence of temperature increment on the reactor dynamics, the t_{Pr_rec} show the maximum value of 155 s for m_{fr}^{M} of 0.76 kg.hr^{-1}; see Figure AI.10 (c). The influence on reactor pressure and its recovery upon expansion could be acknowledged based on various factors involved with this process, like,

1. The mass and heat transfer resistances often observed in the laminar flow regime.
2. The changes in the physical properties of reaction medium as a result of significant temperature rise.
3. The increasing conversion of monomer, thus altering the fluid dynamics of the reactor.
4. The increasing shear resistance of the flow due to the presence of polymer-phase.

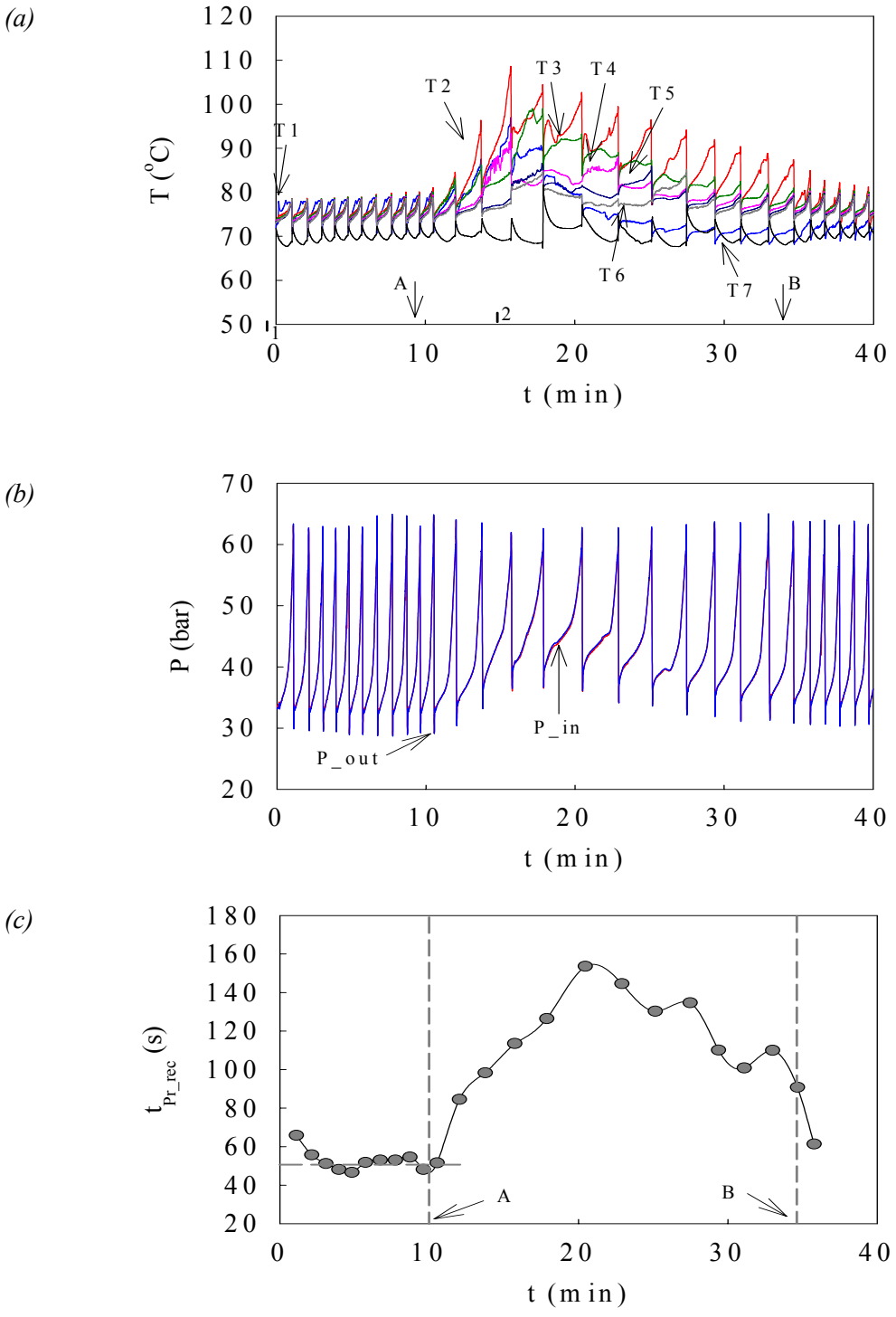

Figure AI.10: Measured profiles for the polymerization test carried out with continuous injection of preactivated catalyst, (a) reactor temperature profiles, (b) reactor pressure profiles, (for experimental condition, see Table AI.2 and Table AI.3, Run75, 1: Catalyst injection started and 2: Catalyst injection stopped).

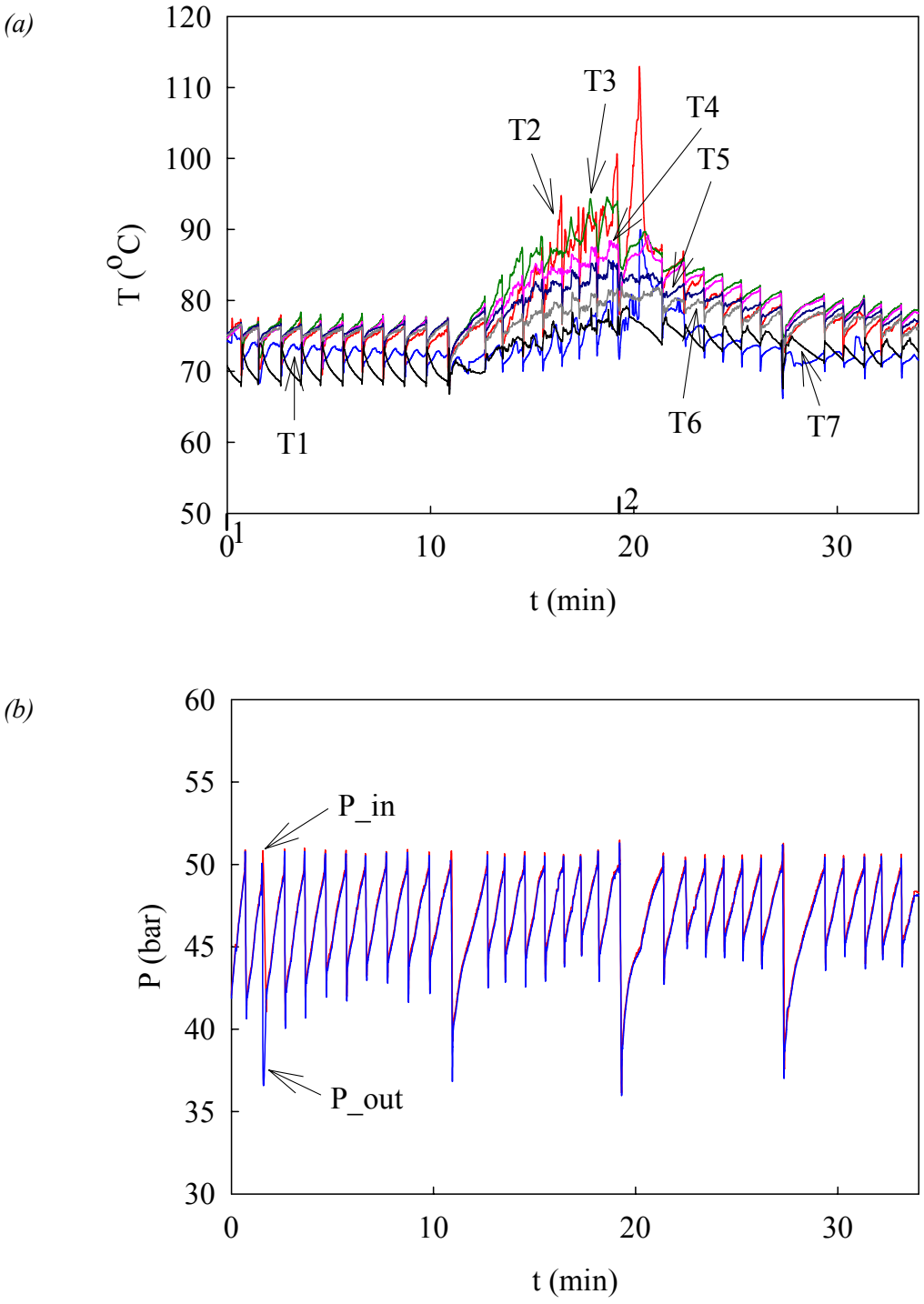

Figure AI.11: Measured profiles for the polymerization test carried out with continuous injection of preactivated catalyst and X value of 0.002, (a) reactor temperature profiles, (b) reactor pressure profiles, (for experimental condition, see Table AI.2 and Table AI.3, Run76, 1: Catalyst injection started and 2: Catalyst injection stopped).

In experiment (Run76), the polymerization test was performed in the presence of hydrogen and with the continuous injection of active catalyst. The experimental conditions for Run76 are reported in Table AI.2 and Table AI.3. The flow rate of hydrogen was set to a constant value in order to have a 0.002 mole ratio of hydrogen to liquid propylene (X). Similar to Run75, a low mass flow rate of catalyst was used with the m_{fr}^{Cat} value set to 0.002 $kg.hr^{-1}$. The points denoted by 1 and 2 on the Figure AI.11 (a) show the complete injection period of active catalyst slurry. Similar to Run75, a low mass flow rate of catalyst was used for Run76 with the m_{fr}^{Cat} value set to 0.002 $kg.hr^{-1}$. Due to possible high activity of the catalyst, the m_{fr}^{M} was kept constant over the complete reaction time. This experiment was particularly executed to see the effect of high activity of catalyst obtained in the presence of hydrogen on the dynamics of tubular reactor ♦. The measured profiles of temperature and pressure are shown in Figure AI.11 (a) and (b), respectively.

Similar to Run75, Figure AI.11 (a) shows an "initial-phase" effect in the first 10 min of the reaction period for Run76. According to the m_{fr}^{M} and 45 ^{o} of exit valve opening, the average fraction of catalyst mass should pass through the reactor within 480 s. Thus, after the 12 min of reaction time the active catalyst mass was dispersed over a complete reactor length. From Figure AI.11 (a), the temperature change was observed at all thermocouple junctions of the reactor, exhibiting the accumulation of heat as the polymerization reaction progressed with the continuous injection of catalyst slurry. It is believed that the varying thermal response of tubular reactor with the advancement of polymerization reaction would lead to a complex hydrodynamics of the reactor, especially, in the presence of hydrogen. Usually, it is considered that in the case of a completely filled reactor, hydrogen is completely dissolved in the liquid propylene. However, this may not be appropriate when the reactor flow is disturbed with the frequent cycles of expansion and pressurization, which might show an influence of liquid monomer evaporation and degassing of some reactive components on the flow behavior. The impact of such complex hydrodynamics of the reactor behavior could be observed from the measured pressure profiles shown in Figure AI.11 (b). The drop in the reactor pressure upon expansion was reduced with the increasing reaction time. On the other hand, unlike Run75, the frequency of the pressure fluctuations did not change, and the values of t_{Pr_rec} were estimated to be constant over the period of reaction. This might suggest that the

♦ The catalyst activity in the presence of hydrogen during liquid propylene polymerization has been discussed in Chapter 3, Chapter 4 and Chapter 5.

consequence of monomer conversion on the pressure recovery and on the expansion of the reactor is very limited.

DSC measurements were carried out for three polypropylene (PP) samples prepared from Run71, Run73, and Run76, to study the heating and cooling behavior of an individual sample. The selected DSC data are summarized in Table AI.4. The thermal history of these samples was scanned in order to understand the impact of the distinct flow conditions of tubular reactor used in this work on the properties of the polymer. The height to width ratio (HWR) of the melting peaks, reported in Table AI.4, describes qualitatively the crystallite size distribution of a semi-crystalline material [8]. The melt enthalpy (H_f) representing the crystallinity of PP sample was estimated using the similar procedure that has been described in Chapter 5. The % Crystallinity data was estimated using the procedure described by Pater et al. (1999) [7] ⊕.

At this moment, the data shown in Table AI.4 is very limited, and therefore, it is difficult to make any final conclusion on the properties of produced polymer samples. However, few interesting points are highlighted. It is important to note that the measured crystallization temperature (T_{c1}) and melting temperature (T_{m2}) from 2nd heating cycle for PP samples prepared from Run71 and Run73 are closed to the standard values. However, the lower values T_{c1} and T_{m2} for PP sample obtained from Run71 clearly show the absence of external donor during the catalyst activation. Kissin et al. (2004) [4] observed the effect of external donors on the characteristic properties of polymers. The authors mentioned that in the absence of an external donor, the crystalline fraction of the polymer decreases. This finding can also be seen from the lower value of % Crystallinity for Run71 as compared to Run73, wherein the % Crystallinity for Run71 was lower by 30 %. The values of T_{c1} and T_{m2} for PP sample obtained from Run76 were found to be very low. It seems that with the present flow conditions, the presence of hydrogen during the polymerization plays an important role in the formation of the particle morphology. The lower % of crystallinity for a PP sample prepared from Run76 represents the polymer sample with high amorphous nature. Another observation made from the lower values of HWR for the 2nd cycle of heating indicates that all the PP samples seem to have achieved the broad crystallite size distribution and therefore represented a more heterogeneous crystallinity [8].

⊕ The calculated heat of fusion for the 100 % crystalline PP sample was taken from Pater et al. (1999) [7]. The authors used 209 J.g^{-1} of heat of fusion for estimating the % Crystallinity of their PP samples.

Table AI.4: DSC data for different PP samples prepared from scale-up tubular reactor

Experiment Code	1st Heating			1st Cooling	2nd Heating			% Crystallinity
	T_{m1} (°C)	HWR (W.g^{-1}.°C^{-1})	H_{f1} (J.g^{-1})	T_{c1} (°C)	T_{m2} (°C)	HWR (W.g^{-1}.°C^{-1})	H_{f2} (J.g^{-1})	
Run71	152.40	0.1711	44.75	104.15	154.66	0.1296	34.75	16.6
Run73	153.43	0.7531	57.76	108.10	162.89	0.2254	50.40	24.1
Run76	144.54	0.1876	17.29	82.51	138.11	0.0855	13.88	6.6

Conclusions

A comprehensive experimental program has been demonstrated to investigate the dynamics of non-isothermal laminar flow of a reacting fluid in a scaled-up tubular reactor. The discussed methodology could assist in carrying out the statistical analysis of catalytic liquid-phase propylene polymerization in a tubular reactor operating under a laminar flow regime. Usually, at industrial level, the tubular reactor are built with larger sizes of tubes in order to operate it to maximize throughput while maintaining the desired conversion and molecular weight, without exceeding the pressure drop limitations of the equipment. This task is difficult because of the non-linear response of the system. The reactor behavior observed in this work may appeared in any part of the scaled-up reactor as a result of unavoidable circumstances like varying properties of the reaction fluid leading to unwanted thermal fluxes or in extreme cases, the plugging possibilities of the reactor. Therefore, the investigations presented in this appendix are very important in understanding the link between reaction kinetics and the scaling of the dimensions of tubular reactor.

The performance of tubular reactor has been explained based on the different process parameters and operating conditions. It has been noticed that the selection of these parameters is very critical in predicting the thermal instability or flow restrictions in the reactor, operating under laminar flow conditions. The mixing patterns observed during the polymerization reaction are quite unpredictable. The frequent expansion of the reactor fluid has exhibited an impact on the transport properties of the reactive catalyst mass. It has been observed that the increase in the amount of catalyst, monomer conversion, as well as shear resistance during reaction can affect the compressibility of the reactor, when working at high-pressures. It is concluded from the measured reactor performance that the proper mixing and heat transfer criteria are very important for the higher productivity of the reactor. The productivity obtained with the present reactor is very low and could be related to the presence of limited mixing in the laminar regime of flow. An unexpected behavior of the catalyst has been observed during the polymerization experiment performed in the presence of hydrogen. The unique characteristics of mass and heat transfer exist due to laminar flow can also be evaluated from the thermal properties of the produced PP samples. The crystallinities of the polymer samples have found to be very low, and have been assumed to exhibit broad distributions of crystallite sizes.

Nomenclature

d_i : Inside reactor diameter (cm)
H_f : Heat of fusion ($J.g^{-1}$)
L : Tubular reactor length (cm)
m_{fr}^{Cat} : Mass flow rate of catalyst ($kg.hr^{-1}$)
m_{fr}^{M} : Mass flow rate of monomer ($kg.hr^{-1}$)
P_{set} : Set reactor pressure (bar)
Re : Reynolds number
t_c : Ratio of reactor pressurization to depressurization time
t_{Pr_rec} : Reactor pressure recovery time (s)
T_c : Crystallization temperature for polymer (^oC)
T_m : Melting temperature for polymer (^oC)
T_o : Initial reactor temperature (^oC)
v_z : Axial velocity ($cm.s^{-1}$)
V_r : Reactor volume (ml)
X : Mole ratio of hydrogen to liquid propylene
y_{di} : Scale-up ratio for reactor inside diameter
y_L : Scale-up ratio for reactor length
y_{Vr} : Scale-up ratio for reactor volume

Greek letters

τ : Average residence time (s)

Sub- and superscripts

avg : Average
c : Crystallization
Cat : Catalyst
f : Fusion
fr : Flow rate
i : Initial or inlet or inside

o	: Initial or outside
r	: Reactor
m	: Melting
M	: Monomer
Pr_rec	: Pressure recovery
set	: Representing the set value of a parameter
z	: Representing the axial direction

Abbreviations

DSC	: Differential scanning calorimetry
$MgCl_2$	: Magnesium dichloride
TEA	: Triethylaluminum
$TiCl_4$	: Titanium tetrachloride

Literature

[1] Agrawal, S. and Nigam, K. D. P. (**2001**), Chemical Engineering Journal, 84, 437 - 444.

[2] Hamer, J. W. and Ray, W. H. (**1986**), Chemical Engineering Science, 56, 6793 - 6800.

[3] Joye, D. D. (**2003**), International Journal of Heat and Fluid flow, 24, 260 - 266.

[4] Kissin, Y. V., Ohmishi, R. and Konakazawa, T. (**2004**), Macromol. Chem. Phys., 205, 284 - 301.

[5] Kleinstreuer, C. and Agarwal, S. S. (**1987**), Int. J. Engng. Sci., 25, 5, 597 - 607.

[6] Palma, M. and Giudici, R. (**2003**), Chemical Engineering Journal, 84, 189 - 198.

[7] Pater, J. T. M. and Kopmels M. (**1999**), Polymerization of liquid propylene using Zeigler- Natta catalyst system, Project Report, University of Twente, Enschede, The Netherlands.

[8] Stern, C., Frick, A. R., Pater, J. T. M. and Weickert, G. (**2005**), Macromolecular Material and Engineering, 290, 372 - 383.

[9] Ujhidy, A., Németh, J. and Szépvölgyi, J. (**2003**), Chemical Engineering and Processing, 42, 1 - 7.

Acknowledgement

Finally, a successful end to the long episode of my Ph. D. study is reached. I am really delighted. My journey towards the Ph. D. degree could not have been better than this, and I appreciate the concern and support provided by many people, which made this journey more exciting and rather less frustrating.

I am highly grateful to my supervisor Prof. Günter Weickert, who helped me in shaping up the research work presented in this thesis. Günter, thank you for allowing me to share some of your experiences and achievements in the field of polyolefins and social culture in general. Your attitude of "dare to dream" always kept me motivated and busy in learning the different aspects of the science and technology. Your most needed guidance and constant support during this project was unquestionable and highly appreciable. Your overall teaching in maintaining the balance between the fundamental understanding and the industrial applicability has assisted me a lot in gaining the confidence while doing this research work, and I am confident that it will help me further in excelling in my future career.

I would like to express my kind gratitude to my Ph. D. promotion committee members, Prof. L. Böhm, Dr. A. B. Mathur, Prof. W. P. M. van Swaaij, Prof. G. Versteeg, Prof. P. D. Idema, Prof. K-H. Reichert and Prof. J. Mejzlík. Your comments and recommendations on this work were highly encouraging and important in fine tuning the content of this thesis. I am thankful to all of you for sharing your valuable experience with me and spending your precious time in evaluating my thesis.

The research work described in this thesis was financially supported by DPI (Dutch Polymer Institute), The Netherlands, and I gratefully acknowledge. DPI has provided me support and valuable information exchange. I would like to thank all people, who were involved with this project. The regular meetings and discussions at the DPI Polyolefin Cluster Day, have contributed a lot in broadening my knowledge of polyolefins.

I am indebted to the HDL (Hoge Druk Lab) for its facility and support. The technical support provided by HDL is appreciable and certainly advanced my knowledge of designing and developing the pilot plants. Gert Banis, your help in solving the safety problems and providing the administration support in the lab was very great. I had the

luxury of utilizing the amazing ideas and technical skills of Fred ter Borg. Fred, your excellent support with practical ideas and constructions of the tubular reactor set-ups is greatly admirable. My “special” thanks to you. I am also thankful to Karst van Bree, for his additional support during the building-up of the pilot plant. Karst, your help was much needed and very valuable. I would like to thank Geert Monnink, “always a happy person”, for his continuous technical support over the last five years. Geert also thanks for the warm snacks during the weekends. Madhavi and I will never forget it. Thanks also goes to Johan Agterhorst, “always a quiet person”, for fixing-up all small problems during the experiments.

I would like to express my deepest gratitude to my master student Ide Engelsma, for his extensive support in start-up of the pilot plant as well as for his assistance in performing the polymerization experiments using a tubular reactor set-up. Ide, your keenness and hard work in achieving perfection in the results can clearly be seen from the high value of this thesis as evaluated by the committee members. Ide, many thanks to you for keeping the moral high by using your most favorite words like humongously…, banana…, etc. Olga, please forgive me for keeping Ide very busy during his nine month project. I also appreciate your support.

I wish to thank the secretaries of the IPP (Industrial Polymerization Processes) group especially Wies Elfers, Annet Rip and Bartie Bruggink-debraal, for their assistance in solving all the administration problems occurred over the last five and half years. I am highly obliged to Mrs. Bauke Visser (PA&O), for her help in communication with Dutch Immigration Department (IND) and the Gemeente Enschede. Mrs. Visser, I will never forget your kind support. I would like to express my deep gratitude to Mrs. Yvonne van der Kuil (Center for Work and Income, Enschede), for her recommendation to UWV for unemployment benefits in The Netherlands. Mrs. Visser and Mrs. Van der Kuil, only because your kind help I could able to stay in The Netherlands for last six months, and able to complete my Ph. D. thesis successfully. Thanks a lot! I would like to convey my appreciation to my former IPP colleagues Jochem Pater, Parasu Veera, Inge van Putten, Michiel Bergstra, Rob Emonds and Makarand Pimplapure, for their extensive scientific support and numerous discussions. My special thanks to Rob Emonds for his help in carrying out the experiments in Box 2. Most gratitude goes to my present IPP colleagues Yahya Banat, Mohammad Al-haj Ali, Shankara, Majid Daftari, Erik Eriksson and Peng Fei. Mohammad, many thanks to you for providing me the raw experimental data of some of the propylene polymerization experiments performed in the presence of

hydrogen. I highly appreciate. Yahya, my heartiest thanks to you for your caring and support provided to me over the last five years. It was really a great time sharing the office with you. I will always remember your sentence, “I love tomorrow”. Yahya and Majid, please convey my appreciation to your respective families for providing me the homely atmosphere away from my home land. Madhavi and I will always be indebted.

Thanks to my mathematics teachers at University of Twente, Dr. P. Mandal, Dr. S. Tomar, Dr. A. Nandi and Dr. K. Hiremath. Thank you very much for giving me a crash course and short-term assistance for mathematical modeling. My personal thanks are due to numerous Indian friends especially, Salim, Vishwas, Kiran, Makarand-Pallavi, Pramod-Vishakha, Kiran-Kavitha, Sirji-Shashibhabhiji-Ishani, Rahul-Shubhangi, Vishal-Shalaka, Supriyo-Anindita, Manish-Neha, Vasughi, Ranjana, Chandrashekhar, Charudatta, Amol, Santosh, Vijaya, Ramakrishna, Sameer, Digvijaya, Sandeep, Sreevatsa and Jeetendra. Kiran Thumma, thanks for all your assistance. My gratitude to everyone else who has made the past five and half years memorable and enjoyable, thanks a lot.

I wish to extend the deepest sense of appreciation to my mother (Aai) and my brother (Tushar), who missed me at home for last four years, and always inspired and motivated me to go for the best, in spite of many testing times at their end. I would like to express my kind gratitude to my grandmother (Aaji) and grandfather (Aajoba) for their blessings and immense belief in my ability, which helped me to sail through many turbulent times. I also owe hearty thanks to my all mama, mami, kaka, kaki, atya and other respected relatives. I am highly indebted to Dr. V. N. Dhobale and family, Mr. and Mrs. R. Velhankar and family, and Mrs. L. Gadgil and family for their much needed support at critical times. Akka Mavashi, thank you very much for your blessings and praying. Kokane mama and family, thanks a lot for your support and blessings. Sunil kaka, your frequent visit to Enschede was truly refreshing, I really appreciate.

More importantly, heartiest thanks to my wife, Madhavi, whose contribution I cannot even begin to acknowledge. Madhavi, I highly appreciate your patience and understanding. Your altruistic love and constant encouragement enabled me to complete this work.

I thank all those whom I missed to mention explicitly for helping me to see this day. Thank you very much to all of you.

Ravindra

About the author

Ravindra Radhakisan Tupe was born on September 11th 1976 in Mumbai, Maharashtra, India. After completing his Diploma in Chemical Technology (1994) from S. A. K. Polytechnic, Mumbai, he joined Dr. B. A. Technological University (an autonomous University) Lonere, Maharashtra, India, to obtain his Bachelor of Technology in Petrochemical Engineering.

In August 1997, he joined M. S. University of Vadodara, Gujarat, India, for his Master of Engineering in Chemical Technology with the specialization in Polymer Technology. During his masters, he received Golden Jubilee Scholarship from Indian Oil Corporation, Vadodara, India. For his master project work, he was selected as a Research Student at Indian Petrochemical Corporation Limited (IPCL), Vadodara, India. He worked on a dissertation titled "Melt Rheology of Polyethylenes and Their Blends" with the guidance of Dr. A. B. Mathur, (VP) R&D, IPCL, Vadodara, India. In 1999, for his master's project, he received a National award from the Indian Society of Technical Education (ISTE) and IPCL, India, for the "Best Master Thesis in Chemical Engineering".

From July 1999, he was appointed as a Lecturer at the Department of Petrochemical Engineering, teaching primarily second and third year Bachelor degree students in Petrochemical Engineering.

In February 2001, he started his Ph. D. project in the group of Industrial Polymerization Processes (IPP), University of Twente, Enschede, The Netherlands, to conduct the research on the "Tubular Reactor for Liquid-Phase Propylene Polymerization". He was guided in his research work by Prof. Dr. -Ing. Habil Günter Weickert. The Ph. D. project was financially supported by Dutch Polymer Institute (DPI), The Netherlands.